Design and rheological performance of microgel suspensions and microgel stabilised emulsions

Samuel Stubley

Submitted in accordance with the requirements for the degree of
Doctor of Philosophy

The University of Leeds
School of Food Science and Nutrition

January 2023

This thesis is dedicated to my mother, Maria.

Without her this would not have been possible.

The candidate confirms that the work submitted is his own, except where work which has formed part of jointly-authored publications has been included. The contribution of the candidate and the other authors to this work has been explicitly indicated below. The candidate confirms that appropriate credit has been given within the thesis where reference has been made to the work of others.

This research has been carried out by a team which has included Professor Brent Murray, Dr Olivier Cayre, Dr Isabel Celigueta Torres and Dr Isabel Fernández Farrés. My own contributions, fully and explicitly indicated in the thesis, have been in the conceptualization of experiments and the development of research methodology. I performed almost all of the experiments and formal data analysis for the data presented. I prepared the first drafts of the three publications presented and wrote and edited the remainder of the thesis alone.

The other members of the group and their contributions have been as follows:

- Brent Murray and Olivier Cayre were the academic supervisors for the research project. They acquired funding and provided supervision, feedback and resources throughout. They contributed to the editing and the reviewing of the manuscripts. Brent Murray was also involved in some of the formal data analysis.
- Isabel Celigueta Torres and Isabel Fernández Farrés were the industrial supervisors for the project. They were involved in project administration, acquired funding, provided resources and reviewed the manuscripts presented in this thesis.

The drafting and development of the patent which resulted from this project was a collective effort by all named authors and Dr John Slaven, lead patent counsel for the Institute of Material Sciences, Nestlé Research.

List of Publications

Chapter 3 - Stubley, S., Cayre, O., Murray, B., Celigueta Torres, I., & Fernández Farrés, I. (2021). Enzyme cross-linked pectin microgel particles for use in foods. *Food Hydrocolloids*, **121**, 107045.

Chapter 4 - Stubley, S., Cayre, O., Murray, B., Celigueta Torres, I. (2022). Pectin-based microgels for rheological modification in the dilute to concentrated regimes. *Journal of Colloid and Interface Science*, **628**, 684-695.

Chapter 5 - Stubley, S., Cayre, O., Murray, B., Celigueta Torres, I. (2023). Emulsifying properties of sugar beet pectin microgels. *Food Hydrocolloids*, **137**, 108291.

Patent Application – Cayre, O., Celigueta Torres, T., Fernández Farrés, I., Lazidis, A., Murray, B., Stubley, S. Whitehouse, A. Enzyme cross-linked sugar beet pectin microgel particles for use in foods. Filed February 2021 (expected publication date August 2022). Reference number: 18031-EP-EPA.

List of Accepted Conference Abstracts

Poster Presentations

'Stimuli Responsive Microgels as Rheology Modifiers'

- School of Food Science & Nutrition annual PhD conference (30th Nov 2018), University of Leeds, UK
- School of Food Science & Nutrition Industry Day (18th Jan 2019), Weetwood Hall, Leeds, UK

'Soft Colloids as Rheology Modifiers; Aqueous vs Sugar Systems'

- The 8th International Symposium of Food Rheology and Structure (17-20 June 2019), ETH Zurich, Switzerland
- The 5th Soft Matter and Functional Interfaces CDT Showcase (27-28 June 2019), University of Leeds, UK
- The 4th UK Hydrocolloids Symposium (12 September 2019), University of Leeds, UK

'Rheology of Sugar Beet Pectin Microgel Suspensions'

- The 35th ECIS 2021 Conference of the European Colloid & Interface Society (5-10 September 2021), Athens, Greece
- The 35th EFFoST International Conference 2021 (1-4 November 2021), Lausanne, Switzerland

Acknowledgements

I will be eternally grateful for the guidance and assistance of my academic supervisors Professor Brent Murray and Associate Professor Olivier Cayre. Not only did they mentor me from relative naivety to a well-rounded colloid scientist, they were also there to provide emotional support when I needed it most. I express my utmost gratitude for their knowledge and willingness to share it. I also sincerely thank my industrial supervisors Dr Isabel Celigueta Torres and Dr Isabel Fernández Farrés for their input and knowledge that they brought into the project.

A special thanks to those members of family and friends that believed in me for their support over the years. I would also like to thank my co-workers and laboratory technicians for their support in and outside of work and for their friendship. In particular Dr Liam Morris, Dr Lorenzo Metilli, Miss Aygül Can, Miss Katherine Lefroy, Mr Neil Rigby, Mr Miles Ratcliffe and Dr Nataricha Phisarnchananan.

I acknowledge the Engineering and Physical Sciences Research Council (EPSRC) funded Centre for Doctoral Training in Soft Matter and Functional Interfaces (SOFI), Grant Ref. No. EP/L015536/1 as well as Nestlé Product Technology Centre, Confectionery (York, UK) for the opportunity to conduct this research and for financial support.

Abstract

This thesis describes the fabrication, characterization and applications of pectin based microgels. A variety of techniques commonly used to characterize colloidal and soft matter systems (*i.e.*, particle size analysis, microscopy techniques and shear rheometry) were used throughout.

Microgel suspensions were prepared in large quantities using a simple and scalable 'top-down' technique. This involved the fabrication of crosslinked 'parent' pectin hydrogels which were subsequently combined with a suitable solvent and subjected to mechanical disruption to yield microgel suspensions. Such systems are promising candidates as novel food additives for purposes of rheology modification and emulsification.

It was shown that the rheological properties (viscosity and elasticity) of microgel suspensions can be tailored by varying the elasticity and effective volume fraction of microgel particles. The former is easily controlled via the elasticity of parent hydrogels, which in turn depends on the crosslinking density. The use of microgel suspensions as rheology modifiers is shown to provide distinct benefits over native polymer solutions and crosslinked polymer gels respectively. The ability to engineer desirable flow behaviour is likely to be a significant advantage to the manufacturer when developing new products or processes.

Converting pectin to pectin microgels also improved their functional properties when such systems were used as stabilizers of oil-in-water emulsions. Microgel stabilized emulsions were more resistant against droplet coarsening on prolonged storage and when subjected to temperature cycling as compared to native pectin stabilized emulsions. Furthermore, the particulate nature of the microgels resulted in emulsions with enhanced rheological properties at the same overall biopolymer concentration.

Table of Contents

List of Tables

List of Figures

Chapter 1: General Introduction

1.1 Overall Objectives

The overall objective of this thesis was to develop, produce and characterize biopolymer microgel suspensions suitable for use in foods. The food applications of interest to the project co-sponsor (Nestlé) include the use of microgel particles as (i) novel rheology modifiers for confectionary systems and (ii) novel stabilizers and emulsifiers for beverages. Nowadays, there is an increasing demand for plant-based food additives which is being driven by ethical, religious and/or sustainability considerations. This trend is expected to continue into the future so that replacing animal-based additives (*e.g.*, gelatine for rheology modification and whey protein for emulsion stabilization) with more sustainable alternatives has become a primary objective for food manufacturers.

Even in their native state, pectin appears promising for the applications suggested when used in foods. For example, pectin has been used as a rheology modifier for many decades by home cooks in the preparation of jams and preserves. For industrial applications, pectin has also found uses in the production of confectionary and dessert jellies, glazing agents for baked goods and texture modification of low-calorie soft drinks (May, 1990; Thakur et al., 1997). Hydrocolloid rheology modifiers (*e.g.*, modified starches, gums) are typically used to replace macronutrients such as sugar and lipids in the development of calorie reduced food products (Saha and Bhattacharya, 2010).

For application (ii), pectins have frequently been used for the stabilization of acidified protein beverages. In dairy products, pectins adsorb onto casein micelles via electrostatic interactions which prevents their aggregation as the pH of the system approaches the isoelectric point of the proteins through a steric mechanism (Maroziene and de Kruif, 2000). By extension, it has been demonstrated that the deposition of pectin onto protein stabilized emulsion droplets can improve the physical stability of emulsions under similar conditions (Littoz and McClements, 2008). Furthermore, there is plenty of experimental evidence in the literature for the direct use of certain pectin preparations as emulsifiers (Ngouémazong et al., 2015), where they have been shown to have a similar effectiveness to gum Arabic (Bai et

al., 2017). Since pectin is considered a ‘clean label’ food additive and is well accepted by the consumer, it was considered as an ideal starting material for the development of biopolymer microgels.

By converting native polymers into microgel particles, improvements in their functional properties might be achieved. For example, concentrated microgel suspensions demonstrate a time independent elasticity, but can be made to flow on the application of external forces. This contrasts with polymer solutions that are typically viscous fluids at all polymer concentrations and polymer gels which typically fracture instead of flowing. The ability to tailor the rheological properties of concentrated microgel suspensions by controlling the mechanical properties of discrete particles has also been demonstrated (Adams et al., 2004). In addition, (microgel) particle stabilized emulsions have been shown to demonstrate exceptional physical stability (Dickinson, 2015).

To gain fundamental insight into the rheological and emulsifying properties of microgels, a model system based on synthetic, poly(N-isopropylacrylamide) (*p(NIPAM)*) microgel particles was considered. The synthesis and characterization of this system has been studied in detail over the years and they were selected here with a view to compare and validate the findings of pectin microgel systems. The advantages of synthetic microgels lie in the precise control available over their particle size, polydispersity and crosslinking density. All of these physical properties are expected to influence the functionality of microgel suspensions. Unfortunately, due to time constraints and disruptions brought about by COVID-19, in addition to the preferences of industrial sponsors, most of the work undertaken was focused on pectin microgel systems. To that end, such systems were found to be sufficiently interesting and novel to allow for three publications which make up the major chapters (**Chapters 3**, **4** and **5**) of this thesis, in addition to a patent application funded by the industrial sponsor.

1.2 Thesis Outline

In line with the submission of this thesis by jointly authored publications, the document is organised into the following sections;

Chapter 1: The remainder of chapter one aims to introduce some key topics required to understand and appreciate any subsequent chapters. Firstly, a general

discussion on colloids and colloidal interactions is required to introduce microgels as ‘soft colloids’, their comparison to ‘solid’ particles (primarily ‘hard-spheres’) and general features of the rheological and emulsifying properties for the two systems.

Chapter 2: Contains details on the synthesis, scale-up and characterization of *p(NIPAM)* microgels. The influence of temperature and solvent composition on particle size and surface charge density was investigated via dynamic light scattering and laser Doppler micro-electrophoresis respectively. The rheological characterization of such systems was limited to the determination of an effective volume fraction (Φ_{eff}) and an investigation of the Φ_{eff} dependence on the viscosity of suspensions. Whilst the initial aim to compare these system in detail with pectin microgels was not realized (due to the reasons given above), this work does show that the rheology of pectin microgels discussed in subsequent chapters is similar to more well defined, synthetic systems. Furthermore, it provides future workers in our research group with a starting point if they wished to scale up the synthesis of *p(NIPAM)* microgels.

Chapter 3: Food Hydrocolloids published article titled “Enzyme cross-linked pectin microgel particles for use in foods”. This manuscript describes the fabrication and characterisation of sugar beet pectin (*SBP*) hydrogels and the microgel particles generated from them using a ‘top-down’ technique. We highlight the benefits of chemically crosslinked *SBP* microgels compared to physically crosslinked, low methyl ester pectin microgels prepared in the same way. The rheological properties of *SBP* microgels are shown to offer distinct advantages over native, non-crosslinked *SBP* when compared at the same total pectin concentration.

Chapter 4: Journal of Colloid and Interface Science published article titled “Pectin-based microgels for rheological modification in the dilute to concentrated regimes”. This manuscript describes a detailed study into the rheological properties of *SBP* microgel suspensions with respect to Φ_{eff} and the elasticity of microgel particles. The linear and non-linear viscoelasticity of suspensions as a function of Φ_{eff} was assessed with capillary viscometry, rotational and oscillatory shear rheometry respectively.

Chapter 5: Food Hydrocolloids published article titled “Emulsifying properties of sugar beet pectin microgels”. This manuscript describes the stabilization of oil-in-water emulsions with *SBP* microgels via a ‘Pickering’ mechanism. Microgels differing in their crosslinking density, either ‘soft’ or ‘firm’ were used for these

purposes. The droplet size distributions and microstructure of emulsions were characterized via laser diffraction and microscopy techniques. Comparisons to native (*i.e.*, non-crosslinked) *SBP* stabilized emulsions were made throughout. Significant improvements in the physical stability of emulsions on (i) prolonged storage at ambient temperature and (ii) temperature cycling could be achieved by processing *SBP* into microgel particles.

Chapter 6: Contains a critical discussion which ties the results of previous chapters together. Some concluding remarks and suggestions for how these materials might be utilized in real food systems is provided, including some ideas for future investigations.

Appendix: Chapters 2-6 contain much of the details on the various experimental methods used, which were mainly: shear rheometry, capillary viscometry, light scattering (static and dynamic), confocal laser scanning microscopy, light microscopy and scanning electron microscopy. Most of these techniques are standard to the characterization of colloidal and soft matter systems. Therefore, instead of a dedicated materials and methods section, some additional remarks on the principles of these techniques are provided in the appendix section, where appropriate.

1.3 Key Topics

1.3.1 Colloidal Dispersions and Colloidal Interactions

A brief discussion into colloidal dispersions and colloidal interactions is necessary to introduce the concept of soft colloids (*i.e.*, deformable microgel particles and emulsion droplets) thereby allowing the reader to appreciate the novelty of this work. A colloidal dispersion refers to a heterogeneous, two component system in which fluid (*i.e.*, liquid or gas) or solid matter is dispersed uniformly within a continuous fluid phase. The dimensions of the dispersed phase, the colloid, are most often on the order of 10-1000 nm. Systems containing larger (> 1000 nm) or anisotropic ‘particles’ are often referred to as suspensions although they may still exhibit colloidal character providing at least one dimension is on this length scale. A distinguishing feature of colloids is that they are considerably larger than the molecules comprising the continuous phase, yet small enough to be influenced by thermal energy, k_BT, where k_B is the Boltzmann’s constant (1.381 x 10-23 J K^{-1}) and

T is the absolute temperature (°K). In these systems, molecules of the continuous phase continuously collide with the colloidal particles and this is sufficient to influence their motion. This phenomenon, referred to as Brownian motion, is characterised by the diffusion of colloids throughout the system in a random 'zig-zag' motion (Everett, 1988; Lekkerkerker and Tuinier, 2011).

Dispersions and suspensions are ubiquitous in everyday life with pertinent examples in foods (*e.g.*, milk, mayonnaise), cosmetics (*e.g.*, aerosols, shaving foam) and coatings (*e.g.*, inks, paints). Brownian motion contributes to the stability of colloidal systems by counteracting the gravity induced creaming or sedimentation resulting from density differences between the dispersed and continuous phases. The attractive and repulsive interactions experienced by colloidal particles dispersed in the continuous phase further govern the stability of the system and hence its possible applications. An imbalance in attractive to repulsive forces make colloidal particles prone to aggregation which is generally considered undesirable (Mewis and Wagner, 2012).

Similarly to the atoms or molecules from which they are composed, colloidal particles experience attractive forces due to van der Waals (*VDW*) interactions. In a vacuum, atoms and molecules interact with a Lennard-Jones potential which approximates the pairwise interaction energies (pair potential, *V* (J)) with respect to their (centre-centre) distance of separation, *r* (m).

$$V_r = \frac{b}{r^{12}} - \frac{c}{r^6} \qquad [1.1]$$

The constant *b* in Equation 1.1 describes a repulsive force originating from the Born repulsion, which implies that electron orbitals surrounding atoms cannot overlap due to the principle of excluded volume. The negative term in Equation 1.1 describes an attractive force originating from the *VDW* interactions. In all cases, the *VDW* attraction is a result of the interactions between electrical dipoles in atoms or molecules at small distances of separation. The constant *c* contains the contribution from the three *VDW* components namely Keesom, Debye and London, which represent different types of dipole-dipole interactions. Each of these *VDW* forces demonstrate an interaction potential that decays with inverse distance to the 6^{th} power (Briscoe, 2010; Israelachvili, 2011).

The London dispersion forces have the greatest influence on the magnitude of the *VDW* attraction and hence the pair potential. Such forces originate from the random fluctuation of the electron clouds surrounding nonpolar atoms or molecules. The stochastic nature of these fluctuations can result in the accumulation of electrons in a given region thereby resulting in the development of a transient 'instantaneous' dipole moment (Briscoe, 2010; Israelachvili, 2011). This dipole moment is essentially an electromagnetic field that can propagate to displace the electron distribution of a neighbouring atom or molecule inducing a temporary dipole upon it. The effect of the London dispersion force is that the dipole moments (and hence atoms or molecules) in close proximity become correlated in their motions resulting in an attraction. It should be noted that dispersion forces can also arise due to the 'instantaneous' dipoles induced on an atom or molecule by permanent dipoles or charges nearby (Hunter, R., 2001).

Colloidal particles are macrobodies composed of assemblies of atoms or molecules. Assuming that the constituent atoms or molecules within discrete colloids interact with a Lennard-Jones potential and that these interactions are pairwise additive (*i.e.*, they can be summed over large collections of atoms or molecules), the Hamaker theory can be used to approximate the potential energy of the interaction between two macrobodies. The most simple geometry to colloid science, which is generally used as a starting point, is that of two spheres (Hunter, R., 2001; Everett, 1988).

Since colloidal particles inherently demonstrate a large surface area to volume ratio, it is more appropriate to consider surface forces between colloidal particles in terms of the potential energy of the interaction as a function of separation distance, *W(h)* (*cf.* centre-centre distance discussed previously for atoms/molecules). Pairwise summation is achieved by integrating the interactions of all molecules over the volume of two spheres;

$$W_{(h)} = \int_{v_1} dv_1 \int_{v_2} dv_2 \, \rho_1 \rho_2 \left(\frac{c}{r^6}\right) \qquad [1.2]$$

Where v and ρ refer to the volume (m^3) and number density of molecules respectively (*i.e.*, in spheres 1 and 2). This leads to;

$$W_{(h)} = -\frac{\pi^2 \rho_1 \rho_2 c}{6}\left[\frac{2R_1R_2}{r^2-(R_1+R_2)^2} + \frac{2R_1R_2}{r^2-(R_1-R_2)^2} + ln\frac{r^2-(R_1+R_2)^2}{r^2-(R_1-R_2)^2}\right] \qquad [1.3]$$

Where r is the centre-centre distance of separation (m) ($r = R_1 + R_2 + h$) and h is the surface separation distance (m). For two equal sized spheres ($R_1 = R_2 = R$) in the limit of close approach ($h << R$) Equation 1.3 reduces to;

$$W_{(h)} = -\frac{AR}{12}\frac{1}{h} = -\frac{AR}{12h} \qquad [1.4]$$

In which A is the Hamaker constant (J) given by;

$$A = \pi^2 \rho_1 \rho_2 c \qquad [1.5]$$

Compared to Equation 1.1 which suggests the potential energy of attraction between atoms/molecules decays like $1/r^6$, it becomes apparent that the surface forces between colloids acts over a much longer range (*i.e.*, $1/h$, Equation 1.4). Consequently, while the range of intermolecular forces are on the order of several nanometres, the surface forces that are important for the stability of colloidal bodies act even at separation distances as large as *ca.* 100 nm (Briscoe, 2010).

Equation 1.4 describes the interaction potential between two colloidal spheres in isolation and in a vacuum. In reality, colloids are dispersed in a continuous fluid phase, often a liquid solvent, the presence of which is generally found to reduce the range of the interaction. A combined Hamaker constant accounting for the presence of the dispersion medium can be defined by;

$$A_H = \left(\sqrt{A_{particle}} - \sqrt{A_{medium}}\right)^2 \qquad [1.6]$$

Hamaker constants of various materials commonly used in colloid science are on the order of 10^{-20} J. The more closely matched the individual Hamaker constants of the particle and the medium, the smaller the combined Hamaker constant. This is an important observation since the Hamaker constant sets the magnitude rather than the range of the interaction (Everett, 1988; Hunter, R., 2001).

A further discrepancy arises from the longer range of interaction in colloidal systems. In a vacuum, the electromagnetic wave responsible for polarisation of electron distributions travels at the speed of light. Therefore, at short distances of separation and in the absence of any intervening medium, its propagation is assumed to occur almost instantaneously. When the colloids are separated by larger distances, there is a delay between the propagation of the electromagnetic field from its origin, the polarisation of the electron distribution in a 2nd colloid and the subsequent dipole-induced-dipole interaction. Under these circumstances, the electron

distribution in the first colloid could be in a different state to what it was originally. As a result, the two dipoles no longer oscillate in unison and hence the attraction is weakened due to these so-called retardation effects. Such effects are observed at surface separations exceeding ~10 nm (Everett, 1988; Israelachvili, 2011).

The above discussion treats the interparticle potential between two colloidal bodies in isolation. In reality, multi-body interactions arise between collections of colloidal particles. In this case, the total potential energy of the system can be estimated by summation of the interactions between a colloid and its nearest neighbours. The *VDW* attraction implies that at short distances of separation, particles become trapped in a deep energy minimum (compared to k_BT) and aggregate irreversibly. It is found that those atoms or molecules occupying the interfacial region of colloidal particles have the greatest influence on the short range (Born) repulsive term. In order to obtain a stable colloidal dispersion, additional repulsive forces owing to charge- or steric- stabilisation mechanisms are required (Everett, 1988; Tadros, 2010).

The repulsive interactions in colloidal dispersions may be defined as either ‘hard’ or ‘soft’ depending on the nature of the interfacial region and composition of the continuous phase. Quantifying the attractive and repulsive forces (*i.e.*, the total interaction potential) allows the construction of energy-distance curves which can be used to explain the stability of colloidal dispersions under a given set of conditions (Tadros, 2010).

1.3.2 Colloidal Hard Spheres

Colloidal particles demonstrating a ‘hard-sphere interaction’ represent the simplest system. Being fabricated from incompressible materials, the dimensions of hard-spheres remain constant even when particles come into contact. In addition, the surface of hard-spheres is assumed to be featureless (*i.e.*, ‘smooth’) such that the radius of the hard-sphere is comparable to the radius of the particle core (Tadros, 2010) as is shown schematically in Figure 1.1A.

Since the range of the *VDW* interaction depends on the propagation of an electromagnetic wave through the continuous phase, the interaction in hard-sphere systems can be screened by matching the refractive indices of the colloid and the continuum respectively (Lekkerkerker and Tuinier, 2011). Surface charges, usually originating from the ionisation of surface groups, result in long-ranged interactions

and in hard-sphere systems such charges are screened with salt addition or by dispersing particles in non-aqueous media. For these reasons, hard-sphere colloids are said to demonstrate ‘net neutrality’ in the sense that particles experience no net interaction until they come into ‘contact’ at which point the repulsive interaction potential approaches infinity (Figure 1.1B). The sharp repulsion on inter-particle contact is due the inability for incompressible spheres to overlap (Tadros, 2010; Mewis and Wagner, 2012).

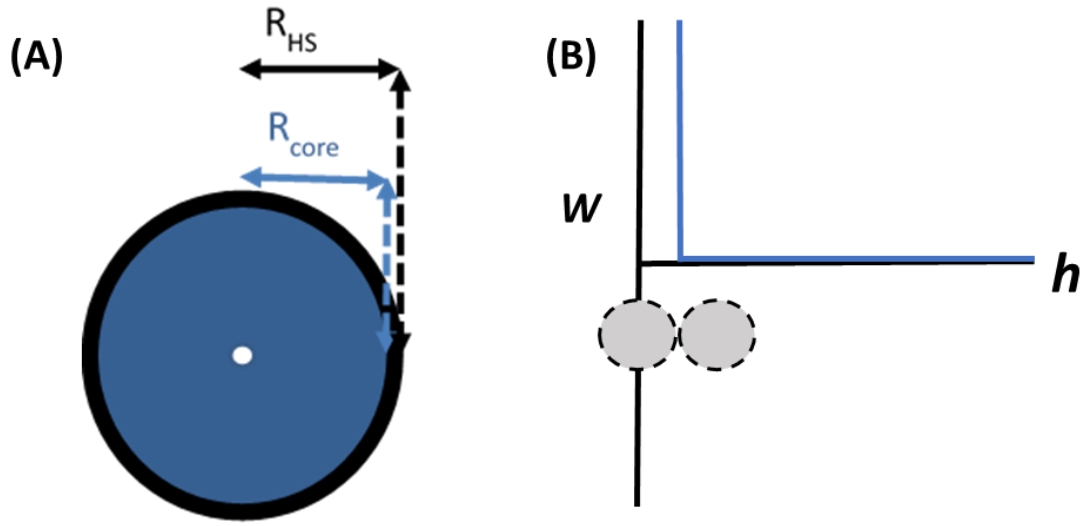

Figure 1.1 - Schematic of (A) a colloidal hard sphere showing the particle radius (R_{HS}) is approximately equal to the radius of the particle core (B) Potential energy of particle-particle interactions (W) for hard spheres as a function of the surface separation distance (h). Adapted from (Tadros, 2010). Not drawn to scale.

1.3.3 ‘Soft’ Colloids

Evidently, the hard-sphere system is highly idealised and is consequently dissimilar to any ‘real’ colloidal dispersion encountered in practice. Due to the materials and techniques available for their fabrication, colloidal particles will generally demonstrate some ‘softness’ (Royall et al., 2013). The term soft may correspond either to the mechanical properties of the dispersed phase or to the nature of the inter-particle interactions. For mechanically soft colloids, the particle size and shape becomes dependent on inter-particle contacts (Vlassopoulos and Cloitre, 2014). The elastic deformation of soft particles on contact adds additional complexities in determining the pair potential (Israelachvili, 2011). Softness in the interaction potential manifests where the contribution of the interfacial region to the effective

particle radius is appreciable relative to the radius of the particle core. Depending on the nature of dispersed and continuous phases, particles experience long range repulsive forces due to ‘soft electrostatic’ or ‘soft steric’ interactions. The combination of these interactions results in so called ‘electro-steric stabilisation’ (Tadros, 2010).

1.3.4 Soft Electrostatic Interaction

Surface charges in colloidal particles mostly arise from the ionisation of surface groups. When immersed in an aqueous solvent, a so called electrical double layer develops in which counter- and co- ions from the bulk surround the colloid to an extent which balances the charges at the surface. There is an uneven distribution of ions in the electrical double layer which extends with a distance known as the Debye length (*1/k*) from the colloid surface. The counter-ions outweigh co-ions due to their accumulation at the oppositely charged surface. Beyond this region, known as the Stern layer, the distribution of ions is more diffuse (Fig. 1.2A). As the electrical double layers of discrete colloids begin to overlap, the ‘soft’ electrostatic interaction manifests as a repulsion of like-charged particles which is driven by the local imbalance of osmotic pressure in this region (Fig. 1.2B). The range of the interaction depends on *1/k*, which in turn depends on the ionic environment (*i.e.*, the ion concentration and valency) in the continuous phase. An increase or decrease in the concentration of ions leads to compression or extension of the double layer respectively. Hence the addition of salt to a dispersion of charged colloids influences the stability of the system (Lekkerkerker and Tuinier, 2011; Everett, 1988; Tadros, 2010).

Figure 1.2 shows a schematic of the soft electrostatic repulsion between like-charged colloids. When combined with the *VDW* attraction (Figure 1.2C), the energy-distance curves for electrostatically stabilised dispersions show an energy barrier where electrostatic repulsion prevents particles from approaching to a distance where the *VDW* attraction begins to dominate. This is the principle of the *DLVO* theory of colloidal stability, after Derjaguin-Landau-Verwey-Overbeek.

The height of the energy barrier depends on the surface charge and the ionic environment (Lekkerkerker and Tuinier, 2011; Tadros, 2010). The energy barrier must be sufficiently large with respect to k_BT to prevent Brownian collisions resulting in the (irreversible) aggregation of colloids. The average energy brought

into inter-particle collisions undergoing Brownian motion is approximately $(3/2)k_BT$. If the energy barrier exceeds ~10 k_BT, the probability of particles overcoming this energy barrier through collisions becomes very small ($\propto e^{-k_BT}$). However, it should be noted that external forces can provide sufficient energy to drive colloids into an aggregated state and therefore in practice, a higher energy barrier would be preferable (Everett, 1988).

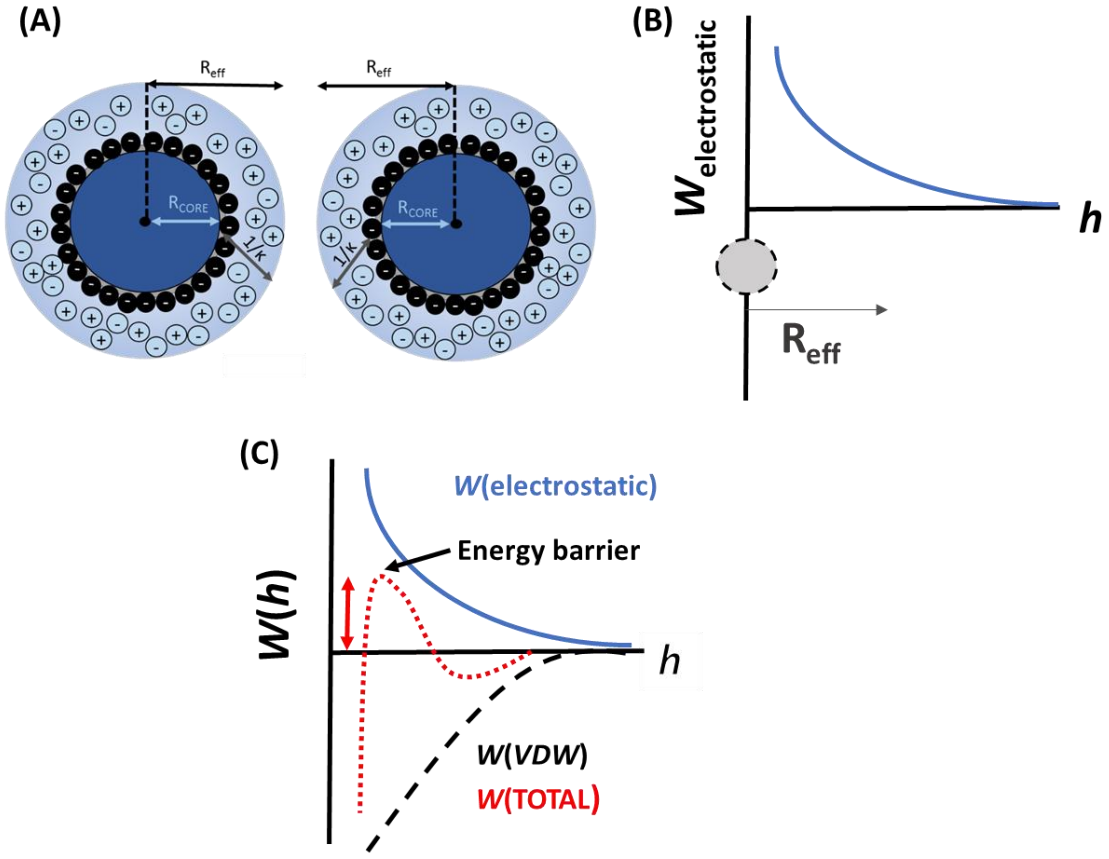

Figure 1.2 - Schematic of (A) a charged colloid showing that the effective particle radius (R_{eff}) is larger than the radius of the particle core. (B) Potential energy of particle-particle interactions (W) for electrostatically stabilized colloids as a function of the surface separation distance (h). In (C), the potential energy of the *VDW* interaction ($W(VDW)$) and the total potential energy (W(TOTAL)) resulting from its combination with the electrostatic repulsion is shown depicting an energy barrier. Adapted from (Tadros, 2010). Not drawn to scale.

1.3.5 Soft Steric Interaction

In systems demonstrating a 'soft' steric interaction, the interfacial region is heterogeneous in contrast to the featureless surface of hard-sphere colloids. Steric

repulsive forces might also arise due to the characteristic morphology of non-spherical particles. In all such cases, the effective radius (R_{eff}) is larger than the core radius (R_{core}). Considering a hard-sphere stabilized by the adsorption of a polymer as an example of such systems, one can define a stabilizing chain length, δ as is shown in Figure 1.3A. Since $R_{eff} = R_{core} + \delta$, the range of the interaction can vary from (nearly) hard to soft (Tadros, 2010).

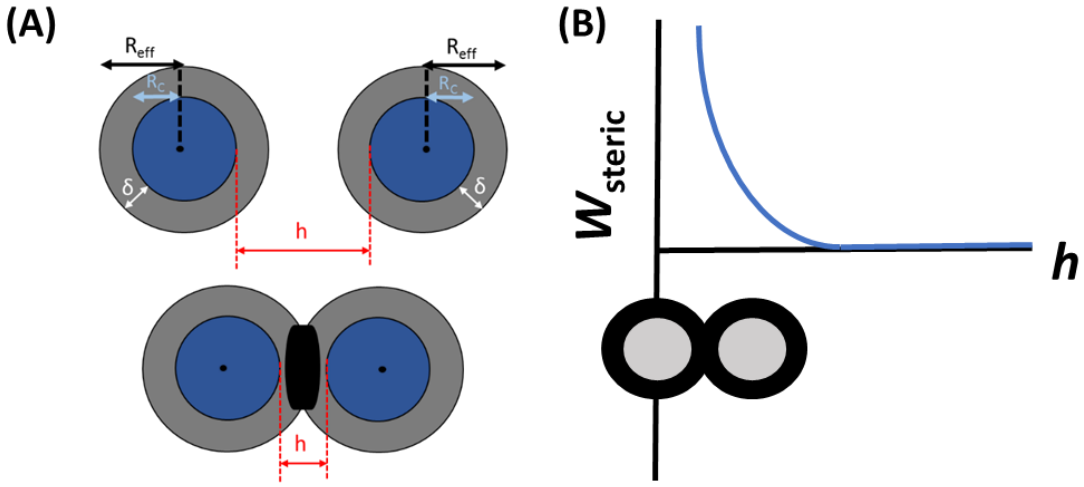

Figure 1.3 - Schematic of (A) a sterically stabilized colloid showing that the effective particle radius (R_{eff}) is larger than that of the particle core (R_C) by an amount that depends on the stabilizing chain length (δ) (B) Potential energy of particle-particle interactions (W) for sterically stabilized colloids as a function of the surface separation distance (h). Adapted from (Tadros, 2010). Not drawn to scale.

As two similar particles approach each other to a distance where the interfacial stabilising chains overlap, a strong repulsive force develops which may be either osmotic or entropic in nature. In the first instance, the local increase in polymer density due to the interpenetration of the steric layers of discrete particles results in a local increase in the osmotic pressure. Providing the solvent is 'good' for the stabilising chains, the subsequent diffusion of solvent into this region acts to separate the particles. The entropic effect arises from the loss of configurational entropy in the stabilising chains due to the principle of excluded volume. The number of available configurations on overlap is less than the number of configurations at infinite distances of separation. This is energetically unfavourable and consequently, the repulsive potential rapidly increases as depicted in Figure 1.3B (Tadros, 2010; Everett, 1988).

1.3.6 Introduction to Gels and Microgels

Despite extensive experimental and theoretical considerations, the term ‘gel’ is somewhat ambiguous (Almdal et al., 1993). The term ‘microgel’ is perhaps even more so. The earliest attempts at defining the gel state suggest the presence of a solvent, potentially in large quantities, as a pre-requisite to gelation (Hermans, 1949). Only gels containing water or electrolyte are considered here which will be referred to as hydrogels. Despite the large amount of solvent present, hydrogels tend to appear ‘solid-like’, at least on the timescales of human perception (Clark and Ross-Murphy, 2009; Almdal et al., 1993). This implies the presence of some other structural component, typically macromolecules (polymer gels) or colloids (colloidal gels) dissolved or dispersed in the solvent. It is well established that the evolution from a liquid state to a solid state, the so-called sol-gel transition or gel point, results from the development of an interconnected microstructure between these entities. Gelation has been studied theoretically as a percolation process which describes the progressive increase in connectivity of the system ultimately resulting in a solvent holding network. Consequently, attractive interactions between the polymers or colloids need to be induced in some manner (Nishinari, 2009; Djabourov et al., 2013).

Considering polymer gels for a more detailed explanation, intermolecular crosslinks between neighbouring molecules initially results in the formation of molecular clusters of finite size. At some point in time (*i.e.*, the gel point), a critical number of crosslinks is formed corresponding to the point where a percolated network of molecules spanning the entire system is formed (Djabourov et al., 2013). In addition to a critical number of crosslinks, percolation theory also implies a critical polymer concentration for gelation. The magnitude of either critical parameter is system specific depending on numerous intrinsic (*e.g.*, polymer molar mass and persistence length) and extrinsic (*e.g.*, pH and ionic strength) factors. The latter affect the polymer conformation in solution and their interactions (Clark and Ross-Murphy, 2009; Nishinari, 2009).

In the broadest sense, gels can be categorised as ‘physical’ or ‘chemical’ depending on the mechanism of crosslinking. The latter involves the introduction of irreversible, covalent crosslinks resulting in ‘strong’ gels. Whereas intermolecular crosslinks in chemical gels are ‘point-like’, those in physical gels extend over larger distances and are often referred to as junction zones. The mechanism of junction

zone formation depends on both the starting material and environmental conditions (Djabourov et al., 2013). Gelation occurs as a result of attractive physical interactions between the polymer chains, for example *VDW* interactions and hydrogen bonding. The energetics of individual physical interactions between the polymer chains are relatively lower than covalent crosslinks and are on the order of k_BT. Despite this, such forces are co-operative and hence stable junction zones can be generated (Daniel et al., 1994). Nonetheless, physical gels are often referred to as 'weak' and gelation is often reversible. For example, junction zones in physical gels can be disrupted on the application of heat and subsequently reform under quiescent conditions. Other extrinsic factors such as solvent quality (*e.g.,* pH, ionic strength) and mechanical disruption can also cause the dissociation of physical gels (Djabourov et al., 2013).

Microgels are particulate, solvent holding polymer networks of tens of micrometres (or below) in size, stabilized by intra- and/or intermolecular crosslinks which may be of chemical or physical origin. Direct analogies can therefore be made between microgels and their macroscopic, bulk gel counterparts. The main difference between the two systems is that microgels take the form of suspensions, the discrete particles being swollen by the same solvent in which they are dispersed (Pelton, 2000). This definition highlights the importance of the solvent. Both aqueous (water swollen) and non-aqueous (organic solvent swollen) microgel systems composed of synthetic polymers have been studied for decades with the first experimental reports being on *p(NIPAM)* (Pelton and Chibante, 1986) and poly(styrene) (Staudinger and Husemann, 1935) microgels, respectively. Only aqueous microgel systems are considered here. These have been proposed as model soft colloids demonstrating properties intermediate between particles and polymers (Lyon and Fernandez-Nieves, 2012). The softness of microgels can be appreciated from their mechanical properties as well as in their interaction potential. The latter will depend on the chemistry of the polymers used and the nature of the interface, which is typically poorly defined.

The technique chosen for microgel synthesis depends largely on the starting materials available. Possible routes to microgel formation from synthetic polymers exist from bulk hydrogels, linear polymers or reactive monomers. For example, the mechanical disruption of a hydrogel network is a facile approach to the fabrication of microgel particles (Griffin et al., 2007). Microgels can be prepared by

crosslinking aqueous polymer solutions in the dispersed phase of water-in-oil emulsions (Kim et al., 2007) or through the electrostatic complexation of oppositely charged, polyelectrolyte macromolecules in solution (Feng et al., 2007). The same techniques have been used to fabricate microgel particles from biopolymers (Adams et al., 2004; Paques et al., 2014; Azarikia et al., 2015). The fabrication, characterization, and rheological properties of *p(NIPAM)* microgels synthesised directly from reactive monomers are discussed in **Chapter 2**.

Biopolymers tend to be more structurally complex than synthetic polymers with respect to the diversity of monomeric subunits and their configuration in the polymer molecules. In developing microgels from biopolymers, it is therefore to be expected that less control will be available over the physiochemical properties of the particles. Furthermore, due to the low retail cost of most food products, the cost of microgel production needs to be reasonable and the method of production needs to be straight forward and scalable. For these reasons, the mechanical disruption of bulk hydrogels in the presence of an excess of solvent appears promising. This so-called 'top-down' technique has been used to fabricate microgel suspensions from a host of different gel forming biopolymer molecules, usually proteins or polysaccharides. The characterization and rheological properties of pectin microgels prepared using a top-down technique are described in **Chapters 3** and **4** respectively and the emulsifying properties of such microgels is described in **Chapter 5**. General features of (i) the phase behaviour and rheological properties of hard spheres and soft colloids and (ii) the emulsifying properties of hard and soft particles are discussed in the following sections.

1.3.7 Phase Behaviour and Rheology of Suspensions

Hard sphere colloidal suspensions demonstrate a rich phase behaviour which largely depends on the volume fraction (ϕ) occupied by the dispersed phase. This can be defined by:

$$\Phi = nV_p \qquad [1.7]$$

$$V_p = 4\pi R^3/3 \qquad [1.8]$$

: where n is the number of particles with volume (V_p) and R is the particle radius (m). For monodisperse systems, which are cooled or concentrated slowly, the onset of crystallization, also known as the freezing point, occurs at ϕ = 0.494. The

coexistence of liquid and crystal phases is observed until ϕ = 0.545. Samples will crystallize completely beyond this ϕ. The maximum ϕ attainable for monodisperse hard spheres is 0.74 corresponding to hexagonal close packed or face centred cubic crystal configurations. Crystallization can be observed visually or investigated analytically, with scattering techniques for example (Schöpe et al., 2007; Pusey et al., 2009).

The introduction of polydispersity (around 8%) or rapid cooling can be used to supress crystallization. The former is the preferred technique since the crystal is the most thermodynamically favourable state for monodisperse systems (Zaccarelli et al., 2009; Hunter, G. and Weeks, 2012). Under these circumstances, the suspension is a disordered fluid until at $\phi \approx 0.58$, a so-called glass transition (ϕ_G) is observed (Pusey and van Megen, 1986). The glass transition extends to ϕ = 0.64 which is the theoretical random close packing (ϕ_{RCP}) limit of equal sized spheres. It has previously been suggested that $\phi_G = \phi_{RCP}$ although polydispersity is known to push the ϕ required for phase transitions to higher values (Schöpe et al., 2007; Pusey et al., 2009). A glass refers to a dynamically arrested state of matter. The glass transition can therefore be identified by monitoring the diffusion, or more appropriately the mean square displacement, of particles as a function of ϕ. This can be achieved by confocal microscopy (Weeks and Weitz, 2002) or light scattering (Zaccarelli et al., 2009) among other techniques. On approach to ϕ_G, the dynamics are slowed due to particles being caged in by their nearest neighbours. Particles can escape from their cages at long (relaxation) times, although this is thought to require collective particle motions. Beyond ϕ_G, the particle dynamics are completely arrested, at least on experimental timescales (Hunter, G. and Weeks, 2012).

Rheology is routinely used to investigate the phase behaviour of suspensions. In the dilute regime, hard sphere dispersions are typically free-flowing Newtonian fluids (*i.e.*, the dispersion viscosity (η) is independent of shear rate). At intermediate ϕ, shear thinning (*i.e.*, a shear rate dependent reduction in η) is observed making the measurement of the low ('zero') shear viscosity (η_0) experimentally challenging (Cheng et al., 2002). Above a critical volume fraction (typically $\phi > 0.3$), shear thickening (*i.e.*, an increase in η with shear rate), is observed. The cause of shear thickening is still poorly understood however it appears to become more pronounced with increasing ϕ. The two main theories that have been proposed to describe shear thickening, namely the 'dilatancy' and 'hydrocluster' models, both suggest that

shear thickening is due to frictional contacts between particles. Shear thickening can be exploited, for example, in the development of protective clothing but is mostly considered undesirable since thickening suspensions are difficult to process (Brown and Jaeger, 2014).

The volume fraction dependence on η_0 is another way to identify the glass transition. The increase in (relative) η is initially gradual, but diverges over a narrow range of ϕ, typically in the vicinity of ϕ = 0.58 - 0.64 (Cheng et al., 2002; Mewis et al., 1989). The exceptionally high relative viscosity demonstrated by such systems is analogous, though not as profound, to the viscosity increase in molecular glasses (Hunter, G. and Weeks, 2012).

Colloidal glasses can therefore be considered amorphous solids. This is because they demonstrate a true, finite yield stress (σ_y). In other words, the suspensions behave as solids until some critical stress (σ) is applied, at which point the suspensions yield and flow as viscous fluids. The flow of colloidal glasses arises due to the disruption of particle cages and subsequent particle rearrangements. The application of small stresses and strains can be achieved using oscillatory shear rheometry. This allows one to probe the mechanical properties of colloidal glasses non-invasively and such systems generally demonstrate a frequency (time) independent elasticity (van der Vaart et al., 2013; Le Grand and Petekidis, 2008).

Some authors discuss a jamming transition for colloidal hard spheres at $\phi > \phi_{RCP}$, however this term is more frequently used to describe dense packings of non-colloidal particles, where Brownian motion is negligible and particles can be packed to such high ϕ that they form permanent contacts. The particle modulus and inter-particle friction then become important for the bulk rheological properties. Soft particles such as microgels can be compressed and even interpenetrate at high phase volumes. Furthermore, their volume depends on the environmental conditions such as the osmotic pressure and temperature (Seth et al., 2006; Vlassopoulos and Cloitre, 2014). An effective volume fraction (ϕ_{eff}) is usually defined for such systems, commonly achieved by mapping their phase diagram onto that of hard spheres or via dilute suspension rheology (Royall et al., 2013).

The formation of crystals, glasses and jammed phases in soft particle suspensions depends on a complex interplay between ϕ_{eff}, the particle mechanical properties and particle-particle interactions. Experimental studies into phase transitions in soft

particle suspensions have been reviewed elsewhere (Vlassopoulos and Cloitre, 2014; Lyon and Fernandez-Nieves, 2012). The determination of ϕ_{eff} and a study into the rheological properties of suspensions as a function of ϕ_{eff} is demonstrated for *p(NIPAM)* microgels in **Chapter 2** and for sugar beet pectin microgels in **Chapter 4**. The rheology of sugar beet pectin microgel stabilized oil-in-water emulsions prepared at oil volume fractions of 20% and 40% is described in **Chapter 5**.

1.3.8 Particle Stabilized 'Pickering' Emulsions

Emulsions stabilized by solid particles, so called 'Pickering emulsions' (Pickering, 1907: Binks, 2002), have been known for over a century however the widespread interest in such systems has only increased in the last two decades. In contrast to low molecular weight surfactants and surface active polymers, which may be either synthetic (*e.g.,* polyglycerol polyricinoleate (*PGPR*)) or natural (*e.g.,* proteins), such particles do not necessarily require surface activity to adsorb to the interface between two immiscible fluid phases (Binks, 2002).

For surfactants and polymers, surface activity originates from the molecules simultaneously containing hydrophilic and hydrophobic regions. This enables them to assemble at the interface of immiscible fluid phases such as oil-water and air-water interfaces, resulting in the stabilization of emulsions and foams respectively. The presence of surface active molecules reduces the number of unfavourable contacts between molecules of the dispersed and continuous phases and consequently reduces the interfacial tension. This provides kinetic stability to the system. Long term emulsion stability is achieved through electrostatic and/or steric mechanisms, depending on the surfactant and environmental conditions (McClements, 2005).

For solid particles, the wettability of the particle by either fluid phase affects the type of emulsion obtained, with the three-phase contact angle θ (measured through the aqueous phase) at the interface dictating whether oil-in-water (*O/W*) or water-in-oil (*W/O*) emulsions are generated. Particles can partition at planar and curved interfaces as depicted in Figure 1.4A. Particles with a hydrophilic character make contact at $\theta < 90°$ and therefore most of the particle surface is located in the aqueous phase resulting in the formation of *O/W* emulsions. In contrast, particles with a hydrophobic character make contact at $\theta > 90°$ and are consequently more suitable for stabilizing *W/O* emulsions. The same arguments can be used to describe the

mechanisms of stabilization operating in particle stabilized foams and aerosols, respectively (Binks, 2002).

One feature of solid particles at interfaces is the significant amount of energy required for particle desorption, which is typically much greater than k_BT. This implies that once particles are situated at the interface, they are essentially irreversibly anchored in this position. This high energy required for particle desorption, in addition to the dense film of particles assembled at the interface is the origin of the remarkable stability of Pickering emulsions against droplet coalescence. This is in contrast to more conventional surfactants which are in a state of 'dynamic equilibrium' meaning that they can readily adsorb and desorb from interfaces. The energy (E) required for particle detachment can be quantified according to;

$$E = \pi R^2 \gamma_{s_{\alpha\beta}} (1 \pm cos\theta)^2 \qquad [1.9]$$

: where γ_s is the surface tension (N m^{-1}) between the two immiscible fluids (α and β) and R is the particle radius (m). The plus or minus sign is used for removal of the particles into the oil or water phases, respectively. Equation 1.9 implies that particle adsorption is strongest for oil-water mixtures with the highest γ_s and for particles with larger radii. For a given oil-water mixture and particle size, E is at its maximum at θ = 90°. At the extremes of contact angle (e.g. θ = 0-20° or θ = 160-180°), the particles are poorly wetted by one of the fluid phases and thus do not adsorb efficiently at the interface (Binks, 2002). Particles can be functionalized post-synthesis to adjust their wettability or specifically designed to be amphiphilic (Nakahama et al., 2000). The former can be achieved simply by promoting some degree of particle aggregation, for example by inducing attractive interactions to charged colloids with the addition of salts (Frith et al., 2008).

The use of large (several μm) particles in fundamental studies on Pickering emulsions facilitates the determination of contact angle and/or the particle assembly at the interface by optical microscopy techniques (Binks, 2002). In this way, millimetre sized emulsion droplets with high stability against coalescence can be produced (Arditty et al., 2003). In practice, emulsions with submicron droplets are preferred, and consequently, the size of the stabilizing particles must be relatively (typically an order of magnitude) smaller. For the most part, stability is attributed to

the mechanical barrier provided by particles, which prevents the close approach of droplet interfaces during collisions.

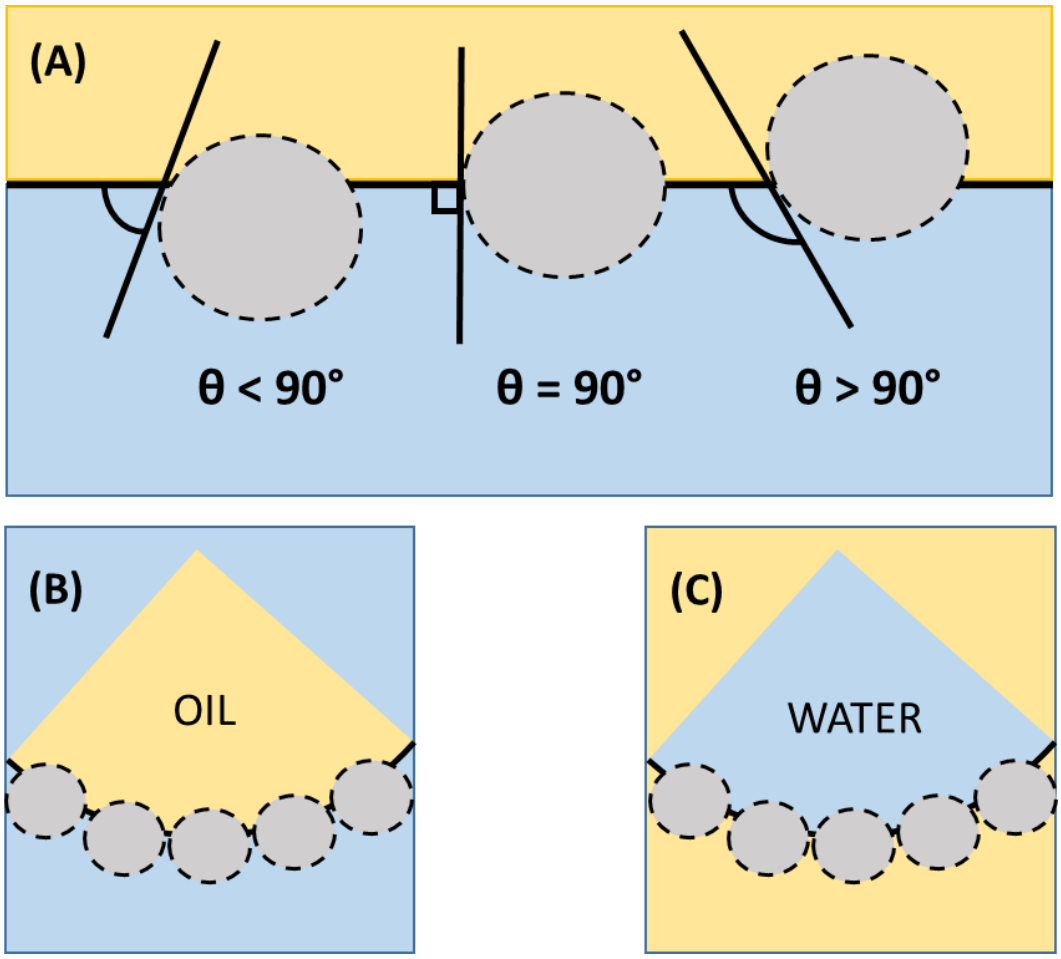

Figure 1.4 - The partitioning of spherical particles at (A) planar interfaces showing the contact angle (θ) measured through the aqueous phase. (B) and (C) show the partitioning of spherical particles at curved interfaces depicting the cross section of *O/W* and *W/O* emulsion droplets respectively.

Another feature of Pickering emulsions that is worth noting is so-called 'limited coalescence', which refers to the merging of droplets that are insufficiently coated by particles on the cessation of shear (*i.e.*, following emulsification) until they achieve a sufficient interfacial coverage to provide stability. The same phenomenon takes place in surfactant and polymer-stabilised emulsions but is usually too fast to observe analytically. Taking advantage of limited coalescence, particle stabilized emulsions with narrow droplet size distributions can be produced, resulting from the fact that only the smaller droplets with lower particle surface coverage are involved

in coalescence events (Arditty et al., 2003). Limited coalescence implies that the surface coverage needs to be high enough to prevent further droplet coarsening, but the formation of a 'complete' monolayer of adsorbed particles is not necessarily required for good stability in Pickering emulsions (Binks and Kirkland, 2002; Tarimala and Dai, 2004).

Whether emulsion droplets with high or low particle surface coverage (or in some cases, particle multilayers) are achieved likely depends on the particle-particle interactions (Deshmukh et al., 2015). Interestingly, with the presence of excess particles in the bulk, attractive interactions can result in the development of a continuous, space filling network of particles and droplets analogous to a colloidal gel. This enhances the stability of the emulsions (*e.g.*, to creaming and coalescence) due to droplet immobilization (Katepalli et al., 2017; Abend et al., 1998).

The stabilization of emulsions is also possible with soft particles (*i.e.*, microgels) of the types described above. Synthetic microgels have been used as model systems for such studies with the behaviour of microgels at interfaces being sufficiently different compared to solid colloidal particles that the resulting emulsions are sometimes separately referred to as 'Mickering*'* emulsions (Schmidt et al., 2011). Microgel particles often demonstrate core-shell type structures, which results from an inhomogeneous distribution of crosslinks across the particle radius, as depicted in Figure 1.5A and described in detail in **Chapter 2**.

Since the interfacial region of microgels is typically diffuse and poorly defined, so is the contact angle between a microgels 'surface' and the *O/W* interface. Furthermore, there is an abundance of experimental evidence demonstrating the deformation of soft particles following adsorption to fluid-fluid interfaces. To that end, microgel laden interfaces are best described by a polymer density profile rather than a contact angle (Dickinson, 2015). An inhomogeneous polymer density has been shown to promote adhesion between microgel stabilized emulsion droplets via particles that bridge relatively sparsely coated droplets (Destribats et al., 2012).

At a constant crosslinking density, the interfacial packing density depends on the particle size since smaller particles can pack more efficiently (Destribats et al., 2014). Through geometric considerations, the size distribution will also be important although synthetic microgels are typically monodisperse and thus polydispersity in particle size has received little attention. An increase in the particle concentration

usually results in the stabilization of smaller droplets (Destribats et al., 2014), as for hard-spheres (Arditty et al., 2003). The amount of energy used in the emulsification process has also been shown to affect the conformation and arrangement of microgels at the interface (Destribats et al., 2013).

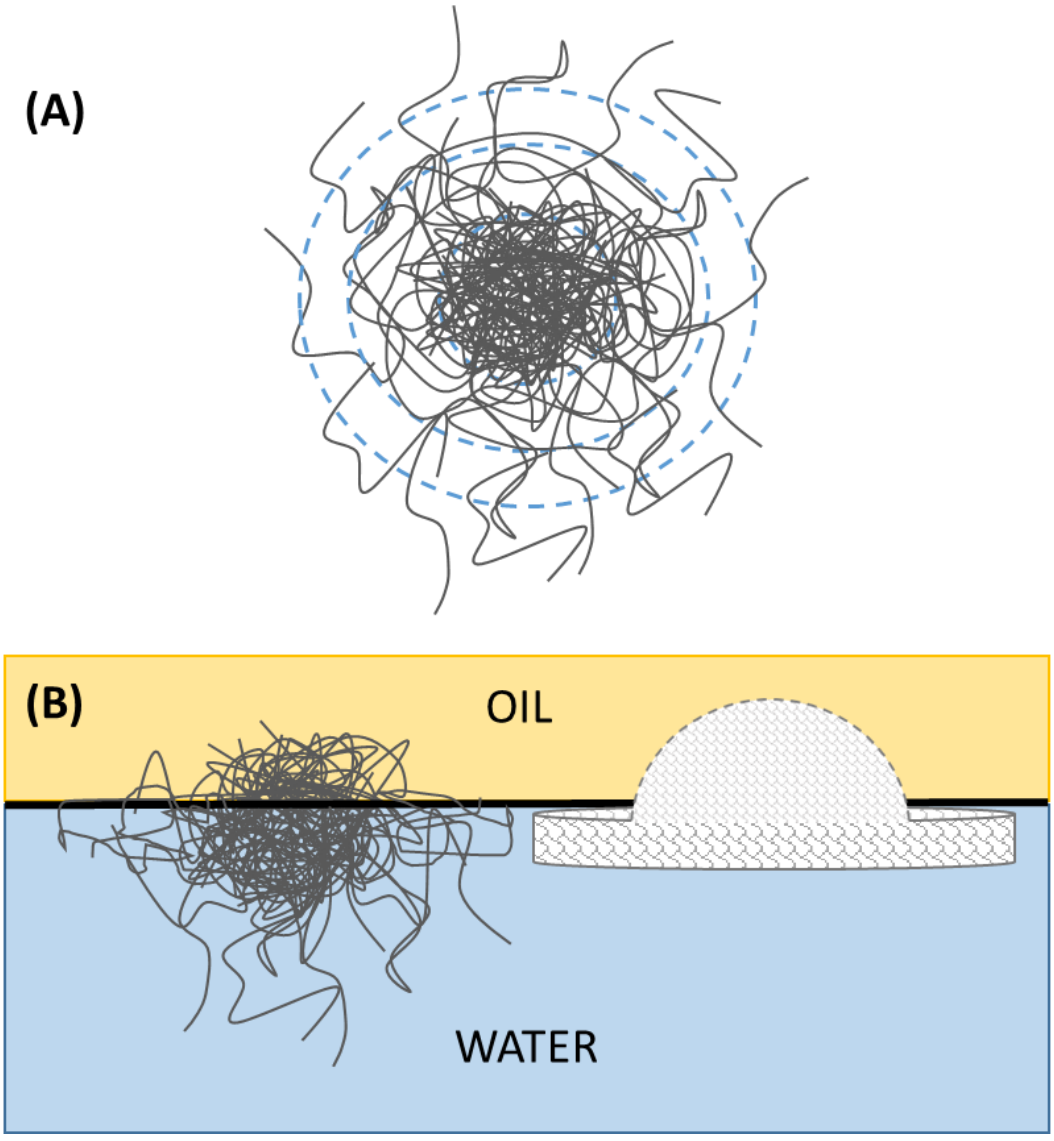

Figure 1.5 - (A) Schematic of a microgel particle with an inhomogeneous crosslinking density and a diffuse interfacial region. (B) The deformation of a microgel assembled at the *O/W* interface showing the stretching of the polymer network (left) and simplified schematic showing the typical 'fried egg' like morphology (right) of adsorbed microgels.

The deformation and subsequent structural rearrangement following adsorption at interfaces is related to the mechanical properties of the microgel particles which

furthermore depends on the density and distribution of internal crosslinks. Deformation of microgels at interfaces has been inferred from surface tension measurements at the air-water (Zhang and Pelton, 1999) and *O/W* interface (Wu et al., 2014). For example, the reduction in interfacial tension was found to be fastest for microgels with a lower crosslinking density, suggesting stretching at the interface (Wu et al., 2014). The same study showed that microgels adsorb to *O/W* interfaces without a significant energy barrier. This contrasts with the adsorption behaviour observed in solid particle systems and is thought to result from the more polymeric character of the particles (Li et al., 2015; Wu et al., 2014).

Interfacial deformation has been observed directly by electron microscopy techniques (Schmidt et al., 2011; Brugger et al., 2010) where microgels have been shown to adopt a 'fried-egg' like morphology (see Figure 1.5) due to their core-shell structure (Destribats et al., 2011). For softer microgels, polymer molecules within the shell region can overlap and interpenetrate resulting in the generation of 2D networks of assembled particles. This has been shown to increase the interfacial elasticity, which appears to be correlated with long-term emulsion stability. In contrast, interfaces decorated with densely crosslinked microgels are brittle and the resulting emulsions are relatively less stable (Brugger et al., 2010). Li et al., (2015) co-polymerized styrene and *NIPAM* in different ratios to obtain hard and soft particles. The particles were of similar charge and size, but the emulsions stabilized by soft particles demonstrated higher interfacial elasticities due to interpenetration. The same authors showed that soft particles were the most efficient stabilizers since more oil could be incorporated into the emulsions, which were stable for longer periods of time (Li et al., 2015). Besides the potential for interpenetration, particle-particle interactions in adsorbed microgel layers are generally not well understood (Deshmukh et al., 2015).

There is a lack of biocompatible particles suitable for the stabilization of food grade Pickering emulsions and foams. Some 'Pickering-like' particles are present naturally in foodstuffs or are generated during processing. For example, edible foams such as whipped cream contain air bubbles stabilized by partially coalesced, semi crystalline oil droplets. Naturally occurring 'particles' such as casein micelles, (hydrated) starch granules and polyphenol crystals require extraction and/or functionalization to improve their surface activity. The potential for (i) enhanced emulsion stability and (ii) the replacement of synthetic surfactants (*e.g.*, polysorbates, *PGPR*) has prompted

researchers to design suitable particles from edible materials (Dickinson, 2015; Tavernier et al., 2016). One such class of particles are biopolymer microgels which are typically composed of proteins, and thus inherently surface active. Surface active polysaccharides such as certain pectins have also been used to prepare microgels that were subsequently used to stabilize emulsions. To what extent the constituent (surface active) polymers in biopolymer microgels rearrange on adsorption at fluid-fluid interfaces is not well understood but some authors have already noted similarities in microgel deformation at the interface and the structural rearrangements known to occur in protein stabilized emulsions (Dickinson, 2015). In **Chapter 5**, *SBP* microgels were used to stabilize *O/W* emulsions at oil volume fractions of up to 40%. Their properties were compared to non-crosslinked (*i.e.*, native) *SBP* throughout. In addition, the findings were compared to similar microgel (*i.e.*, synthetic and biopolymeric) stabilized emulsions reported on in the literature.

1.4 References

Abend, S., Bonnke, N., Gutschner, U. and Lagaly, G. 1998. Stabilization of emulsions by heterocoagulation of clay minerals and layered double hydroxides. Colloid and Polymer Science. 276(8), pp.730-737.

Adams, S., Frith, W.J. and Stokes, J.R. 2004. Influence of particle modulus on the rheological properties of agar microgel suspensions. Journal of Rheology. 48, pp.1195-1213.

Almdal, K., Dyre, J., Hvidt, S. and Kramer, O. 1993. Towards a phenomenological definition of the term 'gel'. Polymer Gels and Networks. 1(1), pp.5-17.

Arditty, S., Whitby, C.P., Binks, B.P., Schmitt, V. and Leal-Calderon, F. 2003. Some general features of limited coalescence in solid-stabilized emulsions. The European Physical Journal E. 11(3), pp.273-281.

Azarikia, F., Wu, B., Abbasi, S. and McClements, D.J. 2015. Stabilization of biopolymer microgels formed by electrostatic complexation: Influence of enzyme (laccase) cross-linking on pH, thermal, and mechanical stability. Food Research International. 78, pp.18-26.

Bai, L., Huan, S., Li, Z. and McClements, D.J. 2017. Comparison of emulsifying properties of food-grade polysaccharides in oil-in-water emulsions: Gum arabic, beet pectin, and corn fiber gum. Food Hydrocolloids. 66, pp.144-153.

Binks, B. 2002. Particles as surfactants—similarities and differences. Current Opinion in Colloid & Interface Science. 7(1), pp.21-41.

Binks, B. and Kirkland, M. 2002. Interfacial structure of solid-stabilised emulsions studied by scanning electron microscopy. Physical Chemistry Chemical Physics. 4(15), pp.3727-3733.

Briscoe, W. 2010. Surface Forces. In: Cosgrove, T. ed. Colloid Science: Principles, Methods and Applications. 2nd ed. UK: Wiley.

Brown, E. and Jaeger, H.M. 2014. Shear thickening in concentrated suspensions: phenomenology, mechanisms and relations to jamming. Reports on Progress in Physics. 77(4), p046602.

Brugger, B., Vermant, J. and Richtering, W. 2010. Interfacial layers of stimuli-responsive poly-(N-isopropylacrylamide-co-methacrylicacid) (PNIPAM-co-MAA)

microgels characterized by interfacial rheology and compression isotherms. Physical Chemistry Chemical Physics. 12(43), pp.14573-14578.

Cheng, Z., Zhu, J., Chaikin, P.M., Phan, S.-E. and Russel, W.B. 2002. Nature of the divergence in low shear viscosity of colloidal hard-sphere dispersions. Physical Review E. 65(4), p041405.

Clark, A. and Ross-Murphy, S. 2009. Biopolymer Network Assembly: Measurement and Theory. In: Kasapis, S., et al. eds. Modern Biopolymer Science. USA: Academic Press, pp.1-27.

Daniel, C., Dammer, C. and Guenet, J.-M. 1994. On the definition of thermoreversible gels: the case of syndiotactic polystyrene. Polymer. 35(19), pp.4243-4246.

Deshmukh, O.S., van den Ende, D., Stuart, M.C., Mugele, F. and Duits, M.H.G. 2015. Hard and soft colloids at fluid interfaces: Adsorption, interactions, assembly & rheology. Advances in Colloid and Interface Science. 222, pp.215-227.

Destribats, M., Eyharts, M., Lapeyre, V., Sellier, E., Varga, I., Ravaine, V. and Schmitt, V. 2014. Impact of pNIPAM Microgel Size on Its Ability To Stabilize Pickering Emulsions. Langmuir. 30(7), pp.1768-1777.

Destribats, M., Lapeyre, V., Sellier, E., Leal-Calderon, F., Ravaine, V. and Schmitt, V. 2012. Origin and Control of Adhesion between Emulsion Drops Stabilized by Thermally Sensitive Soft Colloidal Particles. Langmuir. 28(8), pp.3744-3755.

Destribats, M., Lapeyre, V., Wolfs, M., Sellier, E., Leal-Calderon, F., Ravaine, V. and Schmitt, V. 2011. Soft microgels as Pickering emulsion stabilisers: role of particle deformability. Soft Matter. 7(17), pp.7689-7698.

Destribats, M., Wolfs, M., Pinaud, F., Lapeyre, V., Sellier, E., Schmitt, V. and Ravaine, V. 2013. Pickering Emulsions Stabilized by Soft Microgels: Influence of the Emulsification Process on Particle Interfacial Organization and Emulsion Properties. Langmuir. 29(40), pp.12367-12374.

Dickinson, E. 2015. Microgels — An alternative colloidal ingredient for stabilization of food emulsions. Trends in Food Science & Technology. 43(2), pp.178-188.

Djabourov, M., Nishinari, K. and Ross-Murphy, S.B. 2013. Physical Gels from Biological and Synthetic Polymers. Cambridge: Cambridge University Press.

Everett, D.H. 1988. Basic Principles of Colloid Science. London: Royal Society of Chemistry.

Feng, X., Pelton, R., Leduc, M. and Champ, S. 2007. Colloidal Complexes from Poly(vinyl amine) and Carboxymethyl Cellulose Mixtures. Langmuir. 23(6), pp.2970-2976.

Frith, W.J., Pichot, R., Kirkland, M. and Wolf, B. 2008. Formation, Stability, and Rheology of Particle Stabilized Emulsions: Influence of Multivalent Cations. Industrial & Engineering Chemistry Research. 47(17), pp.6434-6444.

Griffin, J.M., Robb, I. and Bismarck, A. 2007. Preparation and characterization of surfactant-free stimuli-sensitive microgel dispersions. Journal of Applied Polymer Science. 104(3), pp.1912-1919.

Hermans, P. 1949. Gels. In: Kruyt, H. ed. Colloid Science. 2nd ed. New York: Elsevier.

Hunter, G. and Weeks, E. 2012. The physics of the colloidal glass transition. Reports on Progress in Physics. 75(6), p066501.

Hunter, R. 2001. Foundations of Colloid Science. 2nd ed. New York: Oxford University Press.

Israelachvili, J. 2011. Intermolecular and Surface Forces. 3rd ed. USA: Academic Press.

Katepalli, H., John, V.T., Tripathi, A. and Bose, A. 2017. Microstructure and rheology of particle stabilized emulsions: Effects of particle shape and inter-particle interactions. Journal of Colloid and Interface Science. 485, pp.11-17.

Kim, J.-W., Utada, A.S., Fernández-Nieves, A., Hu, Z. and Weitz, D.A. 2007. Fabrication of Monodisperse Gel Shells and Functional Microgels in Microfluidic Devices. Angewandte Chemie International Edition. 46(11), pp.1819-1822.

Le Grand, A. and Petekidis, G. 2008. Effects of particle softness on the rheology and yielding of colloidal glasses. Rheologica Acta. 47(5), pp.579-590.

Lekkerkerker, H. and Tuinier, R. 2011. Depletion interaction. Colloids and the depletion interaction. Dordrecht: Springer, pp.57-108.

Li, Z., Harbottle, D., Pensini, E., Ngai, T., Richtering, W. and Xu, Z. 2015. Fundamental Study of Emulsions Stabilized by Soft and Rigid Particles. Langmuir. 31(23), pp.6282-6288.

Littoz, F. and McClements, D.J. 2008. Bio-mimetic approach to improving emulsion stability: Cross-linking adsorbed beet pectin layers using laccase. Food Hydrocolloids. 22(7), pp.1203-1211.

Lyon, L.A. and Fernandez-Nieves, A. 2012. The Polymer/Colloid Duality of Microgel Suspensions. Annual Review of Physical Chemistry. 63(1), pp.25-43.

Maroziene, A. and de Kruif, C.G. 2000. Interaction of pectin and casein micelles. Food Hydrocolloids. 14(4), pp.391-394.

May, C.D. 1990. Industrial pectins: Sources, production and applications. Carbohydrate Polymers. 12(1), pp.79-99.

McClements, D.J. 2005. Food Emulsions: Principles, Practices, and Techniques. 2nd ed. USA: CRC Press.

Mewis, J., Frith, W.J., Strivens, T.A. and Russel, W.B. 1989. The rheology of suspensions containing polymerically stabilized particles. AIChE Journal. 35(3), pp.415-422.

Mewis, J. and Wagner, N.J. 2012. Colloidal Suspension Rheology. New York: Cambridge University Press.

Nakahama, K., Kawaguchi, H. and Fujimoto, K. 2000. A Novel Preparation of Nonsymmetrical Microspheres Using the Langmuir−Blodgett Technique. Langmuir. 16.

Ngouémazong, E.D., Christiaens, S., Shpigelman, A., Van Loey, A. and Hendrickx, M. 2015. The Emulsifying and Emulsion-Stabilizing Properties of Pectin: A Review. Comprehensive Reviews in Food Science and Food Safety. 14(6), pp.705-718.

Nishinari, K. 2009. Some Thoughts on The Definition of a Gel. In: Tokita, M. and Nishinari, K. eds. Gels: Structures, Properties, and Functions. Berlin: Springer, pp.87-94.

Paques, J.P., Sagis, L.M.C., van Rijn, C.J.M. and van der Linden, E. 2014. Nanospheres of alginate prepared through w/o emulsification and internal gelation with nanoparticles of CaCO3. Food Hydrocolloids. 40, pp.182-188.

Pelton, R. 2000. Temperature-sensitive aqueous microgels. Advances in Colloid and Interface Science. 85(1), pp.1-33.

Pelton, R.H. and Chibante, P. 1986. Preparation of aqueous latices with N-isopropylacrylamide. Colloids and Surfaces. 20(3), pp.247-256.

Pickering, S.U. 1907. CXCVI.—Emulsions. Journal of the Chemical Society, Transactions. 91(0), pp.2001-2021.

Pusey, P.N. and van Megen, W. 1986. Phase behaviour of concentrated suspensions of nearly hard colloidal spheres. Nature. 320(6060), pp.340-342.

Pusey, P.N., Zaccarelli, E., Valeriani, C., Sanz, E., Poon, W.C.K. and Cates, M.E. 2009. Hard spheres: crystallization and glass formation. Philosophical Transactions of the Royal Society A: Mathematical, Physical and Engineering Sciences. 367(1909), pp.4993-5011.

Royall, C.P., Poon, W.C.K. and Weeks, E.R. 2013. In search of colloidal hard spheres. Soft Matter. 9(1), pp.17-27.

Saha, D. and Bhattacharya, S. 2010. Hydrocolloids as thickening and gelling agents in food: a critical review. Journal of Food Science and Technology. 47(6), pp.587-597.

Schmidt, S., Liu, T., Rütten, S., Phan, K.-H., Möller, M. and Richtering, W. 2011. Influence of Microgel Architecture and Oil Polarity on Stabilization of Emulsions by Stimuli-Sensitive Core–Shell Poly(N-isopropylacrylamide-co-methacrylic acid) Microgels: Mickering versus Pickering Behavior? Langmuir. 27(16), pp.9801-9806.

Schöpe, H.J., Bryant, G. and van Megen, W. 2007. Effect of polydispersity on the crystallization kinetics of suspensions of colloidal hard spheres when approaching the glass transition. The Journal of Chemical Physics. 127(8), p084505.

Seth, J.R., Cloitre, M. and Bonnecaze, R.T. 2006. Elastic properties of soft particle pastes. Journal of Rheology. 50(3), pp.353-376.

Staudinger, H. and Husemann, E. 1935. Über hochpolymere Verbindungen, 116. Mitteil.: Über das begrenzt quellbare Poly-styrol. Berichte der deutschen chemischen Gesellschaft (A and B Series). 68(8), pp.1618-1634.

Tadros, T. 2010. Rheology of Dispersions: Principles and Applications. Weinheim: Wiley.

Tarimala, S. and Dai, L.L. 2004. Structure of Microparticles in Solid-Stabilized Emulsions. Langmuir. 20(9), pp.3492-3494.

Tavernier, I., Wijaya, W., Van der Meeren, P., Dewettinck, K. and Patel, A.R. 2016. Food-grade particles for emulsion stabilization. Trends in Food Science & Technology. 50, pp.159-174.

Thakur, B.R., Singh, R.K., Handa, A.K. and Rao, M.A. 1997. Chemistry and uses of pectin — A review. Critical Reviews in Food Science and Nutrition. 37(1), pp.47-73.

van der Vaart, K., Rahmani, Y., Zargar, R., Hu, Z., Bonn, D. and Schall, P. 2013. Rheology of concentrated soft and hard-sphere suspensions. Journal of Rheology. 57(4), pp.1195-1209.

Vlassopoulos, D. and Cloitre, M. 2014. Tunable rheology of dense soft deformable colloids. Current Opinion in Colloid & Interface Science. 19(6), pp.561-574.

Weeks, E.R. and Weitz, D.A. 2002. Subdiffusion and the cage effect studied near the colloidal glass transition. Chemical Physics. 284(1), pp.361-367.

Wu, Y., Wiese, S., Balaceanu, A., Richtering, W. and Pich, A. 2014. Behavior of Temperature-Responsive Copolymer Microgels at the Oil/Water Interface. Langmuir. 30(26), pp.7660-7669.

Zaccarelli, E., Valeriani, C., Sanz, E., Poon, W.C.K., Cates, M.E. and Pusey, P.N. 2009. Crystallization of Hard-Sphere Glasses. Physical Review Letters. 103(13), p135704.

Zhang, J. and Pelton, R. 1999. The dynamic behavior of poly(N-isopropylacrylamide) at the air/water interface. Colloids and Surfaces A: Physicochemical and Engineering Aspects. 156(1), pp.111-122.

Chapter 2: Synthesis, Characterization and Rheological Properties of Poly(N-isopropylacrylamide) Microgel Suspensions *

Summary

The synthesis of poly(N-isopropylacrylamide) (*p(NIPAM)*) microgel suspensions is reported with a focus on scaling up the reaction volumes used and improving the yield of product. The particle size and surface charge density of microgels differing in their crosslinking density was investigated as a function of temperature using photon correlation spectroscopy (*PCS*) and laser Doppler micro-electrophoresis respectively. The influence of ionic strength and pH on the stability of microgels was investigated with *PCS*. Dispersing *p(NIPAM)* microgels in potassium chloride solutions ≥10 mM or water at pH 3 caused destabilisation above the volume phase transition temperature (~32°C). For a microgel sample of intermediate crosslinking density, the effective volume fraction (Φ_{eff}) was estimated through the relationship between the relative viscosity and polymer concentration using a modified form of the Einstein-Batchelor equation. Measurements were performed using capillary viscometry on swollen and de-swollen microgels. At the same polymer concentration and therefore particle number, swollen microgels occupy a larger Φ_{eff} and therefore demonstrate higher relative viscosities. Freeze dried microgels could be efficiently re-dispersed in water with negligible hysteresis in the particle size distributions. Using freeze dried microgel powders enabled the preparation of suspensions over a wide range in Φ_{eff} which facilitated a detailed study into the rheological properties of concentrated suspensions. The shear rate dependence of the viscosity for swollen microgels was investigated as a function of Φ_{eff} using shear rheometry. It was shown that the microgel particles could be concentrated to higher Φ_{eff} than the theoretical limit of random close packing for monodisperse hard spheres.

** As mentioned in **Chapter 1**, this chapter is based on unpublished work but is presented in the form of a research article for consistency throughout the document.*

2.1 Introduction

Microgel particles were previously defined as particulate, crosslinked polymer networks typically of colloidal dimensions (Pelton, 2000). The most well documented approach to fabricate synthetic microgels is directly from reactive (monofunctional) monomer species in chain growth polymerisations. In most cases, the inclusion of a relatively smaller amount of polyfunctional co-monomer is necessary to permit the formation of crosslinks. To avoid the formation of macrogel, different variations of heterogeneous polymerisation (*e.g.*, emulsion polymerisation, precipitation polymerisation) techniques are used. Consequently, the reaction conditions can be elegantly tailored to give rise to microgel particles which differ in their material properties, for example, the particle size and particle size distribution can be tightly regulated (Sanson and Rieger, 2010). Considering synthetic microgels as model soft colloids, the molar ratio of crosslinking monomer relative to the main monomeric species influences the elasticity of the resulting microgel particles (Aufderhorst-Roberts et al., 2018; Wyss et al., 2010).

A major reason for the widespread interest in microgel systems stems from their stimuli responsive behaviour. Depending on the chemistry of the monomeric sub-units, microgels can adjust their shape and volume in response to variations in the environmental conditions, the extent of which is largely controlled by the crosslinking density. Irrespective of the stimulus, the responsive behaviour of microgels arises due to the balance between attractive and repulsive polymer-polymer and polymer-solvent interactions. Microgel particles swell in good solvents and de-swell (therefore expelling solvent) due to a reduction in the solvent quality in a phenomenon known as a volume phase transition (*VPT*) (Saunders and Vincent, 1999). The conformational changes at the *VPT* originate from the entropy gain associated with minimising polymer-solvent contacts and are accompanied by changes in other physiochemical properties of the microgel for example in their mechanical (Hashmi and Dufresne, 2009) and optical properties (Gao and Hu, 2002) and surface charge density (Daly and Saunders, 2000b). Fascinatingly, such behaviour is reversible on removal of the stimulus.

Microgels incorporating ionic monomers can be viewed as polyelectrolytes which demonstrate responsiveness to the pH and ionic strength of the solvent. The most intensively studied ionic microgel systems contain acrylate monomers (*e.g.*,

(meth)acrylic acid) (Borrega et al., 1999). The inclusion of more exotic (co-)monomers extends the range of environmental stimuli able to induce a *VPT* in microgels. For example, systems which respond to; electrochemical stimuli (Zhang et al., 2014), glucose (Hoare and Pelton, 2008) and/or other monosaccharides (Ancla et al., 2011) and light (Phua et al., 2016) have been synthesised.

Most studies in the literature are based on thermally responsive microgel particles such as poly(N-isopropylacrylamide) (*p(NIPAM)*) which are composed of the vinyl monomer *NIPAM* and a crosslinking co-monomer, typically N,N''-Methylenebisacrylamide (*MBA*). Linear *p(NIPAM)* molecules demonstrate a lower critical solution temperature (*LCST*) which corresponds to the temperature at which the oligomer or polymer molecules undergo a coil-globule transition (Winnik, 1990). The volume phase transition temperature (*VPTT*) for crosslinked polymer networks (*e.g.,* bulk gels and microgels) is the analogue of the *LCST* and occurs around the same temperature (*T*) ($T \sim 32$ °C). Below this temperature, the microgel networks are swollen due to hydrogen bonding between water molecules and the amide groups of *NIPAM* and the cage-like structuring of water molecules around the isopropyl groups. Above this temperature, molecular vibrations disrupt the polymer-solvent interactions and the hydrophobic interaction between alkyl groups becomes dominant. In combination, these factors lead to the dehydration of polymer chains and concomitant collapse of the polymer network (Pelton, 2000; Saunders and Vincent, 1999).

The suitability of a co-monomer for a given polymerisation depends on its reactivity and stereochemistry relative to the main monomeric species. Despite being used in relatively lower quantities, *MBA* is consumed more rapidly than *NIPAM* due to its higher reactivity. Therefore, with the batch addition of monomers, the microgel crosslinking density is expected to be greatest in the innermost section of the particle network (Wu et al., 1994). Kinetic modelling studies were originally used to confirm this hypothesis for a variety of different monomers (Hoare and McLean, 2006). Direct structural information on *p(NIPAM)* microgels prepared using a batch addition of monomers has been obtained from neutron scattering experiments (Fernández-Barbero et al., 2002; Saunders, 2004; Stieger et al., 2004b; Kratz et al., 2001). Above the *VPTT*, the scattering wave vector (*q*) dependence on the scattered neutron intensity suggests that de-swollen microgels have a 'smooth' interfacial region and a homogeneous internal polymer density. For swollen microgels

(*T<VPTT*), structural inhomogeneities within particles resulted in different power law dependences of *q* (Fernández-Barbero et al., 2002). The polymer density was found to decrease radially with distance from the centre of the microgel particle due to a progressive decrease in crosslinking density (*i.e.*, due to the premature consumption of crosslinking co-monomer). At the periphery of the microgel network, the crosslink density is very low so that polymer chains protrude from the particle 'surface' (Stieger et al., 2004b). This led authors to describe a type of 'core-shell' structure for swollen *p(NIPAM)* microgels prepared using a batch addition of monomers. Microgel crosslinking can be made more homogeneous with modifications to the synthesis conditions, for example using the semi batch addition of (co-)monomers or by utilising different crosslinking chemistry (Sanson and Rieger, 2010).

The expected structure of *p(NIPAM)* microgel particles synthesized in this study shown schematically in Figure 2.1 for *T<VPTT* and *T>VPTT*. For swollen microgels, there is no well-defined interface and in inhomogeneous polymer density throughout. The use of common free radical initiators such as persulphates leads to the presence of negatively charged initiator fragments attached to the polymer chain ends which tend to accumulate in the interfacial region of microgel particles (Utashiro et al., 2017; Daly and Saunders, 2000b). The 'softness' of microgel particles can therefore be appreciated with respect to the particle-particle interactions, in addition to the particle elasticity.

The softness of microgel particles will consequently affect their functionality. Numerous applications have been suggested for synthetic microgel systems in the scientific literature. Whilst not an exhaustive list, some interesting suggestions are; in the removal of heavy metal ions (Morris et al., 1997) and organic dyes (Parasuraman et al., 2012) from contaminated water, the removal of water from biodiesel (Nur et al., 2009) and in the preparation of stimuli responsive Pickering emulsions (Schmidt et al., 2011). Owing to the great control available over the physiochemical properties of microgels on synthesis and their stimuli responsiveness which enables facile control of the particle (effective) volume fraction (ϕ_{eff}), microgels have been used to address fundamental colloidal physics problems in studies on crystallisation (Lyon et al., 2004) and the glass transition (Mattsson et al., 2009). A contemporary application of non-aqueous microgels is in the rheology modification of paints and coatings where they have been shown to

provide benefits during application and in the performance of the dried films (Murray and Snowden, 1995). Similarly, Carbopol® (Lubrizol) and Sepimax Zen™ (Seppic) are examples of commercially available, aqueous polyacrylate microgels which can be used as rheology modifiers in cosmetic products such as skin creams and lotions (Anon, 2022a; Anon, 2022b).

In this study, we report on the synthesis and characterisation of *p(NIPAM)* microgels which differ in their crosslinking density. The stability of microgels towards the environmental ionic strength and pH was assessed at temperatures below and above the *VPTT*. For microgels of intermediate crosslinking density, the ϕ_{eff} was estimated at 'infinite dilution' for swollen and de-swollen microgels respectively. For the former, the shear rate dependent viscosity was investigated as a function of ϕ_{eff}.

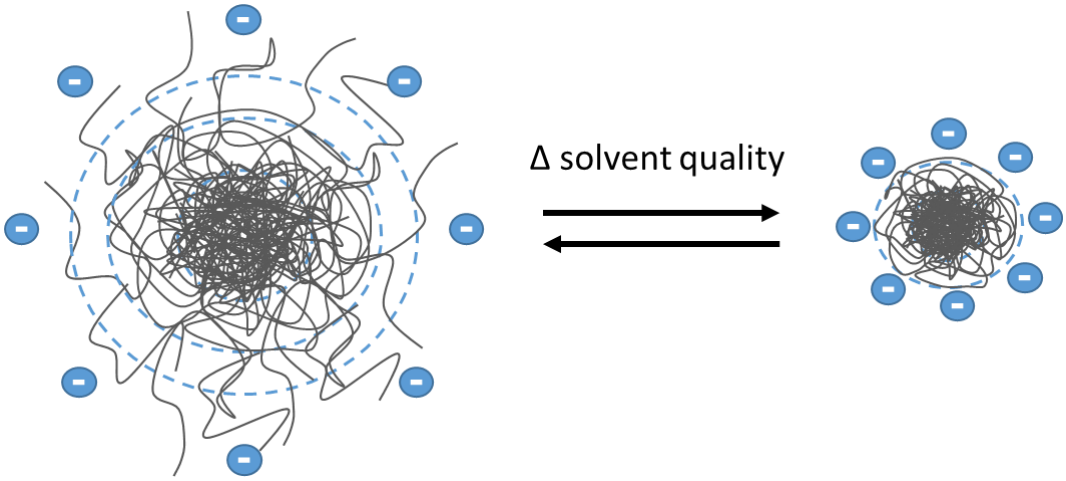

Figure 2.1 - The expected structure of *p(NIPAM)* microgels prepared by free radical polymerization using the batch addition of monomers and an anionic initiator. Structure at *T<VPTT* (left) and *T>VPTT* (right).

2.2 Materials and Methods

2.2.1 Materials

N-isopropylacrylamide (*NIPAM*) (≥99%), N,N'methylenebisacrylamide (*MBA*) (≥99.5%), sodium dodecyl sulphate (*SDS*) (≥99%), potassium peroxodisulfate (*KPS*) (99.99% trace metals basis) and potassium chloride (KCl) (99%) were purchased from Sigma-Aldrich (Dorset, UK) and used as received. Glucose monohydrate was purchased from Alfa Aesar (Lancashire, UK). The water used for polymer synthesis and characterisation was Type-1 ultrapure water (Millipore, Bedford, UK). Type-2 deionised water was used for microgel purification via dialysis.

2.2.2 Methods

2.2.2.1 Microgel synthesis

The protocol for microgel synthesis was based on one previously described (Senff and Richtering, 2000). In attempts to improve the yield of microgel dispersions, the quantities of reagents used in synthesis were varied between batches. In all cases, the conditions of the reaction (*viz.*, stirrer speed, temperature, duration) remained constant.

The experimental protocol used for microgel synthesis is as follows; *NIPAM*, *MBA* and *SDS* were accurately weighed and dissolved in type 1 water under manual stirring before being transferred to a three-necked round bottom flask. The aqueous monomer solution was pre-heated in a paraffin oil bath under reflux conditions and magnetic stirring. The temperature (75 °C) and stirrer speed (250 RPM) were controlled with a digital stirrer plate equipped with an external thermostat probe (IKA, Oxford, UK). High vacuum silicon grease and rubber septa were used to create a sealed environment. Separately, the initiator solution was prepared by manually dissolving *KPS* in a relatively smaller amount of type 1 water. Following its transferral into a suitable round bottom flask, the initiator solution (ambient temperature) and preheated monomer solutions were degassed with nitrogen for at least 30 minutes. The initiator solution was subsequently added dropwise to the preheated monomer solution with a glass syringe. Polymerisation ran for a duration of 4 hours under a nitrogen blanket. The microgel dispersions were allowed to cool slightly under mild magnetic stirring and subsequently filtered through glass wool to remove any coagulum formed during the reaction. The resulting suspensions were dialyzed (dialysis tubing pore size 8 – 10 kDa) against pure water for two weeks

with daily water changes. Typically, the conductivity of microgel dispersions following dialysis was ≤ 15 μs cm^{-1}. Dialysis was necessary to remove low molecular weight contaminants, residual surfactant and any unreacted monomer or initiator molecules before further use.

2.2.2.2 Photon correlation spectroscopy

The instrument used in this study was a Zetasizer Nano ZS (Malvern Instruments, Worcestershire, UK) equipped with a He-Ne laser (λ = 633 nm). Temperature sweeps were performed to study the variation of microgel particle size associated with the thermally induced *VPT*. Measurements were performed in non-invasive backscatter mode (scattering angle, θ = 174°) in the range 20 – 40 °C increasing in 1 °C increments. An equilibration time of 240 seconds elapsed between measurements at different temperatures. Reported values of hydrodynamic diameter are based on the average of 3 individual measurements each of which was computed in the software based on a 50 second measurement duration (5 x 10 s measurements). Hence, 150 seconds of scattering data was collected at each temperature and the translational diffusion coefficient, D (m^2 s^{-1}) was subsequently used to calculate the hydrodynamic radius, R_H (m) based on the Stokes-Einstein relation (Pecora, 2008);

$$D = \frac{k_B T}{6\pi\eta R_H} \qquad [2.1]$$

Where k_B is the Boltzmann constant (1.381 x10^{-23} J K^{-1}), T is the absolute temperature (°K) and η the viscosity of the solvent (Pa s).

2.2.2.3 Laser doppler micro electrophoresis (*LDME*)

LDME monitors the velocity of a charged particle under the influence of an external electrical field (*i.e.*, the electrophoretic velocity). The charged particle moves in the direction of an electrode with opposite sign to the surface charge and the velocity is measured with phase analysis light scattering. The frequency shift (Δf) of scattered light due to particle motion in the electrical field is given by;

$$\Delta f = \frac{2v.\sin\left(\frac{\theta}{2}\right)}{\lambda} \qquad [2.2]$$

Where v is the particle velocity (m s^{-1}), λ is the wavelength of the laser (m) and θ is the scattering angle (rad). Monitoring Δf over time allows the determination of the phase shift (Tscharnuter, 2001; Malvern, 2010). Subsequent analysis of the phase shift signal at the 'beat' frequency compared to a reference frequency allows

detection of small phase differences which, when averaged over time, gives information on the electrophoretic mobility of the particle (Malvern, 2010). Electrophoretic velocity (v_e) is related to the electrophoretic mobility (u_e) through the magnitude of the electric field strength, E (V m^{-1}) (Delgado et al., 2007).

$$v_e = u_e E \qquad [2.3]$$

The zeta potential can subsequently be determined with the Henry equation;

$$u_e = \frac{2\varepsilon\xi f(k_D R)}{3\eta} \qquad [2.4]$$

Where ε is the relative permittivity, ξ the zeta potential (V) and η is the viscosity of the solvent (Pa s). The term $f(k_D R)$, where R is the particle radius (m) and k_D is the reciprocal of the Debye length (m^{-1}) is approximated to equal 1 for small particles immersed in low ε media (Huckel approximation) and 1.5 for larger particles (> 0.2 µm) dispersed in more concentrated electrolyte solution (Smoluchowski approximation) (Tscharnuter, 2001; Malvern, 2009).

Zeta potential in this study was determined using the Zetasizer Nano ZS (Malvern Instruments, Worcestershire, UK). Poly(*NIPAM*) microgel particles were dispersed in water at a concentration of 0.005 wt.% and transferred into folded capillary cells (*DTS1070*) with a disposable syringe. The measurement duration was set to automatic and measurements were performed in the range 20-40 °C. Each reported value of zeta potential is based on the average of three measurements computed in the software using the Smoluchowski equation.

2.2.2.4 Calculating yield of microgel suspensions

The yield of microgel synthesis is reported in terms of polymer concentration (wt. %) which is calculated based on the wet and dry weight of purified dispersions. Aliquots (2 ml) of suspensions were transferred into small volume sample vials and solvent (water) was removed by evaporation in a vacuum oven until no further change in mass was observed. The polymer concentration is calculated according to the following equation;

$$Microgel\ Yield = \frac{Dry\ weight\ dispersion\ (g)}{Wet\ weight\ dispersion\ (g)} \times 100 \qquad [2.5]$$

2.2.2.5 Capillary viscometry

The capillary viscometry experiments were conducted in a thermostated water bath. An Ostwald-type U-tube viscometer was used (Reservoir size A, calibration constant, K = 0.003 $mm^2\ s^{-2}$). The temperature was kept constant to ± 0.1 °C as monitored with a digital thermometer (Comark 2001, Norfolk, UK). The efflux time (*i.e.*, the time required for a known volume of fluid to flow under hydrostatic pressure through a capillary between two specified markers) was measured manually using a digital stopwatch with millisecond resolution. The efflux time can be used to determine the kinematic viscosity (v) of a sample according to the following equations (Wilke et al., 2015; Mezger, 2014);

$$v = \frac{\pi {R_{cap}}^4 g h_m}{8LV} t \qquad [2.6]$$

Where R_{cap} is the capillary radii (m), g is the gravitational acceleration constant (m s^{-2}), h_m is the average hydrostatic pressure height (m), L is the length of the capillary (m), V is the sample volume (m^3) and t is the efflux time (s). Besides the efflux time, Equation 2.6 contains only constants and geometrical data which are accounted for in the capillary calibration constant, K such that;

$$v = Kt \qquad [2.7]$$

Hence, the units of kinematic viscosity, v, are $mm^2\ s^{-1}$. Kinematic viscosity is related to the dynamic viscosity, η (Pa s) through the fluid density, ρ (kg m^{-3}) by;

$$v = \frac{\eta}{\rho} \qquad [2.8]$$

In this study, the efflux times of a series of dilute microgel dispersions were compared to the efflux time of the pure solvent (water) measured in the same viscometer to give the relative viscosity (η_{rel}). The density of water and the microgel dispersions were determined ultrasonically with a densitometer (Anton Paar DMA 4500M, Anton Paar GmbH, Graz, Austria) to give the relative dynamic viscosity;

$$\eta_{rel} = \frac{Kt_0\rho_0}{Kt_s\rho_s} \qquad [2.9]$$

Where the subscripts *0* and *s* refer to the dispersion and the pure solvent respectively. Reported values for η_{rel} are based on the mean efflux times determined over at least 3 measurements.

2.2.2.6 Freeze drying

The instrument used was the VirTis benchtop freeze drier 4K (SP Scientific, Pennsylvania, USA) equipped with a stainless steel vertical manifold. Approximately 25 ml aliquots of *p(NIPAM)* microgel dispersions were pre-frozen (conventional freezing at -80°C) in 50 ml Falcon tubes prior to being transferred to the freeze drier flasks. Solvent was removed at -170 °C at a pressure of 50 mTorr. Freeze drying experiments using these volumes and conditions ran for a typical duration of 72 hours.

2.2.2.7 Shear rheometry

Rotational shear rheometry was performed using a stress controlled rheometer (MCR 302, Anton Paar GmbH, Graz, Austria). Stainless steel cone-plate measuring sets (*CP50/2°*, gap = 0.352 mm or *CP75/1°*, gap = 0.151 mm) were used throughout. Raw data was analysed in the RheoCompass software package (Anton Paar GmbH, Graz, Austria). Logarithmic ramps through shear rate ($\dot{\gamma}$) were used ($\dot{\gamma} = 10^{-4}$ - 10^{3} s^{-1}) depending on the sample viscosity. The measurement duration was set to automatic and the steady state condition was satisfied at each measuring point. Before starting the measurements, samples were preheated to 25 °C for at least 10 minutes and pre-sheared at the lowest shear rates tested for a further 10 minutes to ensure material was homogeneously distributed in the geometry gap. A custom-made solvent trap was used to prevent sample evaporation.

2.3 Results and Discussion

2.3.1 Microgel synthesis

The typical quantities of reagents used in the synthesis of *p(NIPAM)* microgel suspensions in a 50 ml reaction volume are shown in Table 2.1. The quantities of surfactant (*SDS*) and initiator (*KPS*) were initially kept constant between batches and only the molar ratio of *NIPAM*:*MBA* was varied. This allowed for the synthesis of microgels which differ in their crosslinking density. The numbers in sample codes correspond to the molar ratio of *NIPAM*:*MBA*. Hence, sample *MG16* contains a ten-fold excess of crosslinking co-monomer relative to sample *MG160*.

Following purification, this protocol typically yielded microgel dispersions with polymer concentrations on the order of 1 – 1.5 wt. %. Since the overall goal of this work was to study the rheological properties of *concentrated* microgel suspensions, extensive solvent removal would be required to access this regime. It was therefore

necessary to optimise the synthesis protocol to increase both the *yield* and the *volume* of the resulting dispersions. The first step towards achieving this was to investigate the effect of increasing the monomer concentrations by 50 wt.% while keeping the volume of water constant, as shown in Table 2.1. The prefix letter '*S*' was used in sample codes for such scaling of reagents. As expected, this modified protocol resulted in improved yields which were typically on the order 2-2.5 wt.%.

Table 2.1 - Typical quantities of reagents used in the synthesis of *p(NIPAM)* microgels using the original protocol after Senff and Richtering (2000) ('*MG'* samples) and using the modified protocol ('*S*' samples). The typical yield of the product with respect to polymer concentration is given for each protocol.

Code	***NIPAM*** **/ g**	***MBA*** **/ g**	***SDS*** **/ g**	***KPS*** **/ g**	**H_2O / ml**	**Typical Concentration / wt. %**
MG16	0.76	0.065	0.015	0.03	50	1 – 1.5
MG160	0.76	0.0065	0.015	0.03	50	1 – 1.5
S16	1.14	0.0975	0.015	0.03	50	2 – 2.5
S160	1.14	0.00975	0.015	0.03	50	2 – 2.5

Figure 2.2 shows the hydrodynamic diameter (D_H) as a function of temperature (T) for some representative samples fabricated according to Table 2.1. To facilitate the following discussion, samples *MG16* and *S16* will be referred to as 'densely crosslinked' and samples *MG160* and *S160* will be referred to as 'sparsely crosslinked'. The D_H at T = 20 °C for these samples is approximately 200 nm and 280 nm respectively. Evidently, the molar ratio of *NIPAM*:*MBA* controls the particle size, in addition to the particle microstructure (McPhee et al., 1993).

In either case, the D_H gradually decreases with an increase in T. At around 32 °C, an abrupt reduction in D_H is observed corresponding to the collapse of the microgel network (*i.e.*, the *VPT*). This was to be expected since 32 °C is widely reported as the *VPTT* for *p(NIPAM)* microgels in the literature and corresponds to the lower critical solution temperature (*LCST*) of linear *p(NIPAM)* molecules (Winnik, 1990).

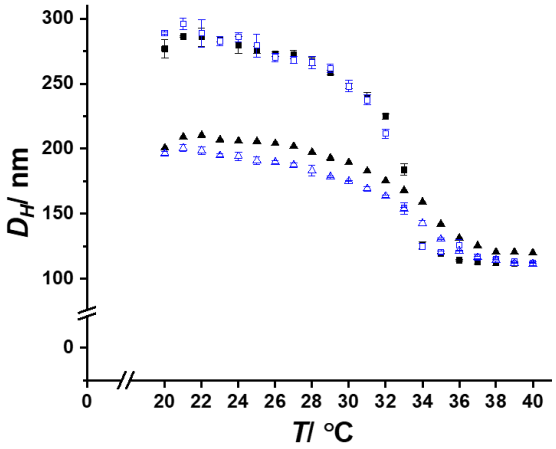

Figure 2.2 - Hydrodynamic diameter (D_H) as a function of temperature (T) for thermally responsive *p(NIPAM)* microgel particles of different crosslinking density. Molar ratio *NIPAM*:*MBA* is ■ = 160 and ▲ = 16. Closed symbols show microgels prepared using the original synthetic protocol (*'MG'* samples) and open symbols are '*S*' samples prepared using a scaled increase in monomers (Table 2.1).

For densely crosslinked microgels, the *VPT* is more gradual and appears to occur over a wider range of *T*. The waiting time between particle size measurements was sufficiently long for temperature equilibration indicating that the greater number of crosslinks within the microgel network are sufficient to resist particle deswelling when induced by temperature (Kratz et al., 2001). Nonetheless, for collapsed microgel particles at T = 40 ° C (*i.e.*, well beyond the *VPTT*), the D_H was similar for all samples ranging from ~110 – 120 nm.

The standard error in the D_H is greater for swollen microgels ($T<VPTT$) than in de-swollen microgels ($T>VPTT$). This is a common observation for microgels synthesised by dispersion polymerisation in batch, which typically have a heterogeneous microstructure (Figure 2.1). The error in such measurements is attributed to the sensitivity of *PCS* to the 'fuzzy interface' of swollen microgels (Boon and Schurtenberger, 2017). Neutron scattering studies on de-swollen microgels indicate the absence of such structural features at the microgel interface (Fernández-Barbero et al., 2002; Kratz et al., 2001) and hence the error in the *PCS* measurement is reduced. The average polydispersity index (*PDI*) from these measurements in the range T = 20 – 40 °C was < 6%. Whilst admittedly skewed

towards the *PDI* of de-swollen microgels, such a low *PDI* indicates a uniform particle size distribution at all temperatures.

The reproducibility of densely crosslinked microgels synthesised using the original and modified protocols is poor in comparison to sparsely crosslinked microgels, as is shown in Figure 2.2. Significant batch-wise variations were also observed in the former. This lack of reproducibility prompted an investigation into the synthesis of microgels with a lower crosslinking density (molar ratio *NIPAM*:*MBA* = 249 (*MG249*)). However, the $D_H(T)$ plots were very similar to *MG160* (data not shown). It was hypothesised that *MG249* would have a different microstructure although proving this would require complimentary scattering techniques (*e.g.*, neutron scattering). For this reason, sample *MG249* will not be discussed further in this work.

Figure 2.3 shows the variation of particle size as a function of *T* for S160 and S16. In this case, D_H at a given temperature is normalised by the D_H of de-swollen microgels at 40 °C to show the extent of swelling and the *VPT* more clearly. At *T* = 21 °C, microgels *S160* and *S16* swell to approximately 2.6 and 1.8 times their fully de-swollen diameter. The corresponding volumetric swelling ratios, *Q* ($Q = (D_{H\,21°C}/D_{H\,40°C})^3$) are *Q* = 17.7 and *Q* = 5.8 respectively (Omari et al., 2006). Figure 2.3 also shows the variation of zeta potential (ζ) with *T*. Measurements were performed on purified microgel suspensions which are assumed to be free of residual *SDS*. The negative charges originate from the ionic initiators used during synthesis (see Introduction). Potassium persulfate (*KPS*) was used in this study however we also observed similarities in the sign and magnitude of ζ for microgels synthesised with ammonium persulfate (data not shown). Initiator fragments are covalently bound to the polymer chain ends suggesting that they reside primarily in the interfacial region (Utashiro et al., 2017; Daly and Saunders, 2000b). The ζ of swollen microgels is approximately -10 mV which increases in magnitude to a value of around -30 mV in de-swollen microgels. The variation of the ζ is due to the conformational changes associated with the *VPT*. The number of charged polymer chains per particle is constant and an increase in the magnitude of ζ corresponds to the distribution of charges over a smaller particle volume (McPhee et al., 1993). The ζ measurements were made at *T* = 2 °C intervals however there appears to be a pronounced difference in the *T* dependence of the particle size and surface charge density, with the former decreasing significantly first. Other authors have reported a

discontinuous de-swelling behaviour for the *p(NIPAM)* microgel core and shell regions respectively. The presence of charges in the 'shell' pushes the *LCST* of polymer molecules in this region to higher values (Daly and Saunders, 2000b).

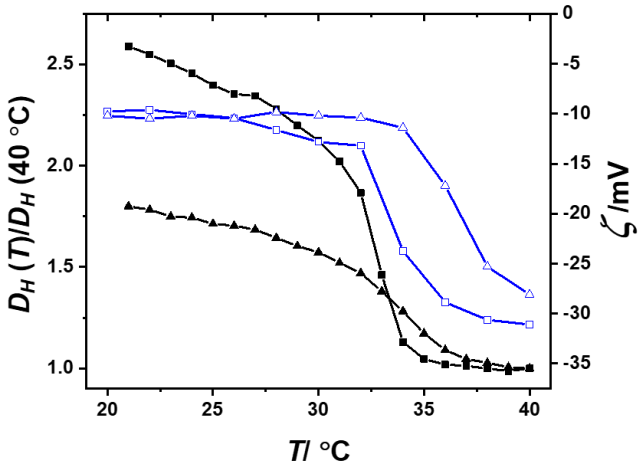

Figure 2.3 - Hydrodynamic diameter (D_H) scaled by D_H of de-swollen microgels at 40 °C (closed symbols) and zeta potential (ζ) (open symbols) as a function of temperature (T). Molar ratio *NIPAM*:*MBA* is ■ = 160 and ▲ = 16 using '*S*' samples synthesized in the presence of 1.04 mM *SDS* (Table 2.1). Lines are to guide the eye.

Increasing the concentration of monomers for densely crosslinked microgels (*S16*) led to experimental difficulties since the resulting suspensions were found to be susceptible to destabilization where $T > VPTT$, for example, towards the end of the synthesis and during filtration through glass wool. For these reasons, it was decided to investigate the effect of increasing the surfactant concentration used during the synthesis, with a hypothesis that this would improve the stability of the de-swollen microgels when prepared at the higher monomer concentrations desired (*'S'* samples).

Figure 2.4 shows the effect of increasing the *SDS* concentration ([*SDS*]) from 1.04 mM to 1.56 mM for *S16* and *S160*. An increase in the surfactant concentration is clearly shown to lead to a reduction in particle size for microgels prepared at both crosslinking densities over the full range in T. This suggests that the [*SDS*] influences the mechanisms of particle nucleation and growth operating during synthesis by precipitation polymerization. Following homogeneous nucleation between monomer and initiator molecules (*i.e.*, the generation of unstable 'precursor

particles'), molecular weight development initially occurs by coagulation mechanisms until the surface charges provided by covalently bound initiator fragments and physically adsorbed *SDS* are sufficient to provide the growing particles with colloidal stability. These 'mature' particles subsequently grow in a more controlled way by incorporation of monomer from the bulk (Pich and Richtering, 2010). Increasing [*SDS*] therefore has the effect of reducing the extent of particle coagulation in the early stages of polymerisation corresponding to an increase in the number of mature particles which ultimately attain smaller dimensions. The influence of varying [*SDS*] during microgel synthesis has been observed before (McPhee et al., 1993; Deen et al., 2011) and remains a facile technique to control particle size. Interestingly, large amounts of surfactant used in microgel synthesis have been shown to result in a more homogeneous microstructure probably due to *SDS* facilitating polymer-solvent interactions at the elevated temperatures used in synthesis (Andersson and Maunu, 2006; Arleth et al., 2005).

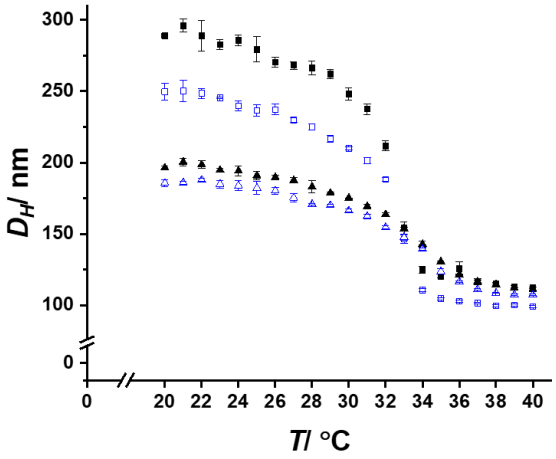

Figure 2.4 - Hydrodynamic diameter (D_H) as a function of temperature (T) for thermally responsive *p(NIPAM)* microgel particles of different crosslinking density. Molar ratio *NIPAM*:*MBA* is ■ = 160 and ▲ = 16 using 'S' samples synthesized in the presence of 1.04 mM *SDS* (closed symbols) (Table 2.1). Open symbols show the effect of increasing the *SDS* concentration to 1.56 mM.

Increasing [*SDS*] was not sufficient to improve the stability of densely crosslinked microgel suspensions at $T > VPTT$. Therefore, it was decided not to pursue a further scaling of this synthesis with respect to the reaction volume. For this, the quantities

of reagents were scaled with the amount of water used in the synthesis. The synthesis of *S160* was successful and reproducible in a reaction volume of 100 ml. This sample was used for the subsequent studies on the stability and rheology of *p(NIPAM)* microgel suspensions discussed in the remainder of this chapter.

2.3.2 Microgel stability

Figure 2.5A shows the variation of D_H with T for microgel *S160* dispersed in KCl solutions over a range of ionic strength (I). Similar results were obtained when microgels were dispersed in phosphate buffered saline (data not shown). For I = 1 mM KCl, there is little variation in the apparent D_H compared to when microgels are dispersed in pure water, irrespective of T. Increasing the KCl concentration influences the stability of *p(NIPAM)* microgels to different extents. At 10 mM KCl, flocculation is observed above 33 °C and no reliable data could be collected beyond the horizontal lines in Figure 2.5. At I = 100 mM KCl, flocculation was observed above 32 °C and microgels showed a significant reduction in D_H on approach to the *VPTT* ($T \geq 29$ °C) compared to when dispersed in pure water. This phenomenon is frequently observed in the literature, often at lower salt concentrations than where it becomes apparent here (McPhee et al., 1993; Daly and Saunders, 2000b; Daly and Saunders, 2000a; López-León et al., 2006; Utashiro et al., 2017). It has been attributed to the dehydration of polymer chains which promotes polymer-polymer interactions at lower temperatures, thus reducing the *VPTT*. Figure 2.5B shows the variation of D_H with T for microgel *S160* dispersed in water at pH 3-11. At pH 3, microgels were flocculated above 33 °C. At T > 35 °C, D_H at pH 11 was greater than at pH 6.

Swollen *p(NIPAM)* microgels consist of a densely crosslinked, largely neutral core (owing to the differences in the reactivity of *NIPAM* and *MBA*) with a sparsely crosslinked, negatively charged shell. The interfacial region could therefore be viewed as a ‘polyelectrolyte shell’ which contributes to colloidal stability through electrostatic and steric repulsive mechanisms (Daly and Saunders, 2000b; Daly and Saunders, 2000a). Furthermore, the solvent swollen microgels inherently have a low effective Hamaker constant and therefore a small attractive van der Waals force (McPhee et al., 1993; Daly and Saunders, 2000a). This explains the exceptional stability of microgels at T < *VPTT*.

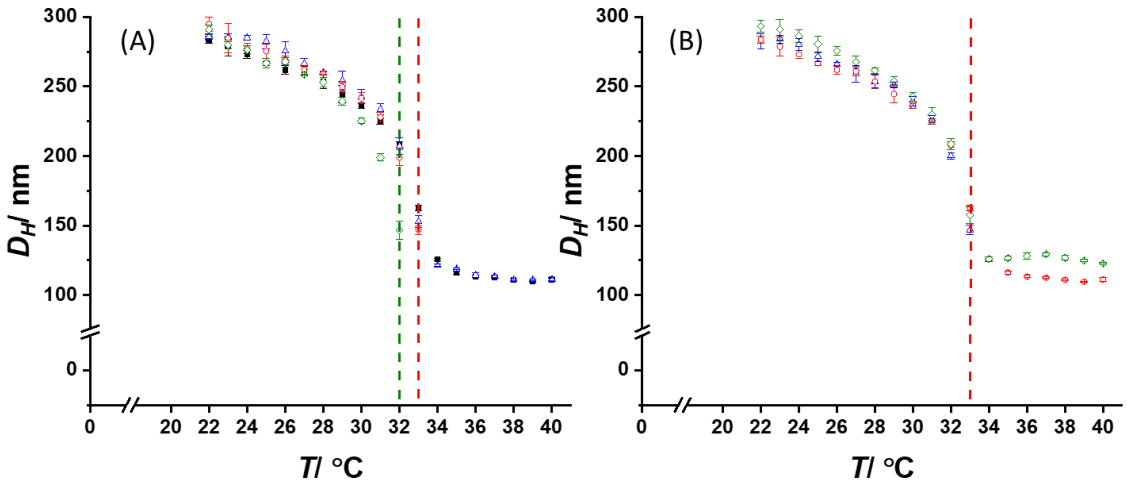

Figure 2.5 - (A) Hydrodynamic diameter (D_H) as a function of temperature (T) for microgel sample *S160* dispersed in pure water (■), 10^{-3} M KCl (▲), 10^{-2} M KCl (●) and 10^{-1} M KCl (◆). (B) $D_H(T)$ plots for the same microgels dispersed in water at pH 3 (▲), pH 6 (●) and pH 11 (◆). The horizontal dashed lines show the T at which microgel particles are destabilized.

The hydrophilic-hydrophobic transition at $T > VPTT$ and concurrent expulsion of water from the polymer network result in a significant increase in the van der Waals attraction. The collapse of the shell onto the surface of de-swollen microgels results in the loss of the steric repulsive barrier. Consequently, all ionic groups are located at the interface and the effective interactions between de-swollen microgel particles are well described by the *DLVO* theory (Daly and Saunders, 2000a; López-León et al., 2006; Pelton, 2000). McPhee et al. (1993) observed a reduction in the electrophoretic mobility in similar microgels with increasing ionic strength. This would suggest that at $I > 10$ mM KCl and at pH 3, charge screening occurs such that the repulsive electrostatic forces become insufficient to overcome the attractive van der Waals forces thereby resulting in flocculation.

The preparation of microgel suspensions over a range of polymer concentrations was required for the rheological characterization discussed in Section **2.3.4**. Due to the poor stability of microgels at $T > 32$ °C, freeze drying was preferred over rotary evaporation for this purpose. Freeze drying had additional advantages in the preservation of microgels. Freeze dried *p(NIPAM)* microgels could readily be re-dispersed in water, even at high concentrations (see Figure 2.8B). Furthermore, there

was negligible hysteresis in the particle size distributions of rehydrated microgel dispersions (data not shown).

Figure 2.6 shows the D_H for a freeze dried *S160* sample when rehydrated with water, 20 wt.% glucose and 40 wt.% glucose respectively. Dispersing the freeze-dried powders into sugar solutions was relatively time inefficient compared to dispersing them in water (*i.e.*, this took several days of stirring for complete dissolution). It was investigated here at the request of the industrial sponsor. Dispersing microgels in glucose solutions also enabled the study of particle size in solvents which are known to differ in their osmotic pressure. Figure 2.6 shows a clear effect of the glucose concentration on D_H at selected temperatures below and above the *VPTT*. The D_H was found to decrease with increasing glucose concentration, irrespective of T. This result was partly expected, for example, a technique to determine the bulk modulus of microgel particles is to monitor the reduction in particle size as a function of osmotic pressure, which was achieved by dispersing microgels in dextran solutions of different concentration (Mattsson et al., 2009).

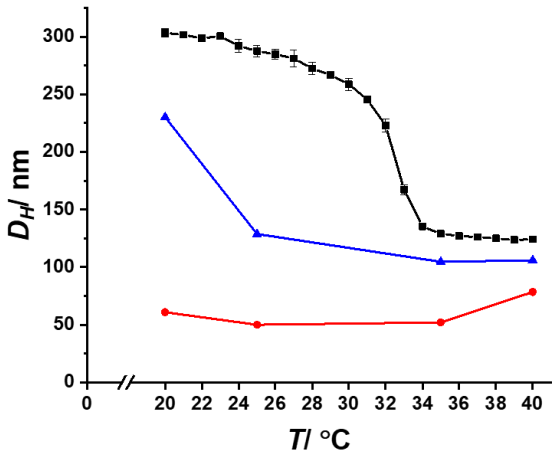

Figure 2.6 - Hydrodynamic diameter (D_H) as a function of temperature (T) for microgel sample *S160* dispersed in pure water (■), 20 wt.% glucose (▲) and 40 wt.% glucose (●). Lines are to guide the eye.

The responsiveness of microgels towards temperature was found to be modified in the presence of glucose. For microgels dispersed in 20 wt.% glucose, the D_H decreased from approximately 230 nm to 130 nm with an increase in T from 20-25 °C. This was followed by a further, small reduction in D_H to 105 nm at 35 °C which remained relatively constant at T = 40 °C. Increasing the glucose concentration from

20 to 40 wt.% led to a further reduction in D_H. The D_H was relatively constant between 50-60 nm with an apparently negligible thermal responsiveness. The apparent increase in D_H ($D_H \approx 78$ nm) between 35-40 °C was an unexpected result and may be due to an error in the viscosity term in the calculation of D_H (Equation 2.1) although this was accounted for in the *PCS* measurement (Telis et al., 2007).

Interestingly, the apparent D_H for microgels dispersed in 40 wt.% glucose was significantly smaller than any aqueous suspensions de-swollen solely with temperature. These results suggest that the addition of glucose progressively reduces the solvent quality and therefore the T dependence of the polymer-solvent interactions. The fact that an increase in osmotic pressure leads to microgel deswelling has consequences for the rheological properties of dense suspensions since the osmotic pressure increases with increasing polymer concentration or more appropriately, the particle volume fraction (ϕ) (Borrega et al., 1999).

2.3.3 Rheology of dilute microgel suspensions

Figure 2.7 shows the variation of the relative viscosity (η_{rel}) with polymer concentration (C) for swollen (T = 25 °C) and de-swollen (T = 40 °C) microgels. The η_{rel} is given by the ratio of the viscosity of a dispersion (η_0) and the viscosity of the solvent at the same temperature (η_s). In dilute colloidal suspensions, η_{rel} is proportional to ϕ according to the Einstein-Batchelor equation (Tadros, 2010):

$$\eta_{rel} = \frac{\eta_0}{\eta_s} = 1 + 2.5\phi + 5.9\phi^2 \qquad [2.10]$$

: For hard-spheres:

$$\phi = nV_p \qquad [2.11]$$

And:

$$V_p = \frac{4}{3}\pi R^3 \qquad [2.12]$$

:Where n is the number of particles, V_p is the particle volume and r is the particle radius (m). For microgels, V_p is not fixed due to their inherent deformability. Nonetheless, experimental viscosity measurements on dilute microgel suspensions can be fitted to a modified form of the Einstein-Batchelor equation (Senff and Richtering, 2000);

$$\eta_{rel} = \frac{\eta_0}{\eta_s} = 1 + 2.5kC + 5.9kC^2 \qquad [2.13]$$

:Where k is a fitting parameter which enables the conversion of C to an *effective* volume fraction (Φ_{eff}) according to;

$$\Phi_{eff} = kc \qquad [2.14]$$

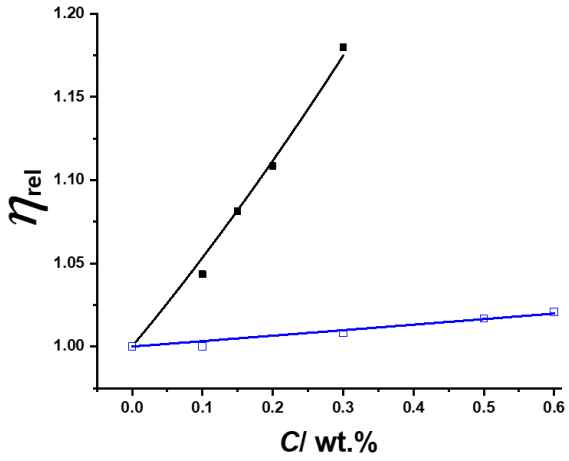

Figure 2.7 - Relative viscosity (η_{rel}) as a function of polymer concentration (C) for *S160* at 25 °C (closed symbols) and 40 °C (open symbols). The solid lines are fits to the data according to the modified Einstein-Batchelor equation (Equation 2.13).

The solid lines in Figure 2.7 are best fits to the data according to Equation 2.13 returning values for k = 203.76 x 10^{-3} and k = 12.99 x 10^{-3} for swollen and de-swollen microgels respectively. For similar microgels studied at the same temperature, Senff and Richtering (2000) found k = 275.5 x 10^{-3} and k = 11.6 x 10^{-3} respectively. The value of k reflects the reduced volume occupied by de-swollen microgels. As an example, for a 2 wt. % *p(NIPAM)* microgel suspension, ϕ_{eff} = 0.41 at 25 °C whereas at 40 °C the same suspension has ϕ_{eff} = 0.03. The typical polymer concentrations obtained in the modified protocol used for microgel synthesis is on the order of 2-2.5 wt.% (Table 2.1). Polymerisation is performed at a high temperature where particles are fully de-swollen and exhibit a low ϕ_{eff}. Subsequent cooling of the freshly synthesised suspension causes an increase in ϕ_{eff}. Interestingly, crystallisation of *p(NIPAM)* microgels has been observed in the dialysis membrane during purification of '*S*' samples, as shown in the photograph in Figure 2.8A. The onset of crystallisation in monodisperse hard-sphere dispersions occurs at ϕ = 0.494 (Lyon et al., 2004). The photographs shown in Figure 2.8B and 2.8C show the interesting concentration dependent optical properties for freeze dried *S160*

redispersed in water at a concentration of 3.07 and 5.93 wt.% corresponding to $\phi_{eff} \approx$ 0.63 and 1.21 respectively.

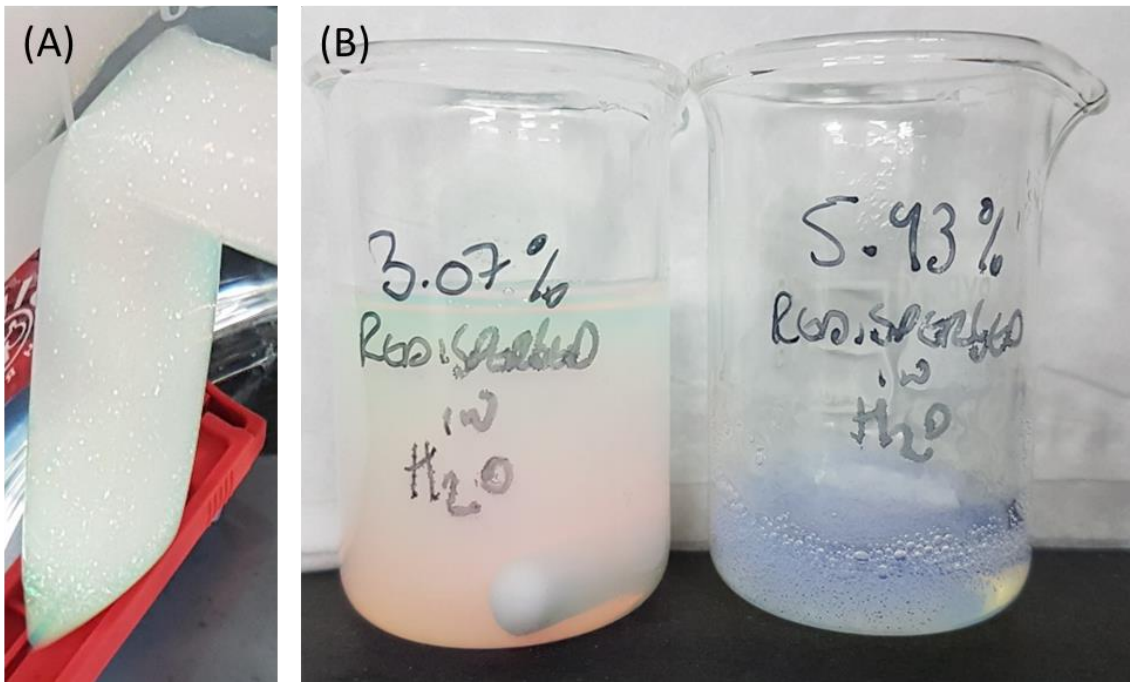

Figure 2.8 - Photographs of *p(NIPAM)* microgel sample *S160* over a range of polymer concentrations. (A) Freshly synthesized microgels undergoing crystallization during dialysis (B) Freeze dried microgel powders rehydrated at polymer concentrations of 3.07 wt.% (left) and 5.93 wt.% (right) in water.

2.3.4 Rheology of concentrated microgel suspensions

Figure 2.9 shows the apparent viscosity (η) as a function of shear rate ($\dot{\gamma}$) for *S160* over a range of ϕ_{eff}. The previous discussion details how ϕ_{eff} varies with temperature due to the thermal responsiveness of *p(NIPAM)* microgels. Using temperature is a facile technique to access different ϕ_{eff}, however the inter-particle interactions change as a consequence (Bergman et al., 2018). The rehydration of freeze dried microgels was used to access a range of ϕ_{eff} here using Equation 2.14. Experiments were performed at 25 °C since k was known and swollen microgels were relatively more stable than de-swollen microgels.

As expected, an increase in ϕ_{eff} corresponds to an increase in η, irrespective of $\dot{\gamma}$. For ϕ_{eff} = 0.38, the suspensions appear Newtonian, with a largely $\dot{\gamma}$ independent η. More concentrated suspensions (ϕ_{eff} > 0.51) demonstrated non-Newtonian flow properties, namely shear thinning (pseudoplastic) behaviour. The extent of

pseudoplasticity clearly depends on ϕ_{eff} (Tan et al., 2010). The origin of shear thinning in concentrated microgel dispersions is not well defined however a decrease in inter-particle distance (corresponding to increased repulsive interactions in swollen microgels) appears to enhance pseudoplasticity. It has been suggested that repulsive microgels form 2D close packed layers as a result of shear forces, and it is the sliding of such layers past each other in flow which gives rise to shear thinning (Stieger et al., 2004a). Pseudoplasticity has also been attributed to the deformation of microgels and their alignment with the direction of the shear flow (Tan et al., 2010).

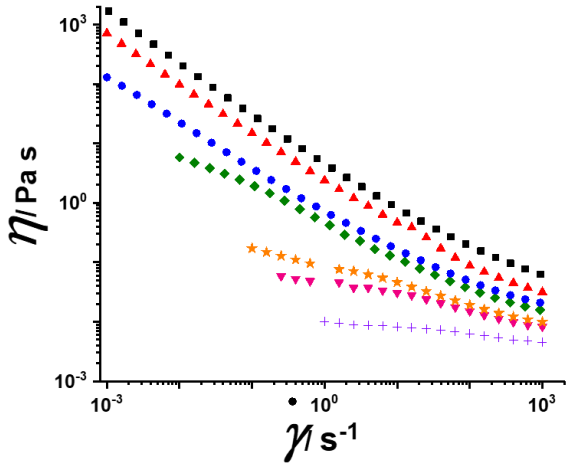

Figure 2.9 - Apparent shear viscosity (η) as a function of shear rate ($\dot{\gamma}$) for *S160* over a range of effective volume fraction (ϕ_{eff}) ■ = 1.04, ▲ = 0.91, ● = 0.82, ◆ = 0.7, ★ = 0.61, ▼ = 0.51 and + = 0.38. Measurements were performed at 25 °C.

It is frequently found that concentrated microgel suspensions demonstrate low shear and high shear Newtonian plateaus, separated by a shear thinning region (Wolfe and Scopazzi, 1989; Senff and Richtering, 2000; Tan et al., 2010). In the low shear plateau (zero-shear viscosity, η_0) region, the rheological properties are dominated by Brownian motion whereas the rheological properties at high shear (infinite shear viscosity, η_∞) are dominated by hydrodynamics (Tadros, 2010).

While these regions were not resolved in the flow curves shown in Figure 2.9, η_0 and η_∞ were estimated by interpolation of the data to $\dot{\gamma} = 10^{-3}$ and 10^3 respectively. Figure 2.10 shows the *relative* η_0 and *relative* η_∞ for *S160* as a function of ϕ_{eff}. This figure was constructed by combining the capillary viscometry and shear rheology

data. The η of the suspensions measured in capillary viscometry is assumed to be Newtonian and hence the initial slope is the same for either curve.

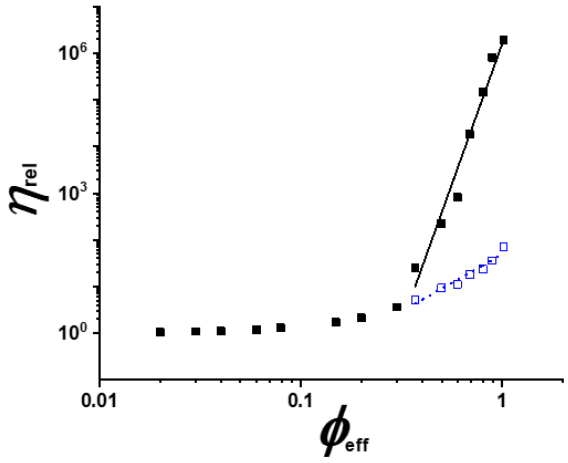

Figure 2.10 - Relative viscosity (η_{rel}) as a function of ϕ_{eff} for sample *S160* at 25 °C. The relative 'zero shear' viscosity (solid symbols) and relative 'infinite shear' viscosity (open symbols) were estimated by interpolation of shear rheometry data shown in Figure 2.9 to $\dot{\gamma}$ = 0.001 s^{-1} and $\dot{\gamma}$ = 1000 s^{-1} respectively. The data points recorded at ϕ_{eff} < 0.3 were taken from capillary viscometry measurements and are assumed to demonstrate a Newtonian (*i.e.,* $\dot{\gamma}$ independent) viscosity. The lines show power law fits to the data with exponents 12 ± 1 (solid line) and 2.4 ± 0.3 (dashed line) with R > 0.97.

The *relative* η_0 of hard-sphere suspensions is well described by the Krieger-Dougherty relation;

$$\eta_{rel} = \left(1 - \frac{\Phi}{\Phi_{max}}\right)^{-[\eta]\Phi_{max}} \qquad [2.15]$$

:Which suggests that η_{rel} diverges on approach to the maximum packing fraction (ϕ_{max}) (Krieger and Dougherty, 1959), commonly observed in the region ϕ = 0.58-0.64, the lower bound corresponding to the glass transition and the upper bound corresponding to the random close packing of equal sized, incompressible spheres (Jones et al., 1991). The intrinsic viscosity ($[\eta]$) takes a value of 2.5. The data for microgel suspensions presented in Figure 2.10 shows deviations from the hard-sphere behaviour predicted by Equation 2.15. Most strikingly, the microgels in this study could be packed to ϕ_{eff} > 0.64 and even to beyond unity. An apparent ϕ_{eff} > 1

seems counterintuitive but has been frequently reported for microgel systems owing to the technique used for the determination of ϕ_{eff} (Senff and Richtering, 2000).

Equation 2.13 is routinely used to determine ϕ_{eff} for microgel systems, however, since ϕ_{eff} is determined at 'infinite dilution' where particle-particle interactions can be neglected and microgels effectively behave as hard-spheres, it can lead to overestimates at high phase volumes. This is due to the potential for particle compression, interpenetration and osmotic deswelling as ϕ_{eff} increases (Brijitta and Schurtenberger, 2019; Royall et al., 2013). In all, these factors suggests that there is a concentration dependence on ϕ_{eff} which isn't accounted for in the modified Einstein-Batchelor equation (Equation 2.13). If this is corrected for, microgel suspensions have been shown to satisfy the hard-sphere behaviour predicted by the Krieger-Dougherty relation (Equation 2.15) (Tan et al., 2010; Borrega et al., 1999).

Further to the discrepancies described above, the shape of the curve in this study is dissimilar to that typical of hard-sphere and microgel systems respectively. Most often, η_{rel} increases more smoothly on approach to ϕ_{max}. A possible reason for the difference in the shape of the curve is the way that η_{rel} was defined via interpolation. The relative η_0 data presented in Figure 2.10 beyond $\phi_{eff} = 0.3$ is better suited to a power law fitting with exponent 12.1. The relative η_∞ of microgel systems generally appears to increase more gradually with ϕ_{eff} (Senff and Richtering, 2000; Wolfe and Scopazzi, 1989). For microgels with a similar crosslink density, Senff and Richtering (2000) did not observe the divergence of η_∞ even up to a $\phi_{eff} \approx 2.5$. For the microgel system in this study (Fig. 2.10), the relative η_∞ can also be described by a power law, but with a much lower exponent of 2.4.

2.4 Conclusions

Overall, the results and associated discussion presented in this chapter serve to introduce microgels as soft colloidal particles and highlights their differences compared to hard-spheres. To that end, thermally responsive microgels are a useful model system for 'soft colloids' since their physiochemical properties can be tailored at the synthesis stage and further adjusted with variations in temperature. It has been shown that *p(NIPAM)* microgel suspensions can be synthesised at reasonably high polymer concentrations with good reproducibility. This work also shows that the particle size (hence ϕ_{eff}) of soft colloids and their resulting stability is sensitive to the solvent composition.

A modified form of the Einstein-Batchelor equation was used to determine ϕ_{eff} for *p(NIPAM)* microgels. Deviations from hard-sphere behaviour were observed at intermediate to high ϕ_{eff} where discrete, solvent swollen microgel particles can interpenetrate, be compressed and/or de-swell due to an increase in the osmotic pressure. A more detailed discussion of the results would be made possible with complementary experimental techniques (*e.g.*, neutron scattering, atomic force microscopy, diffusion wave spectroscopy) providing additional information on the microgel structure, dynamics and inter-particle interactions across a range of phase volumes.

Although no further characterization of the *p(NIPAM)* microgels presented in this chapter was undertaken, it is hoped that the results may assist future researchers in the field, particularly for preparing microgel suspensions at relatively higher ϕ_{eff} than other protocols described in the literature. Furthermore, the experimental results and practical experiences obtained in this study assisted in the fabrication and characterization of the biopolymer microgel systems described in **Chapters 3-5**. For some purposes, *p(NIPAM)* microgels were found to be a more practical system to work with. For example, an investigation into the particle size distributions and stability of microgel suspensions with respect to pH and ionic strength are facilitated by having a well characterized and pure system such as *p(NIPAM)* which is also compatible with *PCS* measurements. Similarly, the definition of an ϕ_{eff} through the Einstein-Batchelor relation, and the associated errors resulting from its definition at infinite dilution, acted to verify some of the results obtained on the rheological properties of biopolymer microgels presented in subsequent chapters.

2.5 References

Ancla, C., Lapeyre, V., Gosse, I., Catargi, B. and Ravaine, V. 2011. Designed Glucose-Responsive Microgels with Selective Shrinking Behavior. Langmuir. 27(20), pp.12693-12701.

Andersson, M. and Maunu, S.L. 2006. Structural studies of poly(N-isopropylacrylamide) microgels: Effect of SDS surfactant concentration in the microgel synthesis. Journal of Polymer Science Part B: Polymer Physics. 44(23), pp.3305-3314.

Anon. 2022a. Carbopol® Polymer Products - Lubrizol. [Online]. [Accessed 05/05/2022]. Available from: https://www.lubrizol.com/Life-Sciences/Products/Carbopol-Polymer-Products

Anon. 2022b. SEPIMAX ZEN™ - Thickening-Stabilizing-Texturizing Polymer. [Online]. [Accessed 05/05/2019]. Available from: https://www.seppic.com/sepimax-zen

Arleth, L., Xia, X., Hjelm, R.P., Wu, J. and Hu, Z. 2005. Volume transition and internal structures of small poly(N-isopropylacrylamide) microgels. Journal of Polymer Science Part B: Polymer Physics. 43(7), pp.849-860.

Aufderhorst-Roberts, A., Baker, D., Foster, R.J., Cayre, O., Mattsson, J. and Connell, S.D. 2018. Nanoscale mechanics of microgel particles. Nanoscale. 10(34), pp.16050-16061.

Bergman, M.J., Gnan, N., Obiols-Rabasa, M., Meijer, J.-M., Rovigatti, L., Zaccarelli, E. and Schurtenberger, P. 2018. A new look at effective interactions between microgel particles. Nature Communications. 9(1), p5039.

Boon, N. and Schurtenberger, P. 2017. Swelling of micro-hydrogels with a crosslinker gradient. Physical Chemistry Chemical Physics. 19(35), pp.23740-23746.

Borrega, R., Cloitre, M., Betremieux, I., Ernst, B. and Leibler, L. 1999. Concentration dependence of the low-shear viscosity of polyelectrolyte micro-networks: From hard spheres to soft microgels. Europhysics Letters (EPL). 47(6), pp.729-735.

Brijitta, J. and Schurtenberger, P. 2019. Responsive hydrogel colloids: Structure, interactions, phase behavior, and equilibrium and nonequilibrium transitions of microgel dispersions. Current Opinion in Colloid & Interface Science. 40, pp.87-103.

Daly, E. and Saunders, B.R. 2000a. A Study of the Effect of Electrolyte on the Swelling and Stability of Poly(N-isopropylacrylamide) Microgel Dispersions. Langmuir. 16(13), pp.5546-5552.

Daly, E. and Saunders, B.R. 2000b. Temperature–dependent electrophoretic mobility and hydrodynamic radius measurements of poly(N-isopropylacrylamide) microgel particles: structural insights. Physical Chemistry Chemical Physics. 2(14), pp.3187-3193.

Deen, G.R., Alsted, T., Richtering, W. and Pedersen, J.S. 2011. Synthesis and characterization of nanogels of poly(N-isopropylacrylamide) by a combination of light and small-angle X-ray scattering. Physical Chemistry Chemical Physics. 13(8), pp.3108-3114.

Delgado, A.V., González-Caballero, F., Hunter, R.J., Koopal, L.K. and Lyklema, J. 2007. Measurement and interpretation of electrokinetic phenomena. Journal of Colloid and Interface Science. 309(2), pp.194-224.

Fernández-Barbero, A., Fernández-Nieves, A., Grillo, I. and López-Cabarcos, E. 2002. Structural modifications in the swelling of inhomogeneous microgels by light and neutron scattering. Physical Review E. 66(5), p051803.

Gao, J. and Hu, Z. 2002. Optical Properties of N-Isopropylacrylamide Microgel Spheres in Water. Langmuir. 18(4), pp.1360-1367.

Hashmi, S.M. and Dufresne, E.R. 2009. Mechanical properties of individual microgel particles through the deswelling transition. Soft Matter. 5(19), pp.3682-3688.

Hoare, T. and McLean, D. 2006. Kinetic Prediction of Functional Group Distributions in Thermosensitive Microgels. The Journal of Physical Chemistry B. 110(41), pp.20327-20336.

Hoare, T. and Pelton, R. 2008. Charge-Switching, Amphoteric Glucose-Responsive Microgels with Physiological Swelling Activity. Biomacromolecules. 9(2), pp.733-740.

Jones, D.A.R., Leary, B. and Boger, D.V. 1991. The rheology of a concentrated colloidal suspension of hard spheres. Journal of Colloid and Interface Science. 147(2), pp.479-495.

Kratz, K., Hellweg, T. and Eimer, W. 2001. Structural changes in PNIPAM microgel particles as seen by SANS, DLS, and EM techniques. Polymer. 42(15), pp.6631-6639.

Krieger, I.M. and Dougherty, T.J. 1959. A Mechanism for Non-Newtonian Flow in Suspensions of Rigid Spheres. Transactions of the Society of Rheology. 3(1), pp.137-152.

López-León, T., Ortega-Vinuesa, J.L., Bastos-González, D. and Elaïssari, A. 2006. Cationic and Anionic Poly(N-isopropylacrylamide) Based Submicron Gel Particles: Electrokinetic Properties and Colloidal Stability. The Journal of Physical Chemistry B. 110(10), pp.4629-4636.

Lyon, L.A., Debord, J.D., Debord, S.B., Jones, C.D., McGrath, J.G. and Serpe, M.J. 2004. Microgel Colloidal Crystals. The Journal of Physical Chemistry B. 108(50), pp.19099-19108.

Malvern. 2009. Zetasizer Nano User Manual. MAN0317 Issue 5.0. England: Malvern Instruments. 15-1 - 15-12. [User Manual]. [Accessed 30/07/2019]. Available from: https://www.malvernpanalytical.com/en/learn/knowledge-center/user-manuals/MAN0485EN

Malvern. 2010. Measuring Zeta Potential Using Phase Analysis Light Scattering (PALS) Zetasizer Nano Application Note MRK571-01. England: Malvern Instruments. pp.1-3. [Application Note]. [Accessed 30/07/2019]. Available from: https://www.malvernpanalytical.com/en/learn/knowledge-center/technical-notes/TN101104PhaseAnalysisLightScattering

Mattsson, J., Wyss, H.M., Fernandez-Nieves, A., Miyazaki, K., Hu, Z., Reichman, D.R. and Weitz, D.A. 2009. Soft colloids make strong glasses. Nature. 462(7269), pp.83-86.

McPhee, W., Tam, K.C. and Pelton, R. 1993. Poly(N-isopropylacrylamide) Latices Prepared with Sodium Dodecyl Sulfate. Journal of Colloid and Interface Science. 156(1), pp.24-30.

Mezger, T. 2014. The Rheology Handbook : 4th Edition. Hannover: Vincentz Network.

Morris, G.E., Vincent, B. and Snowden, M.J. 1997. Adsorption of Lead Ions onto N-Isopropylacrylamide and Acrylic Acid Copolymer Microgels. Journal of Colloid and Interface Science. 190(1), pp.198-205.

Murray, M.J. and Snowden, M.J. 1995. The preparation, characterisation and applications of colloidal microgels. Advances in Colloid and Interface Science. 54, pp.73-91.

Nur, H., Snowden, M.J., Cornelius, V.J., Mitchell, J.C., Harvey, P.J. and Benée, L.S. 2009. Colloidal microgel in removal of water from biodiesel. Colloids and Surfaces A: Physicochemical and Engineering Aspects. 335(1), pp.133-137.

Omari, A., Tabary, R., Rousseau, D., Calderon, F.L., Monteil, J. and Chauveteau, G. 2006. Soft water-soluble microgel dispersions: Structure and rheology. Journal of Colloid and Interface Science. 302(2), pp.537-546.

Parasuraman, D., Leung, E. and Serpe, M.J. 2012. Poly (N-isopropylacrylamide) microgel based assemblies for organic dye removal from water: microgel diameter effects. Colloid and Polymer Science. 290(11), pp.1053-1064.

Pecora, R. 2008. Basic Concepts – Scattering and Time Correlation Functions. In: Borsali, R. and Pecora, R. eds. Soft Matter Characterization. Dordrecht: Springer, pp.2-40.

Pelton, R. 2000. Temperature-sensitive aqueous microgels. Advances in colloid and interface science. 85(1), pp.1-33.

Phua, D.I., Herman, K., Balaceanu, A., Zakrevski, J. and Pich, A. 2016. Reversible Size Modulation of Aqueous Microgels via Orthogonal or Combined Application of Thermo- and Phototriggers. Langmuir. 32(16), pp.3867-3879.

Pich, A. and Richtering, W. 2010. Microgels by Precipitation Polymerization: Synthesis, Characterization and Functionalization. In: Pich, A. and Richtering, W. eds. Chemical Design of Responsive Microgels. Berlin: Springer, pp.3-34.

Royall, C.P., Poon, W.C.K. and Weeks, E.R. 2013. In search of colloidal hard spheres. Soft Matter. 9(1), pp.17-27.

Sanson, N. and Rieger, J. 2010. Synthesis of nanogels/microgels by conventional and controlled radical crosslinking copolymerization. Polymer Chemistry. 1(7), pp.965-977.

Saunders, B.R. 2004. On the Structure of Poly(N-isopropylacrylamide) Microgel Particles. Langmuir. 20(10), pp.3925-3932.

Saunders, B.R. and Vincent, B. 1999. Microgel particles as model colloids: theory, properties and applications. Advances in Colloid and Interface Science. 80(1), pp.1-25.

Schmidt, S., Liu, T.T., Rutten, S., Phan, K.H., Moller, M. and Richtering, W. 2011. Influence of Microgel Architecture and Oil Polarity on Stabilization of Emulsions by Stimuli-Sensitive Core-Shell Poly(N-isopropylacrylamide-co-methacrylic acid) Microgels: Mickering versus Pickering Behavior? Langmuir. 27(16), pp.9801-9806.

Senff, H. and Richtering, W. 2000. Influence of cross-link density on rheological properties of temperature-sensitive microgel suspensions. Colloid and Polymer Science. 278(9), pp.830-840.

Stieger, M., Lindner, P. and Richtering, W. 2004a. Structure formation in thermoresponsive microgel suspensions under shear flow. Journal of Physics: Condensed Matter. 16(38), pp.S3861-S3872.

Stieger, M., Richtering, W., Pedersen, J.S. and Lindner, P. 2004b. Small-angle neutron scattering study of structural changes in temperature sensitive microgel colloids. The Journal of Chemical Physics. 120(13), pp.6197-6206.

Tadros, T. 2010. Rheology of Dispersions: Principles and Applications. Weinheim: WIley.

Tan, B.H., Pelton, R.H. and Tam, K.C. 2010. Microstructure and rheological properties of thermo-responsive poly(N-isopropylacrylamide) microgels. Polymer. 51(14), pp.3238-3243.

Telis, V.R.N., Telis-Romero, J., Mazzotti, H.B. and Gabas, A.L. 2007. Viscosity of Aqueous Carbohydrate Solutions at Different Temperatures and Concentrations. International Journal of Food Properties. 10(1), pp.185-195.

Tscharnuter, W.W. 2001. Mobility measurements by phase analysis. Applied Optics. 40(24), pp.3995-4003.

Utashiro, Y., Takiguchi, M. and Satoh, M. 2017. Zeta potential of PNIPAM microgel particles dispersed in water—effects of charged radical initiators vs. OH^- ion adsorption. Colloid and Polymer Science. 295(1), pp.45-52.

Wilke, J., Kryk, H., Hartmann, J., Wagner, D. and Eich, A. 2015. Visco Handbook. [Online]. New York, USA: SI Analytics. [Accessed 30/05/2022]. Available from: https://www.xylemanalytics.com/File%20Library/Resource%20Library/SIA/10%20Publications/SIA_Visco-handbook_English.pdf

Winnik, F.M. 1990. Fluorescence studies of aqueous solutions of poly(N-isopropylacrylamide) below and above their LCST. Macromolecules. 23(1), pp.233-242.

Wolfe, M.S. and Scopazzi, C. 1989. Rheology of swellable microgel dispersions: Influence of crosslink density. Journal of Colloid and Interface Science. 133(1), pp.265-277.

Wu, X., Pelton, R.H., Hamielec, A.E., Woods, D.R. and McPhee, W. 1994. The kinetics of poly(N-isopropylacrylamide) microgel latex formation. Colloid and Polymer Science. 272(4), pp.467-477.

Wyss, H.M., Franke, T., Mele, E. and Weitz, D.A. 2010. Capillary micromechanics: Measuring the elasticity of microscopic soft objects. Soft Matter. 6(18), pp.4550-4555.

Zhang, Q.M., Xu, W. and Serpe, M.J. 2014. Optical Devices Constructed from Multiresponsive Microgels. Angewandte Chemie International Edition. 53(19), pp.4827-4831.

Chapter 3: Enzyme Cross-Linked Pectin Microgel Particles for Use in Foods *

Abstract

We report on a new enzyme-based method for producing permanently cross-linked pectin microgels. We investigate the shape, size and rheological properties of these microgel particles making comparisons with the more traditional design of calcium cross-linked pectin microgels. Both sets of microgel particles were prepared *via* the 'top-down' mechanical disruption of parent pectin hydrogels. The first hydrogel was prepared from low methoxyl pectin (*LMP*) (2 wt.% pectin) cross-linked using Ca^{2+} (8.3 mM $CaCl_2$). The *LMP* microgels show particle sizes *ca*. 1 to 100 μm, but are stable only in [Ca^{2+}] = 8.3 mM or above, swelling and/or dissolving rapidly in pure water. The second type of microgel was prepared from sugar beet pectin (*SBP*) hydrogels covalently cross-linked *via* laccase. Gelation kinetics were investigated by small amplitude oscillatory shear rheometry. The *SBP* microgels resisted dissolution in water for several months. Light scattering measurements suggested that the *SBP* microgel particle sizes were related to the mechanical properties of the parent hydrogels. Various imaging techniques all suggested that *SBP* microgels have highly irregular shapes, perhaps due to the top-down technique used for their manufacture and their inherent mechanical properties. Concentrating the *SBP* microgels (to 35 – 50 wt.% microgel, or 0.6 – 0.8 wt.% overall pectin concentration) resulted in suspensions with rheological properties typical of yield stress fluids. When compared at similar overall *SBP* concentrations, the *SBP* microgel suspensions offer distinct advantages as bulk rheology modifiers compared to native *SBP* solutions.

*** Published as:** Stubley, S., Cayre, O., Murray, B., Celigueta Torres, I., & Fernández Farrés, I. (2021). Enzyme cross-linked pectin microgel particles for use in foods. *Food Hydrocolloids*, **121**. DOI: https://doi.org/10.1016/j.foodhyd.2021.107045

3.1 Introduction

Hydrogels can be defined as ‘infinitely’ large networks of hydrated polymer molecules which entrap a significant quantity of solvent, either water or electrolyte (Peppas, 1991). In contrast, microgel particles (also referred to as microgels) consist of discrete polymer networks of finite dimensions, swollen by the solvent in which they are dispersed (Pelton and Hoare, 2011). Most (micro)gels with potential applications in foods consist of supramolecular assemblies of biopolymer molecules, more specifically proteins and polysaccharides. Such biopolymers form gels via intermolecular association under different conditions with heat set (*e.g.*, globular proteins), cool set (*e.g.*, gelatine and agarose) and ionotropic (*e.g.*, pectins and alginates) gelation mechanisms being most common (Cao and Mezzenga, 2020). This implies that the specific technique employed to synthesize microgels is dependent on the chosen biopolymer characteristics.

Various techniques have been used to manufacture microgels from biopolymers as reviewed elsewhere (Joye and McClements, 2014; McClements, 2017; Shewan and Stokes, 2013; Farjami and Madadlou, 2017; Burey et al., 2008; Dickinson, 2017; Murray, 2019). In particular, the mechanical disruption of a bulk hydrogel in the presence of excess solvent holds promise as a scalable technique to prepare microgel particles for industrial food applications and has been widely used for the fabrication of proteinaceous microgels (Matsumiya and Murray, 2016; Sarkar et al., 2016; Guo et al., 2016; Zhang et al., 2020; Jiao et al., 2018). However, this ‘top-down’ approach has been used less frequently for preparing polysaccharide microgels. Ellis and Jacquier (2009) dispersed agarose hydrogels into water by ‘blending’ the mixture with a domestic food processor followed by rotor-stator mixing at various operating speeds and durations to obtain agarose microgel suspensions (Ellis and Jacquier, 2009). Saavedra Isusi et al. (2019) fabricated pectin microgel particles based on low-methoxyl pectin (*LMP*), amidated *LMP* and polygalacturonic (pectinic) acid. The pectin hydrogels were fragmented in excess water via sequential rotor stator mixing and wet milling to yield microgel particles (Saavedra Isusi et al., 2019). Note that the mechanism of particle generation via the methods used here are different to the production of shear (fluid) gels. In fluid gel formation, biopolymer solutions are simultaneously sheared and gelled, so that the final gel particle size is a result of the competition between network formation (*i.e.*, particle growth) and

network break-up due to the imposed flow field (Fernández Farrés and Norton, 2014).

Pectins, in particular, have a long history of being used as a gelling agent in foods. They are generally extracted from agro-industrial waste streams (*e.g.*, apple pomace and citrus pulp) and are therefore widely available at a reasonable cost (May, 1990). Thus, they are an ideal polysaccharide to develop food-grade microgel preparations. Applications could include: texture modification for desirable rheological and/or sensory responses (Shewan et al., 2020; Stokes, 2011), stabilization of Pickering emulsions and foams (Murray, 2019; Dickinson, 2017) and the encapsulation of water-soluble pigments, bioactive or flavour molecules (McClements, 2017).

Pectin molecules have chemical structures analogous to block copolymers, with three distinct types of region: homogalacturonan (*HG*), rhamnogalacturonan I (*RGI*) and rhamnogalacturonan II (*RGII*). The HG domain consists of 1,4-linked α-D-galacturonic acid (*GalA*) residues in which some of the carboxyl groups may be esterified at C6 by methyl groups. Degrees of methyl esterification above and below 50% correspond to high-methoxyl (*HMP*) or low-methoxyl (*LMP*) pectins, respectively. The rhamnogalacturonan domains (*RGI* and *RGII*) are more structurally complex and are colloquially referred to as the ‘hairy regions’ due to the presence of pendant sugar side chains (May, 1990). The *RGII* domain contains heteroglycan side chains covalently bound directly to a *HG* backbone (Ishii and Matsunaga, 1996). In contrast, the *RGI* backbone consists of alternating *GalA* and α-L-rhamnopyranose units as a repeating disaccharide. The rhamnose residues in this region bear neutral sugar side chains mainly composed of arabinose and galactose (Renard et al., 1995).

The mechanism of gelation in pectins is related to their fine structure and the solvent composition. For example, gelation of *LMP* (at pH > pKa) is usually achieved by the addition of divalent cations, principally Ca^{2+}, and cross-linking occurs in the *HG* region. It is estimated that 6 to 13 consecutive non-esterified galacturonic acid residues are required for the formation of a stable junction zone (Luzio and Cameron, 2008). If this condition is satisfied, polyanionic pectin chains can be bridged by divalent cations according to the (shifted) egg-box model (Braccini and Pérez, 2001) originally developed to explain the ionotropic gelation of alginates (Grant et al., 1973). Amidated *LMP*, produced by chemical removal of methyl esters

in the presence of ammonia, typically demonstrate improved mechanical properties due to intermolecular hydrogen bonding (Fraeye et al., 2010).

The fine structure of pectins further depends on the botanical source and conditions of extraction. For example, sugar beet pectin (*SBP*) is generally extracted as *HMP* and contains acetyl groups esterified to the secondary alcohols of *GalA*, primarily in the *HG* region (Ralet et al., 2005). The high degree of substitution renders *SBP* incompatible with the conventional gelation mechanisms described above without chemical modification to remove some methyl and/or acetyl groups (Matthew et al., 1990; Williamson et al., 1990; Pippen et al., 1950; Oosterveld et al., 2000a). *SBP* is also known to contain ferulic acid (*FA*) residues esterified to the neutral sugar side chains of *RGI*. This is important because the *FA* moieties can covalently cross-link discrete pectin molecules via oxidative coupling reactions. Under conditions favourable for network development, chemical hydrogels can be generated in this way without the need for removal of methyl or acetyl esters. Such reactions require the generation of free radicals and the use of an effective oxidizing system such as (ammonium) persulfate (Guillon and Thibault, 1987; Guillon and Thibault, 1990; Oosterveld et al., 2000b; Thibault et al., 1987; Thibault and Rombouts, 1986), peroxidase enzymes in combination with hydrogen peroxide (Norsker et al., 2000; Zaidel et al., 2012; Oosterveld et al., 2000b) or laccases (Micard and Thibault, 1999; Kuuva et al., 2003; Norsker et al., 2000; Zaidel et al., 2012). In all cases, the oxidation of polymer bound *FA* and subsequent coupling of phenoxyl radicals results in cross-linking of pectin chains via *FA* dimers and/or higher ferulate oligomers (Bunzel, 2010). Since *SBP* is known to contain protein, it should be noted that laccases can also catalyze the oxidation of aromatic amino acids such as tyrosine, which has been exploited previously, for example to produce casein-xylan conjugates (Selinheimo et al., 2008) and to crosslink bovine serum albumin via tyrosine dimers (Li et al., 2021)”

A critical number of cross-links is required for the sol-gel (liquid-solid) transition and the efficient formation of a hydrogel. The tendency for network development in *SBP* solutions will therefore depend on the number of *FA* residues and their ability to participate in oxidative coupling reactions. However, not all *FA* residues are necessarily able to participate in cross-linking due to their location within the neutral sugar side chains of *RGI*. The galactan side chains of *SBP* mostly consist of linear β-1,4 linked galactopyranose residues esterified by FA at O-6 (Colquhoun et al.,

1994). In contrast, arabinan side chains are highly branched consisting of a main core of α-1,5 linked arabinofuranose (*Araf*) residues, randomly substituted by individual or short chains of α-1,3 linked *Araf* (Guillon et al., 1989). Within arabinan side chains, *FA* is primarily found to be ester linked to *Araf* residues in the main core at O-2 (Colquhoun et al., 1994). Hence, the presence of neutral sugar branches might sterically hinder the access of enzyme to substrate, or the subsequent coupling of phenoxy radicals. For example, it has been shown that gelation of *SBP* can be promoted following treatment with arabinase enzymes to remove some peripheral *Araf* residues (Guillon and Thibault, 1987; Micard and Thibault, 1999).

To be successfully incorporated into commercial formulations, microgel particles must retain their structural integrity throughout any subsequent manufacturing steps, storage and consumer handling. Thus, chemically acceptable cross-linking might be preferable to physical cross-linking in terms of providing a more stable internal structure and more robust particles. Indeed, the mechanical properties of physically cross-linked gels vary with environmental conditions such as ionic strength, pH and temperature (Djabourov et al., 2013). In the current study we report on the fabrication of *SBP* microgels using a top-down technique involving the mechanical disruption of a chemically cross-linked *SBP* hydrogel. To our knowledge, this is the first example of a covalently cross-linked polysaccharide microgel prepared in this way. For comparison, we also present data for calcium cross-linked *LMP* microgels prepared in a similar fashion and provide insight into how their (long-term) stability can be improved.

3.2 Materials and Methods

3.2.1 Materials

Sugar beet pectin (GENU® Beta Pectin) and amidated low methoxyl citrus pectin (GENU® Pectin LM-104 AS), hereafter referred to as *SBP* and *LMP*, respectively, were a generous gift from CP Kelco (Lille Skensved, Denmark). Laccase Y120 (EC 1.10.3.2) was obtained from Amano Enzyme (Nagoya, Japan). Fluorescein isothiocyanate-dextran (average molecular weight 2 x 106 Da) (*FITC-dextran*), sodium azide and 2,2′-azino-di-(3-ethylbenzthiazoline sulfonic acid) (*ABTS*) were obtained from Sigma Aldrich (Dorset, UK). Crystal violet was obtained from Fluorochem Ltd (Hadfield, UK). Citric acid, trisodium citrate dihydrate,

monosodium phosphate monohydrate and calcium chloride dihydrate were of analytical grade from Sigma Aldrich. Silicone oil with viscosity of 350 centistokes (cSt) and 20 cSt were obtained from VWR International (Paris, France) and BDH Silicone Products (Poole, UK) respectively. Type I (Milli-Q) water (Millipore, Bedford, UK) with a minimum resistivity of 18.2 MΩ.cm was used throughout.

Table 3.1 - Degree of methoxylation (*DM*), degree of acetylation (D_{AC}), degree of amidation (D_{AM}) and molecular weight (*MW*) of *LMP* and *SBP*, as specified by the manufacturer.

Pectin Type	***DM* / %**	**D_{AC} / %**	***D_{AM}* / %**	***MW* / kDa**
GENU LM-104 AS	27	-	20	89.1 ± 3.1*
GENU BETA	55	14 - 26	-	> 60

** – Viscosity average MW determined by (Cheng & Lim, 2004)*

3.2.2 Methods

3.2.2.1 Fabrication of low methoxyl pectin (*LMP*) hydrogels and microgel suspensions

LMP powder was used as supplied and dissolved in 10 mM trisodium citrate solution at a concentration of 2.4 wt.% via magnetic stirring for a minimum of 12 h at room temperature. Sodium azide (0.005 wt.%) was added as a preservative. Trisodium citrate was used to chelate calcium ions thereby slowing down gelation and giving rise to more homogeneous hydrogels. The author notes that this may also have resulted in protonation of non-methyl esterified GalA residues, thereby reducing the number of available crosslinking sites.

LMP and 50 mM $CaCl_2$ solutions were separately decanted into sealed glass containers, transferred to a shaking water bath (OLS Aqua Pro, Grant Instruments, Cambridge, UK) set to 85 °C at 20 rpm and pre-heated for 30 min. Gelation of 25 ml of *LMP* solution was initiated via the 'one-shot' addition of 5 ml of $CaCl_2$ stock solution with gentle shaking to prevent the formation of air bubbles. Containers were sealed and the gelling mixture was allowed to cool to ambient temperature and subsequently refrigerated for a minimum of 12 h. *LMP* hydrogels containing 2 wt.% *LMP*, 8.34 mM $CaCl_2$ and 8.33 mM sodium citrate were subsequently used for the fabrication of *LMP* microgels. These conditions were reached by trial and error until

reproducible, clear, homogeneous gels were obtained without any noticeable syneresis. Higher concentrations of $CaCl_2$ led to visible gel inhomogeneity.

LMP microgel suspensions were prepared via the mechanical disruption of 20% volume fraction of coarse *LMP* hydrogel pieces in the presence of excess solvent, hereafter referred to as the dispersion medium. Two different dispersion media were tested: Milli-Q water and 8.34 mM $CaCl_2$ aqueous solution. Two types of disruption were tested. The first was using a T25 ULTRA-TURRAX (IKA, Oxford, UK) rotor-stator device, equipped with a S25N - 18G dispersing tool (gap between rotor and stator = 0.3 mm) operating at a speed of 10,000 rpm for 10 min. The second disruption method utilized firstly a Silverson blender (Model L5MA, Silverson Machines, Buckinghamshire, UK) equipped with a general purpose disintegrating head, operated at 2000 rpm for 60 s, followed by further disruption by passing the dispersion though a high-pressure valve homogenizer (Panda Plus 2000, GEA Niro Soavi Homogeneizador, Parma, Italy), pre-set with water to operate at 350 bar. The pressure was found to fluctuate slightly during homogenization but did not exceed 500 bar. Samples were passed through this homogenizer a total of 3 times. This second method was an attempt to create smaller *LMP* microgel particles – see Results below. Where microgel suspensions were stored for prolonged periods of time, additional sodium azide was added to give a final concentration of 0.005 wt.% of the preservative.

3.2.2.2 Fabrication of sugar beet pectin (*SBP*) hydrogels and microgel suspensions

The concentrations of *SBP* and laccase used were initially optimised for the generation of homogeneous hydrogels displaying no noticeable syneresis on storage for several days. *SBP* powder was dispersed into water using the T25 ULTRA-TURRAX operating at a maximum speed of 15000 rpm, adding the powder gradually to prevent clumping. *SBP* was left to solubilize for a minimum of 12 h with magnetic stirring in sealed glass jars. The *SBP* solutions were then centrifuged (Eppendorf 5810 R, Stevenage, UK) at 4000 rpm for 60 min in approximately 30 ml aliquots to remove any remaining insoluble material. Laccase stock solutions were freshly prepared by solubilizing the enzyme powder in water for a minimum of 20 min. Then 25 ml of *SBP* solution and 5 ml of laccase stock solution were rapidly combined at ambient temperature by vortex mixing. When the two solutions were

visibly well mixed, hydrogels were allowed to develop quiescently in sealed containers for a minimum of 12 h at 25 °C.

The influence of *SBP* and enzyme concentrations, hereafter referred to as C_{GEL} and C_E respectively, on the mechanical properties of the resulting hydrogels was investigated. In order to determine the actual values of C_{GEL}, the gelation procedure outlined above was simulated by replacing enzyme solutions with water and drying the diluted *SBP* solutions in a vacuum oven (Townson and Mercer Limited, Croydon, England) at 75 °C and a pressure of 600 mm Hg until no change in mass was observed. This technique was preferred over drying the hydrogels and allowed us to account for losses due to: potential incomplete solubilization of *SBP* powder, any insoluble material removed by centrifugation and any water associated with the powder before preparing the solutions. The same drying procedure was also used to determine the overall pectin concentration, C_{PTOTAL}, in any microgel suspensions or *SBP* solutions investigated.

SBP microgels (*SBPMG*) were obtained from parent hydrogels prepared by the addition of laccase at a nominal C_E of 0.1 mg ml^{-1} followed by a 12 h storage period. Unless otherwise stated, *SBP* microgel suspensions were fabricated by blending a 20% volume fraction of the hydrogel with deionized water in the ULTRA-TURRAX rotor-stator, *i.e.*, as for the *LMP* microgels described above. Just one set of *SBP* microgel suspensions was created slightly differently, using the Silverson blender method as used for the *LMP* microgels described above (but without the second stage valve homogenization), for comparison with the results of the ULTRA-TURRAX method and also the *LMP* microgels.

Since sodium azide is a known inhibitor of laccase, it could only be added as a preservative after the fabrication of the microgel suspensions (0.005 wt.%). Hygienic handling of glassware and samples was practiced at all prior stages of production, to minimise any microbial growth.

Centrifugation was used to concentrate the *SBP* microgel suspensions for rheological characterization and investigations via microscopy. Suspensions were centrifuged at 4,000 rpm for 60 min to obtain a pellet of microgel particles and the supernatant was subsequently discarded. C_{PTOTAL} was determined from a diluted sample of the pellet as described above.

3.2.2.3 Equilibrium swelling of *SBP* hydrogels

Approximately 2 ml of a gelling pectin solution, mixed with enzyme to give C_E = 0.1 mg ml^{-1}, was transferred to 5 ml disposable syringes with the tips cut off to act as a cylindrical mould. Syringes were covered with Parafilm® and incubated in an upright position at 25 °C for at least 12 hours. The initial mass (M_0) of the hydrogel was determined to two decimal places by transfer to 50 ml centrifuge tubes containing 15 ml of deionized water at pH 6. The mass (M) of hydrogels after a specified time in contact with the swelling medium was determined after draining excess water from the surface of hydrogel cylinders with filter paper and re-weighing. The 'final' ratio of M/M_0 was defined as the swelling ratio, S. Reported values of S are based on at least two measurements. Due to the delicate nature of these hydrogels, particularly when swollen, it was not possible to track the increase in mass over time on the same hydrogel. Rather, hydrogels were swollen in ‘pairs’, each pair being discarded after measuring M.

3.2.2.4 Enzyme activity assay via UV/VIS spectrophotometry

A Specord® 210 PLUS UV/VIS spectrophotometer (Analytik Jena, Jena, Germany) was used to perform enzyme assays. The relative enzyme activity was measured by monitoring the oxidation of *ABTS* substrate *via* absorbance measurements at λ = 420 nm for 10 min at 25 °C. Disposable cuvettes with a path length of 1 cm were used. The final reaction volume (3 mL) contained 2 mM *ABTS* and (10 μL) of enzyme stock solutions, both of which were prepared in McIlvaine buffer (pH 3).

3.2.2.5 Particle size analysis by laser diffraction

A Mastersizer 3000 equipped with the Hydro EV wet sample dispersion unit (Malvern Instruments, Worcestershire, UK) was used to perform laser diffraction measurements on all pectin microgel samples at ambient temperature (20 °C). After optical alignment and measurement of background scattering, microgel samples were added to the dispersion unit until the laser obscuration reached > 1%. Particle size distributions (*PSD*) are inferred in the Mastersizer software from the angular dependence of scattered light intensity via the Mie theory for spherical particles. As such, knowledge of the optical properties of the dispersant and dispersion medium is required. The Mastersizer dispersion medium was water (refractive index = 1.33). For both *LMP* and *SBP* microgels, a refractive index of 1.35 (Nikolova, Panchev, & Sainov, 2007) and an absorption index of 0.01 was used. Representative *PSD*s are

reported alongside mean values of particle diameter, namely the Sauter (surface weighted) mean diameter $D_{3,2}$ and the volume weighted mean diameter $D_{4,3}$, calculated according to;

$$D_{a,b} = \frac{\Sigma n_i D_i^a}{\Sigma n_i D_i^b} \qquad [3.1]$$

Where n_i is the number of particles of diameter D_i. The width of the *PSD* is reported in terms of the *Span*;

$$Span = \frac{Dv_{90} - D_{v10}}{Dv_{50}} \qquad [3.2]$$

Where Dv_x is the diameter of which x percentage of particles are smaller. All values reported are based on the average of 5 measurements on each individual sample.

3.2.2.6 Microscopy of sugar beet pectin microgel (*SBPMG*) suspensions

A Zeiss confocal laser scanning microscope (*CLSM*) (Model LSM 700, Carl Zeiss Microscopy GmbH, Jena, Germany) with a 40x/NA1.4 oil immersion lens was used to image *SBPMG*. A reverse contrast method was employed whereby *FITC*-dextran (0.1 wt. %), used to stain the continuous phase, was dissolved directly into the microgel suspensions before transfer to microscope well slides for imaging. The wavelengths of excitation and emission used were 488 and 528 nm, respectively. Standard transmission optical microscopy was performed using a Nikon SMZ-2T light microscope (Nikon, Japan) equipped with a 10x objective lens. To improve contrast between the continuous phase and solvent swollen microgel particles, crystal violet was used to stain suspensions by adding a few drops of an 0.5 wt.% crystal violet stock solution to 30 ml of suspension. Stained suspensions were gently stirred for one hour, concentrated by centrifugation and placed in well slides. Images were captured with a digital camera (Leica MC120 HD) and scale bars were added in ImageJ.

For scanning electron microscopy (*SEM*), samples were encapsulated in a 3 wt.% agar gel in a plastic tube. The tube contents were fixed by curing for over 8 h in 3.7 wt.% formaldehyde solution. The aqueous phase was then replaced by ethanol *via* successive immersion in baths with increasing ethanol concentration (10 %, 30 %, 50 %, 70 %, 90 % and 100 %). The sample was then dried by immersion in supercritical CO_2, followed by release to atmospheric pressure. The sample tubes

were cut transversely, and the thin sections glued onto an *SEM* stub and coated with a 10 nm gold layer, then imaged in low vacuum mode *via* a Quanta F200 Scanning Electron Microscope. This *SEM* sample preparation has been validated elsewhere (Allan-Wojtas and Kalab, 1984; Kalab, 1988).

3.2.2.7 Rheology of *SBP* solutions, hydrogels and *SBPMG* suspensions

An Anton Paar MCR 302 (Anton Paar GmbH, Graz, Austria) rheometer was used for all shear rheology experiments and all raw data were analyzed in the RheoCompass software. For gelation kinetics, a small volume of the *SBP* + laccase solution was immediately transferred to the gap between a 50 mm parallel plate measuring set (*PP50*), with the gap set to 1 mm. The measurement geometry was covered by a custom-made circular plastic hood with dampened kitchen roll fixed to its inner circumference to prevent solvent evaporation. For experiments > 80 min long, 350 cSt silicone oil was used as a solvent trap in addition to the hood. Dynamic viscoelasticity was monitored with time (*t*) at 25 °C at a frequency of 1 Hz and a strain amplitude of 0.1 % (well within the linear viscoelastic region (*LVER*) of the final hydrogels - data not shown). Data were recorded every 30 s for 60 to 240 min. Amplitude sweeps (at 1 Hz) were also performed on some hydrogels as they formed *in situ*.

Flow curves for *SBP* solutions were measured at 20 °C using a cone-plate measuring set (*CP75*): 75 mm diameter cone, 1° cone angle and 151 μm gap. A 20 cSt silicone oil solvent trap was used to prevent solvent evaporation. Samples were pre-sheared at a shear rate of 50 s^{-1} for 30 s, left at rest for 5 min, then a logarithmic shear stress ramp applied with 10 data points recorded per decade on reaching steady state or after a maximum duration of 5 min at each applied stress.

The *PSD* of the *SBPMG* precluded the use of the same cone-plate measuring set to measure the rheology of these dispersions. Roughened parallel plates (50 mm diameter) were used, since wall-slip appeared to be an issue in preliminary measurements around the apparent yield stress of some dispersions when using smooth plates (data not shown). The plates were roughened by gluing water-resistant silicon carbide sandpaper (600 grit, from 3M) to both the upper and lower plates *via* a multi-purpose silicone rubber sealant (Dow Corning 732), followed by curing for a minimum of 12 h. The sample was loaded and the gap set to 1 mm. Samples were

then pre-sheared at a shear rate of 50 s^{-1} for 30 s, left at rest for 15 min, then a logarithmic shear stress ramp applied as above for the *SBP* solutions.

3.3 Results and Discussion

3.3.1 Low methoxyl pectin microgels

Calcium cross-linked *LMP* microgels were prepared as described in Section 3.2.2.1, using two different dispersion media: pure water and 8.34 mM $CaCl_2$ aqueous solution. Note that the [Ca^{2+}] in the latter matches that used to form the hydrogels in the first place. It was expected that the different media would induce different degrees of microgel swelling, by analogy with bulk gels (Djabourov et al., 2013). In particular, *LMP* hydrogels physically cross-linked via Ca^{2+}, when placed in pure water or NaCl solutions, can undergo pronounced swelling that progressively leads to complete gel dissolution as the cross-linking multivalent cations are replaced with monovalent cations from the bulk (Sriamornsak and Kennedy, 2008).

Figure 3.1 shows the *PSD* of the *LMP* microgels and Table 3.2 gives the corresponding characteristics of these *PSD*s. Figure 3.1A shows the *PSD* of the *LMP* microgels created via the ULTRA-TURRAX in 8.34 mM $CaCl_2$, dispersed in the Mastersizer tank (in water) and measured after 1 and 60 min. During this time there was a distinct shift in the *PSD* to lower sizes, as reflected in the mean particle sizes in Table 3.2. Further analysis of the changes in a diluted dispersion of these particles was carried out during the laser diffraction measurement of their size distribution (Figure 3.1B). The evolution of the size distribution and the laser obscuration of the sample over 60 min shows an apparent increase followed by a substantial decrease. These changes were attributed to the initial swelling of the *LMP* microgels in water, followed by their dissolution. The bulk *LMP* hydrogels were observed to swell significantly over 24 h when incubated in excess water at room temperature (data not shown). It is likely that the sodium citrate, included as a Ca^{2+} chelating agent to slow down and assist in the production of homogeneous *LMP* hydrogels, increased this swelling, as previously observed by others (Gombotz and Wee, 1998).

Figure 3.2 shows the *PSD* of *LMP* microgels created via the two step Silverson blender + valve homogenizer method, with Milli-Q water or 8.34 mM $CaCl_2$ as the dispersion medium during fabrication of the microgels. Much smaller particle sizes were obtained (D_{90} = 1.17 μm) when the microgels were fabricated in water with a

reasonably narrow, monomodal *PSD* (Span = 0.963). However, because of the previous results in Figure 3.1 described above, it is not clear if this *PSD* represents microgels that were created in this size range in the homogenizer, or microgels that have rapidly undergone significant dissolution in water, due to a smaller initial size and therefore much higher surface are to volume ratio (McClements, 2017).

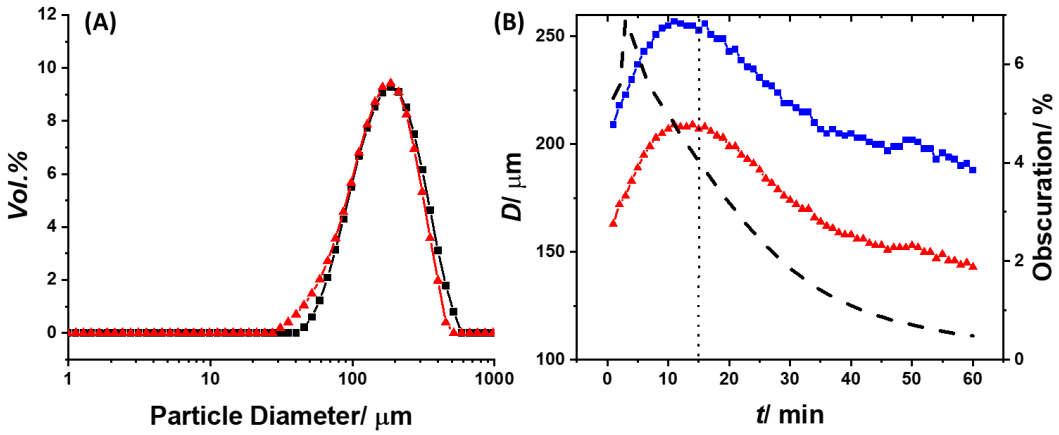

Figure 3.1 - (A) *PSD*s obtained from laser diffraction for *LMP* microgels physically cross-linked via 8.34 mM Ca^{2+} prepared via the ULTRA-TURRAX in 8.34 mM $CaCl_2$, dispersed in the Mastersizer tank (in water) and measured after 1 min (■) and 60 min (▲). (B) Shows values of $D_{3,2}$ (▲) and $D_{4,3}$ (■) as a function of time for the same measurements. Also shown is the corresponding change in the % laser obscuration (dashed curved line) with time. Each individual measurement took 1 min. The changes to the left of the vertical dotted line are assumed to represent swelling of the microgels; to the right, their dissolution.

On the other hand, Figure 3.2 also shows that, when the same two step Silverson blender + valve homogenizer method is used but the hydrogel is broken down to microgels in 8.34 mM $CaCl_2$ (*i.e.*, the same [Ca^{2+}] used to cross-link the parent hydrogel), a *PSD* at much larger particles sizes is observed. In fact, this *PSD* is similar to that obtained with the ULTRA-TURAX only and the $D_{3,2}$, $D_{4,3}$ and D_{90} are only slightly smaller as a result of the two step method (see Table 3.2). More importantly, this *PSD* did not change over time. The data in Table 3.2 corroborates that the mean particle size and *Span* are much larger than for the *LMP* microgels dispersed in water - some particles were even visible to the naked eye and these persisted for at least 7 days. Furthermore, the residuals value was much smaller, suggesting a better measurement quality (Table 3.2). These measurements likely

represent the *PSD* of the microgels in their most swollen state, assuming no dissolution has already taken place. The apparent *PSD*s could also be influenced by the presence of naturally occurring molecular aggregates often found in these systems (Berth et al., 1994; Smith and Stainsby, 1977; Sorochan et al., 1971). For the calcium cross-linked pectin microgel particles fabricated by Saavedra Isusi et al. (2019), a wet milling procedure resulted in a larger particle size (and therefore lower surface area to volume ratio) when compared to the microgels prepared via the valve homogenization in our study. The authors stated that their microgel particles resisted swelling over a period of 24 h, although no data was provided (Saavedra Isusi et al., 2019).

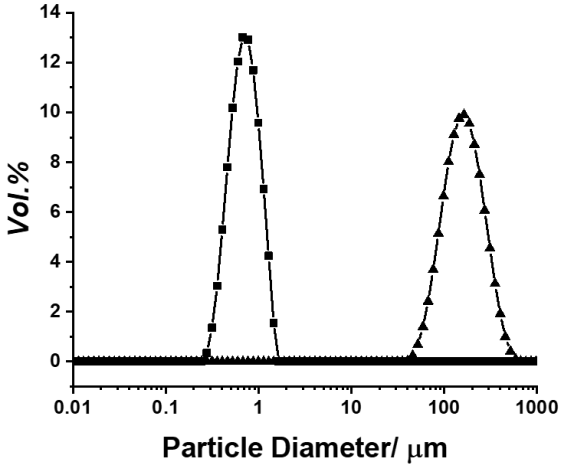

Figure 3.2 - *PSD*s for *LMP* microgels prepared via Silverson and Valve Homogenizer in Milli-Q water water (■) or 8.34 mM $CaCl_2$ (▲), dispersed in Mastersizer tank (in water) and measured after 1 min.

All in all, the data suggest that it is difficult to conclude whether the *PSD*s in water represented swollen but highly dissolved *LMP* microgels or *LMP* molecular aggregates. On the other hand, the *PSD*s in the more Ca^{2+}-rich dispersion medium seemed more likely to represent 'true' microgel particles, since this dispersion medium apparently prevented the *LMP* microgel particle dissolution. It should also be noted that bulk *LMP* hydrogels immersed in 8.34 mM CaCl2 for 24 h at room temperature did not visibly swell (data not shown). Clearly, the high pressure homogenization must break some junction zones in converting the macro-sized gel pieces to microgels, but it is also possible in the high shear conditions that junction zones within the nascent microgels particles are momentarily disrupted but rapidly

reform (in the same or different location), since the released Ca^{2+} ions will still be in the vicinity. This will affect the final form and mechanical properties of the microgel particles, so that the latter might be significantly different from the original bulk gel. However, this will be difficult to prove unless micromechanical measurements on individual microgel particles were made, which is beyond the scope of this study.

Table 3.2 - Particle size distribution measures obtained from laser diffraction measurements of *LMP* microgels formed from bulk *LMP* hydrogels cross-linked via 8.34 mM $CaCl_2$.

Dispersion method	Dispersion medium during microgel formation	Time in Mastersizer tank / min	$D_{3,2}$ / µm	$D_{4,3}$ / µm	D_{90} / µm	Span	Residual / %
UltraTurrax only	8.34 mM $CaCl_2$	1	163	209	355	1.39	0.8
UltraTurrax only	8.34 mM $CaCl_2$	60	143	188	319	1.38	0.9
Silverson + valve homogenizer	Milli-Q water	1	0.69	0.78	1.17	0.963	32.4
Silverson + valve homogenizer	8.34 mM $CaCl_2$	1	151	190	319	1.354	0.7

In addition, the exact osmotic pressure difference between the inside and outside of the microgels will influence their degree of swelling and how much this disrupts the junction zones. Placing the microgels in more 'salty' solutions could lead to their shrinkage but also to ion exchange and further microgel disruption. Being restricted to tight control of the microgel environment to ensure stability would be a significant challenge for practical applications, which would therefore limit their usefulness. On the other hand, the apparently stable calcium cross-linked *LMP* microgels dispersed in 8.34 mM Ca^{2+} may have some useful applications. For example, transfer to physiological fluids could result in changes in particle swelling making the system a possible candidate for drug delivery (Peppas, 1991). The dissolution of such microgels would almost certainly accelerate on heating, since this is what happens with bulk Ca^{2+} cross-linked hydrogels. This would be a disadvantage if the particles are required to survive pasteurization, but an advantage if simple heating can be used to release materials that they encapsulate. Immersion in higher [Ca^{2+}] might allow further strengthening of the microgel particle surface if

the pectin carboxylate groups are not fully saturated with Ca^{2+} ions. However, this is outside of the scope of this article, which aims to use these physically cross-linked microgels as a comparison for chemically crossed-linked *SBP* microgel particles that are predicted to be more robust.

3.3.2 Sugar beet pectin hydrogels

3.3.2.1 Assay of laccase enzyme activity

Figure 3.3 shows the relative activity of the laccase enzyme preparation used to catalyse the oxidative cross-linking of *SBP* as measured *via* the *ABTS* assay at different nominal enzyme concentrations (C_E). The absorbance (A) over time was linear for all C_E ($R > 0.996$ in all cases). Using the data between 0 and 300 s to calculate reaction rates (dA/dt) gave 1.89, 3.51 and 6.07 x 10^{-3} s^{-1} for C_E = 0.15, 0.30 and 0.50 mg ml^{-1} laccase, respectively, as shown in the inset to Figure 3.3. It was not considered relevant to examine the enzyme kinetics in any more detail, since all that we wished to establish was the approximate relative activity of the enzyme with respect to C_E. The more important data were how different enzyme activities affected the kinetics of *SBP* gelation, as discussed below.

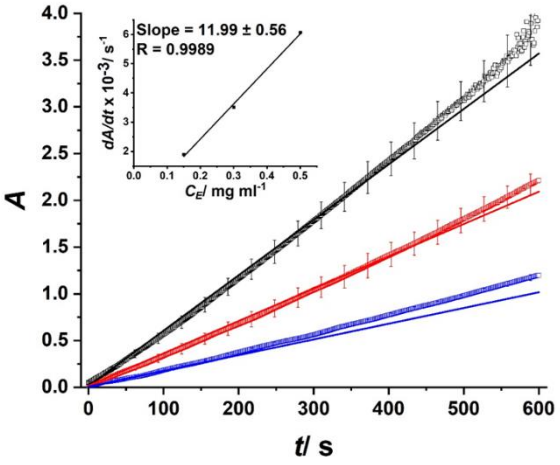

Figure 3.3 - Absorbance (A) vs. time (t) for the assay of enzyme activity measured via oxidation of *ABTS* at λ = 420 nm, for Laccase Y120 enzyme at nominal enzyme concentrations C_E = 0.15 (■), 0.3 (■) and 0.5 (■) mg ml^{-1}. The inset shows the initial rate of *ABTS* oxidation (dA/dt) determined from the gradient of the straight line fit to the data in the first 300 s. Error bars = standard deviation for 3 separate measurements.

3.3.2.2 Gelation kinetics of *SBP* hydrogels

In early studies on *SBP* gelation, the gel state was often evaluated based on a simple qualitative tube inversion test and visual inspection (Micard and Thibault, 1999; Guillon and Thibault, 1990). More recently, rheological techniques have been used to characterize *SBP* hydrogels (Norsker et al., 2000; Kuuva et al., 2003; Oosterveld et al., 2000b; Zaidel et al., 2012) prepared under different conditions. The rate of gelation as well as the final, equilibrium mechanical properties of the *SBP* hydrogels are expected to influence the properties of the corresponding microgels, for example their average particle size and particle elasticity. In small amplitude oscillatory shear experiments, the plateau value of the elastic shear modulus (*G'*) is proportional to the number of intermolecular cross-links (Ross-Murphy, 1995). Thus, studying the evolution of *G'* over time at a constant frequency (1 Hz) and strain amplitude within the *LVER* for the final hydrogels potentially allows one to monitor the rate and extent of cross-linking, which may be affected by both C_{PTOTAL} and C_E. Such experiments also enabled the development of robust protocols to obtain hydrogels compatible with the top-down technique for microgel formation.

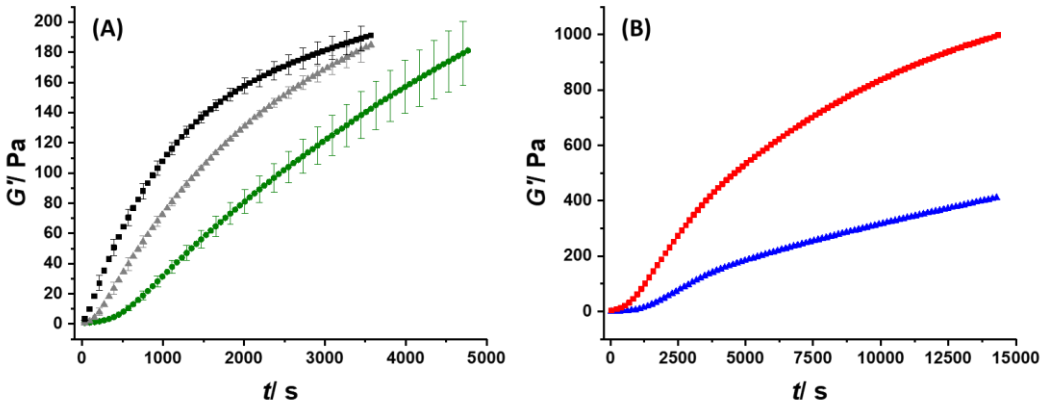

Figure 3.4 - (A) Evolution of *G'* with time for *SBP* hydrogels prepared with C_{GEL} = 2.4 wt.% *SBP* plus C_E = 0.1 (●), 0.2 (▲) and 0.4 (■) mg ml^{-1} laccase. Mean values are shown for 3 separate measurements. For clarity, only every third data point is plotted and error bars (standard deviations) for every three of these data points. (B) Evolution of *G'* with time for *SBP* hydrogels prepared with C_{GEL} = 3.4 (▲) and (■) 4 wt.% *SBP* plus C_E = 0.1 mg ml^{-1} laccase. Every 5th data point is plotted.

Figure 3.4A shows the evolution of *G'* over time for 2.4 wt.% *SBP* hydrogels prepared at different C_E; 0.1, 0.2 and 0.4 mg ml^{-1}, respectively. This figure suggests

that the kinetics of network development are dose-dependent with respect to C_E. The 'final' values of *G'* tended towards a common value of around 200 Pa at the end of the experimental time frame, which suggests that most available ferulic acid residues have been consumed, *i.e.*, the system was approaching the maximum possible cross-linking. Rheological measurements at longer times were difficult due to samples drying out, despite the use of a cover or solvent trap. We therefore attempted to fit the data to a kinetic model that allows 'extrapolation' to a final equilibrium value of *G'* (G'_{inf}). This kinetic model has been successfully applied previously to heat-denatured protein gels setting at constant temperature (Loveday et al., 2011; Gosal et al., 2004):

$$G' = G'_{inf} \exp(-B/t) \qquad [3.3]$$

: where *t* is time and *B* is the kinetic constant, which is lower for faster increase in *G'*. G'_{inf} is a constant that reflects *G'* when $t \rightarrow \infty$ and therefore the exponential terms tends to zero. G'_{inf} and *B* were determined by non-linear regression fits of Equation 3.3 to the data, shown in Figure 3.5.

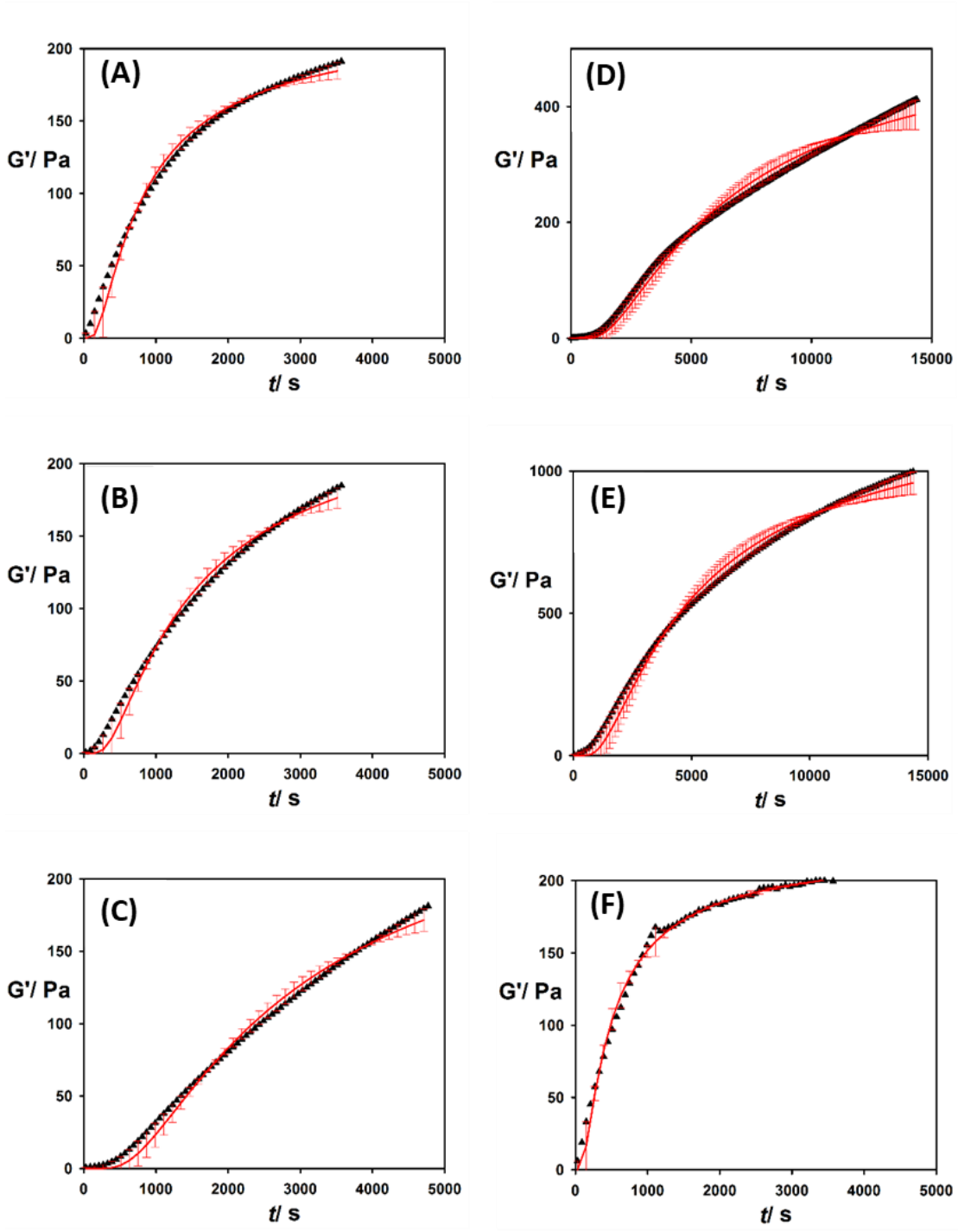

Figure 3.5 - Fits (red data points) of Equation 3.3 to experimental data (black data points). The error bars are the residuals. For clarity, only the fits to every 4th data point are shown. (A) C_{GEL} = 2.4 wt.% plus C_E = 0.4 mg ml^{-1}; (B) C_{GEL} = 2.4 wt.% plus C_E = 0.2 mg ml^{-1}; (C) C_{GEL} = 2.4 wt.% plus C_E = 0.1 mg ml^{-1}; (D) C_{GEL} = 3.4 wt.% plus C_E = 0.1 mg ml^{-1} ; (E) C_{GEL} = 4 wt.% plus C_E = 0.1 mg ml^{-1}. The *SBP* hydrogel in (F) was prepared from a different batch of *SBP* at C_{GEL} = 2 wt.% and corresponds to *SBP* microgels imaged by *CLSM* and *SEM* in Figs. 3.8C and 3.8D, respectively.

Table 3.3 shows the fitted G'_{inf} and B - the residuals were small in all cases (Figure 3.5). For the same C_{GEL} = 2.4 wt.% but 3 different C_E (0.1, 02. and 0.4 mg ml^{-1}) G'_{inf} were similar but decreased slightly with increasing C_E. It has been suggested that, when cross-linking is too rapid, the final cross-link density (and thus the gel strength and G') can be reduced (Zaidel et al., 2012; Kuuva et al., 2003). Indeed, rapid cross-linking can restrict the motion and flexibility of the cross-linked pectin molecules and their neighbours, such that further cross-linking is frustrated. In agreement with this, it was also observed that with C_{GEL} = 2.4 wt.% and C_E > 0.4 mg ml^{-1}, gelation was even more rapid but lower long-time values of G' were obtained (data not shown). Furthermore, such hydrogels exhibited significant syneresis on storage, which is also indicative of a coarser gel network, but also suggested that they were not suitable for producing microgel particles with uniform G'. For this reason, in order to create uniform hydrogels and microgels with a range of different mechanical properties, it is probably best to vary C_{GEL} once an optimum of C_E has been established.

Table 3.3 - Fitted equilibrium dynamic storage moduli (G'_{inf}) and kinetic constant B, according to Equation 3.3 (see Figure 3.5) for the evolution of *SBP* hydrogels at various *SBP* concentrations (C_{GEL}) and laccase concentrations (C_E). R^2 = mean regression coefficient. Also shown are the average particle sizes ($D_{3,2}$, $D_{4,3}$) and *Span* values determined by laser diffraction for the corresponding microgels obtained from these hydrogels.

Concentrations		***SBP* hydrogels**			***SBP* microgels**		
C_{GEL} **/ wt.%**	C_E **/ mg ml^{-1}**	***G'_{inf} / Pa**	***B / s**	R^2	$D_{3,2}$ **/ µm**	$D_{4,3}$ **/ µm**	***Span***
2.4	0.4	223 ± 2	677 ± 13	0.9872	-	-	-
2.4	0.2	250 ± 3	1226 ± 21	0.9898	-	-	-
2.4	0.1	293 ± 3	2515 ± 32	0.9929	16	32	1.78
3.4	0.1	573 ± 3	5662 ± 47	0.9908	37	44	1.14
4	0.1	1286 ± 5	4230 ± 32	0.9918	50	58	1.06

* P < 0.0001 in all cases. ± values are standard errors.

Using both the laccase/O_2 and peroxidase/H_2O_2 oxidizing systems, Zaidel et al. (2012) showed that above a certain enzyme activity, G' tended towards a common value after 20 min, similar to the experimental values in Figure 3.4A. For example,

2.5 wt.% *SBP* + 2 U ml^{-1} laccase resulted in a value of $G' \approx 300$ Pa at t ≈ 20 min. However, the data from Zaidel et al. (2012) showed that *G'* was still increasing slightly after this time, as observed in our results. Using laccases from Trametes hirsute and an *SBP* concentration of 1.5 wt.%, Kuuva et al. (2003) reported similar findings and no plateau in *G'* was reached after 5.5 h. Interestingly, Kuuva et al. (2003) found that at high C_E the addition of $CaCl_2$ slowed down the rate of increase in *G'* but a higher final value of *G'* was reached. It is unclear whether this was due to ionic cross-linking between Ca^{2+} and *HG* regions of *SBP* or an effect of Ca^{2+} on the enzyme activity, although there was no gelation in the absence of enzyme (Kuuva et al., 2003).

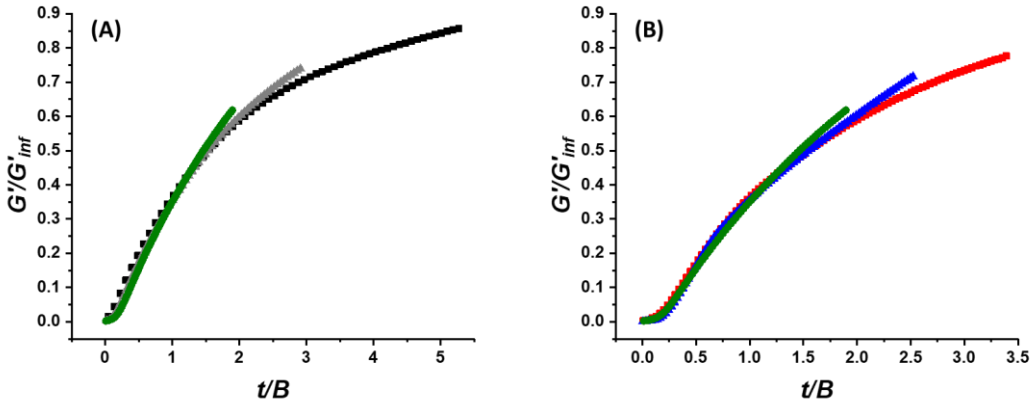

Figure 3.6 - Scaled plots of G'/G_{inf} versus reduced time *t/B* (A) Hydrogels prepared with C_{GEL} = 2.4 wt.% *SBP* plus C_E = 0.1 (●), 0.2 (▲) and 0.4 (■) mg ml^{-1} laccase. (B) Hydrogels prepared with C_{GEL} = 2.4 (●), 3.4 (▲) and 4 (■) wt.% *SBP* plus C_E = 0.1 mg ml^{-1} laccase.

It is seen that C_E mainly affects the gelation kinetics: as C_E increases, this leads to a more rapid increase in *G'*, reflected in a clear trend in the kinetic constant *B*, that is lowest for faster kinetics - see Table 3.3. For example, *B* = 677, 1226 and 2515 s for C_E = 0.4, 0.2 and 0.1 mg ml^{-1}, respectively. Zaidel et al. (2012) also showed that the rate of *SBP* gelation was dose-dependent with the rate of cross-linking increasing with C_E. Table 3.3 shows that the final gel strength is determined largely by C_{GEL} and not C_E at least in this range of concentrations. Indeed, there is a clear and sharp increase in *G'inf* with increasing C_{GEL} at fixed C_E (0.1 mg ml^{-1}) rising from 293 to 1286 Pa between C_{GEL} = 2.4 and 4.0 wt.%, which has been shown previously (Oosterveld et al., 2000b). The trend with C_{GEL} is similar to heat-set protein gels (Ross-Murphy, 1995) but, due to the absence of data points at a wider range of C_{GEL},

we have not attempted to extract a critical gelation concentration (*i.e.*, the minimum pectin concentration for gelation to take place) from these data. Nevertheless, the universality of the gelation mechanism can be illustrated by scaling each *G'* vs *t* curve with the appropriate kinetic constants G'_{inf} and *B*, respectively, as shown in Figure 3.6. Either at fixed C_{GEL} and varying C_E (Figure 3.6A) or fixed C_E and varying C_{GEL} (Figure 3.6B) all the data superimpose very well onto a master curve. This gives added credence to the appropriateness of the model. Gosal et al. (2004) and Loveday et al. (2011) observed the same type of scaling for their data on heat-set protein gels, suggesting that the time-dependent formation of enzyme-driven covalent cross-links proceeds in a similar fashion to the formation of strong bonds between elements of unfolded proteins when forming a network.

3.3.2.3 Equilibrium swelling of *SBP* hydrogels

Figure 3.7 shows that the laccase cross-linked *SBP* hydrogels swelled in water to different extents, depending on C_{GEL}. In contrast to the Ca^{2+} cross-linked *LMP* hydrogels, none of the *SBP* hydrogels dissolved, likely as a result of the permanence of covalent cross-links. Indeed, hydrogel cylinders incubated in 0.005 wt.% sodium azide solution for > 1 month resisted any dissolution and retained their cylindrical shape. The rate and extent of swelling depends on factors such as intermolecular cross-link density, temperature, solvent quality and dilution factor (McClements, 2017). Within experimental error the swelling ratio, *S*, indicated by the dashed horizontal lines in Figure 3.7, was constant after 18 to 24 h and decreased in the order 1.42 < 1.45 < 1.50 for C_{GEL} = 4.0 < 3.4 < 2.4 wt.%, respectively. This observed decrease, in order of increasing G'_{inf}, is expected if the cross-link density increases with C_{GEL}.

The values of *S* were used to calculate the final wt.% concentration of microgel particles, C_{MG}, in any subsequent dispersion from:

$$C_{MG} = 100 \times S \times \frac{C_{PTOTAL}}{C_{GEL}} \qquad [3.4]$$

: where C_{PTOTAL}, the total pectin concentration in a given sample of microgel suspension, was determined by vacuum drying as described for C_{GEL} in section 2.2.2. Note that this calculation assumes that no pectin is lost from the bulk hydrogel in its conversion to microgel particles. Like the *LMP* microgels, equilibrium swelling of the *SBP* microgels was assumed to be reached much more rapidly than the hydrogels, due to their much higher surface area to volume ratio. Certainly,

equilibrium swelling was expected to be achieved within the time before which the microgels were analysed for their particle size and rheological properties (see below) and no significant changes in microgel particle size with time were observed in either the *PSD* measurements or microscopy measurements, as described below.

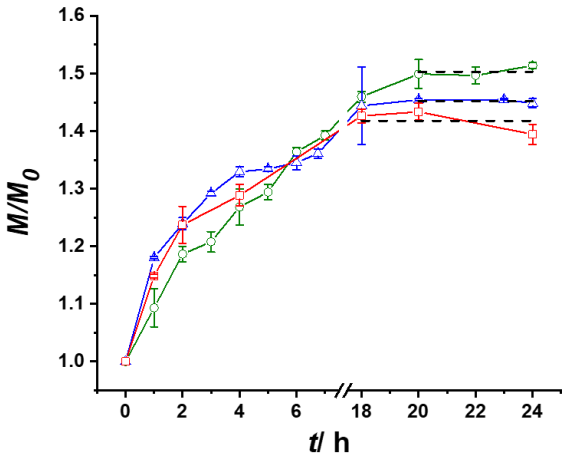

Figure 3.7 - Swelling experiments performed on *SBP* hydrogels prepared with C_{GEL} = 2.4 (●), 3.4 (▲) and 4 (■) wt.% *SBP* plus 0.1 mg ml^{-1} laccase. The mass of the hydrogels relative to their initial mass (M/M_0) is plotted versus time (t) immersed in deionized water at pH 6. The solid lines are to guide the eye and the error bars correspond to the standard deviation based on a minimum of two separate experiments. The dashed horizontal lines show the averages of the final three data points in each case, used to estimate of the final swelling ratio, S (see text).

3.3.3 Sugar beet pectin microgels

3.3.3.1 Characterisation of *SBPMG* via microscopy

Figure 3.8A shows a photograph of a typical free-standing *SBP* hydrogel prior to mechanical disruption. Microgel suspensions imaged via transmission optical microscopy are shown in Figure 3.8B. Addition of crystal violet and concentration of the sample by mild centrifugation was found to improve the image quality (see Section **3.2.2.6**). Highly irregular shaped particles were observed for these microgels, made from C_{GEL} = 2.4 wt.%, *i.e.*, the weakest gel. Alginate-based microgels prepared by fragmenting calcium alginate (macro)gel beads in a commercial food processor were found to have a similar morphology when imaged with light microscopy (Yu et al., 2010). This was also the case for calcium cross-linked *LMP* microgels fabricated by Saavedra Isusi et al. (2019) and the agarose

microgels fabricated by Ellis and Jacquier (2009). On the other hand, polysaccharide microgel particles prepared by a similar top-down disruption of emulsion filled starch hydrogels of higher *G'* (*ca.*, 3 x 10^3 to 6 x 10^3 Pa) showed a much more spherical structure whilst in the same size range (Torres et al., 2017). The average size of the microgels also increased with increasing *G'* of the parent hydrogel. Since the cross-links in starch gels are based on non-covalent interactions, (*i.e.*, hydrogen bonding), possibly the irregular shape of covalently cross-linked *SBP* microgels is a result of stronger cross-links, which likely lead to more random fracture of the hydrogel.

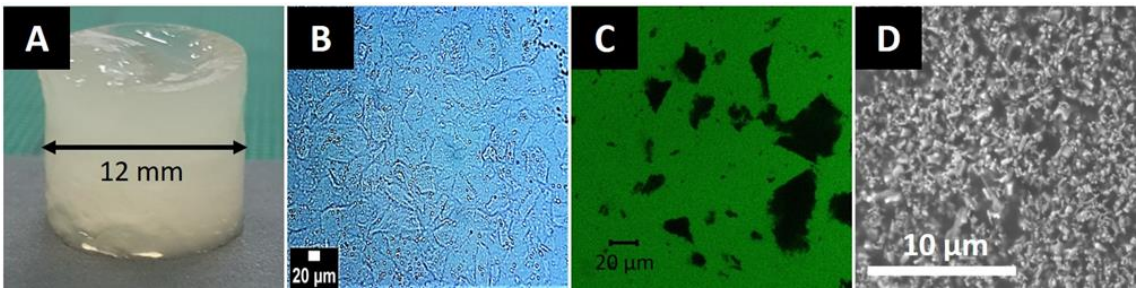

Figure 3.8 - (A) Photograph of a cylinder of *SBP* hydrogel prior to mechanical disruption. (B) Light microscopy image of *SBP* microgels stained by crystal violet. (C) *CLSM* image of *SBP* microgels: microgel particles appear black due to negative staining of the aqueous phase with *FITC*-dextran (green). (D) *SEM* micrograph of *SBP* microgels. Scale bars in (B) & (C) = 20 µm, scale bar in (D) = 10 µm.

CLSM was also used to characterise the microgel samples and provided clear images of the irregular microgel particle structure, as the example in Figure 3.8C shows. Many of the particles seemed to possess flat, smooth sides. Undoubtedly, the interfacial region is more diffuse than this suggests, but such structural features are expected to be well below the resolution of *CLSM*. Scanning electron micrographs of these microgel samples, shown in Figure 3.8D, also seem to preserve this type of morphology, although the average size of the particles was somewhat smaller, with a significant proportion of micron and sub-micron sized particles. It is likely that this apparent difference in size range was a result of the various additional processing steps involved in the *SEM* analysis (see Section **3.2.2.6**). It should also be noted that the images in Figures 3.8C and 3.8D were obtained from a different batch of *SBP* than Figure 3.8B and using a Silverson blender to homogenize the hydrogel (see

Section **3.2.2.2**) - although the final fitted value of *G'inf* (224 ± 2 Pa, see Figure 3.5F) of the gel was almost identical to that in Figure 3.5A (223 ± 2 Pa). A small fraction of particles in this lower size range is suggested in the light scattering measurements of the microgel suspensions made from gels of these *G'*inf values - see next section below. No significant changes in microgel particle size with time were observed in any of the microscopy techniques used.

3.3.3.2 *SBPMG* particle size distributions via laser diffraction

Figure 3.9 shows the *PSD* of *SBP* microgels obtained from parent hydrogels of different C_{GEL}. Table 3.3 shows the various parameters used to describe the resulting *PSD*s, alongside the corresponding hydrogel rheology data discussed above. All microgel suspensions exhibited a *PSD* in which the main peak was between 10 and 100 μm. There is some evidence for a bimodal particle size distribution in the microgels prepared from C_{GEL} = 2.4 wt.%, in the form of a shoulder extending from the major peak to lower particle sizes and a smaller, discrete peak at around 1 μm. It is worth noting that the *SEM* images for this particular sample (Figure 3.8D) also suggested some particles in this lower size range. However, it is also plausible that this peak corresponds to some high molecular weight pectin species or their aggregates, *e.g.*, enzymatically cross-linked pectin components incompletely incorporated into the bulk gel, or liberated from the bulk hydrogel during its comminution. Drying of the pellet and supernatant and comparing this with the known original mass of pectin gel in the sample suggested that if this was the case, these elements represented a minute fraction (*e.g.*, < 1 %) of the total pectin in the system. It has been shown elsewhere that, a more extensive cross-linking in *SBP* hydrogels resulted in a reduced sol fraction and thus a greater yield of cross-linked material (Robertson et al., 2008; Micard and Thibault, 1999). Note that this lower size fraction was only exhibited in the *PSD*s for the microgels prepared from the lowest C_{GEL} = 2.4 wt.% and results in a broadening of the *Span* relative to the (monomodal) *PSD*s for the two stronger hydrogels (see Table 3.3). However, caution should be used in interpreting the *PSD*s since they are calculated via the Mie theory, which assumes spherical particles, whilst Figure 3.8 clearly indicates that this is not the case. Notwithstanding these provisos, Table 3.3 suggests that there is a clear trend for larger particle sizes at the higher C_{GEL} and therefore at the higher the *G'inf, i.e.,* 4 wt.% > 3.4 wt.% > 2.4 wt.%. This suggests that the tougher microgels are harder to break down using the shear procedures employed. Using a combination

of rotor-stator mixing and wet milling, Saavedra Isusi et al. (2019) obtained smaller *LMP* microgels from hydrogels with higher elastic moduli but that had lower yield stresses and strains and the shortest *LVER*. On the other hand, Ellis and Jacquier (2009) found that the average size of agarose microgels increased with increasing polymer concentration in the range 1 to 3 wt.% agarose, but between 4 and 8 wt.% agarose the mean particle size was approximately the same ($D_{3,2} \approx 100$ μm). The authors suggested that this was because, at 3 wt.% agarose and above, the gel yield strain (measured via compression) was approximately the same. Torres et al. (2107) also found that there was a positive correlation between the yield strain (measured via shear rheometry) of their starch-based hydrogels and a larger mean size of the microgels produced from them. Unfortunately, it is difficult to measure or calculate the actual shear stresses and strains applied to the gels in a blender or homogenizer.

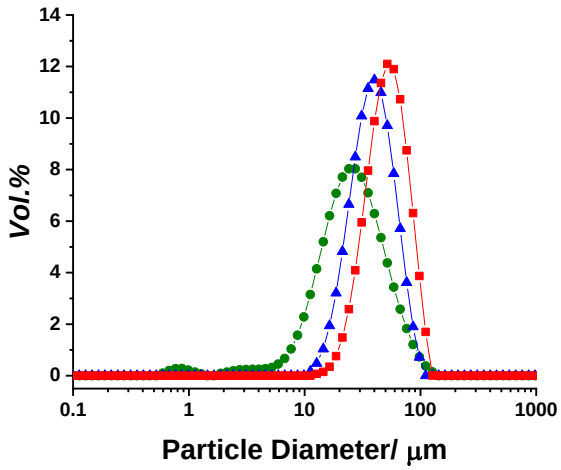

Figure 3.9 - Particle size distributions, as measured by laser diffraction of *SBP* microgels obtained from parent hydrogels prepared with C_{GEL} = 2.4 (●), 3.4 (▲) and 4 (■) wt.% *SBP* + 0.1 mg ml^{-1} laccase.

Oscillatory shear amplitude sweeps were performed on quiescently developed hydrogels allowed to cure for 2 h for C_{GEL} = 2.4 wt.% and for 4 h for C_{GEL} = 3.4 and 4 wt.% *SBP*, *i.e.*, the gels were close to achieving their maximum value of *G'*. (data shown in **Chapter 4**). All 3 gels showed some strain hardening, followed by a sharp decrease in *G'* (and increase in the viscous modulus, *G"*) above a particular strain, *i.e.*, they started to yield. Arbitrarily taking the yield strain and yield stress as the values where the maximum in *G'* occurred, these values were: 84% and 460 Pa for C_{GEL} = 2.4 wt.%, 63% and 747 Pa for C_{GEL} = 3.4 wt.%; 63 % and 853 Pa for

C_{GEL} = 4 wt.%. Therefore, the same correlation between larger particle sizes and higher yield stresses is seen, supporting the preceding discussion. For C_{GEL} = 3.4 wt.% and 4 wt.% no difference in yield strain was observed, but for the weakest gel, *i.e.*, C_{GEL} = 2.4 wt.%, the yield strain was slightly higher, *i.e.*, this gel is slightly less brittle.

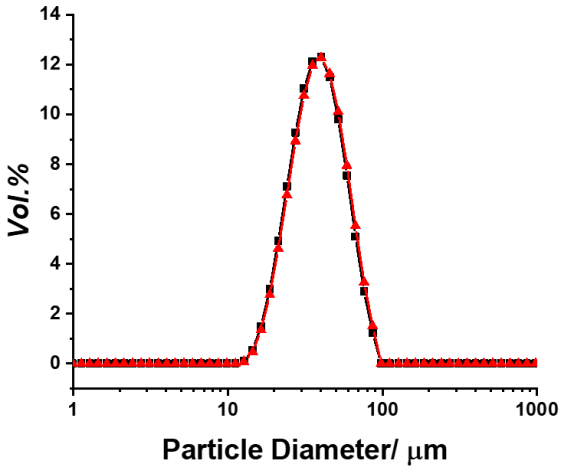

Figure 3.10 - *PSD* of non-heated (■) and heated (▲) *SBPMG* particles (C_{GEL} = 3.4 wt.%). The latter sample was decanted into a plastic falcon tube and heated in a water bath at 85°C for 1 h then cooled to room temperature before re-sizing.

Finally, it was demonstrated that the *SBPMG* seemed perfectly stable to pasteurization-type conditions, at least as far as their *PSD* was concerned. A sample of *SBPMG* (C_{GEL} = 3.4 wt.%) was heated at 85°C for 1 h then cooled to room temperature before re-sizing. There was negligible difference between the *PSD*s before and after the heating procedure, as shown in Figure 3.10.

3.3.3.1 Rheology of *SBPMG* suspensions

A potential application of biopolymer microgels is their use as rheology modifiers in foods. The bulk rheology for such systems is expected to be mainly dependent on the particle volume fraction (ϕ) and shape, though the particle deformability and the potential for inter-penetration will also be important at high ϕ. Characterization of the effective ϕ of microgels requires detailed measurements and modelling at a wide range of C_{MG} and is not the purpose of this current work (although it is the subject of our ongoing investigations). Instead, we wish to highlight the potential of these stable *SBP* microgels for controlling rheological properties.

Figure 3.11 shows viscosity (η) curves as a function of shear stress (σ) for the *SBP* microgel suspensions (C_{GEL} = 2.4 wt.% *SBP*). We describe the systems in terms of C_{MG} as well as C_{PTOTAL}, in order to make comparisons with η of native (*i.e.*, non-cross-linked) *SBP* solutions. The *SBP* solutions showed pronounced pseudoplasticity, with the shear thinning region separated by lower and upper Newtonian plateaus in η. Such behaviour is well known and corresponds to the progressive disentanglement of polymer chains with increasing σ. The stretching and alignment of polymer molecules in the direction of the shear reduces the resistance to flow and thus reduces η (Lapasin and Pricl, 1995). Profound differences were observed in the flow properties of the microgel suspensions when compared to *SBP* solutions at similar C_{PTOTAL}. Most striking is the massive increase in the zero shear viscosity (η_0) at relatively higher σ. The microgel dispersions of C_{PTOTAL} = 0.8 wt.% gave η_0 of the order of 2.3 x 10^4 Pa s. In comparison, native *SBP* solutions prepared at more than double this overall polymer concentration, *i.e.*, the sample with C_{PTOTAL} = 1.7 wt.%, gave an apparent η_0 of only 44 Pa s.

Pseudoplasticity was observed at all C_{MG} but the mechanism is likely to be more complex than the shear thinning behaviour in biopolymer solutions, given that microgels are a hybrid system between a particle and a high *MW* branched polymer molecule. The viscosity curves of the microgel suspensions are more akin to those of so-called ‘structured fluids’ that demonstrate a clear yield stress. The η_0 Newtonian plateau is attributed to creeping flow of the suspensions until a critical stress is reached, at which point the suspensions yield strongly and begin to flow, as characterised by a decrease in η by several orders of magnitude over a narrow range of σ (Barnes, 1999).

Viscosity curves for microgel suspensions were performed in triplicate using a new sample loading for each and it is worth mentioning that the η versus σ curves were, within experimental error, completely reversible on repeating the measurement on the same sample. Figure 3.12 demonstrates this, for a sample at C_{PTOTAL} = 1.1 wt.%, C_{GEL} = 3.4 % *SBP*, where repeated measurement cycles on the same sample but at decreasing gap widths overlap almost perfectly. This test also suggest that any wall slip was negligible. The error in the measurements was always largest in the region of greatest shear thinning, which by analogy to structured fluids is where the microstructure is most greatly disrupted. Future work, to determine an effective ϕ for these microgel dispersions and an investigation of any time-dependent

rheological properties will allow us to determine whether such systems behave as 'soft glassy/jammed materials' or 'particulate gels'.

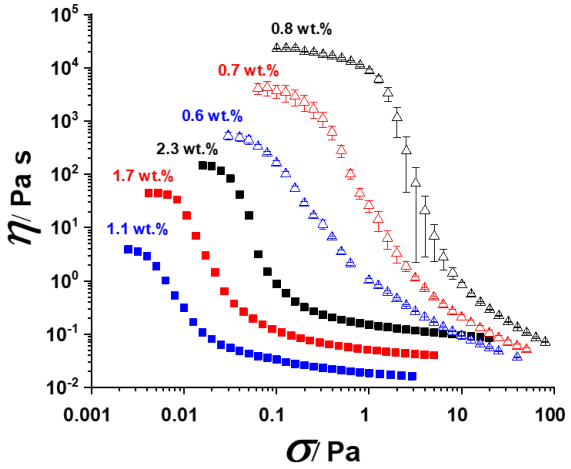

Figure 3.11 - Apparent viscosity (η) as a function of shear stress (σ) for native *SBP* solutions (filled symbols) at C_{PTOTAL} = 1.1 wt.% (■), 1.7 wt.% (■) and 2.3 wt.% (■) and *SBP* microgel suspensions (open symbols) at C_{PTOTAL} = 0.6 wt.% (▲), 0.7 wt.% (▲) and 0.8 wt.% (▲), corresponding to C_{MG} = 37.6, 43.8 and 50.1 wt.%, respectively. The labels on the curves refer to the C_{PTOTAL} values. The microgel suspensions were obtained from parent hydrogels prepared with C_{GEL} = 2.4 wt.% *SBP* + 0.1 mg ml^{-1} laccase and concentrated to the specified C_{MG} by mild centrifugation and appropriate dilution with water. Measurements on microgel suspensions were performed in triplicate using a newly loaded sample for each and error bars = standard deviations. Viscosity curves for *SBP* solutions are based on one measurement.

Another interesting feature of the data in Figure 3.11 is that, despite their 'solid-like' behaviour at low σ, in the range of high σ (> 10 Pa), the microgel suspensions appeared to be still shear thinning and heading for lower η than that of the *SBP* solutions studied. This phenomenon might be a further advantage of *SBPMG* over polysaccharide solutions as thickeners, when material has to mixed, pumped, deposited, *etc.*, at very high shear rates. The highest σ applied to the microgel suspensions corresponds to a shear rate of approximately 1000 s^{-1}, which seemed to be around the maximum accessible shear rate before the microgel samples were ejected from the gap. Therefore, it was not possible to locate a high shear limiting η for the microgel systems. It is possible that the soft microgel particles may change

their shape at high shear, or that water may be squeezed out of them, both of which may result in extra contributions to a reduction in η.

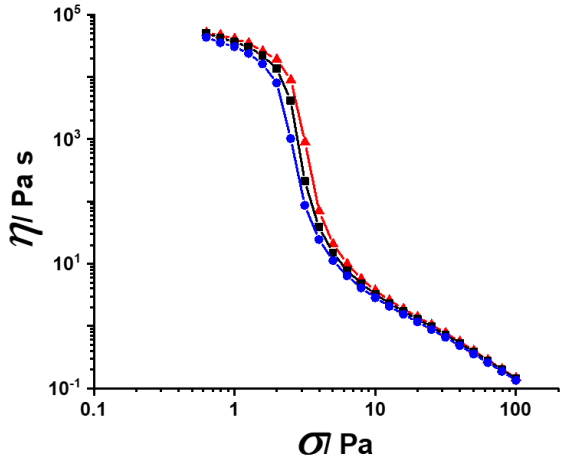

Figure 3.12 - Steady state viscosity curves for C_{GEL} = 3.4 wt.% *SBPMG*'s (C_{PTOTAL} = 1.1 wt.%) at three different gap heights; 1.1 mm (▲), 1 mm (■) and 0.9 mm (●). Each flow curve was performed using the same sample loading at progressively narrower gap heights.

The ULTRA-TURRAX rotor-stator type apparatus is a much simpler method of creating *SBP* microgels than two-stage homogenization, likely to be available much more generally and was seen to generate stable microgel particles with interesting rheological properties. However, in future work we also intend to put such *SBP* gel material through the sort of two stage blender + homogenizer process as initially tested on the *LMP*-Ca^{2+} hydrogels, to see if this generates different sized particles and/or particles with significantly different bulk rheology at equivalent concentrations of the particle sizes studied here. With the *LMP*, this seemed to increase microgel dissolution in water, whereas the *SBP* microgels appear to be perfectly stable in water. Certainly, if the *SBP* microgel particles are surface active, in order to stabilise micron sized emulsion droplets, the stabilizing *SBP* microgels will have to be smaller than those studied here.

3.4 Conclusions

The mechanical disruption of hydrogels in the presence of excess solvent has proven to be a simple and scalable technique to produce microgel suspensions from physically and chemically cross-linked pectin hydrogels. For the former, we have shown how the stability of *LMP* based microgel particles to dissolution can be improved if calcium ions remain in the dispersion medium. However, much more robust polysaccharide-based microgels can be produced from covalently cross-linked *SBP* hydrogels. The latter are of interest for industrial food processing applications because they are resistant to dissolution on prolonged storage in contact with water and can provide a much wider range of viscosities than just solutions of pectin at similar overall pectin concentrations. Furthermore, *SBP* gels cross-linked by laccase are thermally irreversible (Khalighi et al., 2020). The same seems to be true for the *SBP* microgel particles, which will be a clear advantage over other microgel particles, that might dissipate during pasteurization in food applications.

Light scattering measurements suggest that the size (1 to 100 μm) of *SBP* microgels can be tailored via the mechanical properties of the parent hydrogels, which depend strongly on polymer concentration: stronger *SBP* hydrogels lead to larger *SBP* microgels. Microscopy across a range of techniques and magnifications suggested that the microgels consist of highly irregularly shaped particles. Dispersions of between 37 and 50 wt.% *SBP* microgel (equivalent to 0.6 and 0.8 wt.% pectin) were highly pseudoplastic with very high η_0 (approximately 500 to 20,000 Pa s) but extremely shear thinning with increasing σ, with no apparent limiting viscosity up to shear rates of approximately 1000 s^{-1} (the practical limit of measurement). Future work is required to understand the rheology of the *SBP* microgel systems in more detail, in terms of their effective volume fraction, particle deformability and particle interactions. In addition, we hope to demonstrate their use as rheology modifiers and emulsifiers in more complex systems, closer to real foods.

3.5 Acknowledgements

The authors acknowledge excellent technical support from Mark Ambühl and Carine Morgenegg (Imaging Group, Nestle Research Center, Vers-chez-les-Blanc, Switzerland) in obtaining the *SEM* images.

3.6 References

Allan-Wojtas, P. and Kalab, M. 1984. A simple procedure for preparation of stirred yoghurt for scanning electron microscopy. Food Microstructure. 3, pp.197-198.

Barnes, H.A. 1999. The yield stress—a review or ‘παντα ρει’—everything flows? Journal of Non-Newtonian Fluid Mechanics. 81(1), pp.133-178.

Berth, G., Dautzenberg, H. and Hartmann, J. 1994. Static light scattering technique applied to pectin in dilute solution. Part III: The tendency for association. Carbohydrate Polymers. 25(3), pp.197-202.

Braccini, I. and Pérez, S. 2001. Molecular Basis of Ca2+-Induced Gelation in Alginates and Pectins: The Egg-Box Model Revisited. Biomacromolecules. 2(4), pp.1089-1096.

Bunzel, M. 2010. Chemistry and occurrence of hydroxycinnamate oligomers. Phytochemistry Reviews. 9(1), pp.47-64.

Burey, P., Bhandari, B.R., Howes, T. and Gidley, M.J. 2008. Hydrocolloid Gel Particles: Formation, Characterization, and Application. Critical Reviews in Food Science and Nutrition. 48(5), pp.361-377.

Cao, Y. and Mezzenga, R. 2020. Design principles of food gels. Nature Food. 1(2), pp.106-118.

Colquhoun, I.J., Ralet, M.-C., Thibault, J.-F., Faulds, C.B. and Williamson, G. 1994. Structure identification of feruloylated oligosaccharides from sugar-beet pulp by NMR spectroscopy. Carbohydrate Research. 263(2), pp.243-256.

Dickinson, E. 2017. Biopolymer-based particles as stabilizing agents for emulsions and foams. Food Hydrocolloids. 68, pp.219-231.

Djabourov, M., Nishinari, K. and Ross-Murphy, S.B. 2013. Physical Gels from Biological and Synthetic Polymers. Cambridge: Cambridge University Press.

Ellis, A. and Jacquier, J.C. 2009. Manufacture and characterisation of agarose microparticles. Journal of Food Engineering. 90(2), pp.141-145.

Farjami, T. and Madadlou, A. 2017. Fabrication methods of biopolymeric microgels and microgel-based hydrogels. Food Hydrocolloids. 62, pp.262-272.

Fernández Farrés, I. and Norton, I.T. 2014. Formation kinetics and rheology of alginate fluid gels produced by in-situ calcium release. Food Hydrocolloids. 40, pp.76-84.

Fraeye, I., Duvetter, T., Doungla, E., Van Loey, A. and Hendrickx, M. 2010. Fine-tuning the properties of pectin–calcium gels by control of pectin fine structure, gel composition and environmental conditions. Trends in Food Science & Technology. 21(5), pp.219-228.

Gombotz, W.R. and Wee, S. 1998. Protein release from alginate matrices. Advanced Drug Delivery Reviews. 31(3), pp.267-285.

Gosal, W.S., Clark, A.H. and Ross-Murphy, S.B. 2004. Fibrillar β-Lactoglobulin Gels: Part 2. Dynamic Mechanical Characterization of Heat-Set Systems. Biomacromolecules. 5(6), pp.2420-2429.

Grant, G.T., Morris, E.R., Rees, D.A., Smith, P.J.C. and Thom, D. 1973. Biological interactions between polysaccharides and divalent cations: The egg-box model. FEBS Letters. 32(1), pp.195-198.

Guillon, F. and Thibault, J.-F. 1987. Characterization and oxidative cross-linking of sugar beet pectins after mild acid hydrolysis and arabanases and galactanases degradation. Food Hydrocolloids. 1(5), pp.547-549.

Guillon, F. and Thibault, J.-F. 1990. Oxidative cross-linking of chemically and enzymatically modified sugar-beet pectin. Carbohydrate Polymers. 12(4), pp.353-374.

Guillon, F., Thibault, J.-F., Rombouts, F., Voragen, A.G.J. and Pilnik, W. 1989. Enzymic hydrolysis of the “hairy” fragments of sugar-beet pectins. Carbohydrate Research. 190(1), pp.97-108.

Guo, J., Zhou, Q., Liu, Y.-C., Yang, X.-Q., Wang, J.-M., Yin, S.-W. and Qi, J.-R. 2016. Preparation of soy protein-based microgel particles using a hydrogel homogenizing strategy and their interfacial properties. Food Hydrocolloids. 58, pp.324-334.

Ishii, T. and Matsunaga, T. 1996. Isolation and characterization of a boron-rhamnogalacturonan-II complex from cell walls of sugar beet pulp. Carbohydrate Research. 284(1), pp.1-9.

Jiao, B., Shi, A., Wang, Q. and Binks, B.P. 2018. High-Internal-Phase Pickering Emulsions Stabilized Solely by Peanut-Protein-Isolate Microgel Particles with Multiple Potential Applications. Angewandte Chemie International Edition. 57(30), pp.9274-9278.

Joye, I.J. and McClements, D.J. 2014. Biopolymer-based nanoparticles and microparticles: Fabrication, characterization, and application. Current Opinion in Colloid & Interface Science. 19(5), pp.417-427.

Kalab, M. 1988. Encapsulation of viscous food in agar gel tubes for electron microscopy. Food Microstructure. 7, pp.213-214.

Khalighi, S., Berger, R.G. and Ersoy, F. 2020. Cross-Linking of Fibrex Gel by Fungal Laccase: Gel Rheological and Structural Characteristics. Processes. 8(1), p16.

Kuuva, T., Lantto, R., Reinikainen, T., Buchert, J. and Autio, K. 2003. Rheological properties of laccase-induced sugar beet pectin gels. Food Hydrocolloids. 17(5), pp.679-684.

Lapasin, R. and Pricl, S. 1995. Rheology of polysaccharide systems. Rheology of Industrial Polysaccharides: Theory and Application. First edition ed. Glasgow, UK: Blackie Academic and Professional.

Li, Y., Su, J. and Cavaco-Paulo, A. 2021. Laccase-catalyzed cross-linking of BSA mediated by tyrosine. Int J Biol Macromol. 166, pp.798-805

Loveday, S.M., Su, J., Rao, M.A., Anema, S.G. and Singh, H. 2011. Effect of Calcium on the Morphology and Functionality of Whey Protein Nanofibrils. Biomacromolecules. 12(10), pp.3780-3788.

Luzio, G.A. and Cameron, R.G. 2008. Demethylation of a model homogalacturonan with the salt-independent pectin methylesterase from citrus: Part II. Structure–function analysis. Carbohydrate Polymers. 71(2), pp.300-309.

Matsumiya, K. and Murray, B.S. 2016. Soybean protein isolate gel particles as foaming and emulsifying agents. Food Hydrocolloids. 60, pp.206-215.

Matthew, J.A., Howson, S.J., Keenan, M.H.J. and Belton, P.S. 1990. Improvement of the gelation properties of sugarbeet pectin following treatment with an enzyme

preparation derived from Aspergillus niger — Comparison with a chemical modification. Carbohydrate Polymers. 12(3), pp.295-306.

May, C.D. 1990. Industrial pectins: Sources, production and applications. Carbohydrate Polymers. 12(1), pp.79-99.

McClements, D.J. 2017. Designing biopolymer microgels to encapsulate, protect and deliver bioactive components: Physicochemical aspects. Advances in Colloid and Interface Science. 240, pp.31-59.

Micard, V. and Thibault, J.-F. 1999. Oxidative gelation of sugar-beet pectins: use of laccases and hydration properties of the cross-linked pectins. Carbohydrate Polymers. 39(3), pp.265-273.

Murray, B.S. 2019. Microgels at fluid-fluid interfaces for food and drinks. Advances in Colloid and Interface Science. 271, p101990.

Norsker, M., Jensen, M. and Adler-Nissen, J. 2000. Enzymatic gelation of sugar beet pectin in food products. Food Hydrocolloids. 14(3), pp.237-243.

Oosterveld, A., Beldman, G., Searle-van Leeuwen, M.J.F. and Voragen, A.G.J. 2000a. Effect of enzymatic deacetylation on gelation of sugar beet pectin in the presence of calcium. Carbohydrate Polymers. 43(3), pp.249-256.

Oosterveld, A., Beldman, G. and Voragen, A.G.J. 2000b. Oxidative cross-linking of pectic polysaccharides from sugar beet pulp. Carbohydrate Research. 328(2), pp.199-207.

Pelton, R. and Hoare, T. 2011. Microgels and Their Synthesis: An Introduction. In: Fernandez-Nieves, A., et al. eds. Microgel Suspensions. Germany: Wiley-VCH, pp.1-32.

Peppas, N.A. 1991. Physiologically Responsive Hydrogels. Journal of Bioactive and Compatible Polymers. 6(3), pp.241-246.

Pippen, E.L., McCready, R.M. and Owens, H.S. 1950. Gelation Properties of Partially Acetylated Pectins2. Journal of the American Chemical Society. 72(2), pp.813-816.

Ralet, M.-C., Cabrera, J.C., Bonnin, E., Quéméner, B., Hellìn, P. and Thibault, J.-F. 2005. Mapping sugar beet pectin acetylation pattern. Phytochemistry. 66(15), pp.1832-1843.

Renard, C.M.G.C., Crépeau, M.-J. and Thibault, J.-F. 1995. Structure of the repeating units in the rhamnogalacturonic backbone of apple, beet and citrus pectins. Carbohydrate Research. 275(1), pp.155-165.

Robertson, J.A., Faulds, C.B., Smith, A.C. and Waldron, K.W. 2008. Peroxidase-Mediated Oxidative Cross-Linking and Its Potential To Modify Mechanical Properties in Water-Soluble Polysaccharide Extracts and Cereal Grain Residues. Journal of Agricultural and Food Chemistry. 56(5), pp.1720-1726.

Ross-Murphy, S.B. 1995. Rheological Characterisation of Gels. Journal of Texture Studies. 26(4), pp.391-400.

Saavedra Isusi, G.I., Karbstein, H.P. and van der Schaaf, U.S. 2019. Microgel particle formation: Influence of mechanical properties of pectin-based gels on microgel particle size distribution. Food Hydrocolloids. 94, pp.105-113.

Sarkar, A., Murray, B., Holmes, M., Ettelaie, R., Abdalla, A. and Yang, X. 2016. In vitro digestion of Pickering emulsions stabilized by soft whey protein microgel particles: influence of thermal treatment. Soft Matter. 12(15), pp.3558-3569.

Selinheimo, E., Lampila, P., Mattinen, M.L. and Buchert, J. 2008. Formation of protein-oligosaccharide conjugates by laccase and tyrosinase. J Agric Food Chem. 56(9), pp.3118-3128.

Shewan, H.M. and Stokes, J.R. 2013. Review of techniques to manufacture micro-hydrogel particles for the food industry and their applications. Journal of Food Engineering. 119(4), pp.781-792.

Shewan, H.M., Stokes, J.R. and Smyth, H.E. 2020. Influence of particle modulus (softness) and matrix rheology on the sensory experience of ‘grittiness’ and ‘smoothness’. Food Hydrocolloids. 103, p105662.

Smith, J.E. and Stainsby, G. 1977. Studies on pectins I. Light-scattering and MW. British Polymer Journal. 9(4), pp.284-289.

Sorochan, V.D., Dzizenko, A.K., Bodin, N.S. and Ovodov, Y.S. 1971. Light-scattering studies of pectic substances in aqueous solution. Carbohydrate Research. 20(2), pp.243-249.

Sriamornsak, P. and Kennedy, R.A. 2008. Swelling and diffusion studies of calcium polysaccharide gels intended for film coating. International Journal of Pharmaceutics. 358(1), pp.205-213.

Stokes, J.R. 2011. Rheology of Industrially Relevant Microgels. In: Fernandez-Nieves, A., et al. eds. Microgel Suspensions. Weinheim, Germany: Wiley-VCH, pp.327-353.

Thibault, J.F., Garreau, C. and Durand, D. 1987. Kinetics and mechanism of the reaction of ammonium persulfate with ferulic acid and sugar-beet pectins. Carbohydrate Research. 163(1), pp.15-27.

Thibault, J.F. and Rombouts, F.M. 1986. Effects of some oxidising agents, especially ammonium peroxysulfate, on sugar-beet pectins. Carbohydrate Research. 154(1), pp.205-215.

Torres, O., Tena, N.M., Murray, B. and Sarkar, A. 2017. Novel starch based emulsion gels and emulsion microgel particles: Design, structure and rheology. Carbohydrate Polymers. 178, pp.86-94.

Williamson, G., Faulds, C.B., Matthew, J.A., Archer, D.B., Morris, V.J., Brownsey, G.J. and Ridout, M.J. 1990. Gelation of sugarbeet and citrus pectins using enzymes extracted from orange peel. Carbohydrate Polymers. 13(4), pp.387-397.

Yu, C.-Y., Jia, L.-H., Cheng, S.-X., Zhang, X.-Z. and Zhuo, R.-X. 2010. Fabrication of microparticle protein delivery systems based on calcium alginate. Journal of Microencapsulation. 27(2), pp.171-177.

Zaidel, D.N.A., Chronakis, I.S. and Meyer, A.S. 2012. Enzyme catalyzed oxidative gelation of sugar beet pectin: Kinetics and rheology. Food Hydrocolloids. 28(1), pp.130-140.

Zhang, S., Holmes, M., Ettelaie, R. and Sarkar, A. 2020. Pea protein microgel particles as Pickering stabilisers of oil-in-water emulsions: Responsiveness to pH and ionic strength. Food Hydrocolloids. 102, p105583.

Chapter 4: Pectin-based Microgels for Rheological Modification in the Dilute to Concentrated Regimes *

Abstract

A novel range of microgel particles of different internal cross-linking densities can be created by covalently cross-linking sugar beet pectin (*SBP*) with the enzyme laccase and mechanically breaking down the subsequent parent hydrogels to sugar beet pectin microgels (*SBPMG*) via shearing. The bulk rheological properties of suspensions of the different *SBPMG* were expected to depend on the microgel morphology, elasticity (crosslinking density) and volume fraction respectively. The rheology of both dilute and concentrated dispersions of *SBPMG* were studied in detail via capillary viscometry and shear rheometry, supplemented by information on particle size and shape from static light scattering, confocal microscopy and electron microscopy. For dilute suspensions of *SBPMG*, data for viscosity *versus* effective volume fraction (ϕ_{eff}) falls on a 'master' curve for all 3 types of *SBPMG*. In the more concentrated regime, the softer microgels allow greater packing and interpenetration and give lower viscosities at the same ϕ_{eff}, but all 3 types of microgel give much higher viscosities than the equivalent concentration of 'non-microgelled' pectin. The firmer microgels can be concentrated to achieve elasticities equivalent to the original parent hydrogel. All *SBPMG* suspensions were extremely shear thinning but showed virtually no time-dependence.

*** Published as:** Stubley, S., Cayre, O., Murray, B., Celigueta Torres, I. (2022). Pectin-based microgels for rheological modification in the dilute to concentrated regimes. *Journal of Colloid and Interface Science*, **628**, 684-695. DOI: https://doi.org/10.1016/j.jcis.2022.07.147.

4.1 Introduction

Microgel particles are solvent-swollen, particulate polymer networks spanning colloidal to millimetre dimensions. When prepared as suspensions, microgels have been proposed as novel additives to control the rheological properties of formulations of high solvent content, including pharmaceuticals, home and personal care products, agrochemicals and foodstuffs. The use of gels based upon polymer solutions introduces issues during processing due to the ease of which such gels can irreversibly rupture and fracture. In addition, storage stability may be affected due to molecular rearrangements post-processing, which in turn results in the exclusion of solvent from the gel network in a process known as syneresis (Kavanagh and Ross-Murphy 1998). In contrast, concentrated microgel suspensions are essentially 'solid-like' at rest but can be made to flow on the application of external forces that exceed an apparent yield stress (Seth, Cloitre and Bonnecaze 2006), facilitating their 'processability' (*e.g.,* pumping, molding, layering) and application (*e.g.,* as topical pharmaceutical formulations or for appropriate oral sensations). This is potentially one of the great advantages of microgel particles, which in principle can be fabricated from any gel-forming polymer. The rheology of such systems is mainly dictated by the (effective) volume fraction (ϕ_{eff}) occupied by the particles but also by the particle mechanical properties and particle-particle interactions (Vlassopoulos and Cloitre 2014).

The rheological properties of microgels composed of synthetic polymers have received significant interest in the scientific literature. Heterogeneous polymerization techniques are generally used to copolymerize monofunctional monomers with a suitable crosslinking monomer. Such 'bottom-up' techniques allow for great control over particle size and polydispersity. Synthetic protocols also allow for functionalization of the resulting polymer network for specific applications. For example, stimuli responsiveness, in terms of swelling or contraction due to temperature and/or pH changes, can be integrated through the selection of monomers, such that the particle size (and thus ϕ_{eff}) can be controlled by changes in the environmental conditions (Karg et al. 2019). Consequently, such systems have been used as model systems to study the physics of liquid-solid and solid-solid phase transitions, as reviewed extensively elsewhere (Vlassopoulos and Cloitre 2014; Brijitta and Schurtenberger 2019; Yunker et al. 2014).

In most cases, for microgels and ‘model’ hard spheres respectively, polydispersity in particle size suppresses crystallization. Under these circumstances, the suspension is a disordered fluid until at $\phi \approx 0.58$, a so-called glass transition is observed. A glass refers to a dynamically arrested state of matter. Glassy behaviour persists to $\phi = 0.64$ (*i.e.*, the theoretical random close packing limit of equal sized spheres) although polydispersity and the presence of a ‘soft’ stabilizing layer at the particle surface for microgels and hard-sphere systems (i) complicates the definition of ϕ and (ii) pushes the ϕ required for phase transitions to higher values (Pusey et al. 2009; Royall, Poon and Weeks 2013). Soft particles such as microgels can be compressed and even interpenetrate at high phase volumes. Furthermore, their volume depends on the environmental conditions such as the osmotic pressure and, for stimuli responsive microgels, the solvent quality as noted above. Some authors discuss a jamming transition for colloidal hard spheres at $\phi > 0.64$, however this term is more frequently used to describe dense packings of non-colloidal particles, where Brownian motion is negligible and particles can be packed to such high ϕ that they form permanent contacts. The particle modulus and inter-particle friction then become important for the bulk rheological properties, particularly for the yielding behaviour of the dense suspensions (Seth, Cloitre and Bonnecaze 2006; Vlassopoulos and Cloitre 2014).

More recently, microgels based on biopolymers have emerged as attractive alternatives when taking into account both sustainability considerations and regulations for applications where biocompatibility is key. Biopolymer microgel particles have been fabricated using a variety of techniques (see reviews by Joye and McClements 2014; Farjami and Madadlou 2017; Shewan and Stokes 2013)). Notable examples are those prepared using the emulsion templating technique, whereby an aqueous biopolymer solution is emulsified into an immiscible fluid phase, followed by induction of gelation of the dispersed phase in some manner (Shewan et al. 2021; Shewan and Stokes 2015; Adams, Frith and Stokes 2004). A disadvantage of this method is that microgel recovery from the immiscible continuous phase can be laborious due to the requirement for successive separation and washing steps, which can also damage their original templated geometry. Perhaps more scalable for industrial application is the preparation of so-called shear (fluid) gels, where the biopolymer solution is subjected to controlled shearing as gelation conditions are applied (Garrec, Guthrie and Norton 2013; Caggioni et al.

2007). Under these conditions, gel network development is in competition with network break up due to the imposed flow, resulting in suspensions in which particle size and shape can be manipulated via the shear rate, polymer concentration and gelation kinetics (Norton, Jarvis and Foster 1999). An even more simple and scalable method to fabricate microgel suspensions is via the mechanical break-down of a pre-formed gel in the presence of excess solvent. The particle size and shape resulting from such 'top-down' techniques depend on the shear conditions and the mechanical properties of the original bulk 'parent' gel (Torres et al. 2017; Ellis and Jacquier 2009; Saavedra Isusi, Karbstein and van der Schaaf 2019; Stubley et al. 2021).

Pectin is an anionic heteropolysaccharide extracted from plant cell walls of agro-industrial waste streams. The pectin fine structure is complex and varies depending on the botanical origin and extraction conditions (Thakur et al. 1997). Generically, pectins demonstrate a block copolymer type structure with 3 main regions, namely homogalacturonan (*HG*), rhamnogalacturonan II (*RGII*) and rhamnogalacturonan I (*RGI*). The *HG* and *RGII* backbone is a linear polymer of 1,4-linked α-D-galacturonic acid (*GalA*) with the latter containing heteroglycan side chains (Thakur et al. 1997; Ishii and Matsunaga 1996). The polymer backbone of *RGI* contains *GalA* with periodic rhamnose insertions. The rhamnose residues in this region bear neutral sugar side chains composed of arabinose and galactose (Renard, Crépeau and Thibault 1995). In sugar beet pectin (*SBP*), ferulic acid residues are esterified to the neutral sugar side chains of *RGI* which can be deprotonated by oxidoreductase enzymes (*e.g.*, laccases) (Zaidel, Chronakis and Meyer 2012) or chemical oxidizing agents (*e.g.*, persulfates) (Thibault, Garreau and Durand 1987). The resulting phenoxyl radicals can subsequently react, resulting in covalent crosslinking of *SBP* molecules via ferulic acid dimers and/or higher ferulate oligomers (Bunzel 2010). Where the *SBP* concentration exceeds the polymer overlap concentration and there are sufficient ferulic acid residues available to form a percolated biopolymer network, such reactions lead to gelation. This phenomenon is the basis for the creation of the bulk *SBP* hydrogels that are subsequently sheared into smaller microgel particles in this work.

SBP microgels (*SBPMG*) prepared via this route demonstrate some interesting features which may provide significant advantages for commercial applications. For example, they are thermally stable, resist dissolution on extended storage in contact

with aqueous solvents and appear to be robust to shearing - thus retaining their structural integrity under typical conditions experienced during processing and storage of consumer and industrial formulations (Stubley et al. 2021). In this paper, we describe in detail the bulk rheological properties of these novel *SBPMG*s, starting from an estimation of ϕ_{eff} for particles of different cross-linking density for both low and highly concentrated systems. The latter show remarkably high viscosities, reversible shear-thinning, plus some soft solid-like character at much lower concentrations of biopolymer than the native (*i.e.,* 'non-microgelled') *SBP* solutions. The *SBPMG* are therefore much closer to synthetic microgel systems, but are biocompatible and have great potential for rheological control and/or encapsulation.

4.2 Materials and Methods

4.2.1 Materials

Sugar beet pectin (GENU® Beta Pectin) (*SBP*) was a gift from CP Kelco (Lille Skensved, Denmark). Laccase Y120 (EC 1.10.3.2) was obtained from Amano Enzyme (Nagoya, Japan). Silicone oil with a viscosity of 350 cSt was obtained from VWR International (Paris, France). Type I (Milli-Q) water (Millipore, Bedford, UK) with a minimum resistivity of 18.2 MΩ cm was used throughout.

4.2.2 Methods

4.2.2.1 Fabrication of *SBP* hydrogels

SBP powder was dispersed into cold water using a T25 ULTRA-TURRAX rotor-stator mixing device equipped with an S25N - 18G dispersing tool (IKA, Oxford, UK) at 15,000 rpm. The powder was added gradually to prevent clumping and the resulting stock solutions were subsequently stirred magnetically for a minimum of 12 h in sealed Duran® bottles. *SBP* stock solutions at 3 different *SBP* concentrations (C_{PTOTAL}) were then centrifuged (Eppendorf 5810 R, Stevenage, UK) at 4000 rpm for 60 min in approximately 30 ml aliquots, to separate out any remaining insoluble material. The *SBP* solution supernatant was then carefully decanted and stored in sealed containers prior to further use. Separately, laccase stock solutions were prepared by solubilizing the enzyme powder in water for a minimum of 20 min.

For the generation of hydrogels, 25 ml of *SBP* stock solution and 5 ml of laccase stock solution were rapidly combined at ambient temperature by vortex mixing to give a final enzyme concentration of 0.1 mg ml^{-1} laccase, which was found to reproducibly give rise to homogeneous *SBP* gels. When the two solutions were visibly well mixed, hydrogels were allowed to develop quiescently in sealed containers for a minimum of 12 h by incubation at 25 °C. These hydrogels formed the ‘parent’ hydrogels used for the subsequent fabrication of microgel suspensions. Knowledge of the exact *SBP* concentration within bulk hydrogels (C_{GEL}) was required. In order to account for losses due to: potential incomplete solubilization of *SBP* powder, any insoluble material removed by centrifugation and any water associated with the powder before preparing the solutions, the gelation procedure outlined above was simulated by replacing enzyme solutions with water and drying the diluted *SBP* solutions in a vacuum oven (Townson and Mercer Limited, Croydon, England) at 75 °C and a pressure of 600 mm Hg until no change in mass was observed. This method was found to be more practical than attempting to dry

bulk hydrogels. The same drying procedure was used throughout to determine C_{PTOTAL} in any microgel suspensions studied at a later date. The determination of C_{PTOTAL} allows for the calculation of an ϕ_{eff}, as described below.

4.2.2.2 Fabrication of *SBP* microgel (*SBPMG*) suspensions

SBP microgel suspensions (*SBPMG*) were obtained from parent hydrogels prepared at C_{GEL} = 2.4, 3.4 and 4 wt.% respectively. These were fabricated using the same ULTRA-TURRAX rotor-stator setup described above. The 'parent' hydrogels were firstly broken into coarse lumps with a metal spatula. Secondly, 25 g of these gel pieces were combined with 100 g of water (*i.e.,* suspensions were prepared at a nominal weight fraction of bulk gel to water of 20:80 wt.%) prior to blending in the ULTRA-TURRAX at 10000 rpm for 10 min. Sodium azide (0.005 wt.%) was added as a preservative after the fabrication of the microgel suspensions and to inhibit any further enzyme activity (Johannes and Majcherczyk 2000). In addition, the hydrogels were allowed to develop quiescently for at least 12 hours and we have previously shown (Stubley et al. 2021) that gelation is almost complete after just 4 hours (*i.e.,* there were no detectable changes in the elastic modulus after this time), presumably because all available ferulic acid residues had been consumed leaving no available sites for crosslinking *within* and *between* discrete microgel particles. As explained above, C_{PTOTAL} for microgel suspensions was determined by drying + gravimetric analysis to account for any losses during sample preparation. C_{PTOTAL} can be converted to the concentration of *SBPMG* microgels (C_{SBPMG}) by (Stubley et al. 2021):

$$C_{SBPMG}\ (wt.\%) = 100 \times S \times \left(\frac{C_{PTOTAL}}{C_{GEL}}\right) \qquad [4.1]$$

: accounting for C_{GEL} and the capacity for *SBP* gels (and thus microgels) to swell in the presence of excess solvent, pertinent due to the production technique used. The equilibrium swelling ratio, *S*, is already known from a previous study (Stubley et al. 2021) and values for *S* are shown in Table 4.1. The lower degree of swelling for hydrogels prepared at higher C_{GEL} reflects an increased crosslinking density, since there are more ferulic acid residues present and these are the locus of crosslinking.

4.2.2.3 Particle size analysis of *SBPMG* suspensions

Laser diffraction was performed to determine the particle size of *SBPMG*s prepared at different C_{GEL} via a Mastersizer 3000 equipped with the Hydro EV wet sample dispersion unit (Malvern Instruments, Worcestershire, UK). Suspensions were dispersed into pure water (20 °C) in the stirred measurement cell until the laser obscuration reached > 1%.

Particle size distributions (*PSD*) are inferred in the Mastersizer software from the angular dependence of scattered light intensity via the Mie theory for spherical particles. The Fraunhofer approximation gave good agreement in the calculated particle sizes. We are aware that *SBPMG* are not spherical and thus the *PSD*s are estimates, but complementary imaging suggested the apparent *PSD*s are reasonable (see Figure 4.S1). Mean values of particle diameter, namely the Sauter (surface weighted) mean diameter ($D_{3,2}$) and the volume weighted mean diameter ($D_{4,3}$) are calculated according to:

$$D_{a,b} = \frac{\sum n_i D_i^a}{\sum n_i D_i^b} \qquad [4.2]$$

: where n_i is the number of particles of diameter D_i. These are shown in Table 4.1. The *PSD*s were monomodal but naturally demonstrated some polydispersity.

4.2.2.4 Capillary viscometry of dilute *SBP* solutions and *SBPMG*

Capillary viscometry was performed on dilute *SBP* solutions and also *SBPMG* suspensions in order to estimate ϕ_{eff}. An Ostwald-type U-tube viscometer was used (Reservoir size A, calibration constant, K = 0.003 $mm^2\ s^{-2}$) maintained at 20 ± 0.1 °C in a water bath. The efflux time was measured manually using a digital stopwatch with millisecond resolution. The relative (dynamic) viscosity (η_{rel}) is given by:

$$\eta_{rel} = \frac{\eta_s}{\eta_0} = \frac{K.t_0.\rho_s}{K.t_s.\rho_0} \qquad [4.3]$$

: where t is the efflux time, ρ is the density and the subscripts s and 0 refer to the suspensions/solutions and the pure solvent, respectively. Reported values for η_{rel} are based on the mean efflux times for a minimum of 3 measurements in the same viscometer.

4.2.2.5 Shear rheometry of *SBP* hydrogels and *SBPMG* suspensions

An Anton Paar MCR 302 (Anton Paar GmbH, Graz, Austria) rheometer was used for all shear rheology experiments and the raw data were analyzed in the RheoCompass software. All rheological tests were performed using a 50 mm stainless steel parallel plate measuring set (*PP50*), with the gap set to 1 mm. The measurement geometry was covered by a custom-made circular plastic hood with dampened paper towel fixed to its inner circumference to prevent solvent evaporation in all cases. Unless stated otherwise, the measurement point duration was set to automatic using steady state sensing. Any rheological characterisation of *SBPMG* suspensions were performed using roughened plates, which were prepared by gluing water-resistant silicon carbide sandpaper (600 grit, from 3M) to both the upper and lower plates *via* a multi-purpose silicone rubber sealant

(Dow Corning 732), followed by curing for a minimum of 12 h before use. Roughened measuring sets were found to be important for preventing 'wall slip' for microgel samples in preliminary measurements. For characterisation of *SBP* hydrogels the original smooth plates were adequate.

All frequency sweep measurements were performed at strain amplitudes within the linear viscoelastic region (*LVER*) for the corresponding hydrogels or suspensions. The *LVER* was determined through trial and error during preliminary measurements not presented here. All strain amplitude sweeps were performed at an angular frequency (ω) of ω = 6.28 rad s^{-1}. Strain (γ) amplitude sweeps on *SBP* hydrogels were carried out following the same protocol described above but using scaled down reaction volumes. The *SBP* + laccase solutions were rapidly mixed and immediately transferred to the rheometer gap. Following setting of the gap, hydrogels were allowed to develop quiescently at 25 °C for 2 hours for C_{GEL} = 2.4 wt.% or 4 h for C_{GEL} = 3.4 and 4 wt.% respectively, the curing times selected based on the kinetics of gelation of these systems studied previously (Stubley et al. 2021). Due to the long experimental time, the edge of the sample was sealed with a high viscosity silicon oil (350 cSt) to provide additional protection against sample drying. Logarithmic strain sweeps with 8 data points per decade of γ, between γ = 0.01-100% were employed. In separate experiments, frequency sweeps were also performed commencing after the specified setting times. Logarithmic frequency sweeps with 6 data points per decade between ω = 100 – 0.01 rad s^{-1} were employed. For the rheological characterisation of the *SBPMG* suspensions prepared as described above, the samples were concentrated via mild centrifugation (4000 rpm, 60 min) to obtain a close packed pellet of *SBPMG*s followed by careful removal of the supernatant. The pellet was then diluted with a known amount of pure water and left at rest for 30 min (to allow for swelling/equilibration) in order to investigate the rheological properties in the concentrated regime over a range of ϕ_{eff}. This allowed us to prepare samples reproducibly while avoiding any complicating 'aging' effects which may arise from storing the samples in the concentrated regime. Furthermore, a 'shear rejuvenation' protocol was used prior to any measurements on the *SBPMG* suspensions: samples were pre-sheared at a shear rate of 50 s^{-1} for 30 s and left at rest for 15 min at 20 °C prior to commencing further experiments. Strain amplitude sweeps on *SBPMG* suspensions were performed in triplicate. Logarithmic strain sweeps were used with 8 data points per decade between γ = 0.01-100%. For *SBPMG*s from: (a) C_{GEL} = 2.4 wt.%, logarithmic frequency sweeps with 8 data points per decade between ω = 100 – 0.01 rad s^{-1} were employed, performed in duplicate; (b) C_{GEL} = 4 wt.%, a single sample at ω =

100 – 0.1 rad s^{-1} was employed (*i.e.,* over a slightly reduced ω range to reduce the experiment time, since these suspensions were rather ω-independent at low ω).

For rotational tests on *SBPMG* suspensions (*i.e.,* viscosity measurements), logarithmic shear stress ramps were applied with 10 data points recorded per decade. Data points were recorded on reaching steady state or after a maximum of 5 min at each applied stress, whichever came first. Measurements were performed in triplicate using a new sample loading for each.

4.3 Results and Discussion

4.3.1 Characterization of 'parent' *SBP* hydrogels

Figure 4.1 shows the results of oscillatory shear rheometry experiments performed on hydrogels which were allowed to develop quiescently between parallel plates (*i.e., in situ*) due to the difficulty transferring pre-formed hydrogel discs to the rheometer. Over the range of C_{GEL} used (2.4, 3.4 and 4 wt.%) the kinetics of crosslinking is mostly dictated by the enzyme (laccase) concentration (Stubley *et al.* 2021) whilst the final storage modulus (*G'*) is mainly controlled via C_{GEL}. Strain (γ) amplitude sweeps are shown in Figure 4.1A for gels formed from the 3 different C_{GEL} at a fixed enzyme concentration (0.1 mg ml^{-1} laccase). All 3 gels showed a plateau in both *G'* and the loss modulus (*G"*) up until a strain amplitude of approximately 20%, indicated by the vertical solid line and denoted as the 'yield strain' (γ_y), where deviations from the *LVER* were observed.

The length of the *LVER* therefore appears to be constant with respect to strain, although the corresponding yield stresses (σ_y) differ. Indeed, it was found that for C_{GEL} = 4, 3.4 and 2.4 wt.%, σ_y = 126, 72 and 33 Pa, respectively (see Table 4.1), *i.e.,* higher C_{GEL} led to higher moduli and σ_y, as expected. Comparison between the different systems is straightforward only within the *LVER*, but it is noted that all samples showed some evidence for strain hardening beyond γ_y. Thus, it is likely that the actual stresses required for gel fracture may be substantially higher than these values of σ_y. The sharp decline in *G'* at γ beyond the peak in *G'* and *G''* illustrates the brittle fracture of the gels.

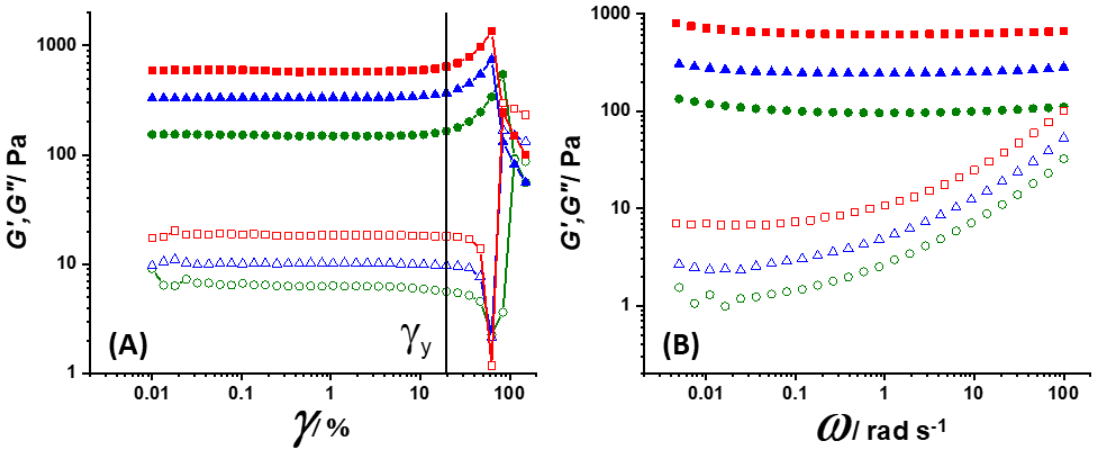

Figure 4.1 - Oscillatory shear rheometry performed on quiescently developed *SBP* hydrogels at C_{GEL} = 2.4 (●), 3.4 (▲) and 4 (■) wt.% *SBP* + 0.1 mg ml^{-1} laccase. Closed symbols = *G'* and open symbols = *G"*. (A) Oscillatory strain amplitude sweeps at ω = 6.28 rad s^{-1}. Coloured lines are to guide the eye. The vertical black line shows the apparent yield strain (γ_y) where *G'* deviates from linearity (B) Oscillatory frequency sweeps at γ = 0.5 %. Experiments began 2 hours (●) or 4 hours (▲) and (■) after gap setting.

Figure 4.1B shows data for frequency sweeps within the *LVER* (γ = 0.5%). From a rheological standpoint, 'true' gel behavior can be defined as a frequency independent plateau in *G'* over an appreciable window in frequency (time), where *G'* >> *G"*, *i.e.*, tanδ = *G"*/*G'* < 0.1 say (Almdal *et al.* 1993). The values of tanδ at ω = 0.01 rad s^{-1} for all samples were < 0.1 and only increased slightly at ω = 100 rad s^{-1} (see Table 4.1) suggesting all 3 could be considered as gels. The increase in tanδ with ω is attributed to increased viscous dissipation due to network defects, for example any trapped sol fraction and dangling polymer chain ends (Mezger 2014; Du and Hill 2018).

The surface weighted ($D_{3,2}$) and volume weighted ($D_{4,3}$) mean particle diameters of the *SBPMG*s produced via the mechanical disruption of the above gels are also given in Table 4.1. The volume weighted particle size distributions were reported previously (Stubley *et al.* 2021). It is seen that the gels with higher *G'* and σ_y gave rise to larger average *SBPMG* sizes. Similar findings have previously been reported for polysaccharide microgels prepared using a comparable 'top-down' approach, although these were gels based on agarose (Ellis and Jacquier 2009) and also low methoxyl pectins physically cross-linked with divalent cations (Saavedra Isusi, Karbstein and van der Schaaf 2019).

Table 4.1 - Elastic modulus (G'), loss factor (tanδ) and yield stress (σ_y) (defined as the shear stress σ at γ_y) measured in oscillatory shear rheology of 'parent' *SBP* hydrogels. The 'swelling ratio', S, was determined from equilibrium swelling experiments on the same hydrogels in a previous study (Stubley et al. 2021). Also shown are the surface weighted ($D_{3,2}$) and volume weighted ($D_{4,3}$) mean particle sizes of the resulting *SBPMG* suspensions determined via laser diffraction measurements.

C_{GEL} /wt.%	$G'_{\omega=0.01}$ /Pa	$G'_{\omega=100}$ /Pa	tan$\delta_{\omega=0.01}$	tan$\delta_{\omega=100}$	σ_y /Pa	S	$D_{3,2}$ /μm	$D_{4,3}$ /μm
2.4	118	110	0.01	0.293	33	1.5 ± 0.01	16.3 ± 0.1	32 ± 0
3.4	275	281	0.008	0.187	72	1.45 ± 0	37 ± 0.1	44.1 ± 0
4	712	662	0.011	0.15	126	1.42 ± 0.02	49.5 ± 0.2	57.9 ± 0.1

In lieu of micromechanical characterization of individual microgel particles, it is usually assumed that the modulus of the microgel particles (referred to as G'_{MG} from hereon) is equal to that of a bulk gel prepared at the same polymer concentration (Adams, Frith and Stokes 2004; Shewan and Stokes 2015). This assumption has recently been shown to be reasonable for agarose microgel particles prepared using an emulsion templating technique with single particle properties then characterized via atomic force microscopy (Shewan *et al.* 2021).

4.3.2 Rheology of dilute *SBPMG* suspensions and estimation of ϕ_{eff}

The main objective for studying the rheological properties of dilute *SBPMG* suspensions was to determine ϕ_{eff}. However, from a technological perspective (*i.e.,* in industrial settings), determination of ϕ_{eff} is not necessarily required and C_{PTOTAL} is a more useful metric to use during formulation. In addition, the C_{PTOTAL} value is useful where ϕ_{eff} is estimated to exceed 1 as a result of the solvent content of the particles and their propensity for inter-penetration (see later). Using C_{PTOTAL} also allows for direct comparison of the microgel suspension properties to the corresponding *SBP* solutions. We will therefore consider the rheological properties of *SBP* microgel suspensions with respect to C_{PTOTAL} where appropriate. For example, Figure 4.2 shows plots of reduced viscosity (η_{red}):

$$\eta_{red} = (\eta_{rel} - 1)/C \qquad [4.4]$$

: against C_{PTOTAL} for native *SBP* solutions (Figure 4.2A) and for *SBP* microgel suspensions obtained from the 3 different parent gels (Figure 4.2B). Extrapolation to $C = 0$ allows one to determine the intrinsic viscosity $[\eta]$ according to:

$$[\eta] = \lim_{c \to 0}(\eta_{red}) \qquad [4.5]$$

: and the corresponding values from Figure 4.2 are shown in Table 4.2, alongside the slope of the curves. For the native *SBP* solutions, $[\eta]$ was found to be 37.6 ± 2.4 dL g^{-1}, in agreement with previous studies (Levigne, Ralet and Thibault 2002; Morris and Ralet 2012). Since microgel particles are cross-linked, supramolecular assemblies of *SBP* molecules, $[\eta]$ is a measure of the specific volume of the particles (with units of volume/mass, dL g^{-1}). It can be observed in Figure 4.2B and Table 4.2 that $[\eta]$ decreases with increasing C_{GEL} and therefore increasing *G', G''* and σ_y (Table 4.1), *i.e.*, the 'softer' microgels demonstrated the highest $[\eta]$. The slope of these plots also follows the same order. Qualitatively, these findings suggest that with respect to C_{PTOTAL}, the softer microgels should be more effective at increasing the viscosity of the solvent with incremental addition of the dispersed material. This is to be expected, as suggested by Omari et al. (2006), who found $[\eta]$ to range from 13.35 to 4.28 dL g^{-1} for colloidal poly(N-isopropylacrylamide) (*p(NIPAM)*) microgels of varying crosslink density, the 'softest' microgels also demonstrating the highest values of $[\eta]$. The same authors also found that $[\eta]$ for linear *p(NIPAM)* was higher (28.4 dL g^{-1}) than any of the microgels composed of the same polymer (Omari *et al.* 2006). Shewan et al. (2015) obtained $[\eta]$ = 12.8 dL g^{-1} for non-colloidal Carbopol suspensions, a commercially available poly acrylic acid microgel (Shewan and Stokes 2015). The $[\eta]$ values reported in Table 4.2 for *SBPMG* therefore seem reasonable.

We note that for C_{GEL} = 3.4 wt.% and C_{GEL} = 4 wt.% the values of $[\eta]$ were almost equal, within the experimental error (24.0 ± 2.6 and 20.3 ± 1.4 dL g^{-1} respectively) whilst for C_{GEL} = 2.4 wt.% $[\eta]$ was significantly larger (54.1 ± 1.1 dL g^{-1}). Considering the results of Omari et al. (2006), the increase in $[\eta]$ suggests a tendency towards linear polymer behavior with increasing particle softness. However, $[\eta]$ for the softest particles presented here was found to be greater even than for the non-gelled *SBP* solutions ($[\eta]$ = 37.6 ± 2.4 dL g^{-1}). This finding suggests (i) the possible presence of some high *MW* aggregates, in effect microgel fragments, released from the softest gel in its conversion to *SBPMG* in addition to 'true' microgel particles or (ii) the presence of particle-particle interactions even at the apparently low particle concentrations used here. Whatever the origin of this

result, in practice it may be exploited to enhance the viscosity above that of simple solutions of *SBP* at the same C_{PTOTAL}.

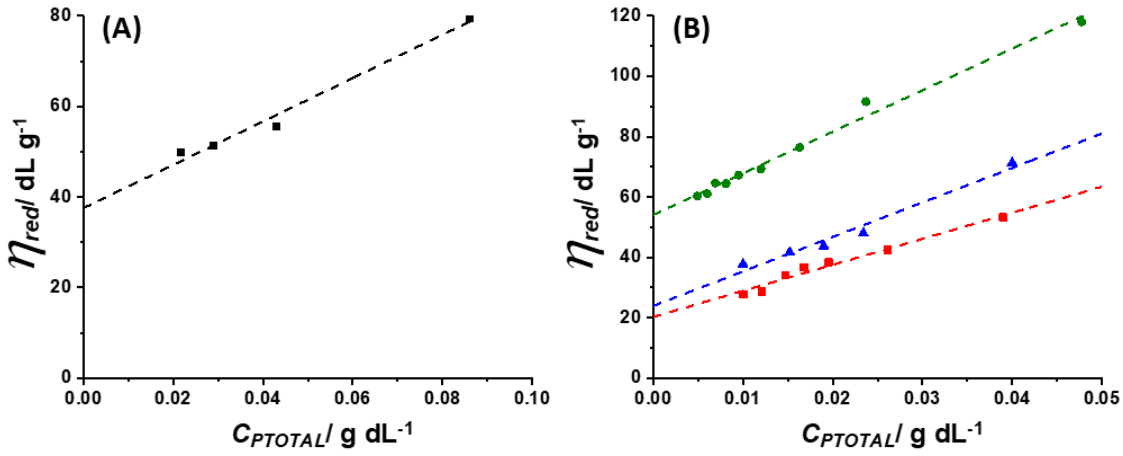

Figure 4.2 - Plots of reduced viscosity (η_{red}) as a function of C_{PTOTAL} for (A) dilute *SBP* solutions and (B) dilute microgel suspensions fabricated via the top-down mechanical disruption of bulk hydrogels C_{GEL} = 2.4 (●), 3.4 (▲) and 4 (■) wt.%. Dashed lines are linear fits to the data. Extrapolation to C_{PTOTAL} = 0 gives the intrinsic viscosity [η] which is shown alongside the slope and coefficient of determination in Table 4.2.

Various complexities arise when interpreting the dilute suspension viscometry data, considering that the *SBPMG*s are *not* spherical (see Figure 4.S1 for images of typical particle morphology). It is well known that the coefficient in the Einstein equation for [η] deviates from 2.5 for particle aspect ratios ≠ 1, due to particle orientation in flow (Mueller, Llewellin and Mader 2010) (which furthermore depends on Péclet number). Particle migration is also known to occur in the flow of non-Brownian suspensions through capillary channels (Nott and Brady 1994). Finally, soft *p(NIPAM)* microgels (Wyss et al. 2010) and swollen starch granules (Desse et al. 2010) have been shown to change their morphology and volume in pressure driven and shear flows respectively, both of which can be experienced in capillary viscometers. While these issues may complicate the rheological analysis and ultimately lead to an overestimation of ϕ_{eff}, capillary viscometry was the best technique available to us to determine the rheological properties of suspensions in the dilute regime. Reassuringly, Figure 4.3A shows that η_{rel} *versus* C_{SBPMG} (calculated according to Equation 4.1) for all 3 types of *SBPMG* appear to fall on a master

curve, indicating that any differences in particle modulus, or minor differences in shape, apparently have a negligible effect on the viscosity in the dilute regime.

Table 4.2 - Intrinsic viscosity [η], slope and R^2 calculated from a linear fit to the data shown in Figure 4.2. Also presented are the calculated values of k and R^2 obtained from fitting of the relative viscosity data shown in Figure 4.3 to the modified Einstein (Equation 4.6) or modified Einstein-Batchelor (Equation 4.7) equations respectively.

	Huggins			**Einstein**		**Einstein-Batchelor**	
Sample	**[η] / dL g^{-1}**	**Slope**	**R^2**	***k* / dL g^{-1}**	**R^2**	***k* / dL g^{-1}**	**R^2**
2.4 wt.% *SBPMG*	54.1 ± 1.1	1375 ± 56	0.989	0.04045 ± 5.7 x 10^{-4}	0.997	0.02939 ± 2.8 x 10^{-4}	0.996
3.4 wt.% *SBPMG*	24.0 ± 2.6	1142 ± 110	0.973	0.03825 ± 1.1 x 10^{-3}	0.993	0.02739 ± 3.2 x 10^{-4}	0.996
4 wt.% *SBPMG*	20.3 ± 1.4	862 ± 64	0.973	0.03224 ± 3.5 x 10^{-4}	0.997	0.02885 ± 3.1 x 10^{-4}	0.995
Native *SBP*	37.6 ± 2.4	478 ± 47	0.981	-	-	-	-

The values of C_{SBPMG} can be converted to ϕ_{eff} by fitting η_{rel} data to both the modified Einstein (Equation 4.6) or modified Einstein-Batchelor (Equation 4.7) equations, respectively, which has become customary for microgel systems (Shewan and Stokes 2015; Mattsson et al. 2009; van der Vaart et al. 2013; Senff and Richtering 2000):

$$\eta_{rel} = 1 + 2.5kC \qquad [4.6]$$

$$\eta_{rel} = 1 + 2.5kC + 5.9kC^2 \qquad [4.7]$$

: where $C = C_{SBPMG}$ and k is a constant that subsequently allows for conversion of C to ϕ_{eff} via:

$$kC = \phi_{eff} \qquad [4.8]$$

: in the absence of inter-particle interactions and assuming spherical, monodisperse particles.

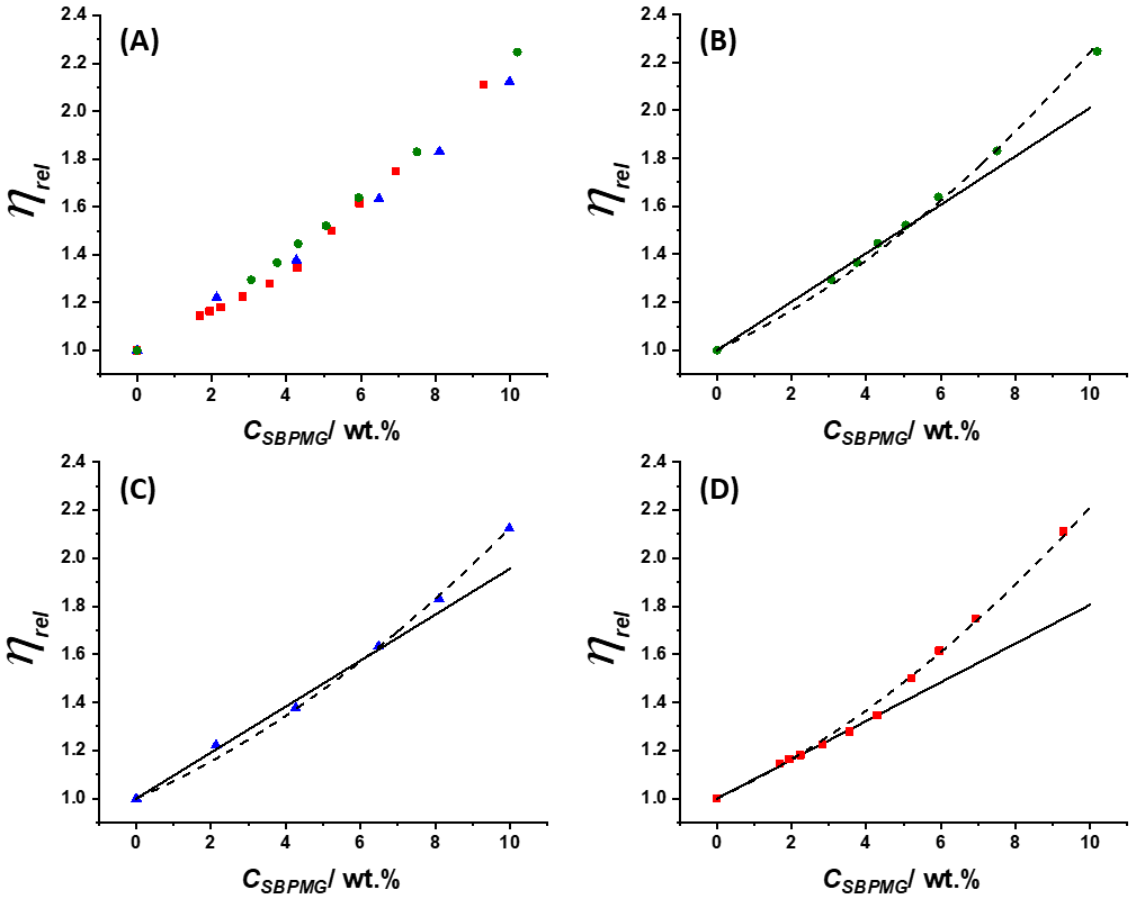

Figure 4.3 - Relative viscosity (η_{rel}) as a function of microgel particle concentration (C_{SBPMG}) for dilute *SBP* microgel suspensions. Equation 4.1 was used to convert C_{PTOTAL} to C_{SBPMG}. (A) All microgel samples prepared from their parent hydrogels C_{GEL} = 2.4 (●), 3.4 (▲) and 4 (■) wt.%. (B-D) Curve fitting to microgel suspensions according to the modified Einstein equation (Equation 4.6, solid lines) or the modified Einstein-Batchelor equation (Equation 4.7, dashed lines) for *SBPMG* samples prepared at (B) C_{GEL} = 2.4 wt.% (C) C_{GEL} = 3.4 wt.% (D) C_{GEL} = 4 wt.%. Calculated values of k and R^2 are given in Table 4.2.

Figure 4.3B and 4.3D shows the lines of best fit to Equation 4.6 in the C_{SBPMG} range of 0 - 5 wt.% and Figure 4.3C in the range 0 - 7 wt.%. Also shown in Figures 4.3B to 4.3D are lines of best fit of Equation 4.7 over the entire data set shown (*i.e.*, C_{SBPMG} up to 10 wt.%). The corresponding fitted values of k are shown Table 4.2. It is seen that, not surprisingly, the modified Einstein-Batchelor equation (Equation 4.7) gives slightly better fits to the data when the higher C_{SBPMG} are included, with correspondingly lower k values. However, as a first approximation we have opted to use the k values from the modified Einstein equation (Equation 4.6) to estimate ϕ_{eff}, in view of the slight uncertainty in the quadratic term of Equation 4.7 and the fact that *SBPMG* particles are not spherical or rigid and that

other complications come to the fore when extrapolating these *k* values to more concentrated microgel dispersions – as discussed below. We simply note here that the *k* values are highest for the microgel particles formed from lowest C_{GEL} and we speculate that this means the microgels formed from the softer gels probably have a more diffuse (or 'hairy') surface than those formed from the stronger gels. For example, other authors (Senff and Richtering 2000) have noted higher *k* values for less densely crosslinked *p(NIPAM)* microgels, which are expected to have a more diffuse interfacial region.

4.3.3 Rotational shear rheometry of concentrated *SBPMG* suspensions

Typical steady state viscosity (η) curves for microgel suspensions prepared from C_{GEL} = 2.4 wt.% are shown as a function of shear stress (σ) in Figure 4.4A and as a function of shear rate ($\dot{\gamma}$) in Figure 4.4B. Repeat measurements were performed using the rheometer in a stress-controlled mode of operation and $\dot{\gamma}$ was calculated according to $\dot{\gamma} = \sigma/\eta$, thus introducing error in the *x*-direction for the $\eta(\dot{\gamma})$ curves. The corresponding viscosity curves for *SBPMG* samples prepared from C_{GEL} = 3.4 wt.% and C_{GEL} = 4 wt.% are shown in Figure 4.S2.

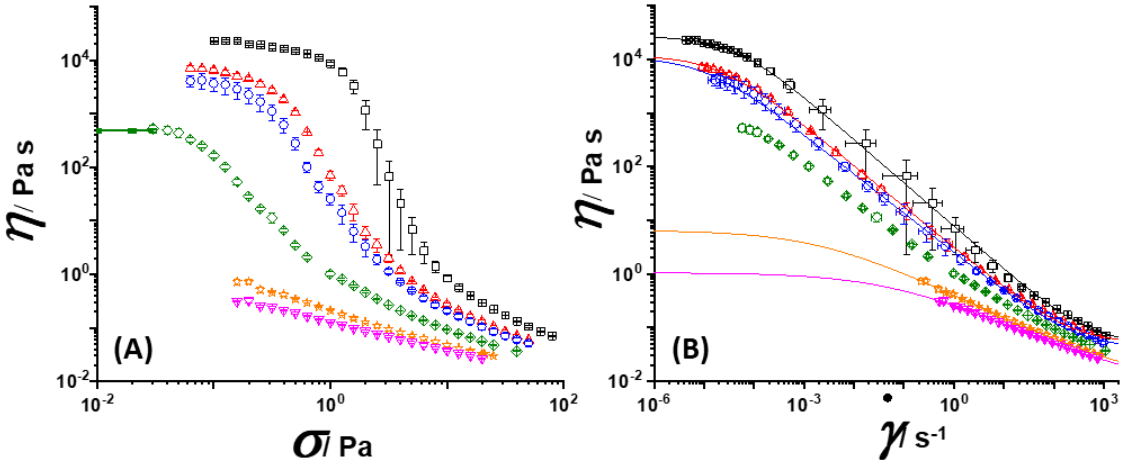

Figure 4.4 - Steady state viscosity (η) curves for concentrated *SBPMG* suspensions (C_{GEL} = 2.4 wt.%) presented as a function of (A) shear stress (σ) and (B) shear rate ($\dot{\gamma}$). ϕ_{eff} for these samples were ■ = 2, ▲ = 1.85, ● = 1.77, ◆ = 1.57, ★ = 1.54 and ▼ = 1.42. Solid lines in 4B are fits to the Cross model (Equation 4.9). Calculated parameters are shown in Table 4.3. The solid line in 4A shows the average η and standard deviation for the first three data points (*i.e.,* data within the pseudo Newtonian plateau). This allows an estimation of the 'zero shear' η where the Cross model cannot be fit to the data.

In most cases, a low shear Newtonian plateau (hereafter referred to as the 'zero shear' viscosity, η_0) is observed where η is essentially independent of σ. This is thought to correspond to creeping flow before a critical σ is reached, at which point the suspensions appear to yield strongly as characterised by a decrease in η by several orders of magnitude over a narrow range of σ. This steep reduction in η has previously been suggested as a hallmark of yield stress fluids (Barnes 1999). However, one may argue that if suspensions flow with a constant η at low σ then a yield stress is, by definition, absent. Indeed, when η is plotted as a function of $\dot{\gamma}$, the corresponding reduction in η appears more gradual. Pseudoplasticity was observed in all cases and η_0 of the order of 10^4 - 10^5 Pa s can be achieved depending on ϕ_{eff} and G'_{MG}. Only in the softest microgel suspensions (Figure 4.4A and 4.4B) is there evidence for the approach to a high shear rate limiting Newtonian plateau (hereafter referred to as the 'infinite shear viscosity' (η_∞)). The η of firmer microgel suspensions appears to continuously decrease with further increases in σ or $\dot{\gamma}$ (Figure 4.S2). The upper σ investigated corresponds to $\dot{\gamma} \approx 1000$ s^{-1} in all cases, which seemed to be the maximum accessible $\dot{\gamma}$ before the samples were ejected from the gap between the parallel plate measuring set. Consequently, only the softest microgel samples could be described by the Cross model (Cross 1965) (Equation 4.9) with the exception of the sample prepared at $\phi_{eff} = 1.57$ (Figure 4.4B):

$$\eta = \eta_\infty + \frac{\eta_0 - \eta_\infty}{1+(K_C\dot{\gamma})^m} \qquad [4.9]$$

: where m is the shear thinning exponent and K_C is the 'consistency' index. This model has previously been used to describe the pseudoplasticity observed in viscosity curves of microgel suspensions (Senff and Richtering 2000; Tan, Pelton and Tam 2010; Garrec, Guthrie and Norton 2013). The fitting parameters are shown in Table 4.3. The shear thinning exponent, m is found to decrease with a reduction in ϕ_{eff} whereas no trend was found in the consistence index, K. The η_0 for all other samples were estimated from the $\eta(\sigma)$ plots by averaging the first 3 data points. The η_∞ were estimated from the $\eta(\dot{\gamma})$ plots using a linear fit to the high shear data in the range $\dot{\gamma} \approx$100-800 s^{-1} and interpolation of η to a value at $\dot{\gamma} = 500$ s^{-1}. Estimates of η_0 and η_∞ (Table 4.3) will be used for a further analysis of the rheological properties of the suspensions described below. The corresponding values of η_0 and η_∞ extracted from the flow curves for $C_{GEL} = 3.4$ wt.% and $C_{GEL} = 4$ wt.% shown in Figure 4.S2 are given in Table 4.S1.

Table 4.3 - Fitting parameters calculated from fitting the Cross model (Equation 4.9) to the data shown in Figure 4.4B. Also shown are the interpolated values of η at $\dot{\gamma}$ = 500 s^{-1}, which are used to compare relative high shear viscosity data for all SBMPG samples shown in Figure 4.5B. For the sample prepared at ϕ_{eff} = 1.57, the Cross model cannot be used and η_0 was estimated from the $\eta(\sigma)$ plots with the average and standard deviation calculated using the first three data points (*i.e.,* data within the pseudo Newtonian plateau) as shown in Figure 4.4A.

ϕ_{eff}	η_0 / Pa s	η_∞ / Pa s	K_C / Pa s	m	η / Pa s ($\dot{\gamma}$ = 500 s^{-1})
2	26959 ± 1215	0.049 ± 0.025	23872 ± 3973	0.809 ± 0.007	0.201 ± 0.003
1.85	11912 ± 1039	0.051 ± 0.003	48886 ± 6989	0.765 ± 0.031	0.105 ± 0.008
1.77	11225 ± 3733	0.041 ± 0.002	94416 ± 55466	0.734 ± 0.010	0.102 ± 0.009
1.57	489 ± 34	-	-	-	0.901 ± 0.001
1.54	6.5 ± 2.55	0.0020 ± 0.0005	459 ± 469	0.448 ± 0.008	0.602 ± 0.002
1.42	1.1 ± 0.20	0.0077 ± 0.0015	0.423 ± 0.017	0.424 ± 0.017	0.052 ± 0.002

The range of ϕ_{eff} apparently tested here was high (ϕ_{eff} > 1 in most cases) (Figure 4.4 and Figure 4.S2). For monodisperse hard spheres, the theoretical maximum random packing fraction, ϕ_{max}, is estimated as ϕ = 0.64. The non-spherical nature, compressibility and polydispersity of particles can all increase ϕ_{max} (Donev et al. 2004; Chong, Christiansen and Baer 1971) as discussed in the Introduction and here ϕ_{eff} was estimated by extrapolation from values determined at 'infinite' dilution. The calculated values of k used to convert C_{SBPMG} to ϕ_{eff} (Equation 4.6) do not account for the possibility of osmotic de-

swelling (Tan, Pelton and Tam 2010; Cloitre et al. 2003) or the potential for deformation and interpenetration of soft particles as ϕ_{eff} increases (Brijitta and Schurtenberger 2019), leading to overestimates in ϕ_{eff}. For these reasons, apparent $\phi_{eff} > 1$ are regularly reported for microgel systems (Omari et al. 2006; Senff and Richtering 2000; Scheffold et al. 2010; Carrier and Petekidis 2009; van der Vaart et al. 2013). The degree of osmotic de-swelling is difficult to observe or measure directly and at a fixed ϕ, de-swelling depends upon a number of different factors including the micromechanical properties of the particles, the change in concentration of ions within and outside the particles as the system is concentrated, plus the other solvent conditions. Nonetheless, when we investigate the dependence of ϕ_{eff} on the *relative* 'zero shear' (η_{0rel}) (Figure 4.5A) and *relative* 'infinite' shear ($\eta_{\infty rel}$) viscosities (Figure 4.5B) we can observe distinct differences between samples which we therefore assume to be dependent only on G'_{MG}.

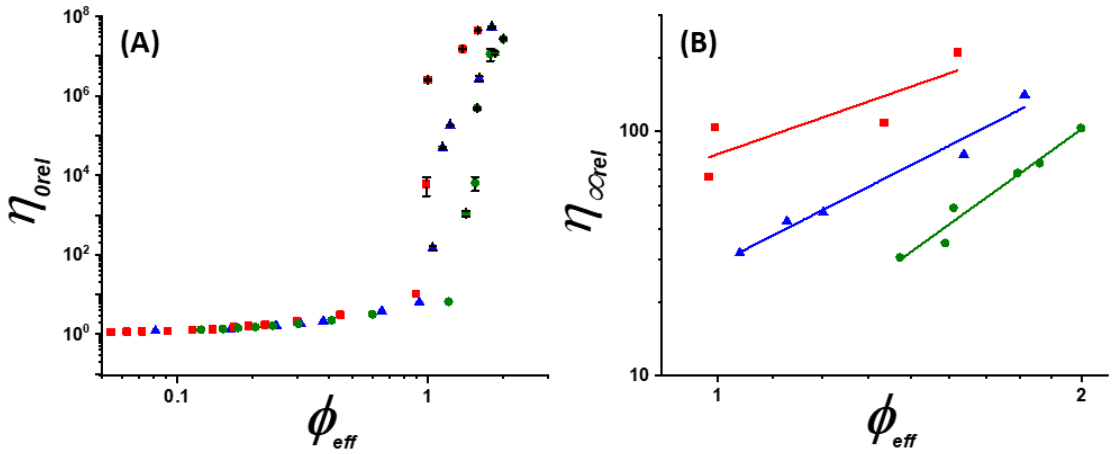

Figure 4.5 - (A) Relative 'zero shear' viscosity (η_{0rel}) and (B) relative 'infinite shear' viscosity ($\eta_{\infty rel}$) as a function of ϕ_{eff} for *SBPMG* suspensions shown on a double logarithmic plot. *SBPMG* suspensions were prepared at C_{GEL} = 2.4 (●), 3.4 (▲) and 4 (■) wt.%. In (B), data are fitted to a power law model and the corresponding power law exponents were 4.2 ± 0.4, 3.3 ± 0.2 and 2.1 ± 0.9 respectively.

Figure 4.5A is constructed from the η_{rel} data determined by capillary viscometry on the dilute suspensions and shear rheometry on more concentrated samples. The increase in η_{0rel} with ϕ_{eff} is initially gradual for all samples before increasing dramatically over a narrow range in ϕ_{eff} which is typical of particle suspensions. According to the Krieger-Dougherty relation (Krieger and Dougherty 1959), the divergence of η_{0rel} occurs at ϕ_{max}, which clearly occurs at relatively higher ϕ_{eff} for the softer particles. The suspensions can

apparently be concentrated further, reflecting the potential for particles to de-swell, interpenetrate and deform, as discussed above. This is evident from the data points recorded beyond the region of divergence where the increase in η_{rel} becomes more linear, resulting in an 'S-shaped' curve (and is even more apparent when plotted on a log-linear plot as in Figure 4.S3). Samples prepared at even higher ϕ_{eff} were studied by oscillatory rheometry and are discussed in the next section.

Shear thickening, *i.e.*, the increase in η with increasing $\dot{\gamma}$ or σ, is a well-known phenomenon in hard sphere systems and can introduce significant challenges during processing (*e.g.*, spraying, coating, mass transport) of suspensions with a high solid content. Figure 4.4 and Figure 4.S2 suggest that shear thickening is absent in *SBPMG* suspensions over the range of ϕ_{eff} and σ investigated here. Figure 4.5B shows that the relative high shear viscosity of *SBPMG*s appears to increase more gradually with ϕ_{eff} and this is typical of soft particle suspensions (Wolfe and Scopazzi 1989; Adams, Frith and Stokes 2004; Senff and Richtering 2000). In addition, there appears to be an effect of G'_{MG} on the high shear viscosity data, with the firmest microgels demonstrating the highest $\eta_{\infty rel}$ at equivalent ϕ_{eff}. This agrees with the limited number of similar studies and has been attributed to the deformability of the particles, which consequently leads to differences in the particle packing efficiency (Adams, Frith and Stokes 2004; Garrec, Guthrie and Norton 2013). Due to the high $\dot{\gamma}$ investigated, one cannot rule out the possibility for solvent (water) to be 'squeezed' out of discrete particles during these measurements which would lead to a reduction in ϕ_{eff} and thus η_{rel} (Desse et al. 2010). The exponents of power law fits in Figure 4.5B are greatest for the softest particles and are higher than those previously reported for κ-carrageenan fluid gels (Garrec, Guthrie and Norton 2013).

4.3.4 Oscillatory shear rheometry of concentrated *SBPMG* suspensions

Figure 4.6A and 4.6B show typical frequency sweep data for a series of *SBPMG* suspensions prepared from C_{GEL} = 2.4 wt.% and C_{GEL} = 4 wt.% respectively (*i.e.*, the softest and most firm microgels, respectively). It can be observed that G' is essentially independent of frequency and $G' > G''$ over a considerable frequency range, indicating solid-like behavior for all samples studied, as expected of concentrated suspensions. The elasticity presumably arises from particle-particle contacts that produce an interconnected microstructure (Adams, Frith and Stokes 2004; Seth, Cloitre and Bonnecaze 2006). This is typical where ϕ_{eff} exceeds the value of close packing or in the presence of some fractal-type particle aggregates which span the entire system, as in particle gels (Koumakis and

Petekidis 2011). Note that here $\phi_{eff} > 1$, so that certainly the former is probably the case. One might expect to find a viscoelastic fluid region ($G'' > G'$) before the onset of elasticity, as observed previously for a variety of hard sphere (Koumakis and Petekidis 2011; Laurati, Egelhaaf and Petekidis 2011) and soft particle suspensions (Shewan et al. 2021; Adams, Frith and Stokes 2004; Senff and Richtering 2000; Koumakis et al. 2012; Mason et al. 1997; Siebenbürger et al. 2009; Crassous et al. 2008). However resolving the viscoelastic moduli of samples more dilute than those shown here proved challenging with the instrument available: experimental data were not very reproducible. The variation of G'' with frequency is more complex and demonstrates a minimum at intermediate frequencies which is more apparent for the softer microgel particles shown in Figure 4.6A. This minimum in G'' appears to become more pronounced with increasing dilution, as found in concentrated emulsions (Mason et al. 1997). Also, this behavior has been observed for other soft particle suspensions at ϕ beyond the glass transition (Koumakis et al. 2012; Helgeson, Wagner and Vlassopoulos 2007; Crassous et al. 2008; Siebenbürger et al. 2009), perhaps providing further evidence that the samples studied here are 'jammed' systems and not particle gels possessing a true yield stress.

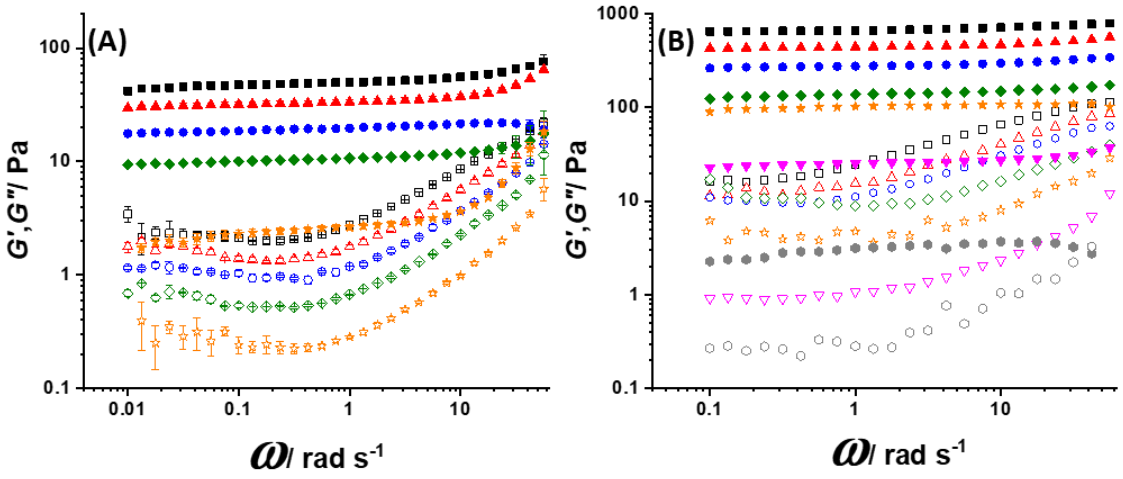

Figure 4.6 - Frequency sweeps performed at strain amplitudes within the *LVER* on *SBPMG* suspensions prepared over a range of ϕ_{eff} for (A) C_{GEL} = 2.4 wt.% and (B) C_{GEL} = 4 wt.%. Closed symbols = G' and open symbols = G''. In (A), ϕ_{eff} for these samples were: ■ = 2.35, ▲ = 2.22, ● = 2.02, ◆ = 1.9 and ★ = 1.44. In (B), ϕ_{eff} for these samples were: ■ = 1.97, ▲ = 1.82, ● = 1.75, ◆ = 1.59, ★ = 1.41, ▼ = 1.32 and ⬢ = 1.24.

Figure 4.7 shows the strong dependence of G' on ϕ_{eff} for these samples and captures the influence of particle modulus (G'_{MG}) on the bulk rheological properties, G' reaching higher values for the most firm microgels. From the linear fits (gradient n) to the plots of $\log_{10}G'$ versus $\log_{10}\phi_{eff}$, it is clear that G' of the firmer microgel particles increases more strongly (n = 7.6 ± 0.9) with ϕ_{eff} than those prepared with softer microgels (n= 6.2 ± 0.3). Other studies have reported similar exponents (Carrier and Petekidis 2009; Koumakis et al. 2012; Seth, Cloitre and Bonnecaze 2006; Adams, Frith and Stokes 2004) suggesting some universality between the rheological properties of soft particle suspensions in the concentrated regime, irrespective of particle type, size or morphology. For example, exponents ranging from 3.19 – 8.3 have been reported for *p(NIPAM)* microgel particles, exponents increasing with crosslinking density and thus particle modulus (Senff and Richtering 2000; Scheffold et al. 2010). Exponents of 7 and 7.7 were found for κ-carrageenan fluid gels (Garrec, Guthrie and Norton 2013) and swollen poly(methyl methacrylate) (*PMMA*) spheres (Paulin, Ackerson and Wolfe 1996) respectively.

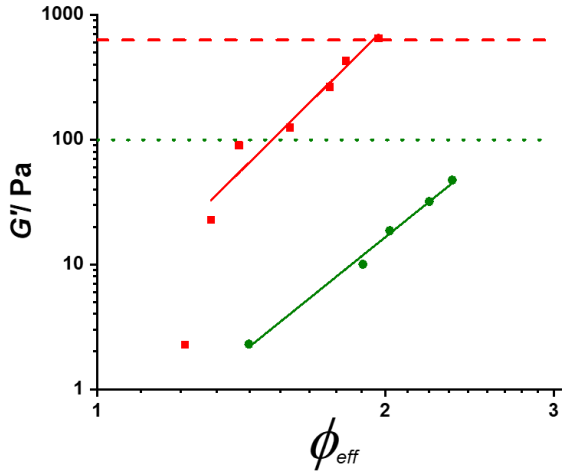

Figure 4.7 - Storage modulus (G') of *SBPMG* suspensions (C_{GEL} = 2.4 (●) and 4 (■) wt.%) as a function of ϕ_{eff}. Data points are taken from frequency sweeps shown in Figure 4.6 at ω = 0.1 rad s^{-1} and at 20 °C. The solid lines show a power law fit to the data (neglecting the first data point in samples prepared at C_{GEL} = 4 wt.%). The power law exponents were ● = 6.2 ± 0.3 and ■ = 7.6 ± 0.9. The horizontal dashed lines show the G' of 'parent' hydrogels at ω = 0.1 rad s^{-1} for C_{GEL} = 2.4 wt.% (green dotted line) and 4 wt.% (red dashed line) at 25 °C.

The above behavior is in contrast to hard spheres, for which *G'* has been reported to demonstrate a much stronger dependence on ϕ depending on the range of ϕ investigated. For example, van der Vaart et al. (2013) showed that *G'* for dense *PMMA* spheres diverged in the vicinity of ϕ_{max} in a similar fashion to the viscosity (*i.e.*, according to the Krieger-Dougherty relation) (van der Vaart et al. 2013) whereas Koumakis et al. (2012) found exponents ranging from 30 at $0.54 > \phi < 0.6$ and 50 at $\phi > 0.6$. Meanwhile, 'ultra-soft' colloidal suspensions such as star-like polymer micelle glasses were found (Koumakis et al. 2012) to demonstrate exponents of around 2. A theoretical study on the rheology of multi- arm star polymers predicts a linear increase above $\phi_{\max}$ (Yang and Schweizer 2010). Thus, the *SBPMG* and other microgel particles behave as intermediate between hard spheres and ultra-soft colloidal systems. The definition of the latter system could be extended to include polymer coils in solution, which are currently more widely used for rheology modification (Heyes and Brańka 2009).

The horizontal lines in Figure 4.7 shows *G'* of the respective 'parent' hydrogels at 25 °C. The suspensions were studied at a slightly lower temperature of 20 °C, but despite this caveat, it can be observed that *G'* of the suspensions closely approaches that of the parent hydrogels at the highest ϕ_{eff} investigated. Interestingly, this occurs at substantially lower values of C_{PTOTAL} for the suspensions, again showing how processing can be made more economical when *SBP* hydrogels are converted to microgel suspensions in order to impart solid-like rheological properties to a given formulation. For example, the corresponding C_{PTOTAL} for the firm microgels (C_{GEL} = 4 wt.%) at ϕ_{eff} = 1.97 was 1.72 wt.%. The highest C_{PTOTAL} investigated for the microgels prepared at C_{GEL} = 2.4 wt.% was 0.93 wt.%. The microgel samples evidently display significant elasticity even at low overall C_{PTOTAL}. In contrast, elasticity in linear polymer solutions generally arises at high polymer concentrations and on timescales shorter than the relaxation time, since it originates from chain entanglements (Omari et al. 2006; Kavanagh and Ross-Murphy 1998). van der Vaart et al. (2013) showed that *G'* for dense *p(NIPAM)* microgel suspensions was around an order of magnitude lower than the Young's modulus (E_P = 5.2 kPa) of the discrete *p(NIPAM)* microgel particles (as measured by atomic force microscopy (AFM)) (van der Vaart et al. 2013). The *p(NIPAM)* microgels were significantly firmer than those presented in our study, assuming that $G'_{MG} = G$' of the corresponding hydrogel, so that our *SBPMG* probably have a greater capacity for interpenetration and 'merging together' to reform a structure similar to the parent hydrogel.

Shewan et al. (2021) analyzed their $G'(\phi)$ data for emulsion templated agarose microgel suspensions (Shewan et al. 2021) with the model of Evans and Lips (Evans and Lips 1990), which is based on the theory of Hertzian contact mechanics and incorporates the elastic modulus of microgel particles. The use of the Young's (compressive) modulus measured by AFM was found to give a better fit to the data compared to the use of a particle shear modulus (*i.e.*, G'_{MG}), estimated from the G' of a hydrogel prepared at the same polymer concentration. However, in neither case did G' of the dense suspensions reach the measured or estimated G' of the particles, which again were substantially firmer than those presented here. These comparisons perhaps emphasize further the potential advantages of using *SBPMG* or similar microgels as rheology modifiers and shows how the mechanical properties of formulations could be tailored simply by incorporating combinations of particles which differ in their material properties.

Figure 4.8 shows the results of strain amplitude (γ) sweeps performed on *SBP* microgel suspensions over a wide range in ϕ_{eff}. The G' data has been scaled as G'/G'_0 where $G'_0 = G'$ in the *LVER*. This analysis shows deviations from the *LVER* more clearly when data for several samples are plotted on the same figure. The viscous modulus is evaluated through tanδ, that is, tan$\delta = G''/G'$. The variation of G' and G'' with γ, showing absolute values of the viscoelastic moduli, are shown in Figure 4.S4 and are in good agreement with the frequency sweep data presented in Figure 4.6 and discussed above.

The data shows that with decreasing ϕ_{eff}, the plateau modulus (see Figure 4.S3) and length of the *LVER* (Figure 4.8A and 4.8B) are reduced for both samples studied, implying a concurrent reduction in the number and strength of inter-particle interactions with increasing dilution. Such interactions will include entanglements of the 'fuzzy' surface of such particles and any weak non-covalent forces operating between the constituent sugars of the polysaccharide chains. The value of tanδ increases with γ from < 1 to values > 1 at the γ tested, suggesting that the initially solid-like samples yield and begin to flow as a viscoelastic fluid (Ching, Bansal and Bhandari 2016; van der Vaart et al. 2013), since this corresponds to the condition where $G'' > G'$. Similarly, the maximum in G'' observed before this crossover (Figure 4.S4) has previously been associated with the dissipation of energy on yielding of colloidal gels (Laurati, Egelhaaf and Petekidis 2011) and glasses (Carrier and Petekidis 2009; Koumakis et al. 2012). Repeat measurements were performed on the same sample using the rejuvenation protocols described in the Methods section prior to starting each measurement. The error between measurements was very small, suggesting that the particle material properties were largely unchanged after exposing the

suspensions to high γ. The solid-fluid transition must therefore be attributed to deformation of the suspension microstructure with respect to the location and orientation of discrete particles (Petekidis, Moussaïd and Pusey 2002; Pham et al. 2006). However, the *SBPMG* particles appear to assume a close packed microstructure following shear rejuvenation (*i.e.*, on the cessation of shear after an appropriate time at rest) since the plateau modulus was recovered on repeating the measurement. The γ where deviations from the *LVER* occur (Figure 4.8) could be taken as a measure of the critical strain (γ_c) for yielding. Other authors have noted increases in γ_c as a function of ϕ for soft particle suspensions (Koumakis et al. 2012; Le Grand and Petekidis 2008; Ching, Bansal and Bhandari 2016). However it should be noted that Ketz et al. (1988) found dense Carbopol suspensions (polyacrylic acid microgels) to yield at a constant γ_c, independent of particle concentration (ϕ) (Ketz, Prud homme and Graessley 1988).

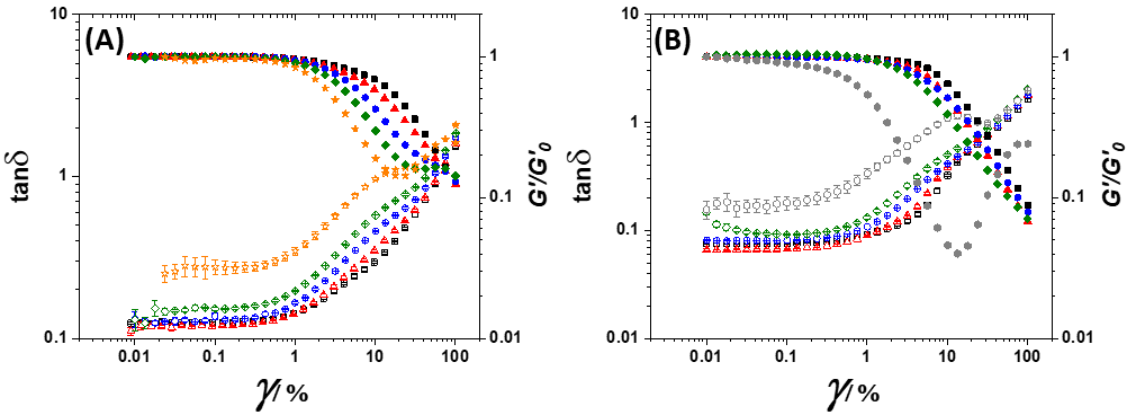

Figure 4.8 - Oscillatory strain amplitude (γ) sweeps for *SBPMG*s over a range in ϕ_{eff} for (A) C_{GEL} = 2.4 wt.% and (B) C_{GEL} = 4 wt.%. On the right-hand side *y*-axis, experimental *G'* was normalized by *G'* in the *LVER* (G'_0). Closed symbols = G'/G'_0. On the left-hand side *y*-axis, the variation of tanδ (*i.e., G"/G'*) with γ is also plotted. Open symbols = tanδ. In (A), ϕ_{eff} for these samples were: ■ = 2.35, ▲ = 2.22, ● = 2.02, ◆ = 1.9 and ★ = 1.44. In (B), ϕ_{eff} for these samples were: ■ = 1.97, ▲ = 1.82, ● = 1.75, ◆ = 1.59, ★ = 1.41, ▼ = 1.32 and ⬢ = 1.24.

The *G'* of *SBPMG* samples prepared at C_{GEL}= 4 wt.% and ϕ_{eff} = 1.24 (Figure 4.8B and Figure 4.S4B) is relatively low ($G' \approx 5.7$ Pa at γ = 0.01%) and appears to drop off more strongly and at substantially lower γ_c ($\gamma_c \approx 0.1\%$) than any other samples tested, for both firm and soft microgels (Figures 4.8 and 4.S4). This may suggest that these particles are in contact but not yet interpenetrating despite the high apparent ϕ_{eff} (ϕ_{eff} = 1.24). One might

expect that microgels formed from the stronger gels would have a less ‘fuzzy’ and open surface, either due to their inherently higher cross-linking density or the way this cross-linked structure survives on fragmentation to microgels under shear. At present, however, we do not have microscopy tools of sufficient resolution to prove this by direct observation. The *G’* appeared to reach a minimum at $\gamma \approx 10\%$ before increasing again as γ increased. Similar behavior was observed in other more dilute samples over the γ range studied. Such behavior may be attributed to wall slip at high γ (Laurati, Egelhaaf and Petekidis 2011), despite the use of roughened measuring sets and the reproducibility of the measurements. Another possibility for the increase in *G’* at high γ is due to shear thickening, as found in hard sphere glasses (Koumakis, Schofield and Petekidis 2008) although this was not observed in any of our steady state viscosity measurements performed at lower ϕ_{eff}. Taking γ even higher may reveal the same behavior in the most concentrated samples and requires further investigation.

4.4 Conclusions

Building on previous work (Stubley et al. 2021) showing that it is possible to create a range of robust microgel particles from *SBP* via laccase catalyzed crosslinking, we have addressed our hypothesis that the viscoelasticity of suspensions of these *SBPMG* depends strongly on ϕ_{eff} and the elasticity of the discrete microgel particles (G'_{MG}), which is easily controlled by C_{GEL} (and therefore the crosslinking density). *SBPMG*s therefore represent an important practical analogue for comparison with highly pure, covalently cross-linked synthetic microgels studied and applied elsewhere (*e.g., p(NIPAM)*). Furthermore, the use of natural biopolymers, biocompatible solvents and a facile production technique suggests that covalently cross-linked *SBPMG*s hold promise as functional ingredients for rheology modification (among other applications *e.g.,* encapsulation, stabilization) in formulations where biocompatibility is very important. Varying the ϕ_{eff} of *SBPMG* allows for much higher viscosities to be achieved compared to pectins in their native (*i.e.*, ‘non-microgel’) state for the same (or lower) overall pectin concentration in the system (Stubley et al. 2021). Similarly, elasticity can be delivered due to the dense packing of particles rather than polymer chain entanglements as in non-cross-linked *SBP* solutions. This should allow design of desirable flow behavior during processing and during use by the consumer.

4.5 Supplementary Figures

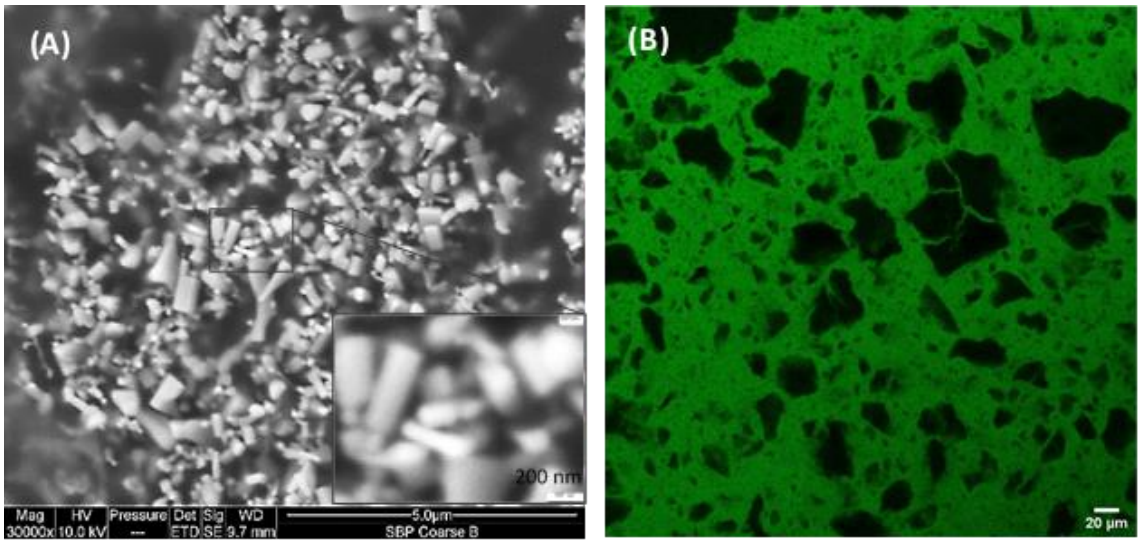

Figure 4.S1 - (A) Representative scanning electron microscopy image of *SBPMG* particles illustrating their non-spherical shape. The inset shows a selected area at higher magnification. (B) Typical morphology of *SBPMG* particles as observed with a confocal laser scanning microscope. For details of the sample preparation procedure the reader is referred to **Chapter 3**.

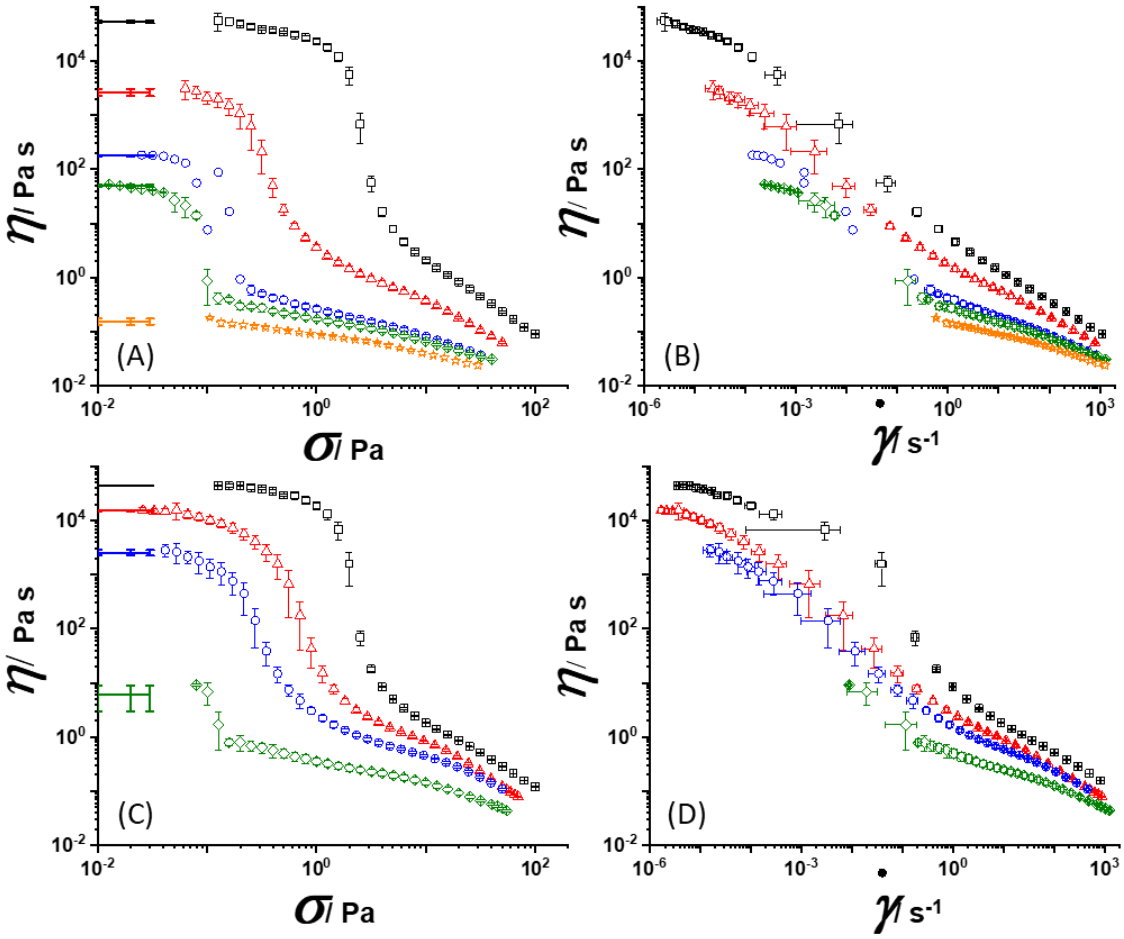

Figure 4.S2 - Steady state viscosity (η) curves for *SBPMG* suspensions as a function of shear stress (σ) for samples prepared from (A) C_{GEL} = 3.4 wt.% and (C) 4 wt.% and also as a function of shear rate ($\dot{\gamma}$) for (B) C_{GEL} = 3.4 wt.% and (D) 4 wt.%. The ϕ_{eff} of suspensions of the C_{GEL} = 3.4 wt.% samples are 1.79 (□), 1.59 (△), 1.22 (○), 1.14 (◇), 1.04 (☆) and for the C_{GEL} = 4 wt.% samples 1.58 (□), 1.37 (△), 0.99 (○), 0.98 (◇). The solid lines close to the η axis indicate the estimated values of η_0 obtained by averaging the first three data points and shown in Table S4.1 below.

Table 4.S1 - Summary of values of η_0 and η_∞ (see text) extracted from the flow curves for C_{GEL} = 3.4 wt.% and C_{GEL} = 4 wt.% shown in Figure 4.S2

C_{GEL} = 3.4 wt.%			C_{GEL} = 4 wt.%		
ϕ_{eff}	η_0 / Pa s	η_∞ / Pa s	ϕ_{eff}	η_0 / Pa s	η_∞ / Pa s
1.79	53189 ± 11384	0.301 ± 0.006	1.58	44196 ± 1754	0.500 ± 0.007
1.59	2669 ± 788	0.107 ± 0.006	1.37	15164 ± 1564	0.202 ± 0.004
1.22	180 ± 4	0.080 ± 0.004	0.99	2538 ± 756	0.203 ± 0.007
1.14	50 ± 2	0.075 ± 0.003	0.98	5.9 ± 1.6	0.102 ± 0.006
1.04	0.15 ± 0.01	0.050 ± 0.003			

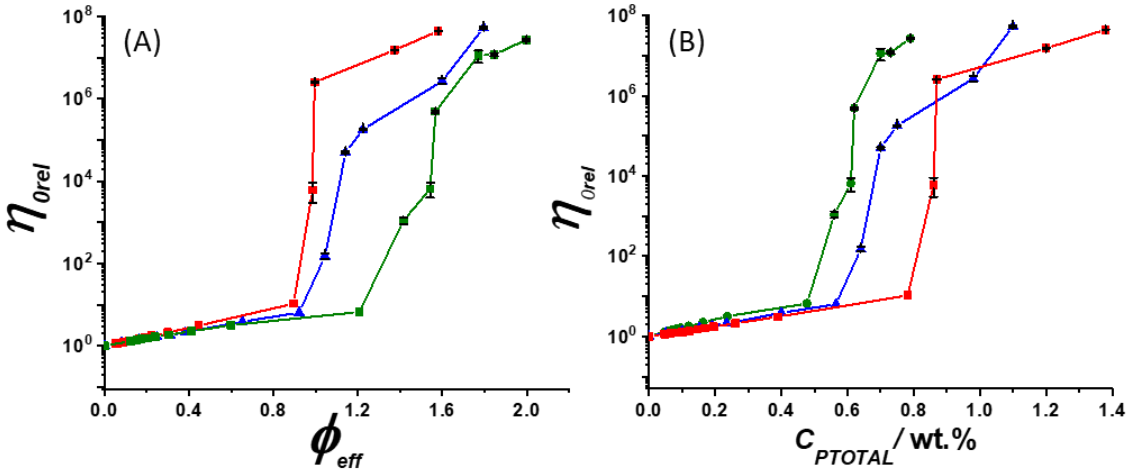

Figure 4.S3 - Relative zero shear viscosity on a LOG-LIN plot for *SBPMG* prepared at C_{GEL} = 2.4 (●), 3.4 (▲) and 4 (■) wt.% as a function of (A) ϕ_{eff} and (B) C_{PTOTAL}.

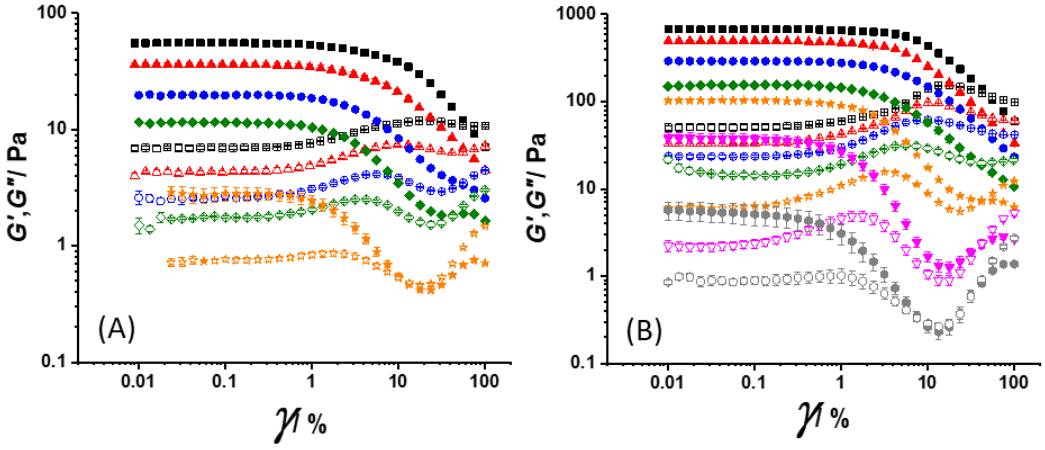

Figure 4.S4 - Oscillatory strain amplitude (γ) sweeps for *SBPMG*s over a range in ϕ_{eff} for (A) C_{GEL} = 2.4 wt.% and (B) C_{GEL} = 4 wt.%. Closed symbols = *G'* and open symbols = *G"*. In (A), ϕ_{eff} for these samples were: ■ = 2.35, ▲ = 2.22, ● = 2.02, ◆ = 1.9 and ★ = 1.44. In (B), ϕ_{eff} for these samples were: ■ = 1.97, ▲ = 1.82, ● = 1.75, ◆ = 1.59, ★ = 1.41, ▼ = 1.32 and ⬢ = 1.24.

4.6 References

Adams, S., Frith, W. J., & Stokes, J. R. (2004). Influence of particle modulus on the rheological properties of agar microgel suspensions. Journal of Rheology, 48(6), 1195-1213.

Almdal, K., Dyre, J., Hvidt, S., & Kramer, O. (1993). Towards a phenomenological definition of the term 'gel'. Polymer Gels and Networks, 1(1), 5-17.

Barnes, H. (1999). The yield stress—a review or 'παντα ρει'—everything flows? Journal of Non-Newtonian Fluid Mechanics, 81(1), 133-178.

Brijitta, J., & Schurtenberger, P. (2019). Responsive hydrogel colloids: Structure, interactions, phase behavior, and equilibrium and nonequilibrium transitions of microgel dispersions. Current Opinion in Colloid & Interface Science, 40, 87-103.

Bunzel, M. (2010). Chemistry and occurrence of hydroxycinnamate oligomers. Phytochemistry Reviews, 9(1), 47-64.

Caggioni, M., Spicer, P. T., Blair, D. L., Lindberg, S. E., & Weitz, D. A. (2007). Rheology and microrheology of a microstructured fluid: The gellan gum case. Journal of Rheology, 51(5), 851-865.

Carrier, V., & Petekidis, G. (2009). Nonlinear rheology of colloidal glasses of soft thermosensitive microgel particles. Journal of Rheology, 53(2), 245-273.

Ching, S. H., Bansal, N., & Bhandari, B. (2016). Rheology of emulsion-filled alginate microgel suspensions. Food Research International, 80, 50-60.

Chong, J. S., Christiansen, E. B., & Baer, A. D. (1971). Rheology of concentrated suspensions. Journal of Applied Polymer Science, 15(8), 2007-2021.

Cloitre, M., Borrega, R., Monti, F., & Leibler, L. (2003). Structure and flow of polyelectrolyte microgels: from suspensions to glasses. Comptes Rendus Physique, 4(2), 221-230.

Crassous, J. J., Siebenbürger, M., Ballauff, M., Drechsler, M., Hajnal, D., Henrich, O., & Fuchs, M. (2008). Shear stresses of colloidal dispersions at the glass transition in equilibrium and in flow. The Journal of Chemical Physics, 128(20), 204902.

Cross, M. (1965). Rheology of non-Newtonian fluids: A new flow equation for pseudoplastic systems. Journal of Colloid Science, 20(5), 417-437.

Desse, M., Fraiseau, D., Mitchell, J., & Budtova, T. (2010). Individual swollen starch granules under mechanical stress: evidence for deformation and volume loss. Soft Matter, 6(2), 363-369.

Donev, A., Cisse, I., Sachs, D., Evan, V., Frank, S., Connelly, R., Torquato, S., & Chaikin, P. (2004). Improving the Density of Jammed Disordered Packings Using Ellipsoids. Science, 303(5660), 990-993.

Du, C., & Hill, R. J. (2018). Linear viscoelasticity of weakly cross-linked hydrogels. Journal of Rheology, 63(1), 109-124.

Ellis, A., & Jacquier, J. C. (2009). Manufacture and characterisation of agarose microparticles. Journal of Food Engineering, 90(2), 141-145.

Evans, I., & Lips, A. (1990). Concentration dependence of the linear elastic behaviour of model microgel dispersions. Journal of the Chemical Society, Faraday Transactions, 86(20), 3413-3417.

Farjami, T., & Madadlou, A. (2017). Fabrication methods of biopolymeric microgels and microgel-based hydrogels. Food Hydrocolloids, 62, 262-272.

Garrec, D., Guthrie, B., & Norton, I. (2013). Kappa carrageenan fluid gel material properties. Part 1: Rheology. Food Hydrocolloids, 33(1), 151-159.

Helgeson, M., Wagner, N., & Vlassopoulos, D. (2007). Viscoelasticity and shear melting of colloidal star polymer glasses. Journal of Rheology, 51(2), 297-316.

Heyes, D. M., & Brańka, A. C. (2009). Interactions between microgel particles. Soft Matter, 5(14), 2681-2685.

Ishii, T., & Matsunaga, T. (1996). Isolation and characterization of a boron-rhamnogalacturonan-II complex from cell walls of sugar beet pulp. Carbohydrate Research, 284(1), 1-9.

Johannes, C., & Majcherczyk, A. (2000). Laccase activity tests and laccase inhibitors. Journal of Biotechnology, 78(2), 193-199.

Joye, I. J., & McClements, D. J. (2014). Biopolymer-based nanoparticles and microparticles: Fabrication, characterization, and application. Current Opinion in Colloid & Interface Science, 19(5), 417-427.

Karg, M., Pich, A., Hellweg, T., Hoare, T., Lyon, L. A., Crassous, J. J., Suzuki, D., Gumerov, R. A., Schneider, S., Potemkin, I. I., & Richtering, W. (2019). Nanogels

and Microgels: From Model Colloids to Applications, Recent Developments, and Future Trends. Langmuir, 35(19), 6231-6255.

Kavanagh, G., & Ross-Murphy, S. (1998). Rheological characterisation of polymer gels. Progress in Polymer Science, 23(3), 533-562.

Ketz, R., Prud homme, R., & Graessley, W. (1988). Rheology of concentrated microgel solutions. Rheologica Acta, 27, 531-539.

Koumakis, N., Pamvouxoglou, A., Poulos, A. S., & Petekidis, G. (2012). Direct comparison of the rheology of model hard and soft particle glasses. Soft Matter, 8(15), 4271-4284.

Koumakis, N., & Petekidis, G. (2011). Two step yielding in attractive colloids: transition from gels to attractive glasses. Soft Matter, 7(6), 2456-2470.

Koumakis, N., Schofield, A. B., & Petekidis, G. (2008). Effects of shear induced crystallization on the rheology and ageing of hard sphere glasses. Soft Matter, 4(10), 2008-2018.

Krieger, I., & Dougherty, T. (1959). A Mechanism for Non-Newtonian Flow in Suspensions of Rigid Spheres. Transactions of the Society of Rheology, 3(1), 137-152.

Laurati, M., Egelhaaf, S. U., & Petekidis, G. (2011). Nonlinear rheology of colloidal gels with intermediate volume fraction. Journal of Rheology, 55(3), 673-706.

Le Grand, A., & Petekidis, G. (2008). Effects of particle softness on the rheology and yielding of colloidal glasses. Rheologica Acta, 47(5), 579-590.

Levigne, S., Ralet, M.-C., & Thibault, J.-F. (2002). Characterisation of pectins extracted from fresh sugar beet under different conditions using an experimental design. Carbohydrate Polymers, 49(2), 145-153.

Mason, T. G., Lacasse, M., Grest, G., Levine, D., Bibette, J., & Weitz, D. A. (1997). Osmotic pressure and viscoelastic shear moduli of concentrated emulsions. Physical Review E, 56(3), 3150-3166.

Mattsson, J., Wyss, H. M., Fernandez-Nieves, A., Miyazaki, K., Hu, Z., Reichman, D. R., & Weitz, D. A. (2009). Soft colloids make strong glasses. Nature, 462(7269), 83-86.

Mezger, T. G. (2014). The Rheology Handbook: For Users of Rotational and Oscillatory Rheometers (4th ed. Vol. 4). Hanover, Germany: Vincentz Network.

Morris, G. A., & Ralet, M.-C. (2012). The effect of neutral sugar distribution on the dilute solution conformation of sugar beet pectin. Carbohydrate Polymers, 88(4), 1488-1491.

Mueller, S., Llewellin, E. W., & Mader, H. M. (2010). The rheology of suspensions of solid particles. Proceedings of the Royal Society A: Mathematical, Physical and Engineering Sciences, 466(2116), 1201-1228.

Norton, I. T., Jarvis, D. A., & Foster, T. J. (1999). A molecular model for the formation and properties of fluid gels. International Journal of Biological Macromolecules, 26(4), 255-261.

Nott, P. R., & Brady, J. F. (1994). Pressure-driven flow of suspensions: simulation and theory. Journal of Fluid Mechanics, 275, 157-199.

Omari, A., Tabary, R., Rousseau, D., Leal Calderon, F., Monteil, J., & Chauveteau, G. (2006). Soft water-soluble microgel dispersions: Structure and rheology. Journal of Colloid and Interface Science, 302(2), 537-546.

Paulin, S. E., Ackerson, B. J., & Wolfe, M. S. (1996). Equilibrium and Shear Induced Nonequilibrium Phase Behavior of PMMA Microgel Spheres. Journal of Colloid and Interface Science, 178(1), 251-262.

Petekidis, G., Moussaïd, A., & Pusey, P. N. (2002). Rearrangements in hard-sphere glasses under oscillatory shear strain. Physical Review E, 66(5), 051402.

Pham, K. N., Petekidis, G., Vlassopoulos, D., Egelhaaf, S. U., Pusey, P. N., & Poon, W. C. K. (2006). Yielding of colloidal glasses. Europhysics Letters (EPL), 75(4), 624-630.

Pusey, P. N., Zaccarelli, E., Valeriani, C., Sanz, E., Poon, W. C. K., & Cates, M. E. (2009). Hard spheres: crystallization and glass formation. Philosophical Transactions of the Royal Society A: Mathematical, Physical and Engineering Sciences, 367(1909), 4993-5011.

Renard, C. M. G. C., Crépeau, M.-J., & Thibault, J.-F. (1995). Structure of the repeating units in the rhamnogalacturonic backbone of apple, beet and citrus pectins. Carbohydrate Research, 275(1), 155-165.

Royall, C. P., Poon, W. C. K., & Weeks, E. R. (2013). In search of colloidal hard spheres. Soft Matter, 9(1), 17-27.

Saavedra Isusi, G. I., Karbstein, H. P., & van der Schaaf, U. S. (2019). Microgel particle formation: Influence of mechanical properties of pectin-based gels on microgel particle size distribution. Food Hydrocolloids, 94, 105-113.

Scheffold, F., Díaz-Leyva, P., Reufer, M., Ben Braham, N., Lynch, I., & Harden, J. (2010). Brushlike Interactions between Thermoresponsive Microgel Particles. Physical Review Letters, 104(12), 128304.

Senff, H., & Richtering, W. (2000). Influence of cross-link density on rheological properties of temperature-sensitive microgel suspensions. Colloid and Polymer Science, 278(9), 830-840.

Seth, J., Cloitre, M., & Bonnecaze, R. (2006). Elastic properties of soft particle pastes. Journal of Rheology, 50(3), 353-376.

Shewan, H., Yakubov, G., Bonilla, M., & Stokes, J. (2021). Viscoelasticity of non-colloidal hydrogel particle suspensions at the liquid–solid transition. Soft Matter, 17(19), 5073-5083.

Shewan, H. M., & Stokes, J. R. (2013). Review of techniques to manufacture micro-hydrogel particles for the food industry and their applications. Journal of Food Engineering, 119(4), 781-792.

Shewan, H. M., & Stokes, J. R. (2015). Viscosity of soft spherical micro-hydrogel suspensions. Journal of Colloid and Interface Science, 442, 75-81.

Siebenbürger, M., Fuchs, M., Winter, H., & Ballauff, M. (2009). Viscoelasticity and shear flow of concentrated, noncrystallizing colloidal suspensions: Comparison with mode-coupling theory. Journal of Rheology, 53(3), 707-726.

Stubley, S., Cayre, O., Murray, B., Celigueta Torres, I., & Fernández Farrés, I. (2021). Enzyme cross-linked pectin microgel particles for use in foods. Food Hydrocolloids, 121, 107045.

Tan, B. H., Pelton, R. H., & Tam, K. C. (2010). Microstructure and rheological properties of thermo-responsive poly(N-isopropylacrylamide) microgels. Polymer, 51(14), 3238-3243.

Thakur, B. R., Singh, R. K., Handa, A. K., & Rao, M. A. (1997). Chemistry and uses of pectin — A review. Critical Reviews in Food Science and Nutrition, 37(1), 47-73.

Thibault, J.-F., Garreau, C., & Durand, D. (1987). Kinetics and mechanism of the reaction of ammonium persulfate with ferulic acid and sugar-beet pectins. Carbohydrate Research, 163(1), 15-27.

Torres, O., Tena, N. M., Murray, B., & Sarkar, A. (2017). Novel starch based emulsion gels and emulsion microgel particles: Design, structure and rheology. Carbohydrate Polymers, 178, 86-94.

van der Vaart, K., Rahmani, Y., Zargar, R., Hu, Z., Bonn, D., & Schall, P. (2013). Rheology of concentrated soft and hard-sphere suspensions. Journal of Rheology, 57(4), 1195-1209.

Vlassopoulos, D., & Cloitre, M. (2014). Tunable rheology of dense soft deformable colloids. Current Opinion in Colloid & Interface Science, 19(6), 561-574.

Wolfe, M. S., & Scopazzi, C. (1989). Rheology of swellable microgel dispersions: Influence of crosslink density. Journal of Colloid and Interface Science, 133(1), 265-277.

Wyss, H. M., Franke, T., Mele, E., & Weitz, D. A. (2010). Capillary micromechanics: Measuring the elasticity of microscopic soft objects. Soft Matter, 6(18), 4550-4555.

Yang, J., & Schweizer, K. (2010). Tunable dynamic fragility and elasticity in dense suspensions of many-arm-star polymer colloids. EPL (Europhysics Letters), 90(6), 66001.

Yunker, P. J., Chen, K., Gratale, M. D., Lohr, M. A., Still, T., & Yodh, A. G. (2014). Physics in ordered and disordered colloidal matter composed of poly(N-isopropylacrylamide) microgel particles. Reports on Progress in Physics, 77(5), 056601.

Zaidel, D. N. A., Chronakis, I. S., & Meyer, A. S. (2012). Enzyme catalyzed oxidative gelation of sugar beet pectin: Kinetics and rheology. Food Hydrocolloids, 28(1), 130-140.

Chapter 5: Emulsifying Properties of Sugar Beet Pectin Microgels *

Abstract

Particle stabilized ('Pickering') oil-in-water (*O/W*) emulsions were fabricated using sugar beet pectin (*SBP*) microgel particles (*SBPMG*) that differed in their crosslinking density and therefore elasticity. Droplet size distributions and emulsion microstructures were investigated via static light scattering and complementary imaging techniques: light microscopy, confocal laser scanning microscopy and scanning electron microscopy. Comparisons to emulsions stabilized by native (*i.e.*, non-microgelled) *SBP* at equivalent overall *SBP* content were made throughout. The *SBPMG*-stabilized emulsions (20 and 40 vol.% oil) were shown to have an improved physical stability compared to those stabilized by *SBP*. For example, droplet coarsening on prolonged (9 weeks) storage at ambient temperature (25 °C) and on temperature cycling (75 °C) was substantially reduced for *SBPMG*-stabilized emulsions. This is attributed to greater steric barrier provided by *SBPMG* particles and their higher energy of displacement. Furthermore, the higher viscoelasticity of the *SBPMG*-stabilized emulsions (particularly at 40 vol.% oil) retarded droplet creaming. This higher viscoelasticity could be due to weak flocculation of the *SBPMG*-stabilized droplets or the strong influence of the *SBPMG* on the viscoelasticity of the intervening aqueous phase, even at relatively low *SBPMG* concentrations.

*** Published as:** Stubley, S., Cayre, O., Murray, B., Celigueta Torres, I. (2023). Emulsifying properties of sugar beet pectin microgels. *Food Hydrocolloids*. **137,** 108291. DOI: https://doi.org/10.1016/j.foodhyd.2022.108291

5.1 Introduction

Pectin is a heteropolysaccharide extracted from plant cell walls and its chemical structure is complex and depends on the plant source and extraction conditions. However, some general features are preserved in all cases. For example, the main structural component, Homogalacturonan (*HG*), is essentially a linear polymer of galacturonic acid (*GalA*) where some of the *GalA* residues may be methylated or acetylated. The second major structural region is Rhamnogalcturonan I (*RGI*), whose backbone consists of *GalA* interspersed with rhamnose residues. In *RGI*, branching from the polymer backbone occurs in the form of neutral sugar side chains composed mainly of arabinose and galactose residues (Thakur et al., 1997; Ngouémazong et al., 2015). In addition, protein has frequently been observed in some extracted pectins, including sugar beet pectin (*SBP*), although the origin, location and distribution of such proteinaceous elements is currently not entirely clear. The key point is that such protein elements confer surface activity on these pectins, allowing for their use as emulsifiers, as reviewed elsewhere (Ngouémazong et al., 2015; Alba and Kontogiorgos, 2017). At the same time, the non-surface active polysaccharide elements confer excellent ‘electrosteric’ stability by protruding into the aqueous continuous phase of oil-in-water (*O/W*) emulsions (Akhtar et al., 2002; Dickinson, 2003). *SBP* tends to contain more protein and also a greater proportion of acetyl groups (Leroux et al., 2003; Schmidt et al., 2015) compared to other commonly utilized pectins from apple and citrus sources and their emulsifying properties have been studied in some detail. The acetyl groups are believed to increase the hydrophobicity and therefore the surface activity of the *SBP* (Dea and Madden, 1986). Indeed, synthetic acetylation of depolymerized citrus pectins improved their performance as emulsifiers, enabling the stabilization of finer *O/W* emulsion droplets (Leroux et al., 2003). The measured proportion of protein associated with *SBP* seems to vary greatly between studies, probably due to differences in the extraction conditions (Chen et al., 2016; Yapo et al., 2007). Protein has apparently been confirmed as being directly attached to the polymer backbone via atomic force microscopy studies - approximately 66% of the imaged *SBP* molecules contained protein (Kirby et al., 2006). This is in agreement with previous observations that pectins adsorb to *O/W* interfaces via their protein-rich fractions (Akhtar et al., 2002; Leroux et al., 2003; Williams et al., 2005; Siew and Williams, 2008) and that treatment of *SBP* with proteases significantly decreases

their performance as emulsifiers (Chen et al., 2016; Funami et al., 2007). For example, compared to a non-protease treated *SBP*, proteolysis resulted in a higher *O/W* interfacial tension and larger droplets that exhibited significant creaming over 2 hours storage (Funami et al., 2007).

Another significant feature of *SBP* is the presence of ferulic acid residues esterified to the neutral sugar side chains of the *RGI* regions (Levigne et al., 2004). While ferulic acid has been suggested as also increasing the *SBP* hydrophobicity and surface activity (Siew and Williams, 2008; Williams et al., 2005), it also makes the *SBP* susceptible to chemical crosslinking via oxidative coupling reactions. Oxidation of ferulic acid can be catalyzed by persulphates (Thibault et al., 1987) or oxidoreductase enzymes, resulting in the generation of phenoxy radicals. Radical coupling leads to *SBP* molecules that are cross-linked via ferulic acid dimers and/or higher ferulate oligomers (Bunzel, 2010).

Such oxidative crosslinking has been exploited to improve the stability of *SBP*-stabilized emulsions by crosslinking the *SBP* molecules in dilute solution prior to their use as emulsifiers. For example, *SBP* has been cross-linked via laccase (Jung and Wicker, 2012) and horseradish peroxidase (Zhang, L. et al., 2015). In each case, the increase in the *SBP* molecular weight (*MW*), as confirmed by size exclusion chromatography, led to emulsions with improved storage stability compared to the native *SBP*. This was attributed to the development of a thicker and more viscoelastic film adsorbed at the interface, which was more effective at reducing droplet coalescence.

Another interesting use of oxidative crosslinking of *SBP* is in the preparation of chemical hydrogels (Thibault et al., 1987) which are thermally irreversible (Khalighi et al., 2020) and resist dissolution when placed in excess solvent (Stubley et al., 2021). We recently exploited this technique to prepare sugar beet pectin microgels (*SBPMG*), by homogenizing bulk SBP hydrogels (cross-linked via laccase) in the presence of excess solvent (water) to produce aqueous suspensions of microgel particles (Stubley et al., 2021; Stubley et al., 2022). Microgels are solvent swollen polymer networks of finite dimensions, a type of soft colloid demonstrating the properties of both polymers and particles (Dickinson, 2016; Lyon and Fernandez-Nieves, 2012). In general, microgel suspensions appear to be very promising for bulk rheology modification, as an alternative to polymer solutions (Adams, Frith, &

Stokes, 2004; Stubley et al., 2022; Stubley et al., 2021). However, since SBP is surface active, it might be expected that SBPM would also be surface active and testing the ability of SBPM to stabilize O/W emulsions is the main topic that this paper seeks to address.

The use of biopolymer-based microgels as particulate ('Pickering') stabilizers of emulsions, foams, *etc*. has been reviewed extensively elsewhere (Dickinson, 2015; Murray, 2019). In general, they are thought to provide superior stability to coalescence and Ostwald ripening, via the general Pickering mechanism of strong and irreversible adsorption of the particles to the interface, whist their large size (*i.e.*, larger than the polymer molecules of which they are composed) provides a thicker steric barrier. In addition the particle-stabilized systems may provide extra benefits such as the reduction of oil oxidation (Kargar et al., 2012; Atarés et al., 2012) and the rate of lipid digestion (Sarkar et al., 2019), depending on the nature of the stabilizing particles.

There are several recent publications on the use of polysaccharide based microgels to stabilize emulsions (Ishii et al., 2018; Hu et al., 2021; Lefroy et al., 2021; Huang et al., 2021). Other pectin based microgels have already been developed and used as Pickering emulsifiers. For example Mironov et al. (2012) used a 'bottom-up' approach to microgelation in dilute solution. Their synthesis involved chemical crosslinking of pectinic acid via a basic isocyanide and amine leading to the development of polyampholyte microgels which precipitated around their pI. Stable emulsions could be prepared at low pH, where particles were strongly positively charged, while emulsions could be broken by raising the pH > pI (Mironov et al., 2013). However, the use of such chemicals and the organic solvents utilized in their synthesis probably make such microgels unsuitable for use in food and drinks. Also, Saavedra Isusi and coworkers have published a series of papers (Saavedra Isusi et al., 2020a; Saavedra Isusi et al., 2020b; Saavedra Isusi et al., 2021a; Saavedra Isusi et al., 2021b) investigating the emulsifying properties of low methyl ester pectin microgels which are physically cross-linked by divalent calcium ions and that may be promising for stabilizing emulsions where biocompatibility is important. Building on these previous works, the chemical crosslinking mechanism exploited in the study reported here yields robust microgel particles whilst maintaining biocompatibility.

Taking inspiration from the debate in the literature as to whether ‘softer’ or ‘harder’ microgels give better emulsion stability (Murray, 2019), this work studies the *O/W* emulsion stabilizing properties of two sets of *SBPMG*, which differed in their crosslinking density. We investigate the physical stability of *SBPMG* stabilized emulsions towards droplet coarsening and phase separation on prolonged storage (9 weeks) at 25 °C and on temperature cycling at 75 °C making comparisons to native (*i.e.*, non-cross-linked) *SBP* stabilized emulsions throughout. Complementary imaging techniques and rheological characterization were used to explain the factors which promote long term stability.

5.2 Materials and Methods

5.2.1 Materials

Sugar beet pectin (GENU® Beta Pectin) (*SBP*) was a gift from CP Kelco (Lille Skensved, Denmark). Laccase Y120 (EC 1.10.3.2) was obtained from Amano Enzyme (Nagoya, Japan). Type I (Milli-Q) water (Millipore, Bedford, UK) with a minimum resistivity of 18.2 MΩ cm^{-1} was used throughout. Fluorescein isothiocyanate-dextran (*FITC*-dextran, average $MW = 2 \times 10^6$ Da), Nile Red and n-Tetradecane were obtained from Sigma Aldrich (Dorset, UK).

5.2.2 Methods

5.2.2.1 Preparation of *SBP* solutions

SBP powder was dispersed into cold water via a T25 ULTRA-TURRAX blender (IKA, Oxford, UK) equipped with an S25N - 18G dispersing tool at speed of 15,000 rpm. The powder was added gradually to prevent clumping and the resulting stock solutions were stirred magnetically for a minimum of 12 h in sealed Duran® bottles. The *SBP* solutions were then centrifuged (Eppendorf 5810 R, Stevenage, UK) at 4000 rpm for 60 min in approximately 30 ml aliquots to remove any remaining insoluble material. The supernatant was carefully decanted and stored in sealed containers prior to further use.

The total *SBP* concentration in the supernatants, referred to as C_{PTOTAL} throughout, was determined by drying the purified solutions in a vacuum oven (Townson and Mercer Limited, Croydon, England) at 75 °C and a pressure of 600 mm Hg until no change in mass was observed. To allow for a direct comparison between the emulsifying properties of native (*i.e.*, non-cross-linked) *SBP* and *SBPMG*, solutions or suspensions were diluted to the same C_{PTOTAL} = 0.5 wt.%.

5.2.2.2 Fabrication of *SBP* hydrogels and *SBPMG* suspensions

Laccase stock solutions were prepared by solubilizing the enzyme powder in water for a minimum of 20 minutes. Subsequently, 5 ml laccase was combined with 25 ml *SBP* stock solution via vortex mixing to give a final enzyme concentration of 0.1 mg ml^{-1} laccase. When the two solutions were visibly well mixed, ‘parent’ hydrogels were allowed to develop quiescently in sealed containers for a minimum of 12 h by incubation at 25 °C. The elasticity of *SBP* hydrogels depends strongly on the *SBP* concentration in the gel (C_{GEL}) (Stubley et al., 2021). In this work, we have chosen

to refer to the hydrogels, plus the microgels derived from them, as ‘soft’ when C_{GEL} = 2.4 wt% and ‘firm’ when C_{GEL} = 4 wt.%. The development and rheology of these gels has been described in detail earlier (Stubley et al., 2021) and these designations of soft and firm are based on yield strain and stress values of 84% and 460 Pa for C_{GEL} = 2.4 wt% and corresponding values of 63% and 853 Pa for C_{GEL} = 4 wt% (as described in Section 4.3.1).

For the fabrication of the *SBPMG* suspensions, the parent hydrogels were broken into coarse lumps with a metal spatula and 25 g of the parent hydrogel were combined with 100 g of deionized water and blended via the ULTRA-TURRAX at 10000 rpm for 10 min. To account for any losses during sample preparation, C_{PTOTAL} of any *SBPMG* suspensions used as emulsifier was determined by drying the suspensions as described above for the *SBP* supernatants.

5.2.2.3 Fabrication of oil-in-water (*O/W*) emulsions

Tetradecane (ρ = 0.76 g cm^{-3}) was used as the dispersed phase in the fabrication of *O/W* emulsions at oil volume fractions (ϕ_{OIL}) of 20 or 40 %, to avoid complications from competing surface active species present in other oils such as vegetable oils. For the continuous phase, *SBP* solutions or suspensions of the soft or firm *SBPMG* were used at an overall C_{PTOTAL} = 0.5 wt.%. Emulsions were prepared in 100 ml batches. Coarse emulsions were prepared by combining the oil and aqueous phases in the ULTRA-TURRAX at 18000 rpm for 2 min. Fine emulsions were prepared immediately afterwards by passing the coarse emulsions through a high pressure jet homogenizer once at 300 bar. Emulsions were mixed gently with a vortex mixer, decanted into sealed containers and incubated at 25 °C until further use. Sodium azide (0.005 wt.%) was added as a preservative.

In one set of experiments, the *SBPMG* suspensions prepared in Methods section 5.2.2.2 were separately subjected to the same the same mechanical treatment used to prepare the fine emulsions, *i.e.,* the combination of both ULTRA-TURRAX shearing and jet homogenization. These microgel suspensions are referred to as ‘fine’ *SBPMG* in the text. This experiment was conducted to understand how the *SBPMG* particle size might be further affected by the emulsification conditions.

5.2.2.4 Particle size analysis of *SBPMG* suspensions and *O/W* emulsions

A Mastersizer 3000 equipped with the Hydro EV wet sample dispersion unit (Malvern Instruments, Worcestershire, UK) was used to investigate the particle size distribution (*PSD*) of *SBPMG* suspensions and emulsions. Samples were dispersed in pure water (20 °C) in the stirred measurement cell of the Mastersizer until the laser obscuration reached >1%. A stirrer speed of 2500 rpm was used throughout. In the Mastersizer, *PSD*s are automatically calculated via the manufacturer software from the angular dependence of scattered light intensity via the Mie theory for spherical particles. Mean values of particle diameter, namely the Sauter (surface weighted) mean diameter ($D_{3,2}$) and the volume weighted mean diameter ($D_{4,3}$) are calculated according to:

$$D_{a,b} = \frac{\sum n_i D_i^a}{\sum n_i D_i^b} \qquad [5.1]$$

: where n_i is the number of particles of diameter D_i. From the volume distributions, the width of the distribution was assessed by the D_{10}, D_{50} and D_{90} values, where subscripts correspond to the percentage of particles in a distribution. For example, the D_{50} is the median droplet size: 50% of the particles in a distribution are larger than this and 50% are smaller. Similarly, the 90th percentile gives the diameter of which 90% of the particles in a distribution are smaller.

5.2.2.5 Microscopy of *SBPMG* suspensions and *O/W* emulsions

Light microscope (Nikon SMZ-2T, Japan) images were collected with a digital camera (Leica MC120 HD). Emulsions were diluted with water and gently vortex mixed before being transferred to welled glass slides and covered with a cover slip. Microscopy was performed using a 10x objective lens.

A Zeiss confocal laser scanning microscope (*CLSM*) (Model LSM 700, Carl Zeiss Microscopy GmbH, Jena, Germany) equipped with a 20x/0.8 NA objective lens was used. Samples were transferred *undiluted* into welled slides for imaging. To image *SBPMG* suspensions, a reverse contrast was employed whereby the continuous phase (water) was stained using a high *MW FITC*-dextran, added directly to suspensions at a concentration of 0.1 wt.% with mild stirring for 1 hour in the dark. The excitation and emission wavelengths (λ) used were λ = 488 and 528 nm respectively. For the emulsions, the oil soluble stain Nile Red (0.4 mg mL^{-1}) was

dissolved in ethanol and this stain solution was added at 1 v/v % of the emulsions. Stained emulsions were stirred for two hours in the dark before imaging by *CLSM*. The excitation and emission wavelengths used for Nile Red were λ = 488 and 561 nm respectively. Images were processed in ImageJ.

Cryo-scanning electron microscopy (*CRYO-SEM*) was performed on freshly prepared, *undiluted* 40 vol.% emulsions over numerous length scales. The instrument used was a Helios G4 CX (FEI, Oregon, USA). The microscope was operated at 2 kV and a working distance of 6.4-8 mm. Emulsions were deposited into hollow copper rivets and rapidly frozen by dipping into liquid nitrogen slush (-180 °C) before being transferred to the *SEM*. Samples were fractured and imaged at -135 °C without the need for sublimation or sputter coating with metal.

5.2.2.6 Stability of *O/W* emulsions to temperature cycling

The thermal stability of emulsions stabilized by *SBP* and *SBPMG* was investigated by subjecting the emulsions to two consecutive heating and cooling cycles. Twenty ml of freshly prepared emulsion was transferred to a plastic falcon tube and placed in a water bath pre-heated to 75 °C for 30 min. Samples were then cooled by placing the tubes in a separate water bath set to 25 °C for an additional 30 min. An aliquot (5 ml) of each emulsion was removed for investigation via laser diffraction and light microscopy before the samples were subjected to a second heating and cooling cycle under the same conditions. Light microscopy and particle size analysis of the heat-cycled emulsions was performed within 1 h of heating.

5.2.2.7 Creaming stability of *O/W* emulsions

Emulsions were transferred into matching glass vials to obtain an emulsion height of approximately 60 mm. Vials were sealed and incubated at 25 °C until required for measurement of creaming stability. Periodically, over the space of 9 weeks, the serum layer height (*i.e.,* the aqueous continuous phase) was measured at three predefined points via a pair of calipers and the average serum layer height recorded. The creaming index (*CI*) was calculated according to:

$$CI\ (\%) = 100\ \times (\frac{H_s}{H_e}) \qquad [5.2]$$

: where H_s is the height of the serum layer below the cream layer and H_e = the total height of the emulsion, frequently used to assess emulsion stability (McClements, 2007).

5.2.2.8 Shear rheometry of *O/W* emulsions

An Anton Paar MCR 302 (Anton Paar GmbH, Graz, Austria) rheometer was used for all shear rheology experiments and the raw data were analyzed in the RheoCompass software. All rheological tests were performed using a 50 mm stainless steel parallel plate measuring set (*PP50*), with the gap set to 0.5 mm. As a precautionary measure to prevent wall slip, the *PP50* measuring set was roughened by gluing water-resistant silicon carbide sandpaper (600 grit, from 3 M) to both the upper and lower plates with multi-purpose silicone rubber sealant (Dow Corning 732), followed by curing for a minimum of 12 h before use. During rheological characterization, the measuring set was covered with a custom made solvent hood lined with dampened paper towel to minimize solvent evaporation. All emulsions were pre-sheared at a shear rate of 50 s^{-1} for 30 s and left at rest for 10 min before commencing the experiments. The pre-shear, rest and measuring intervals were all performed at 20 °C.

Rotational shear rheometry was conducted in triplicate using a new sample loading for each run. Logarithmic sweeps through shear rate were performed using 5 measuring points per decade and a maximum measuring point duration of 2 minutes. For oscillatory shear rheometry experiments, the measurement point duration was set to automatic using steady state sensing. Strain (γ) amplitude sweeps were conducted in triplicate using a new sample loading for each run. All γ sweeps were performed at an angular frequency (ω) of 3.14 rad s^{-1}. Frequency sweeps are based on single measurements and were performed at γ within the linear viscoelastic region (*LVER*).

5.2.2.9 Statistical analysis

The mean droplet size distributions and standard deviations of individual samples, either (i) freshly prepared emulsions (ii) emulsions after storage for 63 days and (iii) emulsions after one or two heating cycles respectively were analyzed in the Minitab software using the one way analysis of variance and students T-test at a significance level of $p < 0.05$.

5.3 Results and Discussion

5.3.1 Particle size and microstructure of *SBP- versus SBPMG*-stabilized emulsions

Figure 5.1A shows the *PSD*s of the soft and firm *SBPMG* after their initial preparation. The firm microgels demonstrated a Gaussian *PSD* with particle sizes between 20 and 100 μm, whereas the soft microgels showed a bimodal *PSD*. For the latter, the main peak was in a slightly lower size regime: 7 to 70 μm with a second peak at a significantly lower size of around 1 μm. We have previously suggested that this size fraction may represent some *SBP* aggregates liberated from the parent *SBP* hydrogels in their conversion to *SBPMG* suspensions (Stubley et al., 2021).

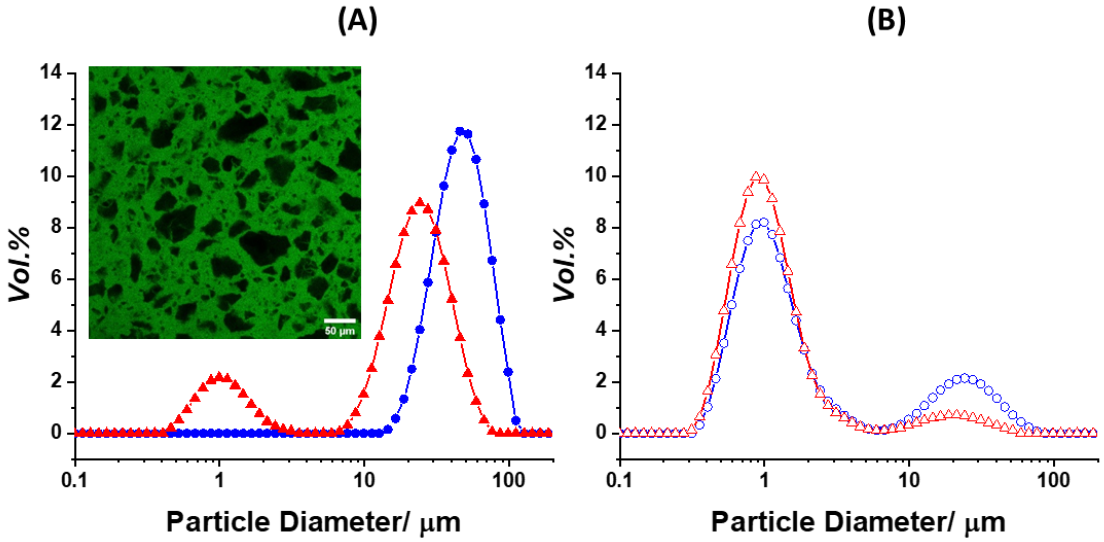

Figure 5.1 – (A) Particle size distributions (*PSD*) of the coarse *SBPMG* particles prepared by rotor-stator mixing: firm (●) and soft (▲). The inset shows a *CLSM* image of firm *SBPMG*s that appear black due to negative staining of the background aqueous phase. Scale bar = 50 μm. (B) *PSD*s of the fine *SBPMG* suspensions, firm (●) and soft (▲), obtained after subjecting the coarse *SBPMG* suspensions to the same homogenization conditions as used to form the emulsions (see text).

Note the calculation of the *PSD*s assumes that the particles are spherical. However, the inset in Figure 5.1A clearly suggests that the *SBPMG*s (in this case the firm ones) have highly irregular morphologies when imaged by *CLSM*. However, the particle sizes in the image seems to be in agreement with the range of sizes in the *PSD*s. In agreement with previous studies on the production of polysaccharide microgels via 'top-down' techniques, differences in average particle size result from

the elasticity of the parent hydrogels. Those hydrogels with higher elastic modulus and/or yield stress tend to result in larger particle sizes when fragmented to smaller gel particles (Ellis and Jacquier, 2009; Saavedra Isusi et al., 2019; Stubley et al., 2021).

Table 5.1 – Average particle sizes of coarse and fine *SBPMG* particles of different particle elasticity. Firm and soft *SBPMG*s were obtained from parent hydrogels prepared at C_{GEL} = 4 wt.% and 2.4 wt.%, respectively.

	Microgel elasticity/preparation method			
	Firm/ 'Coarse'	**Firm/ 'Fine'**	**Soft/ 'Coarse'**	**Soft/ 'Fine'**
$D_{3,2}$ **/ µm**	44.74 ± 0.14	1.26 ± 0.02	4.92 ± 0.2	1.01 ± 0.01
$D_{4,3}$ **/ µm**	52.48 ± 0.16	7.15 ± 0.42	23.22 ± 0.23	2.79 ± 0.08
D_{90} **/ µm**	82.06 ± 0.43	26.58 ± 1.16	43.30 ± 0.13	2.99 ± 0.18
D_{50} **/ µm**	49.22 ± 0.1	1.28 ± 0.02	22.45 ± 0.21	1.07 ± 0.01
D_{10} **/ µm**	28.22 ± 0.15	0.64 ± 0.01	1.20 ± 0.03	0.59 ± 0.01

These 'coarse' *SBPMG* suspensions were subsequently used as Pickering stabilizers of the *O/W* emulsions. However, in preparing the emulsions, the *SBPMG*s were subjected to a further mechanical disruption, more substantial than that used to prepare the *SBPMG*s in the first place. The size of stabilizing particles is expected to influence the extent of interfacial coverage and thus the size of the resulting oil droplets (Destribats et al., 2014a). Therefore, the *SBPMG* were subjected to the emulsion homogenization conditions *in the absence of oil* and the *PSD* re-measured (as described in the Methods). Figure 5.1B shows the *PSD* of these 'fine' *SBPMG* dispersions. A clear shift to smaller particle sizes was observed for both the soft and firm *SBPMG*, with the main peak in each case now being between *ca.*, 0.3 and 3 µm. The peak at larger particle sizes is presumed to derive from the main peak at larger

size prior to these ‘emulsification’ conditions (see Figure 5.1A). Table 5.1 shows the average particle sizes calculated from the laser diffraction measurements on coarse and fine *SBPMG*s. Irrespective of how the average is calculated, it was found to be lower for the fine particles, as expected. For example, $D_{3,2}$ and $D_{4,3}$ decreased from 44.7 and 52.4 μm to 1.3 and 7.2 μm, respectively, for the firm *SBPMG*s and from 4.9 and 23.2 to 1.0 and 2.8 μm, respectively, for the soft *SBPMG*s.

Measurement of the *PSD*s of the emulsions requires considerable dilution in the measurement cell in order to obtain a laser obscuration in the correct range. Figures 5.2A-C show the evolution of mean particle size with time after dispersing 40 vol.% *O/W* emulsions stabilized by native *SBP*, the soft and the firm *SBPMG*, respectively into the measurement cell. For the native *SBP* (Figure 5.2A), the apparent droplet sizes (D_{90}, D_{50} and D_{10}) were found to be independent of measurement time, suggesting that the emulsions were stable to dilution and were not flocculated. In contrast, the droplet sizes of the microgel stabilized emulsions, shown in Figures 5.2B and 5.2C, particularly the larger fractions represented by the D_{90} and D_{50}, were found to decrease with time. We attribute this to weak droplet flocculation. Most of the reduction in particle size sizes occurred during the initial 5 to 6 measurements (*i.e.*, 6 ± 2 min), after which the reduction became more gradual, eventually leading to a near plateau value similar to that with the native *SBP*, shown in Figure 5.2A.

In Figure 5.2D, the volume weighted *PSD*s of the emulsions stabilized by the firm *SBPMG* are plotted at various time intervals (*i.e.*, measurement numbers). Initially, the *PSD* suggests a wide distribution of droplet sizes with a major peak centered around 20 μm and a shoulder peak extending to around 1 μm. Over time, apparent droplet sizes are progressively shifted to smaller dimensions, ultimately resulting (*i.e.*, on measurement 20) in a monomodal *PSD* centered between 1 and 10 μm. A similar reduction in (apparent) droplet diameter was observed in the 20 vol.% *O/W* emulsions stabilized by *SBPMG* (data not shown). From here on, all reported mean droplet sizes for the *SBPMG*-stabilized emulsions are based on these ‘deflocculated values’, *i.e.*, obtained after the *PSD* had stabilized after this continued stirring and calculated by taking an average of at least 5 measurements once the plateau had been established.

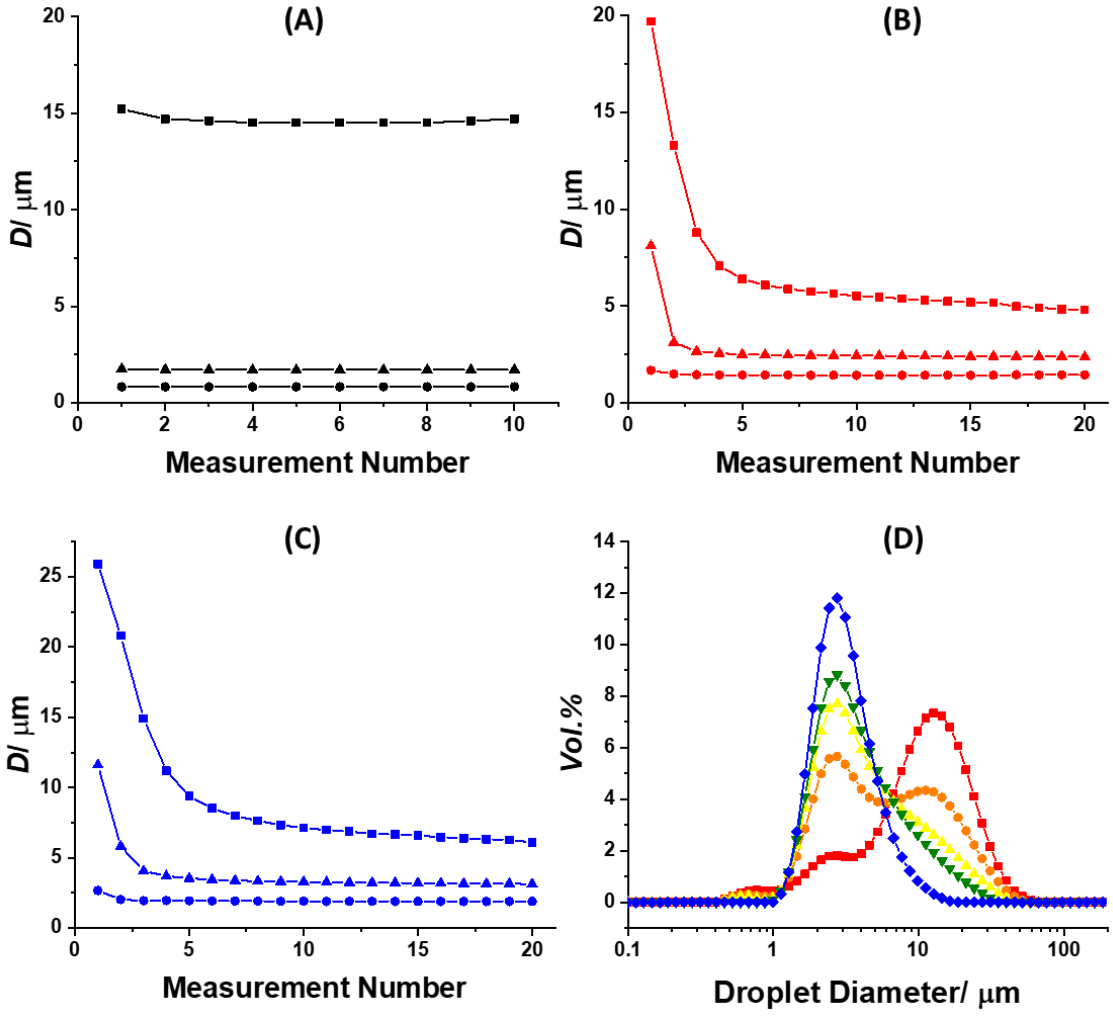

Figure 5.2 – Evolution of particle size with time after dispersing ϕ_{OIL} = 40 % emulsions stabilized by (A) native *SBP* (B) soft *SBPMG* and (C) firm *SBPMG* into the Mastersizer measurement cell. Particle size is represented by the D_{90} (■), D_{50} (▲), D_{10} (●) values. Each measurement number corresponds to approx. 60 s of data collection. In (D) the volume weighted *PSD*s are shown for the emulsions stabilized by the firm *SBPMG* shown in (C) at measurement numbers 1 (■), 2 (●) , 3(▲), 4 (▼) and 20 (◆).

The results of this analysis are shown for the freshly prepared emulsions in Figures 5.3A and 5.3B for 20 vol.% and 40 vol.% *O/W* emulsions stabilized by native *SBP*, soft and firm *SBPMG*, respectively. To make things simpler, we will now refer to these systems using a coding system: 'N' (native *SBP*), 'S' (soft *SPBMG*) and 'F' (firm *SBPMG*) followed by a number, either 20 or 40, to represent whether or not this is a 20 or 40 vol.% emulsion, respectively, as is shown in Table 5.2 alongside the corresponding average droplet sizes.

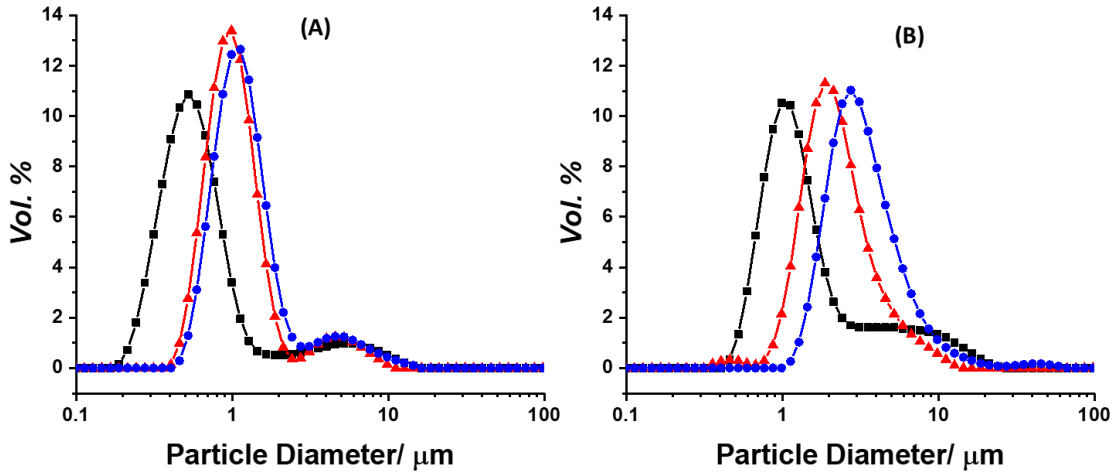

Figure 5.3 – Particle size distributions of (A) 20 vol.% and (B) 40 vol.% emulsions stabilized by native *SBP* (■), soft *SBPMG* (▲) and firm *SBPMG* (●), collected within 2 h of preparation of the emulsions.

Figures 5.3A and 5.3B suggest a clear influence of the nature of the interfacial species on the droplet size distributions. Native *SBP* could stabilize the smallest droplets at both ϕ_{OIL} but the *PSD*s appeared bimodal in each case. Figure 5.3A shows that for S20 and F20 there was a peak centered at ~1 μm and also shoulder peak extending to ~20 μm. The latter probably indicates some limited droplet coalescence or flocculation, due to droplets with an insufficient interfacial coverage immediately after their preparation (Destribats et al., 2014a).

Figure 5.3A shows that the softer microgels appeared to be more capable of stabilizing smaller droplets but this was even more apparent at the higher ϕ_{OIL} investigated (ϕ_{OIL} = 40%), as seen Figure 5.3B for S40 and F40. These observations are reflected in the average droplet diameters shown in Table 5.2. For the most part, irrespective of which average is used, the droplet size increases in the order N20 < S20 < F20 and similarly N40 < S40 <F40. The only exception is in the D_{90} values for N20 and N40, which were larger than S20 and S40 respectively.

Table 5.2 – Average particle sizes of emulsions stabilized by native *SBP* and *SBPMG* (after de-flocculation) as determined by laser diffraction as a function of storage time. The corresponding % change in droplet size between day 1 and day 63 is also shown (ΔD). All droplet size measures were significantly different between samples prepared at the same ϕ_{OIL} on day 1 and the values of ΔD were significant for all samples ($p < 0.05$).

	ϕ_{OIL} = 20 %			ϕ_{OIL} = 40 %		
	NATIVE *SBP* N20	**SOFT *SBPMG* S20**	**FIRM *SBPMG* F20**	**NATIVE *SBP* N40**	**SOFT *SBPMG* F40**	**FIRM *SBPMG* F40**
$D_{3,2}$ / µm	0.58 ± 0.01	1.05 ± 0.01	1.20 ± 0.01	1.32 ± 0.01	2.35 ± 0.01	3.22 ± 0.07
D_{50} / µm	0.60 ± 0.01	1.07 ± 0.01	1.22 ± 0.01	1.31 ± 0.01	2.56 ± 0.01	3.39 ± 0.08
$D_{4,3}$ Day 1 / µm	1.19 ± 0.02	1.47 ± 0.01	1.75 ± 0.01	2.62 ± 0.05	3.14 ± 0.02	4.40 ± 0.29
D_{90} Day 1 / µm	2.39 ± 0.1	2.10 ± 0.02	3.15 ± 0.02	6.74 ± 0.22	5.54 ± 0.1	7.70 ± 0.74
$D_{4,3}$ Day 63 / µm	4.25 ± 0.02	1.67 ± 0.01	2.31 ± 0.09	10.5 ± 0.04	3.79 ± 0.13	5.05 ± 0.03
D_{90} Day 63 / µm	12.12 ± 0.04	2.99 ± 0.03	5.57 ± 0.31	26.13 ± 0.06	7.67 ± 0.4	9.53 ± 0.08
$\Delta D_{4,3}$ / %	257	14	32	301	21	15
ΔD_{90} / %	407	42	77	288	38	24

In the above comparisons, for technological reasons, C_{PTOTAL} in the continuous phase was kept constant at 0.5 wt.% for both *SBPMG*- and *SBP*-stabilized systems. However, considering each *SBPMG* particle as a solvent swollen polymer network, the wt.% *particle* concentration (C_{SBPMG}) can be calculated via Equation 5.2 and is highest in the soft microgel systems.

$$C_{SBPMG}\ (\text{wt.}\%) = 100 \times S \times \left(\frac{C_{PTOTAL}}{C_{GEL}}\right) \qquad [5.2]$$

This is because the soft parent gels, and therefore each microgel particle derived from it, initially contain more water but also swell to a greater extent. The swelling ratios, *i.e.,* the increase in mass (and therefore volume, considering the gels as having a mass density ≈ that of water) were 1.5 and 1.4 for the soft and firm systems, respectively (Stubley et al., 2021). Use of Equation 5.2 yields C_{SBPMG} = 31.3 and 17.5 wt.%, for the soft and firm *SBPMG* respectively. A higher particle concentration might reasonably be expected to result in smaller oil droplets due to more extensive interfacial coverage and/or a reduction in the extent of limited coalescence during preparation (Destribats et al., 2014a).

As already mentioned, an additional factor affecting the subsequent emulsion stability is that the microgels themselves may undergo some size reduction in the process of homogenizing them with oil, whilst static light scattering cannot distinguish emulsion droplets from microgel particles. Saaverda Isusi et al. (2021) also investigated the breakup of pectin microgel particles during emulsification (Saavedra Isusi et al., 2021a). The $D_{3,2}$ of microgels prepared using a rotor-stator mixer was reduced from around 137 μm to 17 μm following high pressure homogenization, although the latter suspensions were suggested to have a "flaky" appearance due to particle aggregation. The 17 μm aggregates were suggested to be assemblies of smaller (around 90 nm) elementary particles. Microgel particles (or aggregates thereof) of different sizes ('small', 'medium' and 'large') were subsequently used to stabilize emulsions. Despite large differences in the initial microgel particle sizes ($D_{3,2}$ = 17 to 137 μm), the $D_{3,2}$ of the resulting emulsions was not significantly different, irrespective of whether emulsions were prepared in a colloid mill or via high pressure homogenization, suggesting the microgels all end up the same in the emulsification process. The $D_{3,2}$ of the resulting oil droplets were also found to be smaller than the $D_{3,2}$ of the initial microgels, which of course is

impossible if the same microgels stabilize the droplets. So this again suggests a significant, simultaneous reduction of microgel particle size during emulsion formation. Similar results have been described elsewhere for microgel stabilized emulsions (Lefroy et al., 2021). It is also possible that presence of oil aids the break-up of the larger microgel particles (Saavedra Isusi et al., 2021a).

A comparison of the average *SBPMG* particle sizes in Table 5.1 and overall emulsion particle sizes in Table 5.2 suggests that the *PSD*s of the microgels and resulting droplets are similar, which also suggests that *SBPMG* particle breakdown is modified in the presence of oil. This makes it difficult to relate the average particle size to the average droplet size, especially once polydispersity and flocculation is accounted for. Nonetheless, in contrast to the work by Saavedra Isusi et al. (2021), the resulting emulsion *PSD*s were significantly different depending on which pectin preparation was used (see Table 5.2). Thus, the average droplet sizes can be tailored by varying ϕ_{OIL} and the nature of the stabilizing species, either free polymer or polymer microgel, though whether the variations with microgels are due to the *SBPMG* size, mechanical properties or particle concentration is not clear.

Figure 5.4 shows some typical light microscopy images of emulsions for S20 and S40 (Figure 5.4A and 5.4B), F20 and F40 (Figure 5.4C and 5.4D), N20 and N40 (Figure 5.4E and 5.4F) systems. In all images, discrete spherical droplets were observed of sizes in good agreement with the corresponding laser diffraction measurements (Figure 5.3). For the N20 and N40 emulsions (Figure 5.4E and 5.4F), the droplets appeared well dispersed. In contrast, the *SBPMG* stabilized emulsions (Figures 5.4A-D) appeared to have heterogeneous microstructures, despite samples being diluted and vortex mixed for the preparation of microscope slides. The clusters such as those observed in Figures 5.4A-D were presumably flocculated emulsion droplets.

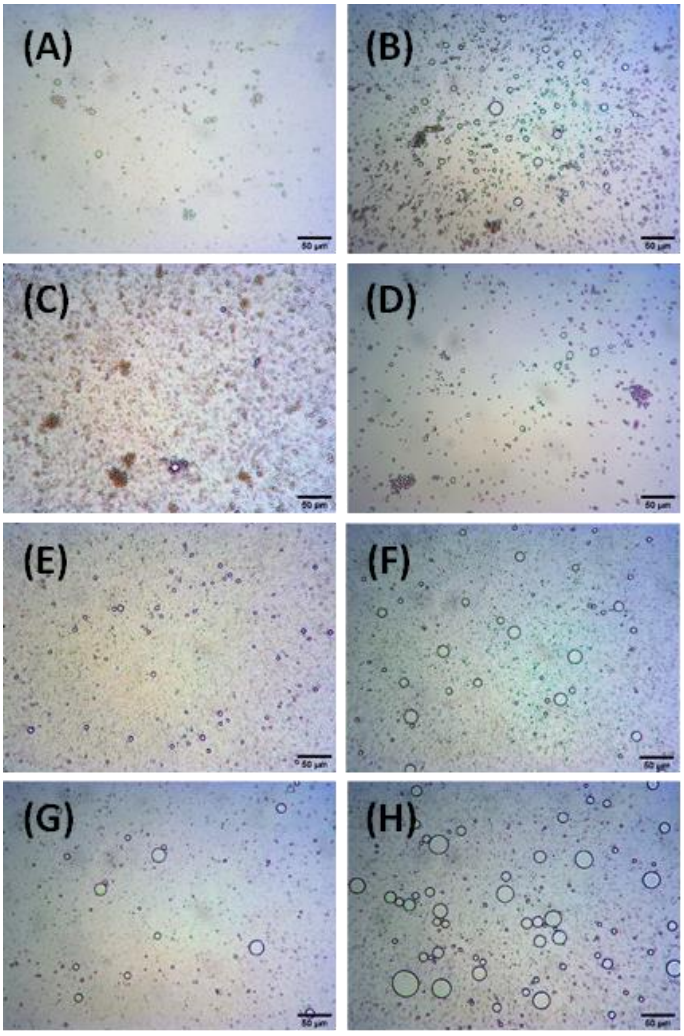

Figure 5.4 – Typical light microscopy images of diluted emulsions: (A) S20, (B) S40, (C) F20, (D) F40, (E) N20 (F) N40. Images (G) and (H) also show N20 and N40, respectively, after 2 heating and cooling cycles as described in Methods. Scale bar = 50 μm.

Figure 5.5 shows typical *CLSM* images of *undiluted* emulsions at 20x magnification. Oil droplets should appear red due to staining with Nile Red, but for N20 and N40 (Figures 5.5A and 5.5B, respectively) few discrete droplets can be observed and the images appear almost homogeneously red, due to their small size, making it difficult for the microscope to resolve clearly and compounded by their Brownian motion. The dark spherical regions were air bubbles. For the microgel samples shown in Figures 5.5C to 5.5F, some clusters of oil droplets, which appear a brighter shade of red, are apparent in agreement with the droplet flocculation in these systems suggested by other techniques. Interestingly, many more dark regions can be seen which, in contrast to Figure 5.5A, were clearly non-spherical and therefore unlikely to be air bubbles. These large, non-spherical entities are reminiscent of the irregular

shaped ‘coarse’ *SBPMG*s shown in the inset of Figure 5.1A. They appeared to be more pronounced in emulsions F20 and F40 (Figure 5.5E and 5.5F) than in S20 and S40 (Figure 5.5C and 5.5D). Indeed, the particle sizing performed on the fine *SBPMG*s shown in Figure 5.1B suggests that microgel particles in the size range 10-100 μm can still survive the additional homogenization stage used in emulsion formation and also that this fraction of particles occupies a larger vol.% in the firm suspensions. Thus, there is good evidence for the persistence of large, non-adsorbed microgel particles in the microgel-stabilized emulsions.

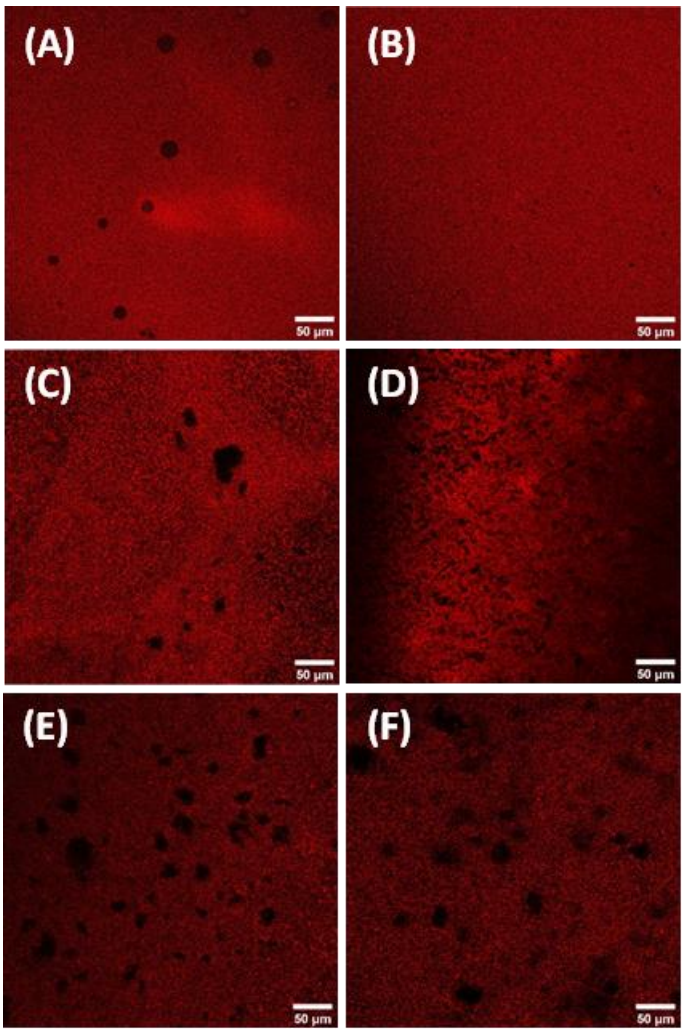

Figure 5.5 – Typical *CLSM* images of undiluted emulsions: (A) N20, (B) N40, (C) S20, (D) S40, (E) F20 (F) F40. Oil phase stained with Nile Red and appears red. Scale bar = 50 μm.

To obtain further microstructural information on undiluted emulsions across wider length scales, 40 vol.% *O/W* emulsions were investigated via *CRYO-SEM* (Figure

5.6). Like the light microscopy and *CLSM* images in Figures 5.4 and 5.5 respectively, emulsions stabilized by native *SBP* (Figures 5.6A-C) appeared much more homogeneous, with no apparent flocculation compared to microgel-stabilized emulsions (Figures 5.6D-I). The droplets in the latter clearly appeared to be more clustered together and, in some cases, the interfaces between adjacent droplets appeared to have merged, as in 'bridging flocculation' described below. Unfortunately, the *CRYO-SEM* images did not reveal convincing evidence for the presence of *SBPMG* particles at the interface. This was probably due to the lack of contrast between the continuous phase (water) and the water-swollen microgel particles. With hindsight, imaging may have been improved by performing sublimation.

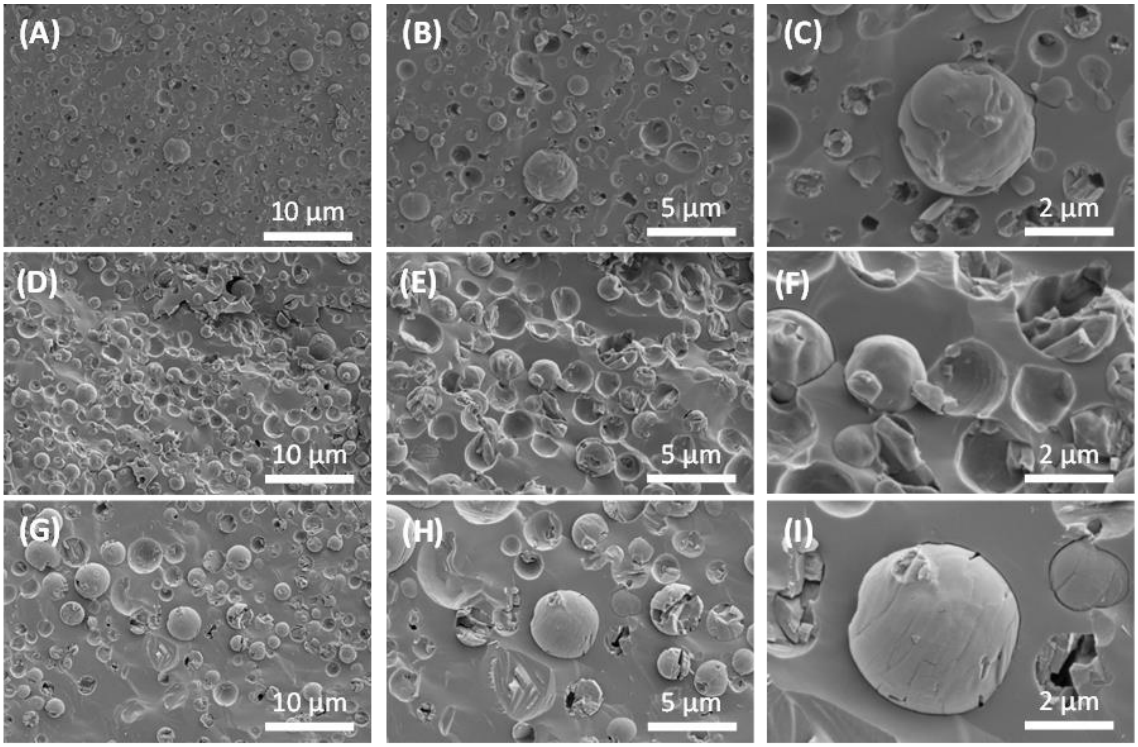

Figure 5.6 – Typical *CRYO-SEM* images of undiluted emulsions. (A)-(C) = N40, (D)-(F) = S40, (G)-(I) = F40. For left hand side, middle and right hand side images the scale bars are 10, 5 and 2 µm, respectively.

Numerous factors can promote flocculation in particle-stabilized (Pickering) emulsions. For example, flocculation in microgel stabilized emulsions has been studied with respect to the interfacial coverage. Using colloidal poly(N-Isopropylacrylamide) microgel particles as emulsifiers, Destribats et al. (2014)

showed that a low interfacial coverage promotes deformation of microgels adsorbed at the *O/W* interface which in turn leads to an inhomogeneous density distribution of material at the interface. Flocculation originates from droplet bridging via interfacial regions where the microgel density is low or depleted on one droplet and high on another. Consequently, more highly cross-linked (and therefore less deformable) and larger microgel particles, which had a reduced packing efficiency and reduced ability to deform and rearrange at the interface, gave rise to more flocculated emulsions. Such 'bridging monolayers' were visualized by *SEM* and it was suggested that they were still able to prevent extensive droplet coalescence (Destribats et al., 2014a; Destribats et al., 2014b). In contrast, Saavedra Isusi et al. (2021) suggested that an excess of microgel particles could promote flocculation of *O/W* emulsions. For example, at a constant pH (pH 3) and ϕ_{OIL} (5%), an increase in the concentration of pectin microgel particles from 0.5 wt.% to > 1 wt.% led to extensive droplet flocculation (Saavedra Isusi et al., 2021b). The minimum C_{SBPMG} used in this study was 10.5 wt.% particles in sample F40. Cursory calculations indicate that the number density of *SBPMG* particles and size differences between the oil droplets and the *SBPMG* are not sufficient for a strong depletion interaction to be responsible for the flocculation. For example, using the expression for the depletion energy, V_{depl}, (Walstra, 2003) as:

$$V_{depl} = 2\pi R\Pi(2\delta - h)^2 \qquad [5.3]$$

: where δ is the excluded volume thickness, R is the radius of the droplets and Π the osmotic pressure due to the microgel particles in the bulk solution. We take δ as the minimum possible diameter of the microgel particles as approximately 1 μm, according to values of $D_{3,2}$ in Table 5.1 for the fine microgels. As a first approximation, the simplest possible expression for $\Pi = Nk_BT$, where N is the number concentration of microgel particles per unit volume, k_B the Boltzmann constant and T the temperature (*i.e.*, no second virial coefficient) may be used. For the firm microgels and the mean droplet surface separation (h) for ϕ_{OIL} = 20 or 40 vol.%, the values of V_{depl} obtained are < 1 k_BT for R = 2 μm droplets, (*i.e.*, droplets larger than any $D_{3,2}$ values observed - see Table 5.2). For the soft microgel–stabilized systems this rises slightly but is still < 2 k_BT for R = 2 μm droplets.

More experiments are required to elucidate the exact flocculation mechanisms observed in the *SBPMG*-stabilized emulsions, however, it should be noted that weak

droplet flocculation is not necessarily a disadvantage, in terms of inhibiting droplet movement and therefore potentially droplet creaming and droplet coalescence. Furthermore, tuning droplet-droplet interactions from repulsive to attractive is routinely used to tailor the rheological properties of emulsions (Fuhrmann et al., 2019) and this was investigated as described in the next section.

5.3.2 Viscoelasticity of *SBP- versus SBPMG-* stabilized emulsions

In addition to droplet-droplet interactions, emulsion rheology depends strongly on the dispersed phase volume fraction (ϕ) (Fuhrmann et al., 2019; Hermes and Clegg, 2013), which for particle-stabilized emulsions includes the volume fraction occupied by both the oil droplets (ϕ_{OIL}) and particles (ϕ_{SBPMG}), where the latter may or may not be adsorbed to the interface.

Figure 5.7 shows the shear rate ($\dot{\gamma}$) dependence of the apparent viscosity (η) for all the emulsions studied. Sample N20 showed some evidence for shear thinning from $\dot{\gamma}$ = 1 to 100 s^{-1}, before η appeared to plateau at η = 6.37 ± 0.66 mPa s between $\dot{\gamma}$ = 100 and 1000 s^{-1}. The microgel-stabilized emulsions S20 and F20 were shear thinning over 5 decades in $\dot{\gamma}$ and showed marked differences in η in the low shear rate region $\dot{\gamma} < 1$ s^{-1}, where η for S20 was consistently greater than η for F20. The $\dot{\gamma}$ dependent η was similar for these samples beyond 1 s^{-1} but never appeared to plateau or reach the same value as N20. The higher viscosities of microgel stabilized emulsions compared with the corresponding native *SBP* emulsions can be attributed in most part to the presence of *SBPMG* particles, which increases ϕ. Furthermore, droplet flocculation also increases the effective ϕ occupied by the dispersed phase since water molecules of the continuous phase become trapped in the interstitial regions of the flocculated emulsion droplets. The more non-spherical (*i.e.*, lower fractal dimension) the clusters become the greater is this effect (Fuhrmann et al., 2019). The shear induced disruption of such flocs resulted in similar flow curves for F20 and S20 at the higher shear rates investigated (Saavedra Isusi et al., 2020b; Zhang, S. et al., 2020; McClements, 2007).

As expected, the emulsions ϕ_{OIL} = 40 % (Figure 5.7) also demonstrated shear thinning flow behavior although marked differences were observed compared to the flow curves for the corresponding emulsions prepared at ϕ_{OIL} = 20 %. For example, at $\dot{\gamma} < 10^{-2}$ s^{-1}, an apparent Newtonian plateau viscosity could be resolved in the microgel stabilized emulsions where η was approximately 100 Pa s for S40 and

around an order of magnitude higher for F40. With increasing $\dot{\gamma}$, this plateau was followed by shear thinning over 5 decades in $\dot{\gamma}$, both samples approaching an η of approximately 0.03 – 0.05 Pa s at $\dot{\gamma}$ =1000 s^{-1}. Interestingly, η for F40 was consistently greater than that of S40 over the entire range of $\dot{\gamma}$ investigated, which is the opposite to the trend found F20 and S20. This likely results from differences in the sample microstructure and potentially reflects the rate at which droplet flocs reform following the pre-shear protocol used (see Section 5.2.2.8)

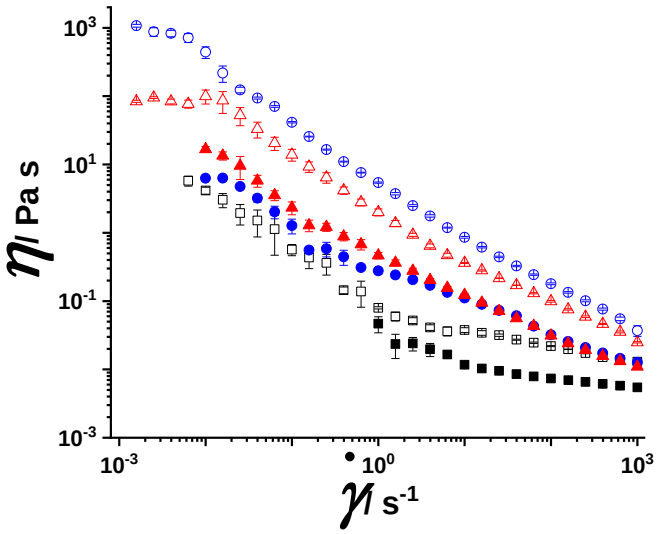

Figure 5.7 – Apparent viscosity (η) as a function of shear rate ($\dot{\gamma}$) for 20 vol.% (filled symbols) and 40 vol.% (open symbols) emulsions stabilized by native *SBP* (■), soft *SBPMG* (▲) and firm *SBPMG* (●).

Oscillatory shear rheometry was therefore employed to probe the sample microstructure non-destructively. Amplitude sweeps were first performed to define the linear viscoelastic region (*LVER*) where the viscoelastic moduli (*G'* = storage modulus and *G"* = loss modulus) were independent of applied strain (γ). Figure 5.8A shows results for the emulsions prepared at ϕ_{OIL} = 40 %. It is shown that *G'* > *G"* over an extended range in γ, suggesting the emulsions were viscoelastic solids 'at rest'. The *G'* values vary with the type of sample in the same way as the viscosity (Figure 5.7) does, that is, *G'* decreases in the order F40 > S40 > N40. The elasticity must arise from an interconnected droplet structure and the magnitude of *G'* is related to the number and strength of the inter-droplet interactions (Hermes and Clegg, 2013; Fuhrmann et al., 2022). The length of the *LVER* was similar for *SBPMG*-stabilized emulsions, extending to $\gamma \approx 2\%$ before the onset of non-linearity and a crossover in *G'* and *G"* was observed at $\gamma \approx 70\%$. Beyond this γ, the

emulsions exhibited an essentially liquid-like response (*i.e.*, *G"*>*G'*) implying that the microstructure was irreversibly perturbed. The length of the *LVER* was significantly shorter for N40, characteristic of a more brittle structure than for the *SBPMG*-stabilized emulsions (Fuhrmann et al., 2022). The *G'* and *G"* determined from frequency sweep measurements on 40 vol.% emulsions at γ within the *LVER* (Figure 5.8B) were in good agreement with the γ sweep measurements. Reliable data could only be collected in a limited frequency range for N40 whereas a plateau in *G'* extended over several decades in frequency for the *SBPMG*-stabilized emulsions was measured, which is again indicative of a more (soft) solid-like structure. Reassuringly, the complex viscosity (η^*) for N40 was in good agreement with the η (Figure 5.7), *i.e.*, obeying the Cox-Merz rule, whilst $\eta^* > \eta$ for the *SBPMG*-stabilized emulsions but the trend of viscosity for F40 > S40 was maintained.

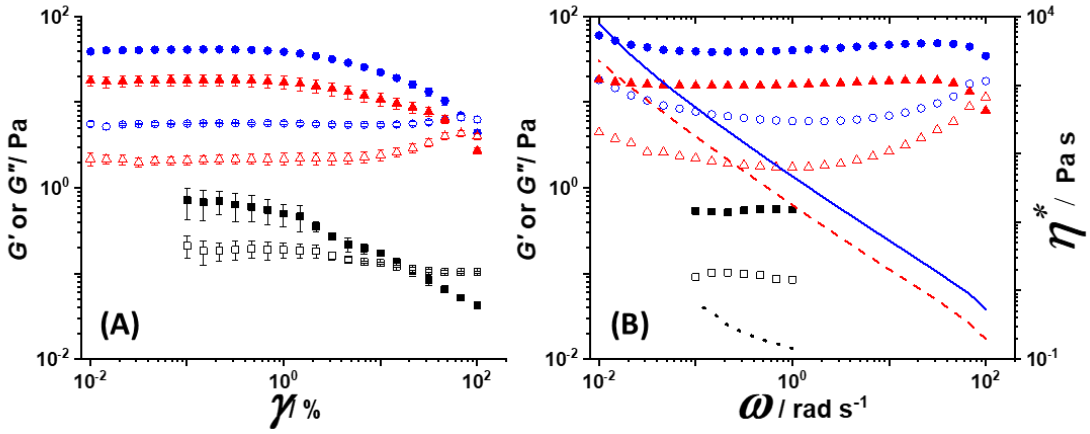

Figure 5.8 – *G'* = storage modulus (filled symbols), *G"* = loss modulus (open symbols) as a function of: (A) strain amplitude (γ) and (B) angular frequency (ω) for emulsions N40 (■), S40 (▲) and F40 (●). In (B), the lines show the complex viscosity (η^*) of N40 (dotted line), S40 (dashed line) and F40 (solid line).

Emulsions prepared at ϕ_{OIL} = 20 % were probed with a liquid-like response (*i.e.*, *G'*>*G"*). Attractive (*i.e.*, flocculated) and concentrated emulsions can demonstrate significant elasticity due to droplet network formation (*i.e.*, emulsion gels) or droplet caging by their nearest neighbors (*i.e.*, soft glassy materials) respectively. Thus, the destruction of droplet networks or cages by external stresses results in a solid-fluid transition transition (Fuhrmann et al., 2022; Hermes and Clegg, 2013). A more detailed study over a wider range of ϕ_{OIL} and ϕ_{SBPMG} is required to speculate on the

origin of elasticity in these emulsions, but the results suggest that the rheological properties of emulsions can be tailored through selection of emulsifier, either native *SBP* or *SBPMG* of different elasticity. It is worth noting here that Saavedra Isusi et al. (2020) began to construct a ternary phase diagram for their pectin microgel stabilized emulsions and suggested that emulsion gel networks were formed above 10 wt.% microgel particles even in emulsions prepared at ϕ_{OIL} = 10% (Saavedra Isusi et al., 2020b).

5.3.3 Physical stability of *SBP- versus SBPMG*-stabilized emulsions

The experimental results discussed so far suggest that native *SBP* is a more efficient emulsifier than *SBPMG*s due to its ability to stabilize finer emulsion droplets with no apparent flocculation. However, this does not address the long-term and process stability of the emulsions, which in industry may be subjected to cycles of heating and cooling as well as prolonged storage. Changes in the visual appearance and the *PSD*s of both set of emulsions were therefore also assessed over 9 weeks storage and also after heating and cooling cycles between 75 °C (held at this temperature for 30 min) and 25 °C. The size parameters $D_{4,3}$ and D_{90} are reported, since these are the most sensitive to any droplet coarsening. These were calculated as described in Section 5.3.1 in relation to Figure 5.2 and 5.3.

The results of the thermal cycling experiments are illustrated in Figures 5.9A and 5.9B for ϕ_{OIL} = 20 and 40%, respectively. It should be noted that none of the emulsions exhibited phase separation due to the heating cycles. For the 20 vol.% emulsions (Figure 5.9A), the histograms show a significant increase in the $D_{4,3}$ and D_{90} after one heating cycle for all samples, compared to the initial non-heated emulsions. A further increase in size between the 1st and 2nd heating cycle was significant for all samples - with the exception of the $D_{4,3}$ for S20. For the 40 vol.% emulsions (Figure 5.9B), the increases in droplet size for N40 were significant but the *SBPMG*-stabilized emulsions (S40 and F40) appeared to be more stable to heating. For example, no significant differences were found in $D_{4,3}$ or D_{90} of S40 after two heating cycles. Furthermore, the D_{90} for F40 increased significantly after the first heating cycle but the increase after the 2nd heating cycle was not significant. The use of softer microgels for emulsion stabilization has been shown to lead to an

increased interfacial elasticity, which should improve the stability of droplets against coalescence under these conditions (Li et al., 2015; Huang et al., 2021).

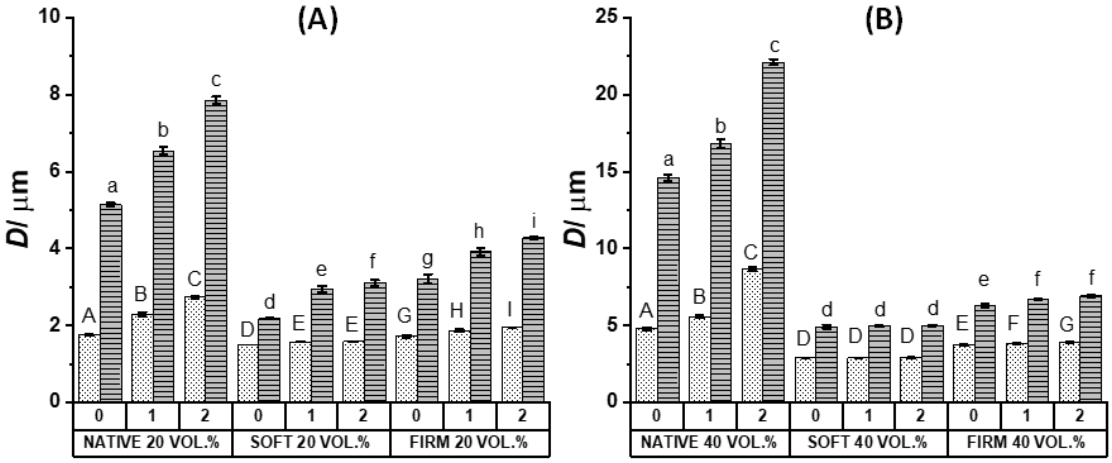

Figure 5.9 – Average particle diameters (*D*) of emulsions represented by the $D_{4,3}$ (dotted columns) and D_{90} (striped columns) values before (0) and after one (1) or two (2) heating cycles as described in the text. (A) and (B) show results for ϕ_{OIL} = 20 vol.% and 40 vol.%, respectively, stabilized by native *SBP*, soft *SBPMG* or firm *SBPMG*. Columns sharing the same letters do not show significant differences between the heating cycles ($p < 0.05$) - upper case letters are used to indicate this for the $D_{4,3}$ values and lowercase letters for the are used for the D_{90} values.

The average droplet sizes and percentage increases in the droplet diameter (ΔD) after two heating cycles are shown in Table 5.3. The ΔD was found to be highest for the *SBP*-stabilized emulsions irrespective of ϕ_{OIL}. For example, the $D_{4,3}$ of N20 and N40 increased from 1.76 to 2.74 µm and from 4.8 to 8.7 µm, respectively, corresponding to large ΔD of 55.7 and 81.3 %, respectively. This is hypothesized as being due to the non-Pickering nature of the *SBP* stabilizer compared to the *SBPMG*, which is therefore less able to prevent coalescence and Ostwald ripening. To confirm this hypothesis, light microscopy was also performed on these emulsions after 2 heating cycles and typical results are shown in Figures 5.4G and 5.4H for N20 and N40, respectively. Compared to the corresponding *unheated* samples (shown in Figures 4E and 4F respectively), a clear increase in droplet size is apparent but with the absence of extensive droplet flocculation. No conclusive differences were observed in the light microscopy images (not shown) of any of the

SBPMG-stabilized emulsions after heating, despite significant increases in the apparent droplet sizes measured by laser diffraction for all samples except S40. However, it should be remembered that the samples were extensively diluted before the light microscopy, which might have disrupted any loose flocs of droplets, whilst the *PSD*s and resultant droplet size measurements may be skewed by a small number of some persistent large flocs (Figure 5.2), which may possibly be strengthened by heating. The *SBPMG*-stabilized emulsions at ϕ_{OIL} = 40% were more stable against heat-induced droplet coarsening compared to those at ϕ_{OIL} = 20 % (Table 5.3). This suggests an additional contribution to emulsion stability from the higher ϕ_{SBPMG} and its effect on the viscoelasticity of the emulsions, as discussed above.

Figure 5.10 shows the evolution of particle size with storage time at 25 °C of the non-heated emulsions. Figures 5.10A and 5.10C shows the D_{90} and $D_{4,3}$ for emulsions with ϕ_{OIL} = 20 %, respectively, whilst Figures 5.10B and 5.10D show the corresponding D_{90} and $D_{4,3}$ for emulsions with ϕ_{OIL} = 40 %. The data presented illustrate a profound between the stability of emulsions stabilized by native *SBP* and that of the *SBPMG*-stabilized emulsions. The sizes in the latter remain more or less constant over 63 days storage, whereas the droplet sizes (Figure 5.10B and 5.10D) in the N40 emulsion appears to increase progressively and continuously over at least 56 days, before appearing to begin to plateau off. The same behavior was observed in the N20 system (Figures 5.10A and 5.10C), although there was slightly more scatter in the data and no clear evidence for a plateau in size at the end of the storage period. Table 5.2 shows the D_{90} and $D_{4,3}$ for each emulsion on day 1 and day 63 and the ΔD over this storage period. In all cases, the increase in droplet size was significant but ΔD was substantially lower for the *SBPMG*-stabilized emulsions. For example, the $D_{4,3}$ for N40 increased by 301% compared to an increase of 21% and 15% for S40 and F40 respectively.

Table 5.3 – Average particle sizes of emulsions stabilized by native *SBP* and *SBPMG* (after de-flocculation) as determined by laser diffraction as a function of heating and cooling cycles. The % change in droplet size (ΔD) after two heating cycles is shown in the final 2 columns.

	Before heating		After 1 heating cycle		After 2 heating cycles		%ΔD after 2 heating cycles	
	$D_{4,3}$ / µm	D_{90} / µm	$D_{4,3}$ / µm	D_{90} / µm	$D_{4,3}$ / µm	D_{90} / µm	$D_{4,3}$ / %	D_{90} / %
N20	1.76 ± 0.01	5.14 ± 0.04	2.29 ± 0.06	6.54 ± 0.1	2.74 ± 0.04	7.85 ± 0.09	55.7	52.7
S20	1.52 ± 0.01	2.18 ± 0.02	1.58 ± 0.01	2.95 ± 0.08	1.59 ± 0.01	3.11 ± 0.08	4.6	42.7
F20	1.72 ± 0.03	3.22 ± 0.12	1.87 ± 0.03	3.92 ± 0.09	1.95 ± 0.01	4.28 ± 0.04	13.4	32.9
N40	4.85 ± 0.08	14.6 ± 0.2	5.64 ± 0.1	16.82 ± 0.29	8.7 ± 0.06	22.1 ± 0.15	81.3	51.4
S40	2.92 ± 0.04	4.94 ± 0.13	2.9 ± 0.01	4.98 ± 0.03	2.93 ± 0.01	5.01 ± 0.05	0.3	1.4
F40	3.73 ± 0.03	6.31 ± 0.13	3.86 ± 0.02	6.71 ± 0.07	3.95 ± 0.03	6.93 ± 0.09	5.9	9.8

At the C_{PTOTAL} used here, the native *SBP* is clearly a poor stabilizer under temperature cycling and prolonged storage conditions. Other authors have previously suggested that although the protein side chains anchor strongly to the oil-water interface, the polysaccharide chains of *SBP* protruding into the continuous phase are insufficient to confer effective (electro-)steric stabilization. Indeed, the stability of *SBP*-based emulsions has been improved by chemical cross-linking of *SBP* (Jung and Wicker, 2012; Zhang, L. et al., 2015) in dilute solution to increase the *MW* before their use as emulsifiers, as noted in the Introduction. In a similar vein, protein side chains of *SBP* have been used as a target for chemical crosslinking via lysine residues in a reaction catalyzed by genipin (Lin et al., 2020). Such supramolecular aggregates could also be regarded as microgel particles, but are

likely substantially 'softer' than those presented here. Nonetheless, in all of these studies, droplet coarsening on storage was reduced for modified *SBP* stabilized emulsions compared to the non-cross-linked controls (Jung and Wicker, 2012; Lin et al., 2020), even at elevated temperatures (60 °C) (Zhang, L. et al., 2015).

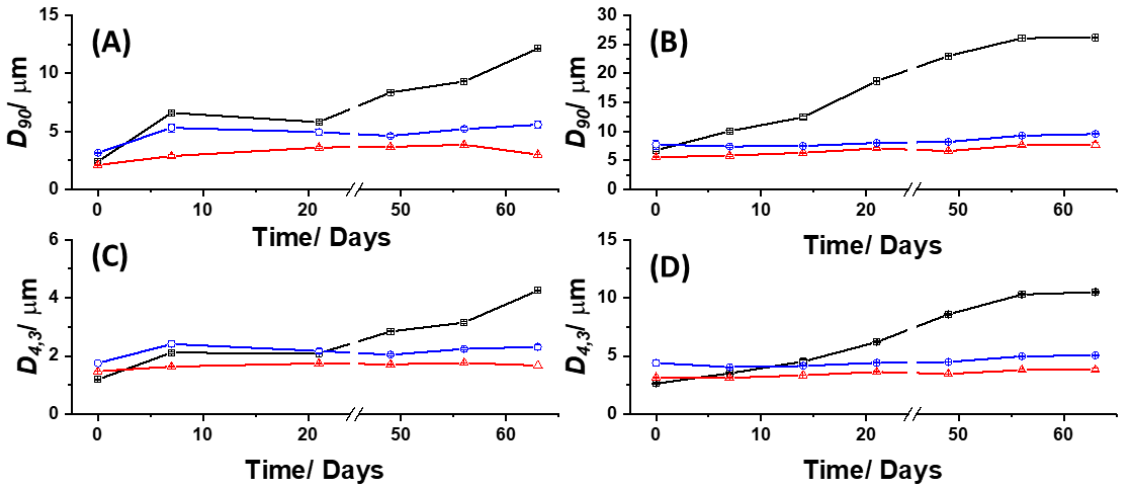

Figure 5.10 – Evolution of (A) D_{90} and (B) $D_{4,3}$ with prolonged storage time at 25 °C for the ϕ_{OIL} = 20 vol.% emulsions stabilized by native *SBP* (■), soft *SBPMG* (▲) and firm *SBPMG* (●). (B) and (D) show the corresponding D_{90} and $D_{4,3}$ values for the ϕ_{OIL} = 40 vol.% emulsions.

Most of the emulsions were found to undergo phase separation into a droplet rich cream layer and a droplet depleted serum layer on prolonged storage, as illustrated by the photographs in Figures 5.11A-B for the 20 vol.% emulsions and 5.11C-D for the 40 vol.% emulsions on day 1 and day 21. This gravitational separation was quantified by the creaming index (*CI*) given by Equation 5.1. For the 20 vol.% emulsions (Figure 5.11E), the rate and extent of creaming over the initial 21 days storage followed the order F20 > S20 > N20. By day 49 creaming in S20 appeared to have accelerated and approached the *CI* of F20. The remaining 2 weeks showed a reduced rate of creaming for the *SBPMG*-stabilized emulsions, which reached a similar *CI* of ~44% on day 63. The cream layer in N20 was accidently disrupted after measuring the *CI* on day 56, although the *CI* already appeared to be approaching a plateau of CI ≈ 30.5%.

The observed trend in creaming stability was reversed for the 40 vol.% emulsions with N40 > S40 > F40, clearly visible in the corresponding photographs (Figures 5.11A-D). Sample F40 showed no evidence for creaming over the entire storage

period. The *CI* of N40 and S40 appeared to have plateaued at around day 49. Taking an average of the final 3 data points gives *CI* = 38.4 ± 0.4 % and 17.3 ± 0.3 % for N40 and S40, respectively (Figure 5.11F). Hence, S40 creamed to a lesser extent than S20, whereas N40 creamed more extensively than N20.

For the *SBP*-stabilized emulsions, the time dependence of the *CI* is well correlated with the progressive increase in droplet size over the same storage period (see Figures 5.10A, 5.10C and Table 5.1) according to Stokes' Law, which can also explain the relatively faster and more extensive creaming of S20 and F20 compared to N20 if the flocculation increases the effective droplet size but does not lead to a droplet gel network entirely preventing creaming (Hermes and Clegg, 2013). Indeed, the improved stability to creaming of the *SBPMG*-stabilized emulsions at the higher ϕ_{OIL} of 40% is probably related to the development of just this sort of interconnected microstructure, as suggested by the oscillatory shear rheometry results (Figure 5.8).

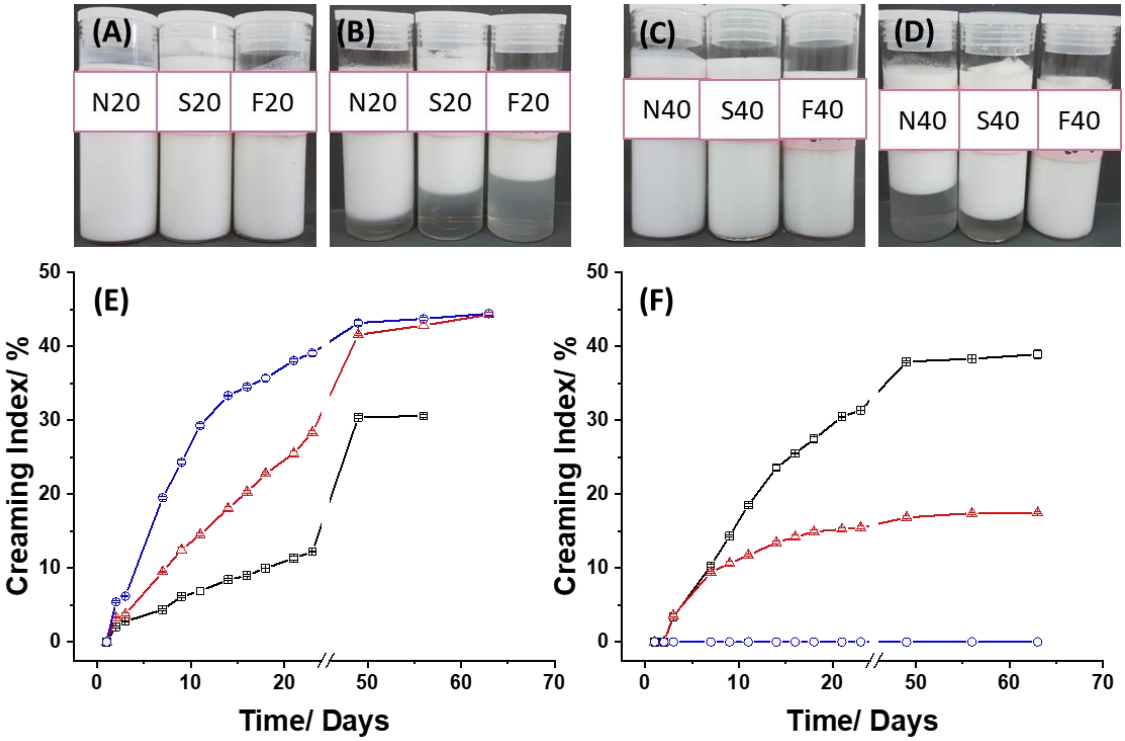

Figure 5.11 – Visual assessment of creaming stability for emulsions on prolonged storage at 25 °C. (A) and (B) show photographs of 20 vol.% emulsions on day 1 and day 21 respectively. (C) and (D) shows photographs of 40 vol.% emulsions on day 1 and day 21 respectively. Each left, middle and right photograph shows emulsions were stabilized by native *SBP*, soft and firm *SBPMG* respectively. (E) and (F) show the creaming index at various time intervals over 63 days storage for 20 vol.% and 40 vol.% emulsions, respectively, stabilized by native *SBP* (■), soft *SBPMG* (▲) and firm *SBPMG* (●).

5.4 Conclusions

In this work we have introduced a novel route to improved emulsion stability by converting *SBP*, a surface active hydrocolloid, into *SBP* microgel particles (*SBPMG*). Owing to the Pickering emulsification mechanism, the *SBPMG*-stabilized emulsions demonstrated improved stability towards droplet coarsening on (i) temperature cycling and (ii) prolonged storage at ambient temperature compared to native *SBP* at the same total *SBP* content (C_{PTOTAL}). Furthermore, the use of *SBPMG*s as emulsifiers enabled significant enhancement of the viscoelasticity of the emulsions, due to a combination of droplet flocculation and the increase in overall volume faction of dispersed particles due to the presence of *SBPMG* themselves. The softer *SBPMG* seemed to give slightly smaller initial droplet sizes than the firm *SBPMG*, but the latter seemed to lead to greater thickening effects, particularly at higher volume fractions of oil droplets, that even more significantly curtailed creaming. Our future work on these systems will aim to investigate separately the influence of ϕ_{OIL} and ϕ_{SBPMG} on the properties of such emulsions and also investigate a wider range of particle elasticities, with the mechanical properties of individual particles also assessed (*e.g.*, via atomic force microscopy). Considering the great potential for *SBPMGs* as emulsifiers in foods, their emulsifying properties should be also be investigated under different environmental conditions, for example, by varying the ionic strength and pH and also with food-grade oils.

5.5 Acknowledgements

We thank Mr. Stuart Micklethwaite of the Leeds electron microscopy and spectroscopy center and Dr. Ruth Hughes of the Leeds bio-imaging and flow cytometry facility for their excellent technical assistance in sample imaging via *SEM* and *CLSM* respectively.

5.6 References

Adams, S., Frith, W.J. and Stokes, J.R. 2004. Influence of particle modulus on the rheological properties of agar microgel suspensions. Journal of Rheology. 48, pp.1195-1213.

Akhtar, M., Dickinson, E., Mazoyer, J. and Langendorff, V. 2002. Emulsion stabilizing properties of depolymerized pectin. Food Hydrocolloids. 16(3), pp.249-256.

Alba, K. and Kontogiorgos, V. 2017. Pectin at the oil-water interface: Relationship of molecular composition and structure to functionality. Food Hydrocolloids. 68, pp.211-218.

Atarés, L., Marshall, L.J., Akhtar, M. and Murray, B.S. 2012. Structure and oxidative stability of oil in water emulsions as affected by rutin and homogenization procedure. Food Chemistry. 134(3), pp.1418-1424.

Bunzel, M. 2010. Chemistry and occurrence of hydroxycinnamate oligomers. Phytochemistry Reviews. 9(1), pp.47-64.

Chen, H., Qiu, S., Gan, J., Liu, Y., Zhu, Q. and Yin, L. 2016. New insights into the functionality of protein to the emulsifying properties of sugar beet pectin. Food Hydrocolloids. 57, pp.262-270.

Dea, I.C.M. and Madden, J.K. 1986. Acetylated pectic polysaccharides of sugar beet. Food Hydrocolloids. 1(1), pp.71-88.

Destribats, M., Eyharts, M., Lapeyre, V., Sellier, E., Varga, I., Ravaine, V. and Schmitt, V. 2014a. Impact of pNIPAM Microgel Size on Its Ability To Stabilize Pickering Emulsions. Langmuir. 30(7), pp.1768-1777.

Destribats, M., Rouvet, M., Gehin-Delval, C., Schmitt, C. and Binks, B.P. 2014b. Emulsions stabilised by whey protein microgel particles: towards food-grade Pickering emulsions. Soft Matter. 10(36), pp.6941-6954.

Dickinson, E. 2003. Hydrocolloids at interfaces and the influence on the properties of dispersed systems. Food Hydrocolloids. 17(1), pp.25-39.

Dickinson, E. 2015. Microgels — An alternative colloidal ingredient for stabilization of food emulsions. Trends in Food Science & Technology. 43(2), pp.178-188.

Dickinson, E. 2016. Exploring the frontiers of colloidal behaviour where polymers and particles meet. Food Hydrocolloids. 52, pp.497-509.

Ellis, A. and Jacquier, J.C. 2009. Manufacture and characterisation of agarose microparticles. Journal of Food Engineering. 90(2), pp.141-145.

Fuhrmann, P.L., Breunig, S., Sala, G., Sagis, L., Stieger, M. and Scholten, E. 2022. Rheological behaviour of attractive emulsions differing in droplet-droplet interaction strength. Journal of Colloid and Interface Science. 607, pp.389-400.

Fuhrmann, P.L., Sala, G., Stieger, M. and Scholten, E. 2019. Clustering of oil droplets in o/w emulsions: Controlling cluster size and interaction strength. Food Research International. 122, pp.537-547.

Funami, T., Zhang, G., Hiroe, M., Noda, S., Nakauma, M., Asai, I., Cowman, M.K., Al-Assaf, S. and Phillips, G.O. 2007. Effects of the proteinaceous moiety on the emulsifying properties of sugar beet pectin. Food Hydrocolloids. 21(8), pp.1319-1329.

Hermes, M. and Clegg, P.S. 2013. Yielding and flow of concentrated Pickering emulsions. Soft Matter. 9(31), pp.7568-7575.

Hu, M., Wu, Y., Wang, J., Lu, W., Gao, Z., Xu, L., Cui, S., Fang, Y. and Nishinari, K. 2021. Emulsions Stabilization and Lipid Digestion Profiles of Sodium Alginate Microgels: Effect of the Crosslink Density. Food Biophysics. 16(3), pp.346-354.

Huang, P., Huang, C., Ma, X., Gao, C., Sun, F., Yang, N. and Nishinari, K. 2021. Effect of pH on the mechanical, interfacial, and emulsification properties of chitosan microgels. Food Hydrocolloids. 121, p106972.

Ishii, T., Matsumiya, K., Aoshima, M. and Matsumura, Y. 2018. Microgelation imparts emulsifying ability to surface-inactive polysaccharides—bottom-up vs top-down approaches. npj Science of Food. 2(1), p15.

Jung, J. and Wicker, L. 2012. Laccase mediated conjugation of sugar beet pectin and the effect on emulsion stability. Food Hydrocolloids. 28(1), pp.168-173.

Kargar, M., Fayazmanesh, K., Alavi, M., Spyropoulos, F. and Norton, I.T. 2012. Investigation into the potential ability of Pickering emulsions (food-grade particles) to enhance the oxidative stability of oil-in-water emulsions. Journal of Colloid and Interface Science. 366(1), pp.209-215.

Khalighi, S., Berger, R.G. and Ersoy, F. 2020. Cross-Linking of Fibrex Gel by Fungal Laccase: Gel Rheological and Structural Characteristics. Processes. 8(1).

Kirby, A.R., MacDougall, A.J. and Morris, V.J. 2006. Sugar Beet Pectin–Protein Complexes. Food Biophysics. 1(1), p51.

Lefroy, K.S., Murray, B.S., Ries, M.E. and Curwen, T.D. 2021. A natural, cellulose-based microgel for water-in-oil emulsions. Food Hydrocolloids. 113, p106408.

Leroux, J., Langendorff, V., Schick, G., Vaishnav, V. and Mazoyer, J. 2003. Emulsion stabilizing properties of pectin. Food Hydrocolloids. 17(4), pp.455-462.

Levigne, S.b.V., Ralet, M.-C.J., Quéméner, B.C., Pollet, B.N.L., Lapierre, C. and Thibault, J.-F.o.J. 2004. Isolation from Sugar Beet Cell Walls of Arabinan Oligosaccharides Esterified by Two Ferulic Acid Monomers. Plant Physiology. 134(3), pp.1173-1180.

Li, Z., Harbottle, D., Pensini, E., Ngai, T., Richtering, W. and Xu, Z. 2015. Fundamental Study of Emulsions Stabilized by Soft and Rigid Particles. Langmuir. 31(23), pp.6282-6288.

Lin, J., Yu, S., Ai, C., Zhang, T. and Guo, X. 2020. Emulsion stability of sugar beet pectin increased by genipin crosslinking. Food Hydrocolloids. 101, p105459.

Lyon, L.A. and Fernandez-Nieves, A. 2012. The Polymer/Colloid Duality of Microgel Suspensions. Annual Review of Physical Chemistry. 63(1), pp.25-43.

Matsumiya, K. and Murray, B.S. 2016. Soybean protein isolate gel particles as foaming and emulsifying agents. Food Hydrocolloids. 60, pp.206-215.

McClements, D.J. 2007. Critical Review of Techniques and Methodologies for Characterization of Emulsion Stability. Critical Reviews in Food Science and Nutrition. 47(7), pp.611-649.

Mironov, M.A., Shulepov, I.D., Ponomarev, V.S. and Bakulev, V.A. 2013. Synthesis of polyampholyte microgels from colloidal salts of pectinic acid and their application as pH-responsive emulsifiers. Colloid and Polymer Science. 291(7), pp.1683-1691.

Murray, B.S. 2019. Microgels at fluid-fluid interfaces for food and drinks. Advances in Colloid and Interface Science. 271, p101990.

Ngouémazong, E.D., Christiaens, S., Shpigelman, A., Van Loey, A. and Hendrickx, M. 2015. The Emulsifying and Emulsion-Stabilizing Properties of Pectin: A Review. Comprehensive Reviews in Food Science and Food Safety. 14(6), pp.705-718.

Saavedra Isusi, G.I., Bindereif, B., Karbstein, H.P. and van der Schaaf, U.S. 2020a. Polymer or microgel particle: Differences in emulsifying properties of pectin as microgel or as individual polymer chains. Colloids and Surfaces A: Physicochemical and Engineering Aspects. 598, p124793.

Saavedra Isusi, G.I., Karbstein, H.P. and van der Schaaf, U.S. 2019. Microgel particle formation: Influence of mechanical properties of pectin-based gels on microgel particle size distribution. Food Hydrocolloids. 94, pp.105-113.

Saavedra Isusi, G.I., Lohner, N., Karbstein, H.P. and van der Schaaf, U.S. 2021a. Emulsions stabilised with pectin-based microgels: Investigations into the break-up of droplets in the presence of microgels. Journal of Food Engineering. 294, p110421.

Saavedra Isusi, G.I., Madlindl, L.B., Karbstein, H.P. and van der Schaaf, U.S. 2020b. Microstructures and conformational arrangement in emulsions caused by concentration ratios of pectin-based microgels and oil. Colloids and Surfaces A: Physicochemical and Engineering Aspects. 602, p125166.

Saavedra Isusi, G.I., Weilandt, M., Majollari, I., Karbstein, H.P. and van der Schaaf, U.S. 2021b. Emulsions stabilised with pectin-based microgels: investigations into the effect of pH and ionic strength on emulsion stability. Food & Function. 12(16), pp.7227-7238.

Sarkar, A., Murray, B., Holmes, M., Ettelaie, R., Abdalla, A. and Yang, X. 2016. In vitro digestion of Pickering emulsions stabilized by soft whey protein microgel particles: influence of thermal treatment. Soft Matter. 12(15), pp.3558-3569.

Sarkar, A., Zhang, S., Holmes, M. and Ettelaie, R. 2019. Colloidal aspects of digestion of Pickering emulsions: Experiments and theoretical models of lipid digestion kinetics. Advances in Colloid and Interface Science. 263, pp.195-211.

Schmidt, U.S., Schmidt, K., Kurz, T., Endreß, H.U. and Schuchmann, H.P. 2015. Pectins of different origin and their performance in forming and stabilizing oil-in-water-emulsions. Food Hydrocolloids. 46, pp.59-66.

Siew, C.K. and Williams, P.A. 2008. Role of Protein and Ferulic Acid in the Emulsification Properties of Sugar Beet Pectin. Journal of Agricultural and Food Chemistry. 56(11), pp.4164-4171.

Stubley, S.J., Cayre, O.J., Murray, B.S., Torres, I.C. and Farrés, I.F. 2021. Enzyme cross-linked pectin microgel particles for use in foods. Food Hydrocolloids. 121, p107045.

Thakur, B.R., Singh, R.K., Handa, A.K. and Rao, M.A. 1997. Chemistry and uses of pectin — A review. Critical Reviews in Food Science and Nutrition. 37(1), pp.47-73.

Thibault, J.-F., Garreau, C. and Durand, D. 1987. Kinetics and mechanism of the reaction of ammonium persulfate with ferulic acid and sugar-beet pectins. Carbohydrate Research. 163(1), pp.15-27.

Walstra, P. 2003. Colloidal interactions. Physical chemistry of foods. 1st ed. USA: Marcel Dekker.

Williams, P.A., Sayers, C., Viebke, C., Senan, C., Mazoyer, J. and Boulenguer, P. 2005. Elucidation of the Emulsification Properties of Sugar Beet Pectin. Journal of Agricultural and Food Chemistry. 53(9), pp.3592-3597.

Yapo, B.M., Robert, C., Etienne, I., Wathelet, B. and Paquot, M. 2007. Effect of extraction conditions on the yield, purity and surface properties of sugar beet pulp pectin extracts. Food Chemistry. 100(4), pp.1356-1364.

Zhang, L., Shi, Z., Shangguan, W., Fang, Y., Nishinari, K., Phillips, G.O. and Jiang, F. 2015. Emulsification properties of sugar beet pectin after modification with horseradish peroxidase. Food Hydrocolloids. 43, pp.107-113.

Zhang, S., Holmes, M., Ettelaie, R. and Sarkar, A. 2020. Pea protein microgel particles as Pickering stabilisers of oil-in-water emulsions: Responsiveness to pH and ionic strength. Food Hydrocolloids. 102, p105583.

Chapter 6: Concluding Remarks and Ideas for Future Work

6.1 Conclusions

As discussed in **Chapter 1**, the overall objective of this thesis was to fabricate and characterize biopolymer microgel suspensions suitable for use in foods. The food applications of interest to the project co-sponsor (Nestlé) included the use of microgel particles as (i) novel rheology modifiers for confectionary systems and (ii) novel stabilizers and emulsifiers for beverages. In addition, a model system based on synthetic microgels was to be investigated to gain fundamental insight into the factors which promote desirable functional properties in microgel systems.

In **Chapter 2**, microgels based on poly(N-isopropylacrylamide) (*p(NIPAM)*) were synthesized using a conventional free radical polymerization. In the end, this chapter mainly served to introduce microgels as soft colloidal particles. Such systems are approximately spherical, compatible with dynamic light scattering and demonstrate narrow particle size distributions, all of which facilitated a study into the stability of microgels with respect to the solvent conditions *i.e.*, pH, ionic strength and temperature. The stability of such microgels is attributed to a combination of surface charges and a 'fuzzy' interface which provides steric stability, analogous to the stabilization of hard-sphere colloids by polymers. This is also expected to be the case for the biopolymer microgels produced in subsequent chapters, although their irregular morphology and larger dimensions made investigations into the stability of suspensions more challenging with the techniques available to us. The most useful finding in **Chapter 2** was that *p(NIPAM)* microgels can be synthesized at higher polymer concentrations than what has previously been reported. These experiments also provided the foundation for subsequent studies into biopolymer (pectin-based) microgels. For example, the rationale behind using dilute suspension viscometry to determine an effective volume fraction (ϕ_{eff}), and the variation of the bulk viscosity with ϕ_{eff} were outlined at this stage.

Due to time constraints and at the discretion of the industrial sponsor, the development of biopolymer microgels was prioritised. **Chapter 3** describes our earliest attempts at producing such a system, using pectin, which was the biopolymer of interest to the sponsor. This was because pectin is plant-based, and

thus renewable and suitable for food products consumed by those with restricted diets, either due to religious or ethical reasons. Pectins are generally considered as ‘clean label’ additives and are therefore well accepted by the consumer.

Within the research group at Leeds and elsewhere, the top-down technique to produce microgel suspensions from bulk, ‘parent’ hydrogels had been used to create microgels from a variety of different biopolymers. This technique is both simple and scalable and thus holds great promise for the production of microgels in large quantities. After some trial and error, the top-down technique was also found to be suitable for pectin microgels. Using low methyl ester pectins (*LMP*), physical crosslinking can be achieved using divalent cations *e.g.*, Ca^{2+}, resulting in bulk hydrogels above a critical polymer concentration. When combined with a *suitable* solvent, their comminution should technically yield microgel suspensions. In a first attempt, for simplicity and to maintain biocompatibility, water was used to facilitate the production of suspensions.

Considering (i) the requirements for thermal treatment during processing, (ii) the high solvent content and (iii) the extended shelf lives of food products where microgels could potentially be used as novel additives, it became apparent that a solvent other than water, or a more robust method of crosslinking was required. This is because *LMP* microgels were found to be prone to dissolution when placed in contact with pure water, and the parent hydrogels (thus presumably microgel particles) were found to disintegrate on the application of heat (data not shown). Dissolution of *LMP* microgels on storage could be prevented by adding crosslinking ions to the continuous phase at equivalent concentration to that used to prepare the hydrogels in the first place. However, controlling the ionic environment in real food systems is expected to be challenging and, in many cases, probably undesirable.

To that end, it was decided to pursue a chemical crosslinking route in the development of pectin microgels. This was achieved by selecting pectins from a different botanical source, namely sugar beet pectins (*SBP*), as it had previously been demonstrated that the presence of ferulic acid residues naturally bound to the polymer backbone allows for intermolecular chemical crosslinking catalyzed by an oxidoreductase enzyme, namely laccase. The permanence of covalent crosslinks was expected to provide structural integrity to the microgel particles under the processing and storage conditions mentioned above. Indeed, *SBP* microgels

(*SBPMG*s) were found to resist dissolution on several months storage in water, and when subjected to heating typical of pasteurization conditions. Although no micromechanical characterization of discrete *SBPMG*s was performed, we assumed that the elasticity of the parent hydrogel, assessed via oscillatory shear rheometry, would directly influence the elasticity of the *SBPMG*s. This is easily controlled by preparing gels at different polymer concentrations (C_{GEL}). Consequently, with the same input of energy during the mechanical disruption of the parent hydrogels, the average microgel particle sizes were also larger for stronger gels. This necessitated a definition of ϕ_{eff} to compare their rheological properties in concentrated suspensions, which was the subject of **Chapter 4**. However, the benefits of using microgel particles as rheology modifiers over native polymers had already become apparent, as highlighted in the comparison of the viscosity curves for either system, studied with respect to the total pectin concentration in the system (C_{PTOTAL}) where microgels provided a significantly enhanced viscosity at equivalent C_{PTOTAL} (see Figure 3.11 and the associated discussion).

Building on this work, a detailed investigation into the rheological properties of *SBPMG* suspensions was performed **(Chapter 4)** with a hypothesis that the viscoelasticity of *SBPMG* suspensions depends on ϕ_{eff} and the elasticity (*i.e.,* crosslinking density) of the discrete microgel particles (G'_{MG}). Capillary viscometry was performed on three sets of dilute *SBPMG* suspensions to determine ϕ_{eff} following the same procedure outlined in **Chapter 2**, *i.e.,* via the modified Einstein(-Batchelor) equation. Native *SBP* solutions were also studied as a comparison. With respect to C_{PTOTAL}, distinct differences were observed in the intrinsic viscosities between samples. For example, Table 4.2 showed that the intrinsic viscosity for *SBPMG* was highest for the 'softest' particles *i.e.,* lowest crosslinking density/G'_{MG}. Furthermore, the latter were shown to demonstrate a higher intrinsic viscosity than native *SBP*. These results suggest that even for fluid-like applications (*e.g.,* beverages, sauces and dressings), *SBPMG* can be used to control the rheological properties. However, this was not investigated in further detail since it was the rheological properties of concentrated suspensions which were of more interest in this thesis.

By concentrating the samples via centrifugation, the rheological properties of suspensions of different G'_{MG} could be studied with respect to ϕ_{eff}. Shear rheometry was performed using rotational techniques to determine the shear rate dependent

viscosities. In all cases, the relative zero shear viscosity (η_{rel0}) increased gradually until at some critical ϕ_{eff}, η_{0rel} diverged strongly, in all cases exceeding 10^6 (*i.e.*, the viscosity of suspensions was more than a million times that of the pure solvent). This occurred at higher ϕ_{eff} for softer particles, reflecting the increased potential for particle deformation and interpenetration as G'_{MG} decreased. In contrast, when assessed with respect to C_{PTOTAL}, the divergence of the η_{0rel} occurred in the opposite order, *i.e.*, the softest microgels were most effective at enhancing the viscosity of the pure solvent. This shows how processing could be made more economical by converting *SBP* to *SBPMG*. For example, if the sole purpose of using *SBPMG*s was to increase the viscosity of a given formulation, then soft microgels, which contain less *SBP* to begin with, might be sufficient.

For some applications, rheological additives might be added to a formulation to impart elasticity on it. For suspensions, this can be delivered at high ϕ_{eff} often resulting in a time independent 'solid-like' behavior. Comparing the elasticity of the softest and most firm *SBPMG*, the elasticity of suspensions (G') increased more strongly as a function of ϕ_{eff} and reached higher values for the latter. Furthermore, the G' of dense suspensions of firm *SBPMG* approached that of the parent hydrogels. In contrast to formulations which have been 'solidified' using polymeric gelling agents, the suspensions can be made to *reversibly* flow on the application of forces exceeding an apparent yield stress (or a critical strain). Similarly, elasticity can be delivered due to the dense packing of particles rather than (relatively short lived) polymer chain entanglements as in native polymer solutions. These results suggest that the elasticity of a given formulation can be tailored simply by using microgel particles of different elasticity, which is easily controlled by varying C_{GEL}. This may be a significant advantage to the manufacturer when developing new products or processes.

An ϕ_{eff} >1 was routinely accessed in *SBPMG* suspensions which was explained in detail in **Chapter 4.** However, it should be noted that the swelling ratio determined from equilibrium swelling experiments on parent hydrogels was used to correct for particle swelling in the determination of ϕ_{eff}. This results in a ϕ_{eff} ranging from 1.42 – 1.5 times higher than if the correction for particle swelling was not used. While we feel that it is reasonable to include the swelling correction for a determination of ϕ_{eff} at high dilution, it may not be appropriate at high phase volumes due to the potential for osmotic deswelling. If this could be quantified, one could potentially remove the

swelling correction, ideally in a concentration (ϕ_{eff}) dependent manner, since the osmotic pressure increases with an increase in the solute concentration (Borrega et al., 1999).

In **Chapter 5**, the *SBPMG*s were used to stabilize oil-in-water (*O/W*) emulsions at oil volume fractions (ϕ_{OIL}) of ϕ_{OIL} = 20 and 40 % respectively. Comparisons with emulsions stabilized by native (*i.e.*, non-crosslinked) *SBP* were made throughout. Therefore, the amount of stabilizer added was controlled by keeping C_{PTOTAL} in the continuous phase constant. While *SBP* is known to be a surface active hydrocolloid (*i.e.*, due to the presence of bound proteins), it was hypothesized that by converting *SBP* to *SBPMG*, significant improvements in the emulsion stability could be achieved. This was due to the potential for *SBPMG* particles to stabilize emulsions through a 'Pickering' mechanism. In previous studies (Zhang et al., 2015; Jung and Wicker, 2012), chemical crosslinking of *SBP* in dilute aqueous solutions (*i.e.*, to avoid the formation of macrogel) could improve emulsion stability compared to emulsions prepared with native *SBP*. To some extent, this crosslinking approach is similar to the production of shear (fluid) gels, which are essentially microgel suspensions.

Compared to native *SBP*, the use of *SBPMG* to stabilize emulsions resulted in a larger initial average droplet size at either ϕ_{OIL} investigated. Microgel stabilized emulsions demonstrated an improved storage stability over 9 weeks at 25 °C and an improved resistance to droplet coarsening on thermal treatment in the form of two temperature cycles at 75 °C and 25 °C respectively. Due to the *SBPMG* behaving as solvent swollen particles and extensive flocculation of microgel stabilized oil droplets, the volume fraction occupied by the dispersed phase was highest in the microgel stabilized emulsions, which consequently led to a higher viscosity than native *SBP* emulsions at either ϕ_{OIL} investigated. Interestingly, at ϕ_{OIL} = 40 %, *SBPMG* emulsions demonstrated a solid-like behaviour with $G' > G''$ over several decades of strain amplitude and frequency. This was sufficient to retard or prevent creaming compared to emulsions prepared at ϕ_{OIL} = 20 %, despite the large density mismatch between the aqueous (water) and dispersed (n-tetradecane ρ = 0.76 g cm^{-3}) phases. Furthermore, *SBPMG* emulsions prepared at ϕ_{OIL} = 40 % appeared to demonstrate an improved stability to heating, which was rationalized as an immobilization of emulsion droplets in a 'gel-like' or 'soft glassy' particle network, which in turn reduces the likelihood of coalescence events.

In summary, we have developed a technique to yield biocompatible *SBP* microgel suspensions focussing on their application as rheology modifiers and emulsifiers in foods, providing benefits over the use of native *SBP* in either case. Due to confidentiality, we were not made aware of all potential applications of interest to the industrial sponsor. With further development, *SBPMG*s may find uses in other soft matter applications where biocompatibility and biodegradability are becoming increasingly important. For example, many coatings (*e.g.*, inks, paints) contain particulate rheology modifiers and cosmetics/personal care products and agricultural products are frequently applied in the form of emulsions. Some suggestions for future works are given in the next section.

6.2 Future Work

Firstly, the regulatory status on the use of laccases in food processing is somewhat unclear. Several review articles on the potential uses of laccases in the food industry have been published recently, all suggesting that regulatory clarity is lacking (Mayolo-Deloisa et al., 2020; Forootanfar and Faramarzi, 2019; Backes et al., 2021). These applications include the use of laccases to catalyze crosslinking of polymers (*e.g., SBP* but also arabinoxylans), colour modification in tea and wine, and the treatment (removal of phenolic compounds) of wastewater from food processing plants, among others. The use of an enzyme to catalyze crosslinking may potentially pose a problem, particularly if the active enzyme is trapped within the (micro)gel networks or free in the resulting suspensions. If laccases were to be permitted as processing aids, techniques such as enzyme immobilization can be used, which would ensure the absence of the enzyme from the final product. While this adds additional complications, immobilization of enzymes is frequently shown to *improve* their activity and immobilized enzymes can often be recycled (Adamian et al., 2021). While scaling up these processes, identifying and quantifying the reaction products (*i.e.*, intermolecular crosslinks and by-products) resulting from laccase catalyzed gelation should be investigated, for optimisation and to ensure consumer safety.

The top-down technique described for the fabrication of pectin microgels has proven to be simple and scalable however the production still requires two stages of preparation. Firstly, the preparation of hydrogels and secondly, the mechanical disruption of bulk gels into microgel particles. The resulting suspensions may or

may not require subsequent concentration, depending on the application. The fabrication of microgel type systems in a single processing step can be achieved using the fluid gel approach, whereby a gelling biopolymer solution is subject to shear throughout the sol-gel transition. By utilizing the same crosslinking chemistry, *SBP* fluid gel particles should retain the promising properties of thermal irreversibility and resistance to dissolution on storage.

Such an approach does not resolve the issue of irregular particle shapes. Perhaps for higher value applications or a rigorous fundamental study into the rheological properties of biopolymer microgels, spherical particles would be preferred. To that end, one could feasibly produce spherical *SBPMG* of well-defined size using an emulsion templating technique providing that crosslinking can be either delayed until after the formation of emulsions or initiated afterward. An example of a high value but realistic application would be in the encapsulation of bioactive compounds for targeted delivery to the gastrointestinal tract, simply by incorporating a hydrophilic payload into the pre-gelled droplets. Pectin has been shown to be promising for delivery to the later stages of the gastrointestinal tract since it is a dietary fibre (*i.e.*, it is resistant to digestive enzymes of the upper gastrointestinal tract but can be degraded by the colonic flora) (Liu et al., 2003).

Some suggestions for additional experiments that should be performed to realize the use of *SBPMG* for rheology modification based on the findings of **Chapters 3** and **4** are as follows:

1. The time dependent flow properties of *SBPMG* suspensions should be investigated in further detail. These will be important to understand to develop new products and processes. For example, the production of layered products will require the initial layer to support the weight of all successive layers. Studies of time dependence should also include investigations into aging, which are pertinent due to the extended shelf lives of food products.
2. This thesis investigated the rheological properties of suspensions in shear flows, which are the simplest flows to generate. All types of complex flow phenomena can occur in extension and compression (*e.g.*, capillary breakup, die swell) and these types of flow are experienced during processing (*e.g.*, pumping, moulding, layering) but also on consumption (*e.g.*, chewing and swallowing). Extensional and compressive rheological characterization

should therefore be performed. These are all examples of bulk techniques. Micro-rheology is another active area of research in materials science and the micromechanical characterization of microgel particles and suspensions may provide some additional insight into which factors promote desirable flow properties.

3. Prior to the disruptions brought about by COVID-19, we were studying the rheological properties of smaller, approximately 1 μm sized *SBPMG* particles. These were obtained by rotor-stator mixing followed by high pressure homogenization, similar to the investigation of how the *SBPMG* particle size evolves during the preparation of emulsions, as described in **Chapter 5**. A few experimental issues arose during these investigations, which appear to be due to the smaller particle size. For example, mild centrifugation was no longer suitable for the concentration of suspensions. Therefore, rotary evaporation was used which was both time consuming and energy intensive. No determination of ϕ_{eff} was performed for these smaller *SBPMG*, but with respect to C_{PTOTAL}, a much higher polymer concentration was required to achieve a more modest increase in the viscosity/viscoelasticity of the suspensions. While the data for such systems was not presented in this thesis, these preliminary results suggest that smaller microgel particles are more polymeric (*i.e.*, 'softer') in nature, possibly resembling star polymers.
4. Smaller microgel particles would be preferred for many applications primarily to deliver stability against sedimentation. However, it is also known that in food products, the presence of particles > 25 μm can lead to the perception of a 'gritty' mouthfeel (Engelen et al., 2005). Therefore, sensory analysis should be conducted on the systems presented in this thesis, which may potentially provide additional insight into the factors that promote desirable sensory properties. For example, it would be particularly interesting to understand whether sensory panels can discern between the use of 'soft' or 'firm' *SBPMG* in model food systems. A recent sensory study using agar microgels suggests that increasing G'_{MG} led to an increased detectability of particles and a reduced perception of creaminess (Shewan et al., 2020). An alternative or supplementary experiment to investigate the sensory properties of microgel systems would be to use (soft) tribology to

assess their lubrication properties. This was done by Fernández Farrés and Norton (2014) for agar fluid gels. The elasticity of particles was varied by disruption of intermolecular hydrogen bonds with the addition of co-solutes during fluid gel formation. It was found that suspensions of softer particles demonstrated increased friction, due to an increased surface area between the tribological surfaces under an applied load (Fernández Farrés and Norton, 2014)."

Some suggestions for additional experiments that should be performed to realize the use of *SBPMG* for emulsification based on the findings of **Chapter 5** are as follows:

1. Firstly, n-tetradecane was selected as the dispersed phase in these emulsions for its purity. However, this oil is not suitable for use in foods. In preliminary investigations, we found that *SBPMG* were also capable of stabilizing rapeseed oil in water emulsions (data not shown) and this requires further investigation.
2. From a fundamental standpoint, it would be interesting to use a protein-deficient *SBP* to prepare microgels. For example, by using proteases to (partially) hydrolyze these fragments. This will allow one to separate out any interfacial activity that is due to their particulate nature from that attributed to the surface active protein fractions.
3. In preliminary investigations, *SBPMG* emulsions could be stabilized up to Φ_{OIL} = 60 % (data not shown). To that end, future work on these systems should systematically investigate the influence of Φ_{OIL} and particle concentration on the properties of emulsions while simultaneously studying the effect of particle elasticity. This will include an investigation into the droplet size and emulsion stability, but interfacial tension measurements and interfacial rheology should be performed to provide additional insight into the behavior (e.g., spreading, interpenetration) of microgels following adsorption. Obtaining good quality microcopy images of microgels adsorbed at oil/water and/or air/water interfaces should also be pursued. Similar work has been done on synthetic microgel systems, as discussed in Section 1.3.8. Considering the potential for *SBPMG* emulsions to be used in foods, their emulsifying properties should also be investigated under different environmental conditions (*e.g.*, ionic strength and pH).

4. The mechanism which promotes flocculation in *SBPMG* emulsions should become clear from the studies suggested above. Droplet flocculation is usually considered as undesirable, but some of the data presented in **Chapter 5** suggest that flocculation promoted additional stability against creaming on prolonged storage and to droplet coarsening on heating. Thus, if droplet flocculation is understood in more detail, it may be exploited in practice.

6.3 References

Adamian, Y., Lonappan, L., Alokpa, K., Agathos, S. and Cabana, H. 2021. Recent Developments in the Immobilization of Laccase on Carbonaceous Supports for Environmental Applications - A Critical Review. Frontiers in Bioengineering and Biotechnology. 9.

Backes, E., Kato, C.G., Corrêa, R.C.G., Peralta Muniz Moreira, R.d.F., Peralta, R.A., Barros, L., Ferreira, I.C.F.R., Zanin, G.M., Bracht, A. and Peralta, R.M. 2021. Laccases in food processing: Current status, bottlenecks and perspectives. Trends in Food Science & Technology. 115, pp.445-460.

Borrega, R., Cloitre, M., Betremieux, I., Ernst, B. and Leibler, L. 1999. Concentration dependence of the low-shear viscosity of polyelectrolyte micro-networks: From hard spheres to soft microgels. Europhysics Letters (EPL). 47(6), pp.729-735.

Engelen, L., de Wijk, R.A., van der Bilt, A., Prinz, J.F., Janssen, A.M. and Bosman, F. 2005. Relating particles and texture perception. Physiology & Behavior. 86(1), pp.111-117.

Fernández Farrés, I. and Norton, I.T. 2015. The influence of co-solutes on tribology of agar fluid gels. Food Hydrocolloids. 45, pp.186-195.

Forootanfar, H. and Faramarzi, M.A. 2019. Recent Developments in Laccase Applications for the Food Industry. Reference Module in Food Science.

Jung, J. and Wicker, L. 2012. Laccase mediated conjugation of sugar beet pectin and the effect on emulsion stability. Food Hydrocolloids. 28, pp.168-173.

Liu, L., Fishman, M.L., Kost, J. and Hicks, K.B. 2003. Pectin-based systems for colon-specific drug delivery via oral route. Biomaterials. 24(19), pp.3333-3343.

Appendix A: Methods

As specified in **Chapter 1**, the materials and methods sections provided in the experimental chapters is in most cases sufficient for the reader to understand and replicate the work. In this section, the principles of shear rheometry and the various microscopy techniques used are described in further detail.

A.1 Shear Rheometry

Rheology is the study of deformation and flow but the technique is not limited to the study of 'ideal materials' *e.g.*, Hookean solids and Newtonian fluids. It has become an important technique to characterize soft materials, which are viscoelastic, meaning that they simultaneously demonstrate features of solids and fluids depending on the magnitude of externally applied forces and the timescale of observation (Mezger, 2014). Rheological experiments can be performed using various types of deformation. For example the response of a material to shear, extensional and compressive forces can be studied with commercially available instruments. The simplest experiment involves the application of shear deformations. The working principle of shear rheometry is best illustrated with the two-plate model (Fig. A.1).

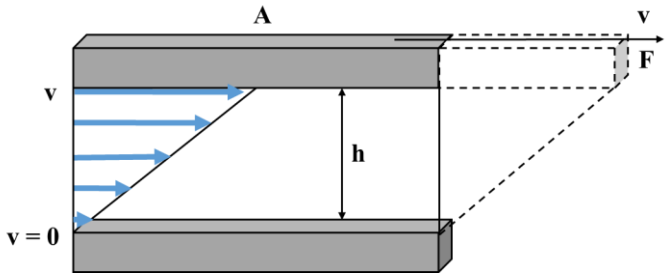

Figure A.1 - Steady shear flow illustrated by the two-plate model.

A given material is loaded between the gap with width, h (m), of two flat plates where it is assumed to adhere to the plates at the upper and lower boundaries, satisfying the no slip boundary condition. A shear force, F (N) is applied to the material over the shear area, A (m^2) by forcing the top plate to move parallel to the bottom plate while the latter is held stationary. This allows the definition of a shear stress σ (Pa) (1 N m^{-2} = 1 Pa);

$$\sigma = \frac{F}{A} \qquad [A.1]$$

In the study of fluids, the deformation due to the application of a shear stress results in fluid flow. To obtain meaningful data, the development of a laminar flow profile is required. Here, the material flows in discrete layers, the velocity of each layer decreasing linearly with distance from the top plate as shown by the blue arrows in Figure A.1. The velocity gradient in the sample is measured with respect to the velocity of the top plate, v (m s^{-1}). This depends on the sample height, the knowledge of which allows the definition of a shear rate, $\dot{\gamma}$ (s^{-1}):

$$\dot{\gamma} = \frac{v}{h} \qquad [A.2]$$

The shear viscosity η (Pa s), defined as the resistance to fluid flow due to internal friction between molecules in the material, is calculated according to:

$$\eta = \frac{\sigma}{\dot{\gamma}} \qquad [A.3]$$

The raw data obtained in a shear rheometry experiment are converted to rheological parameters in the computer software. These depend on the type of measurement geometry used, its dimensions and the rheometer mode of operation (either stress- or strain- control). Measurement of the torque, M (N m) (*i.e.,* in strain control mode) or angular velocity, Ω (rad s^{-1}) (*i.e.,* in stress control mode) at the top plate and their normalisation with geometry specific constants allows one to arrive at the constitutive equations relating σ, $\dot{\gamma}$ and the constant of proportionality, η (Mezger, 2014; Mewis and Wagner, 2012).

The rheology of fluids has industrial relevance since the knowledge of flow behaviour can assist in the design of new or improved products and processes. Performing measurements over a wide range of deformations allows the construction of flow curves and subsequently, viscosity functions. Examples of these are shown in Figures A.2 (A) and (B) respectively.

For ideal (Newtonian) fluids, the stress increases linearly with shear rate, and therefore, the viscosity is constant. Many real fluids demonstrate non-Newtonian flow properties, *i.e.,* the relationship between stress and strain is non-linear giving rise to ‘shear thinning’ if the stress (thus viscosity, Equation A.3) decreases with increasing shear rate or ‘shear thickening’ if the opposite is true. At any given deformation, the steady state response is linear over time, therefore the term ‘apparent shear viscosity’ is often used for non-Newtonian fluids (Mezger, 2014).

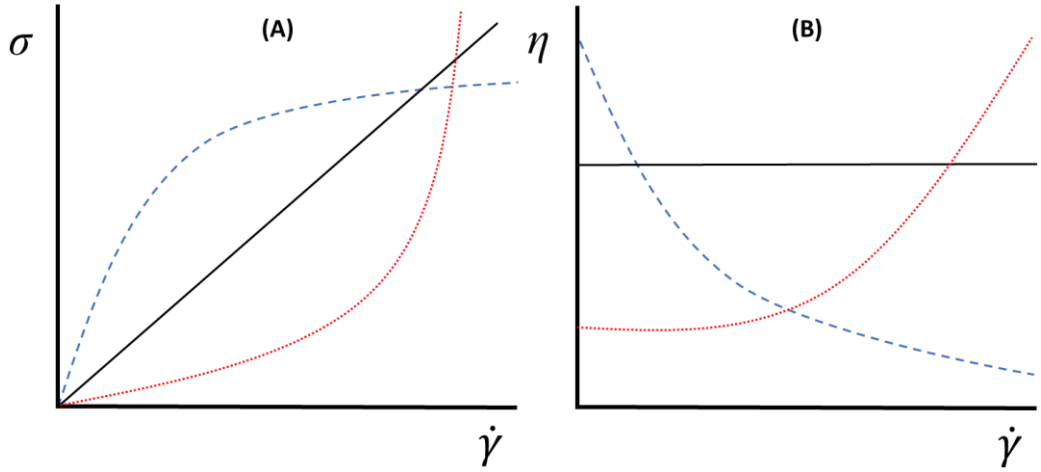

Figure A.2 - (A) Flow curves and (B) the corresponding viscosity curves for a typical Newtonian fluid (solid lines), shear thinning fluid (dashed lines) and shear thickening fluid (dotted lines).

The deformation of a solid material in a shear rheometer can also be illustrated by the two-plate model, as shown in Figure A.3. In this case, the lower plate is fixed and the application of a deformation force in the form of a shear stress, σ, (Equation A.1) at the upper plate leads to its deflection with respect to the lower plate.

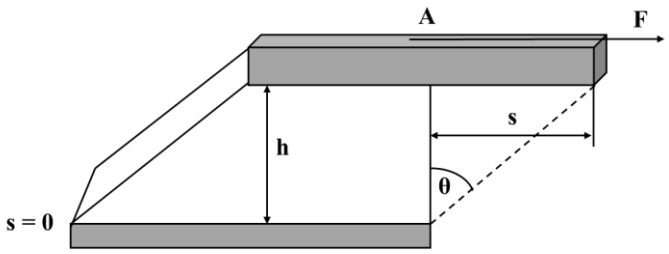

Figure A.3 - Shear deformation of a solid material illustrated by the two-plate model.

The material is deformed homogeneously in the rheometer gap and the resulting shear strain, γ, can be quantified according to:

$$\gamma = \frac{s}{h} = tan\theta \qquad [A.4]$$

: where s is the deflection path (m), h (m) is the distance between the gap and θ the deflection angle (°). Although γ is a dimensionless quantity, it is typically expressed as a percentage (*e.g.*, γ = 100% where s/h = 1). Depending on the material being studied and the device mode of operation, the application of σ or γ allows the

opposing response to be quantified. The constant of proportionality is the elastic shear modulus, *G* (Pa) through Hooke's law:

$$G = \frac{\sigma}{\gamma} \qquad [A.5]$$

: which describes the rigidity of a material. For ideal (Hookean) elastic solids in the limit of low deformation, the material is deformed non-destructively and therefore irreversibly. The removal of the deformation energy results in the restoration of the original unstrained structure. As for fluids, the response of a solid over a range of deformations is required to fully characterize the material. For an ideal elastic solid, the relationship between σ and γ is linear until the so called 'yield point'. For deformations below this value, known as the linear elastic range, the mechanical properties of ideal solids are independent of time. For deformations beyond the yield point, the material will be permanently deformed on removal of the force, or the material may simply fracture. By analogy to non-ideal fluids, so called 'neo-Hookean' solids can undergo strain stiffening or strain softening introducing some curvature to the $\sigma(\gamma)$ response (Mezger, 2014; Tadros, 2010).

More sophisticated experiments can be performed by applying a harmonic, sinusoidal deformation to a material. This is the principle of dynamic mechanical analysis, also known as oscillatory rheometry. The power of this technique arises from the ability to be able to control the amplitude and frequency of deformation. It is particularly useful for the characterization of viscoelastic materials, which may respond with a 'solid-like' response at low deformation and flow at large deformations. Similarly, a viscoelastic material which appears solid at short times (high frequency measurements) may begin to flow if deformed for a long period of time (low frequency measurements) (Mezger, 2014).

The two-plate model is also used to illustrate oscillatory testing, as shown in Figure A.4. The upper plate oscillates back and forth on the application of a force ($\pm F$) which consequently causes homogeneous deformation of the material constrained in the gap with the deflection path ($\pm s$) and deflection angle ($\pm \theta$). As for the rotational tests described above, oscillatory measurements can be performed in stress control and strain control mode of operation and the stress and strain can be defined according to Equations A.1 and A.4 respectively (Mezger, 2014).

Since these measurements are dynamic (*i.e.,* the deformation is sinusoidal with a characteristic frequency) the rheological parameters are expressed with respect to time. Therefore, for ideal elastic materials, Hooke's law applies:

$$\sigma(t) = G^*.\gamma(t) \qquad [A.6]$$

: where G^* is now the complex shear modulus (Pa). Whereas for ideal viscous fluids, Newton's law applies:

$$\sigma(t) = \eta^*.\dot{\gamma}(t) \qquad [A.7]$$

: where η^* is the complex viscosity (Pa s).

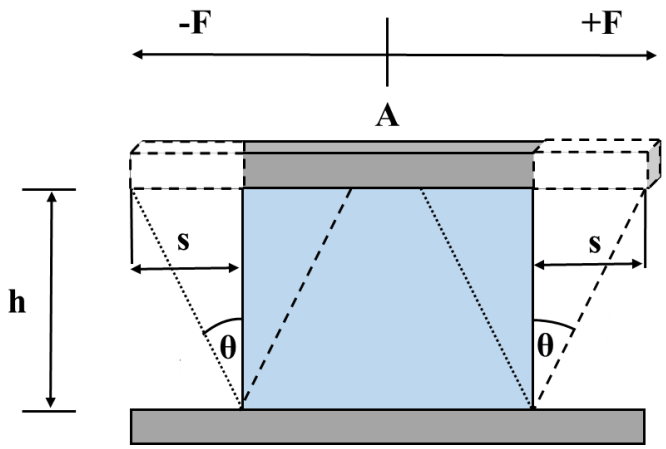

Figure A.4 - Oscillatory shear testing illustrated by the two-plate model.

With the application of a sinusoidal stress or strain, the opposing mechanical response is also sinusoidal and occurs with the same frequency. The red line in Figure A.5 shows the application of a sinusoidal $\gamma(t)$ defined by:

$$\gamma(t) = \gamma_A \,.sin\omega t \qquad [A.8]$$

And the resulting stress response is given by:

$$\sigma(t) = \sigma_A \,.\sin(\omega t + \delta) \qquad [A.9]$$

: where the subscript A corresponds to the stress or strain amplitude, ω is the angular frequency (rad s^{-1}), t is time and δ (°) is the phase shift between the preset and the resulting sine wave. For ideal elastic solids, $G^* = \sigma(t)/\gamma(t)$ = constant. Therefore, the resulting stress response is completely in phase (*i.e.*, $\delta = 0°$) occurring without delay. For ideal viscous fluids, the $\dot{\gamma}$(t) response occurs as a cosine curve:

$$\dot{\gamma}(t) = \gamma_A \,.\omega \,.cos\omega t \qquad [A.10]$$

: *i.e.*, the shear rate function is completely out of phase ($\delta = 90°$). For a viscoelastic material, the phase shift is intermediate between these two responses and thus $0° \leq \delta \geq 90°$ which is shown schematically in Figure A.5 (Mezger, 2014; Tadros, 2010).

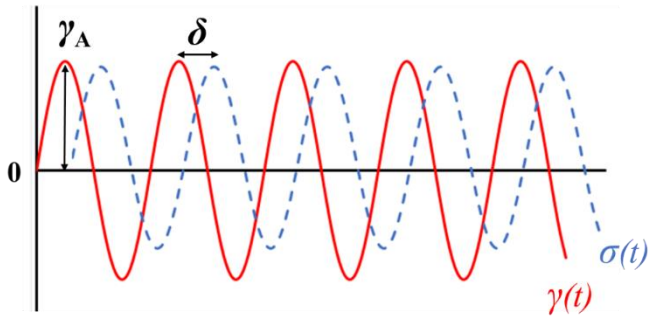

Figure A.5 - Schematic of the application of a sinusoidal shear strain ($\gamma(t)$) and the resulting stress ($\sigma(t)$) response for a viscoelastic material showing a phase shift (δ) of $0° \leq \delta \geq 90°$.

The rheological quantities G^* and η^* introduced in Equations A.6 and A.7 respectively are written in complex form due to their definition in oscillatory shear. Analysis is performed in the rheometer software using complex mathematics to obtain the 'real' (namely G' and η') and 'imaginary' (namely G'' and η'') parts of G^* and η^* respectively. For the purpose of this thesis, it suffices to define these parameters in mathematical notation. G' describes the portion of the deformation energy which is stored in the material and drives the elastic restoration of the unstrained structure when the deformation is removed. G'' describes the portion of the deformation energy which is lost as a viscous dissipation in the form of heat (*e.g.*, to the environment, or within the sample). This provides the relevant nomenclature for the rheological parameters obtained from an oscillatory rheometry experiment: the elastic or *storage* modulus (G') and the viscous or *loss* modulus (G'') defined according to:

$$G' = \left(\frac{\sigma_A}{\gamma_A}\right) cos\delta \qquad [A.11]$$

$$G'' = \left(\frac{\sigma_A}{\gamma_A}\right) sin\delta \qquad [A.12]$$

: G^*, G' and G'' (Pa) are related through:

$$G^* = \sqrt{(G')^2 + (G'')^2} \qquad [A.13]$$

: The loss factor, tanδ, is calculated according to:

$$tan\delta = G''/G' \qquad [A.14]$$

: and hence describes the ratio of viscous and elastic behaviour in a given viscoelastic material (Mezger, 2014).

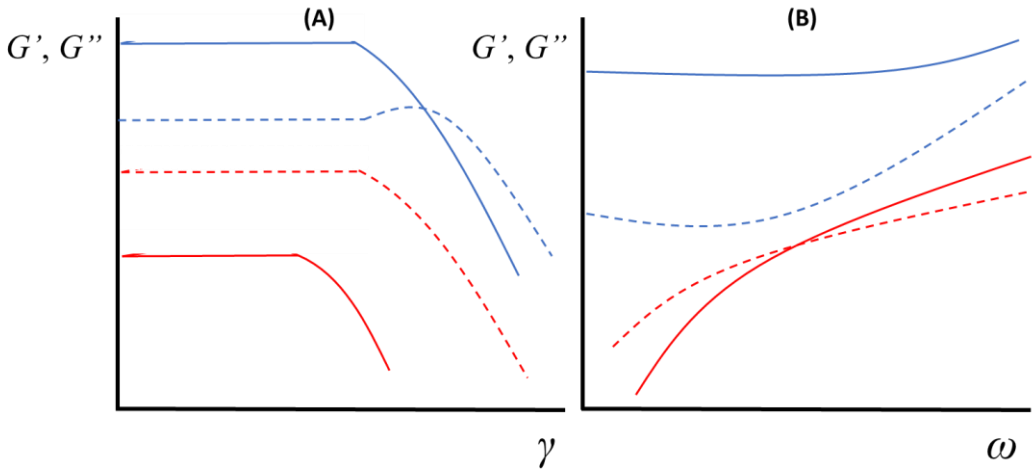

Figure A.6 - (A) Strain amplitude (γ) sweeps for a typical viscoelastic solid (*e.g.,* a hydrogel) (blue lines) where *G'* (solid lines) is greater than *G"* (dashed lines) and a typical viscoelastic fluid (*e.g.,* a polymer solution) where *G"*>*G'*. (B) Shows the typical mechanical response of the same materials during frequency (ω) sweep measurements.

A full characterization of the material can be achieved by first performing stain amplitude sweeps *i.e.*, an incrementally increasing γ applied at a constant ω. This allows one to define the linear viscoelastic region (*LVER*) where the *G'* and *G"* values are γ independent as shown in Figure A.6 (A) for a viscoelastic solid (*G'*>*G"* thus tanδ < 1) and a viscoelastic fluid (*G"*>*G'* thus tanδ > 1). Subsequently, frequency sweeps can be performed at a constant γ (within the *LVER*), to study the time dependence of the applied deformation. This is shown for a solid-like sample (*e.g.,* a hydrogel) and a fluid-like sample (*e.g.,* a polymer solution) in Figure A.6 (B). From frequency sweep measurements, one can also define η^* via:

$$\eta^* = \frac{G^*}{\omega} \qquad [A.15]$$

: By pre-setting a constant strain amplitude and frequency, the rheological properties of a material can be assessed with time or temperature. This is particularly useful for mechanical characterization of samples that change as a result of either or both dependent variable (*e.g.,* for monitoring heat set gelation or the isothermal curing of resins).

A.2 Microscopy

A.2.1 Light Microscopy

Optical microscopy refers to a collection of techniques which can be used to image a material depending on its interactions with light. The simplest experimental setup for these purposes is a compound microscope. The instruments relies on the transmission of light through a specimen to produce an image and this can be achieved using either a ‘brightfield’ or ‘darkfield’ microscope configuration. In either case, a sample is placed on the microscope stage and is illuminated by a light source from below, which is focused onto the sample using a mirror and condenser. In brightfield microscopy, the light arriving at the objective lens is uniformly bright in the absence of a specimen. When light passes through the sample, it is either absorbed or scattered and thus the light arriving at the objective lens appears darker than the background. The objective lens transmits the light to the eyepiece enabling one to produce an image of the sample. Alternatively, the eyepiece can be connected to a digital camera where the image is captured. A limitation of brightfield microscopy is that the resolution of the microscope is limited by the wavelength of the light source and the numerical aperture of the objective lens. Typically, the lower limit for obtaining images of reasonable quality is around 1 µm. In addition, the technique is generally found to be unsuitable for imaging of samples with a low contrast (*e.g.*, materials with similar refractive indices) in the absence of a suitable stain. Finally, optical techniques are best suited to ‘thin’ samples and the collected images are two-dimensional (Clarke and Eberhardt, 2002; Rochow and Rochow, 1978). For these reasons, complementary imaging techniques were used and briefly described below.

A.2.2 Confocal Laser Scanning Microscopy

Confocal laser scanning microscopy (*CLSM*) is typically employed on samples which are inherently fluorescent (auto-fluorescent), or which have been labelled with fluorescent probes although the technique can also be used in reflection and transmission modes of operation. In a typical *CLSM* experiment, the specimen is illuminated by one or more light sources, typically lasers, which scan small sections of the sample either by moving the stage or by moving the light source (*e.g.*, via a series of mirrors). Sectioning can be achieved in the *x*,*y* plane but also vertically such that thick materials can be probed. Since only small sections of the specimen are scanned, the image needs to be reconstructed from the intensity of light arriving at the detector based on the *x*,*y*,*z* coordinates. The advantage of scanning small sections of the sample and reconstructing an image is that out of focus light has already been removed by the optical system (*i.e.*, via a slit or pinhole), thus

improving the resolution of the resulting image. This is one of the great advantages of *CLSM* over conventional light microscopy setups, along with the enhanced contrast provided by (auto)fluorescence. Furthermore, three dimensional images can be obtained in the form of a Z-series (Z-stack). The detectors in a *CLSM* are usually photomultiplier tubes which receive light from a section of the sample via a confocal aperture. The size of the aperture dictates the amount of light arriving at the detector, and consequently, the thickness of the optical section, with a larger sized aperture producing a larger section. Fluorescence arises from the specimen absorbing one wavelength of light and emitting longer wavelengths of light. The emitted fluorescence follows a separate light path to the incident light and contains a combination of different wavelengths. This emitted light is split by filters and detected at separate fluorescent light detectors. In this way, samples can be stained by multiple flurochromes and the resulting images, when reconstructed, provide an even greater contrast enhancement (Paddock, 1999; Singh and Gopinathan, 1998; Clarke and Eberhardt, 2002).

A.2.3 Electron Microscopy

Electron microscopy utilize the interactions of electrons with the atomic nuclei of a specimen to create an image. The two most common forms of electron microscopy are scanning electron microscopy (*SEM*) and transmission electron microscopy (*TEM*) respectively. In either case, electron beams are discharged from an electron gun and directed onto the sample by a condenser lens. *TEM* utilizes the transmission of electrons through a specimen and is therefore only suitable for thin samples (typically around 0.5 μm). Electrons which are transmitted through the material can be counted and sorted based on their energy loss by a detection system, which in turn provides an image with high spatial resolution due to the short wavelengths of the electrons. When a high energy electron beam interacts with a specimen, a variety of products are formed including secondary and backscattered electrons, X-rays, and photons. It is the backscattered electrons which are of most interest in *SEM* experiments, as the detection of these allows one to obtain an image of the material based on their intensity. The electron beam raster scans the surface of the specimen at various positions, and contrast in the image arises from the differences in the angular distribution of backscattered signals, in addition to differences in the nuclear charge. This results in a seemingly three-dimensional image of the specimen (*e.g.*, due to elevations and depressions of the surface). Conventional *SEM* and *TEM* experiments are performed under vacuum to prevent electron beams interacting with molecules in the air. Consequently, the techniques are only suitable for dried samples which limits their potential. Furthermore, drying can significantly change

the properties of a given material and therefore the resulting images may not be entirely representative (Rochow and Rochow, 1978; Clarke and Eberhardt, 2002). Conventional *SEM* was used in **Chapter 3** to investigate the morphology of sugar beet pectin (*SBP*) microgel particles. These were encapsulated within an agarose gel, subjected to solvent exchange with ethanol and finally dried for analysis. Cryogenic *SEM* (*CRYO-SEM*) was used in **Chapter 5** to investigate the microstructure of *SBP* and *SBP* microgel stabilized emulsions. This technique involves freezing samples with a high moisture content prior to imaging, which facilitates their study under vacuum. Samples are frozen rapidly, by liquid nitrogen for instance, to minimize the growth of ice crystals and limit any potential destruction of the sample.

A.3 References

Clarke, A. and Eberhardt, C. 2002. *Microscopy techniques for materials science*. Cambridge: Woodhead Publishing.

Mewis, J. and Wagner, N. 2012. *Colloidal Suspension Rheology*. New York: Cambridge University Press.

Mezger, T. 2014. *The Rheology Handbook: For Users of Rotational and Oscillatory Rheometers*. 4th ed. Hanover, Germany: Vincentz Network.

Paddock, S. 1999. *Confocal microscopy: methods and protocols*. New Jersey: Humana Press.

Rochow, E. and Rochow, T. 1978. *An introduction to microscopy by means of light, electrons, X-rays, or ultrasound*. New York: Plenum Press.

Singh, A. and Gopinathan, K. 1998. *Confocal microscopy: a powerful technique for biological research*. Current Science. pp.841-851.

Tadros, T. 2010. *Rheology of Dispersions: Principles and Applications*. Weinheim: Wiley.

List of Abbreviations

1/k	Debye length
A	Hamaker constant (**Chapter 1**)
A	Absorbance (**Chapter 3**)
A	Shear area (**Appendix**)
A_H	Combined Hamaker constant
ABTS	2,2′-azino-di-(3-ethylbenzthiazoline sulfonic acid)
Araf	Arabinofuranose
b	Constant for Born repulsion
B	Kinetic constant
c	van der Waals constant
C	Concentration
$CaCl_2$	Calcium chloride
C_E	Nominal enzyme concentrations
C_{GEL}	Polymer concentration in pectin hydrogels
CI	Creaming Index
CLSM	Confocal laser scanning microscopy
C_{PTOTAL}	Total pectin concentration
CRYO-SEM	Cryogenic scanning electron microscopy
D	Diffusion coefficient
$D_{3,2}$	Sauter (surface weighted) mean diameter
$D_{4,3}$	De Broukere (volume weighted) mean diameter
D_{90}	Mean diameter of the smallest 90% of particles in suspensions
D_{AC}	Degree of acetylation
D_{AM}	Degree of amidation
D_H	Hydrodynamic diameter
DLVO	Theory of colloidal stability
D_M	Degree of methoxylation
E	Energy of particle detachment (**Chapter 1**)
E	Electric field strength (**Chapter 2**)
E_P	Young’s modulus of particles
f	Frequency
F	Shear force

FA	Ferulic acid
FITC	Fluorescein isothiocyanate
g	Gravitational acceleration constant
G	Shear modulus
G''	Viscous (loss) modulus
G'	Elastic (storage) modulus
*G**	Complex shear modulus
G'_{inf}	Constant that reflects *G'* when $t \rightarrow \infty$
G'_{MG}	Elastic modulus of microgel particles
GalA	Galacturonic acid
h	Surface distance of separation (**Chapter 1**)
h	Gap height (**Appendix**)
h_m	Average hydrostatic pressure height
H_E	Emulsion layer height
H_S	Serum layer height
HG	Homogalacturonan
HLB	Hydrophile-lipophile balance
HMP	High methoxyl pectin
I	Ionic strength
k	Constant to convert particle concentration to an effective volume fraction
K	Capillary constant
K_B	Boltzmann constant
K_C	Consistency index
KCl	Potassium chloride
k_D	Reciprocal of the Debye length
KPS	Potassium peroxodisulfate
L	Length of capillary
LCST	Lower critical solution temperature
LDME	Laser doppler micro electrophoresis
LMP	Low methoxyl pectin
LVER	Linear viscoelastic region
m	Shear thinning exponent
M_0	Mass of hydrogels
M	Mass of swollen hydrogels
MBA	N,N''-Methylenebisacrylamide

n	Power law exponent
O/W	Oil-in-water emulsion
p(NIPAM)	Poly(N-isopropylacrylamide)
PCS	Photon correlation spectroscopy
PDI	Polydispersity index
PGPR	Polyglycerol polyricinoleate
PMMA	Poly(methyl methacrylate)
PSD	Particle size distributions
q	Scattering wave vector
Q	Volumetric swelling ratio
r	Centre-centre distance of separation
R	Particle radius
R_{cap}	Capillary radii
R_{core}	Radius of particle core
R_{eff}	Effective particle radius
RGI	Rhamnogalacturonan I
RGII	Rhamnogalacturonan II
R_H	Hydrodynamic radius
s	Deflection path
S	Swelling ratio
SBP	Sugar beet pectin
SBPMG	Sugar beet pectin microgel
SDS	Sodium dodecyl sulphate
SEM	Scanning electron microscopy
T	Temperature
t	Time
tanδ	Loss factor
u_e	Electrophoretic mobility
$V_{(r)}$	Pair potential
V	Sample volume
VDW	van der Waals
v	Particle velocity (**Chapter 2**)
v	Velocity of the top plate (**Appendix**)
v_e	Electrophoretic velocity
V_P	Volume of sphere
VPT	Volume phase transition

VPTT	Volume phase transition temperature
W	Colloid pair potential
W/O	Water-in-oil emulsion

List of Symbols

$\dot{\gamma}$	Shear rate
γ	Shear strain
γ_c	Critical strain
γ_s	Surface tension
γ_y	Yield strain
η	Viscosity
$[\eta]$	Intrinsic viscosity
η_{red}	Reduced viscosity
η_{rel}	Relative viscosity
η_0	Zero shear viscosity
η_∞	Infinite shear viscosity
η^*	Complex viscosity
ϕ	Volume fraction
ϕ_{eff}	Effective volume fraction
ϕ_G	Volume fraction of glass transition
ϕ_J	Volume fraction of jamming transition
ϕ_{max}	Maximum packing volume fraction
ϕ_{OIL}	Volume fraction of oil
ϕ_{RCP}	Volume fraction of random close packing
δ	Stabilizing chain length (**Chapter 1**)
δ	Excluded volume thickness (**Chapter 5**)
δ	Phase shift
Δ	Increment
ε	Relative permittivity
θ	Contact angle (**Chapter 1**)
θ	Scattering angle (**Chapter 2**)

θ	Deflection angle (**Appendix**)
λ	Wavelength
v	Kinematic viscosity
ξ	Zeta potential
ρ	Number density (**Chapter 1**)
ρ	Fluid density
σ	Shear stress
σ_y	Yield stress
ω	Angular frequency
Π	Osmotic pressure